Study of putative aminotransferases from *Staphylococcus aureus*

This thesis is submitted by

ARELY FERNANDA LEYTON DOMÍNGUEZ

For the degree of Doctor of Philosophy (PhD) in the

Faculty of Medical Sciences, University College London

Department of Microbial Diseases

UCL Eastman Dental Institute

Royal Free Campus, Rowland Hill Street

London NW3 2PF, UK

2023

Declaration

I, Arely Fernanda Leyton Domínguez, confirm that the work presented in this thesis is my own. Where information has been derived from other sources, I confirm that this has been indicated in the thesis.

Abstract

The antimicrobial resistance (AMR) problem was responsible for 4.95 million deaths in 2019, with 10 million people predicted to die annually by 2050. *Staphylococcus aureus* is one of the six leading pathogens associated with AMR deaths, it is considered as a serious threat by the CDC and a high priority pathogen by the WHO.

One of the ways to tackle AMR is by finding new targets. In the work described here, we focused on the study of three putative aminotransferases coded in the genome of *S. aureus* predicted to be involved in the aspartate and haem biosynthetic pathways as potential drug targets.

Mutant strains from the Nebraska Transposon Mutant Library (NTML) with disruptions in the genes coding for a putative aspartate aminotransferase, SAUSA300_1916 (AspB), and for two putative glutamate-1-semialdehyde aminotransferases (GSA-ATs), SAUSA300_1614 (HemL1) and SAUSA300_1845 (HemL2), were used to evaluate the impact of the deficiency of the enzymes in *S. aureus* colonisation using planarian model, virulence using *Galleria mellonella* model, growth in different media, and biofilm formation using the crystal violet assay.

Our results show that, although the putative AspB and HemL enzymes were found not to be essential for the growth or biofilm formation of *S. aureus* under the conditions tested, their deficiency led to a significant virulence attenuation in the *G. mellonella* model. This model had the advantage over the planarian model of being able to precisely inject the bacteria without the need for a sophisticated microinjection instrument and was used for further analysis.

The genes coding the putative enzymes were cloned, expressed in *Escherichia coli* and the purified proteins were assayed for aminotransferase activity. SAUSA300_1916 (AspB) was confirmed to be a pyridoxal phosphate (PLP)-dependent aminotransferase showing a K_m of 1.36 ± 0.13 mM for aspartate and was inhibited by the PLP-dependent aminotransferase inhibitors adapalene and PF-04859989, amongst others.

SAUSA300_1614 and SAUSA300_1845 bound pyridoxamine phosphate (PMP) and PLP, respectively. Furthermore SAUSA300_1614 (HemL1) showed the bioinformatically predicted GSA-AT activity, while SAUSA300_1845 did not. SAUSA300_1614 had a K_m of 8.6 ± 2.9 µM for its substrate, glutamate-1-semialdehyde, and was inhibited by γ-acetylenic GABA and γ-vinyl GABA.

We showed that the enzymes AspB and HemL1 had the annotated activity, while the activity of the putative HemL2 protein remains to be elucidated. Both enzymes, AspB and HemL1, were inhibited by compounds approved to be used in humans that are safe and whose efficacy in *S. aureus* treatment might potentially be tested. Since these pyridoxal dependent enzymes have no homologs in humans, they represent specific targets for the development of new drugs against *S. aureus*.

Impact Statement

Staphylococcus aureus is one of the leading pathogens causing healthcare associated antimicrobial resistant (AMR) infections. The current global crisis caused by AMR combined with a lack of new drugs available makes it crucial to find new targets against multi-drug resistance bacteria.

The finding of this thesis demonstrated that three putative aminotransferases from *S. aureus* involved in the central carbon and haem metabolic pathways were important for the virulence of the pathogen in a *Galleria mellonella* model. Furthermore, our study experimentally determined that SAUSA300_1916 (AspB) had aspartate aminotransferase activity and SAUSA300_1614 (HemL1) had glutatamate-1-semialdehyde aminotransferase activity. Moreover, both enzymes were characterised and inhibited by aminotransferase inhibitors.

This study proposes that the aspartate aminotransferase (AspB) and glutamate-1-semialdehyde aminotransferase (HemL1) from *S. aureus* are good candidates as new targets for drugs development. We have demonstrated that the enzymes AspB and HemL1 can be inhibited by compounds that are used in humans, which are proven to be safe and can be used as a leading compounds to design new antimicrobials. This confirmation can inform pharmaceutical investigations on the development of new drugs against *S. aureus* infections.

Although the identification of potential candidates for drug development is an initial step in the antibiotic development pipeline, it is critical to find valid candidate molecules against those targets. We expect this research will help in the process of drugs development as proposes the aminotransferases of *S. aureus* as new targets to develop antibacterial agents that could ultimately lead to a decrease in the mortality rate due to *S. aureus* infections as well as a reduction in the healthcare costs associated to hospital treatment and drug usage.

More specifically, the results of the present study contribute to the body of knowledge of the characterised enzymes of *S. aureus,* which can be instrumental for future academic research in the subject.

Acknowledgement

I would like to thank to Dr. Sean Nair for his guidance and support throughout this PhD. His comments and critical feedback were invaluable to complete this dissertation. I would also like to thank to Dr. Andrew Smith for his support, feedback and willingness to help whenever was needed.

I would like to thank to Dr. Hellen Allan from the Department of Chemistry, UCL, for her guidance during the synthesis of glutamate-1-semialdehyde and to the staff members of the Department of Microbial Diseases who contributed with their expertise and support during the realisation of this research project, specially thanks to Dr. Haitham Hussain, Dr. Anna Tymon, Ingrid Green, and Tracey Moss.

There has been ups and downs all the way throughout this PhD and I am very grateful to have shared these years with Khadijah, Shatha, Sophia and Hadeel who have been very supportive and helpful. My gratitude also goes to my previous and current colleagues with whom I have shared good memories, specially thanks to Supanan, Shirene, Asyura, Mehmet, Claire, Felix and Badri.

My deepest gratitude goes to Daniel for his endless encouragement and support and to Alejandra for being there when I needed support.

Finally, I would like to thank to the Chilean National Agency for Research and Development (ANID) for funding this research.

Table of contents

List of figures

List of tables

List of abbreviations

µg	Microgram
µL	Microlitre
µm	Micrometre
µM	Micromolar
AhpC	Alkyl hydroperoxide reductase
ALA	5-aminolevulinic acid
AMPs	Antimicrobial peptides
AMR	Antimicrobial resistance
AOA	Amino-oxyacetate
APCs	Antigen presenting cells
Asp-AT	Aspartate aminotransferase
AspB	Aspartate aminotransferase from *Staphylococcus aureus*
ATP	Adenosine triphosphate
Bbp	bone sialoprotein binding proteins
BHI	Brain hearth infusion
bp	Base pair
CA-MRSA	Community-associated methicillin-resistant *Staphylococcus aureus*
CDM	Chemically defined media
CFU	Colony forming units
CHIPS	Chemotaxis inhibitory protein of staphylococci
Clf	Clumping factor
Cna	Collagen adhesin
CP	Capsular polysaccharides
CSE	Cystathionine γ-lyase
CSR	Centre for Staphylococcal research
dH_2O	Distilled water
DHFR	Dihydrofolate reductase
DHPS	Dihydropteroate synthase
DMSO	Dimethyl sulfoxide
DNA	Deoxyribonucleic acid

dpi	Days post infection
Dsg1	Desmoglein 1
dsRNA	Double-stranded RNA
Eap	Extracellular adherence protein
EDTA	Ethylenediaminetetraacetic acid
ETC	Electron transport chain
ETs	Exfoliative toxins
FnBP	Fibronectin binding protein
FPR	Formylated peptide receptors
g	Grams
GABA	gamma-aminobutyric acid
GABA-AT	gamma-aminobutyric acid aminotransferase
GDH	Glutamate dehydrogenase
GOT	Glutamic oxaloacetic transaminase
GSA	Glutamate-1-semialdehyde
GSA-AT	Glutamate-1-semialdehyde aminotransferase
h	Hour
HA-MRSA	Healthcare-associated methicillin-resistant *Staphylococcus aureus*
HEPES	4-(2-hydroxyethyl)-1-piperazineethanesulfonic acid
His	Histidine
Hla	Hemolysin-α
Hlb	Hemolysin-β
HPLC	High performance liquid chromatography
IC_{50}	Half-maximal inhibitory concentration
ICAM-1	Intercellular adhesion molecule-1
IgG	Immunoglobulin G
ileRS	Isoleucyl-tRNA synthetase
IU	International unit
KAT	kynurenine aminotransferase
K_{cat}	Catalytic constant
kDa	Kilodalton
K_m	Michaelis-Menten constant

KYNA	Kynurenic acid
LAs	Lipoteichoic acids
LB	Luria Bertani
LFA-1	Lymphocyte function-associated antigen
LPS	Lipopolysaccharide
L-SOS	L-serine O-sulfate
M	Molar
MBTH	3-methyl-2-benzothiazolinone
MDH	Malic dehydrogenase
MDRSA	Multidrug-resistant *Staphylococcus aureus*
MHC-II	Major histocompatibility complex class II
MIC	Minimum inhibitory concentration
min	Minute
mL	Millilitre
MOPS	3-(N-morpholino)propanesulfonic acid
MORN	Membrane occupation and recognition nexus
MRSA	Methicillin-resistant *Staphylococcus aureus*
MSA	Mannitol salt agar
MSCRAMM	Microbial surface components recognising adhesive matrix molecules
MSSA	Methicillin-sensitive *Staphylococcus aureus*
NADH	Nicotinamide adenine dinucleotide
NADPH	Reduced nicotinamide adenine dinucleotide phosphate
NETs	Neutrophil extracellular traps
Ni-NTA	Nickel-nitrilotriacetic acid
nM	Nanomolar
NTML	Nebraska transposon mutant library
Nuc	Nuclease
OAA	Oxaloacetic acid
PAGE	Polyacrylamide gel electrophoresis
PAMPs	Pathogen-associated molecular patterns
PBP	Penicillin-binding protein
PBS	Phosphate buffer saline

PCR	Polymerase chain reaction
PDA	pancreatic ductal adenocarcinoma
PFTs	Pore forming toxins
PG	Peptidoglycan
PLP	Pyridoxal 5’-phosphate
PMF	Proton motive force
PMP	Pyridoxamine 5’-phosphate
PPP	Pentose phosphate pathway
PSMs	Phenol soluble modulins
PTC	Peptidyltransferase center
PVL	Panton-Valentine leucocidin
RNA	Ribonucleic acid
RNAi	Interference RNA
RNase	Ribonuclease
S	Second
SAA	sulphur-containing amino acid
Sad	Superoxide dismutase
SAgs	Superantigens
SCV	Small colony variant
SDS	Sodium dodecyl-sulfate
SMX	Sulfamethoxazole
SNM	Synthetic nasal extract
SPIN	Staphylococcal peroxidase inhibitor
SSSS	Staphylococcal scalded skin syndrome
TAE	Tris-acetate-EDTA
TAs	Teichoic acids
TCA	Tricarboxylic acid
TCR	T-cell receptor
TEMED	Tetramethylethylenediamine
TEV	Tobacco Etch virus
TMP	Trimethoprim
Tn	Transposon

tRNA	Transfer RNA
TSA	Tryptic soy agar
TSB	Tryptic soy broth
TSST-1	Toxic shock syndrome toxin 1
UV	Ultraviolet
V_{max}	Maximal velocity
VRSA	Vancomycin resistance *Staphylococcus aureus*
WHO	World Health Organisation
WTAs	Wall teichoic acids
α-KG	Alpha- ketoglutaric acid

CHAPTER 1

Introduction

1. Introduction

1.1 Antibiotic resistance as a global health problem

This thesis describes an exploration of potential drug targets against *Staphylococcus aureus* infections and antimetabolite agents in an attempt to aid to the discovery of new antibiotics in the future in order to tackle the increase in antimicrobial resistance (AMR). AMR has become one of the major concerns on human health and it is amongst the top 10 threats facing humanity according to the World Health Organisation (WHO). Depending on the antimicrobial resistance pattern, bacteria are categorised into susceptible, intermediate resistant, and resistant to antibiotics after comparing the minimum inhibitory concentration (MIC) obtained in a susceptibility test with established breakpoints that define the susceptibility of the bacteria for a specific antibiotic (Macgowan & Wise, 2001). A resistant bacteria shows an increased MIC when compared with the susceptibility breakpoint for the antibiotic under study and the drug will no longer show inhibitory activity against the pathogen (Sherrard et al., 2014).

AMR can be caused by different mechanisms categorised into two types: biochemical and genetic mechanisms (Siddiqui, 2019). One of the biochemical mechanisms consists in the target modification, and an example of that corresponds to the alteration in either the DNA gyrase or topoisomerase IV, that reduces the effectiveness of fluoroquinolones, which target the DNA synthesis (Redgrave et al., 2014). A decreased influx of the antibiotic due to modification in the structure of the cell membrane, an active efflux of the antibiotic, an inactivation of the antibiotic as a result of enzymatic modification, or an alteration of the binding site of the antibiotic to its target are different mechanisms of bacterial resistance to antibiotics. In terms of the genetic mechanisms, mutations within the genome results in antimicrobial resistance acquisition by alteration in the drug target or in the composition of the cell wall (Foster, 2017). It was reported that mutations in the genes coding regulatory housekeeping functions, like the gene coding the RNA polymerase β subunit (*rpoB*) or the ribosomal S12 protein (*rpsL*), is a common

mechanism of antibiotic resistance and it is also associated with pleiotropic effects due to the central role of the affected genes in microbial processes (Hershberg, 2017). The horizontal gene transfer is another genetic mechanism involved in the acquisition of resistance by bacteria being conjugation, transduction, and transformation the types of gene transference that significantly contribute to the spread of antimicrobial resistance genes (Andersson & Hughes, 2010).

It has been predicted that by 2050, nearly 10 million people will die per year worldwide due to AMR related infections, this being the leading cause of deaths compared with others like cancer (8.2 million), diabetes (1.5 million), diarrheal disease (1.4 million), and road traffic accidents (1.2 million) according to an official report commissioned by the United Kingdom (UK) government (J. O'Neill, 2016). The fatality rates associated with resistant strains infections is higher when compared with their susceptible counterparts, for example, in patients with bacteraemia caused by methicillin-resistant *Staphylococcus aureus* (MRSA) strains the mortality was significantly higher when compared with patients with bacteraemia caused by methicillin-susceptible *Staphylococcus aureus* (MSSA) strains (Cosgrove et al., 2003).

Regarding the financial consequences of AMR, Thorpe and colleagues found that the costs related to the treatment of AMR infections added an average of 1,383 USD when compared with the treatment costs of non-AMR infections after analysing the data from the Medical Expenditure Panel Survey-Household Component during a 13 years period, from 2002 to 2014 (Thorpe et al., 2018). In the case of the EU/EEA, it was predicted that the costs associated to AMR infections could be around 1.1 billion Euros per year between 2015 and 2050 if no action is taken (ECDC & OECD, 2019) (accessed 2021, Feb 04). To tackle the AMR problem, worldwide efforts have been made, and in 2017 the G20 Health Ministers held the Berlin Declaration in a joint commitment to promote research leading to the development of new antibiotics and to design plans to tackle AMR considering the impact it will have on millions of people and on the economic productivity of the countries if not properly addressed.

Amongst the factors contributing to the AMR crisis, a key one is the decrease in the rate of new drugs discovered since the 1980s, mainly due to a reduced investment in antibiotic research by both, public and private funders (J. O'Neill, 2016). It seems paradoxical that while AMR bugs are increasing, companies researching in drug development are decreasing as seen by the reduction in the number of companies investigating in antibiotics from the 1990 to 2011 with a fall in number from 18 to 4 (Cooper & Shlaes, 2011), which is caused mainly due to the low returns that antibiotic discovery and development provides to pharmaceutical and biotechnological firms (M. J. Renwick et al., 2016).

According to the threat categorisation by the Centers for Disease Control and Prevention (CDC) in urgent, serious, and concerning, MRSA is considered as a serious threat and the vancomycin-resistant *S. aureus* (VRSA) is categorised as concerning, while the priority of *S. aureus* for the WHO remains to be high (Micoli et al., 2021). The serious threat this pathogen represents for the public health and the lack of new antimicrobials available for its treatment make it imperative to find new targets for the development of new drugs to combat its infection.

1.2 *S. aureus* general characteristics and virulence factors

S. aureus is a bacterium belonging to the *Staphylococcus* genus discovered by the Scottish surgeon Alexander Ogston in 1880 while observing microorganisms obtained from samples of abscesses, when he was trying to explain the link between bacteria and wound infections (Ogston, 1881). Amongst the microorganisms observed by Ogston, those arranged in grape-like clusters were named as *Staphylococcus* and the species "*aureus"* was named afterwards by the German surgeon Anton J. Rosenbanch due to the golden colour of the colonies (G. Y. Liu et al., 2005).

S. aureus is a Gram-positive, spherical-shaped microorganism, catalase and coagulase positive, and can be normally found inhabiting the skin (hands, chest, and abdomen), the upper respiratory tract (mainly the nose), gastrointestinal tract, vagina, rectum, and axilla (Presctott et al., 2002; Sakr et al., 2018). The squamous epithelium of the anterior nares is its preferred ecological niche (Cole et al. 2001) and depending on the nasal carriage status, the population can be classified as persistent (~20%), intermittent (~30%) or non-carriers (~50%) of *S. aureus* (Wertheim et al., 2005) or as persistent and non-persistent according to the re-classification made by van Belkum and colleagues (van Belkum et al., 2009). Although it is a commensal microorganism, when our protective mechanical barriers are broken, it can penetrate into our body and cause from local infections of the skin to more severe infections such as osteomyelitis, pneumonia, endocarditis and septicaemia (Cheung et al., 2021).

S. aureus produces a wide range of virulence factors that can be secreted or associated with its surface, contributing to its adhesion, invasion, and evasion of the host immune system. Adhesion of the pathogen to the host cell, specially to the extracellular matrix, is mediated by cell wall-anchored (CWA) proteins that have been classified into four families depending on their structural motifs: microbial surface components recognising adhesive matrix molecules (MSCRAMMs), NET motif family, three-helical bundle family, and G5-E repeat family (Foster et al., 2014). Amongst the MSCRAMMs that are proven to be involved in adhesion to host components like fibrinogen, collagen, cytokeratin, or epithelial cells, we can find the clumping factors: ClfA and ClfB, fibronectin binding proteins: FnBPA and FnBPB, collagen adhesin (Cna), and bone sialoprotein binding proteins (Bbp).

S. aureus has developed the ability to evade the host immune system through the expression of a wide range of evasion molecules that participate in the circumvention of the pathogen to every step of the immune response (de Jong et al., 2019). The chemotaxis inhibitory protein of *Staphylococcus aureus* (CHIPS), the extracellular adherence protein (Eap) and capsular polysaccharides (CPs) type 5 and 8 are examples

of factors involved in the evasion of the neutrophils extravasation and chemotaxis as well as in the inhibition of phagocytosis (de Jong et al., 2019; Foster, 2005). CHIPS binds specifically to two chemoattractant receptors located on the surface of neutrophils, the C5a receptor (C5aR) and formylated peptide receptors (FPR), whose natural ligands are the complement component C5a and bacterial released formylated peptides, respectively. Once the receptors are occupied by CHIPS, the intracellular cascade of events that leads to the migration of neutrophils from blood to the infection site is avoided (Foster, 2005; Postma et al., 2004). Eap interferes with the adhesion between leukocytes and endothelial cells of the blood vessels, a step required for the extravasation of neutrophils to the underlying tissue. The protein binds to the intercellular adhesion molecule-1 (ICAM-1) located on the surface of endothelial cells impairing its union with the lymphocyte function-associated antigen (LFA-1) on the surface of leukocytes, which in normal function allows the migration of leukocytes to the infection site (Foster, 2005). The capsular polysaccharide (CP) protects bacteria from being killed by neutrophils and both, CP5 and CP8, have been shown to cause resistance to phagocytosis (Kampen et al., 2005). Another *S. aureus* protein involved in immune evasion is the protein A (SpA), a cell wall associated protein coded by the *spa* gene, that binds to the Fc region of host immunoglobulin G (IgG) and to the Fab region of type B cells, which is known to promote immune evasion by preventing the union between the Fc region and its receptor located on the surface of phagocytic cells, thus avoiding the phagocytosis of antibody coated bacteria (Falugi et al., 2013). It was reported that SpA specifically restricts the IgG hexamer formation needed for an efficient complement activation, thus facilitating the *S. aureus* immune evasion (Cruz et al., 2021). The nuclease (Nuc) enzyme is an example of a *S. aureus* secreted enzyme able to degrade the neutrophil extracellular traps (NETs) formed to ensnare pathogens for further clearance. This secreted nuclease was reported to participate in immune evasion since a *nuc*-deficient strain showed significantly more susceptibility to be cleared by activated neutrophils compared with the wild-type strain in a murine model (Berends et al., 2010). *S. aureus* has also developed strategies to evade

its killing, either in an oxygen-dependent or independent way, by secreting a wide range of enzymes like staphylokinases, superoxide dismutases SadA and SadM, catalases like KatA and alkyl hydroperoxide reductase (AhpC), the staphylococcal peroxidase inhibitor (SPIN), aureolysins, and O-acethyltransferase A (OatA), amongst other enzymes (de Jong et al., 2019).

According to de Jong and colleagues, there are currently nearly 40 different *S. aureus* molecules described to be involved in the evasion of the pathogen to the host immune system, number that potentially might increase since there are still another 200 secreted proteins from *S. aureus* whose function has not been yet identified (de Jong et al., 2019). Immune evasion molecules of *S. aureus* are not the only defence mechanism this pathogen uses to survive within its host, it also produces a wide range of toxins that increase its pathogenicity and protection from host immunity.

1.3 *S. aureus* toxins

Amongst the machinery of virulence factors found in *S. aureus*, the production of a wide range of toxins enhances its pathogenicity, since they affect the host cell by forming pores in the cell membrane, loosening cell junctions, and causing an excessive stimulation of the host immune system (Grumann et al., 2014). According to Oliveira and colleagues, the *S. aureus* toxins can be divided into three groups: 1) pore forming toxins (PFTs), 2) exfoliative toxins (ETs), and 3) superantigens (SAgs) (D. Oliveira et al., 2018).

1.3.1 Pore forming toxins

The pore forming toxins (PFTs) comprise four types of toxins: hemolysin-α (Hla), hemolysin-β (Hlb), leukotoxins, and phenol soluble modulins (PSMs) (Grumann et al., 2014). The first type, Hla, is secreted as a water soluble molecule and able to form pores in the host membrane upon binding to its plasma membrane receptors (i.e. transmembrane protein ADAM10 or α5β1 integrin) with concomitant changes in its

conformation forming a heptamer, which is a pre-pore structure that finally forms a heptameric transmembrane pore in the host (Seilie & Wardenburg, 2017). It was reported that this toxin affects endothelial cells (Powers et al., 2012) and also epithelial cells (Möller et al., 2020) as well as immune cells like T cells, B cells, and monocytes (Nygaard et al., 2012).

Another PFT that is important for *S. aureus* pathogenicity is Hlb or sphingomyelinase C, which has shown to promote *S. aureus* colonisation on the skin in a murine ear colonisation model, with a 50-fold higher colonisation efficiency when compared with the non Hlb-producing strain (Katayama et al., 2013). It was also reported that Hlb is essential for the development of lung injury by *S. aureus* through an increase in neutrophils influx to the alveolar space and lung inflammation (Hayashida et al., 2009).

Leukotoxins are two-component toxins that lyse immune cells like leukocytes, neutrophils, monocytes, dendritic cells and red blood cells being reported four types of them: 1) the Panton-Valentine Leukocidin (PVL), 2) the LukAB,/LukGH, 3) LukED, and 4) γ-hemolysins (HlgA, HlgB, HlgC) (D. Oliveira et al., 2018). *S. aureus* strains can produce at least three leukocidins and clinical strains involved in human infections can produce up to five different leukocidins (Alonzo & Torres, 2014).

The *S. aureus* phenol soluble modulins (PSMs) are secreted small peptides classified according to their length into two types: α-PSM, the shorter type composed of nearly 20 amino acids and the longer type, the β-PSM, which is composed of nearly 40 amino acids (R. Wang et al., 2007). The PSMs are coded in three operons in the *S. aureus* genome: the *psm*α operon (coding the α-PSMs), the *psmβ* operon (coding the β-PSMs), and the *hld* operon (coding the δ-toxin), which is in the coding sequence of the staphylococci regulator RNA III (D. Oliveira et al., 2018). The PSMs have cytolytic activity, activate inflammatory response, and are produced by almost all *S. aureus* strains except by those showing a defective *agr* quorum-sensing system, since in *S. aureus* the PSMs production is controlled by the Agr regulator (Otto, 2014). It was also reported that

the production of PSMs was higher in community-associated methicillin-resistant *Staphylococcus aureus* (CA-MRSA) strains than in healthcare-associated methicillin-resistant *Staphylococcus aureus* (HA-MRSA) strains which may contribute to the increased virulence showed by those strains in bacteraemia and skin infections models (R. Wang et al., 2007).

1.3.2 Exfoliative toxins

The exfoliative toxins (ETs) are glutamate-specific serine proteases that cleavage desmogleins-1 (Dsg1), which are cadherin-like adhesion molecules that maintain the cell-to-cell adhesion in the mammal epidermis, thus resulting in the loosening of keratinocytes junctions with concomitant formation of blisters and skin desquamation (Kayan & Torres, 2019). The ETs include the ETA, ETB, ETC, ETD, (Kayan & Torres, 2019) and ETE (Imanishi et al., 2019) whose expression is regulated by the *agr*-quorum sensing system (Grumann et al., 2014). The ETs are responsible for the staphylococcal scalded skin syndrome (SSSS), previously known as dermatitis exfoliative, Lyell's disease and Ritter's disease, that affects neonates and children and also adults with compromised immune system or renal dysfunction (Ladhani, 2003).

1.3.3 Superantigens

Superantigens (SAgs) are toxins that have an immune system stimulatory effect, specifically on T cells and mononuclear macrophages, causing an excessive immune response leading to clinical signs like high fever, hypotension, and a progressive organ failure (Grumann et al., 2014; Krakauer et al., 2016). The molecular mechanism by which the SAgs activate T cells has been a matter of study and it was shown, after using x-ray crystallography, that they form a complex with the α-chain major histocompatibility complex class II receptors (MHC-II) expressed on the surface of the antigen presenting cells (APCs) and with the β-variable region of the T cell receptors (TCR) (Rödström et al., 2014). This ability of the SAgs to bind both, the TCR and MHC-II receptors, makes them a potent immunogen since they have the capacity to circumvent the conventional antigen presentation pathway by crosslinking the TCRs and MHC-II on the surface of the

APCs, thus stimulating T cells activation with the concomitant increase in cytokines production (Abdurrahman et al., 2020). There are 26 *S. aureus* SAgs described, including the toxic shock syndrome toxin (TSST-1), 11 staphylococcal enterotoxins, and 14 staphylococcal enterotoxin-like proteins (Abdurrahman et al., 2020) and nearly 80% of the *S. aureus* clinical strains carry an average of between five and six SAgs coding genes (Grumann et al., 2014).

1.4 *S. aureus* and its resistance to antimicrobials

In *S. aureus* the drugs used for its control target mainly protein synthesis, cell wall, DNA replication and transcription, and to a lesser extent the enzymes involved in metabolic processes.

The molecular targets of the antibiotics inhibiting the protein synthesis are the subunits 30S and 50S of the bacterial ribosome, as well as the elongation factor G and the isoleucyl-tRNA synthetase (IleRS), which catalyses the attachment of isoleucine to tRNA (Vestergaard et al., 2019). The antibiotics targeting the 30S subunit bind to the A site where the charged tRNA binds to the ribosome, being antibiotics belonging to the classes tetracyclines (tetracycline, doxycycline), aminoglycosides (gentamicin), and glycylcyclines (tigecycline) used against the 30S subunit of *S. aureus* (Foster, 2017; Vestergaard et al., 2019). Regarding the antibiotics that target the 50S subunit, where the drug binding sites are the peptidyltransferase center (PTC), which is the ribosome main functional centre, and the emerging peptide exit tunnel (Foster, 2017), there are several classes of antibiotics that target the 50S subunit that are used to treat *S. aureus* infections, including oxazolidinones (linezolid and tedizolid), macrolides (erythromycin), streptogramins (quinupristin and dalfopristin), lycosamides (clindamycin), chloramphenicols (chloramphenicol), and pleuromutilins (retapamulin) (Vestergaard et al., 2019). Although there is a wide range of antibiotics used to target *S. aureus* protein synthesis, this pathogen can develop resistance against the most clinically relevant

drugs. For example, the resistance of *S. aureus* against tetracyclines is associated with the presence of the resistance determinants *tetA(K)* and *tetA(L)*, involved in the active efflux of the drug (Jensen & Lyon, 2009), and *tet(M)* or *tet(O)*, involved in the removal of the antibiotic from the ribosome (Lu et al., 2013). It has been reported the resistance of *S. aureus* against gentamicin through the activity of aminoglycoside-modifying enzymes like phosphor-transferases, acetyl-transferases, and nucleotidyl-transferases (Mccallum et al., 2010). Similar situation happened with two of the most relevant drugs to treat MRSA infections that inhibit the protein synthesis by targeting the 50S ribosomal subunit: linezolid and synercid (Foster, 2017). In the case of linezolid its resistance is mediated by the acquisition of the chloramphenicol-florfenicol resistance (*cfr)* gene, which codes a methyltransferase that catalyses the methylation of the 23S ribosomal RNA at the position A2503 conferring resistance to the antibiotic (Morales et al., 2010). In the case of synercid (quinupristin/dalfopristin) that occasionally is used for the treatment of MRSA infections, a study reported the emergence of resistance amongst clinical strains with a prevalence of resistance of 0.4% in MRSA isolates (F. Yu et al., 2014).

The earliest antibiotic targeting the cell envelope in *S. aureus* was penicillin, which was commercialized in the early 1940 and targets the penicillin-binding protein 2 (PBP2) that has transglycosylase and transpeptidase activity (Foster, 2017). The antibiotic binds to the serine residues in the active site of the enzyme blocking the peptidoglycan synthesis (Walsh & Wencewicz, 2016). Resistant strains to this antibiotic were identified as early as two years after its introduction into clinical settings when 29 strains of *S. aureus* developed resistance to it after a prolonged period of exposure (Rammelkamp & Maxon, 1942). The resistance of *S. aureus* to penicillin is due to the presence of the *blaZ* gene, which codes a β-lactamase that hydrolyses the β-lactam ring of the antibiotic leading to its inactivation (Lowy, 2003). To overcome this resistance problem, the new semisynthetic antibiotic, methicillin, was introduced in 1961 but the pathogen developed resistance against it through the acquisition of the genetic determinant *mecA* that codes

a homolog enzyme to the PBP2, the PBP2a, which has a low-affinity for β-lactams antibiotics (Foster, 2017), thus arising the methicillin-resistant *S. aureus* (MRSA) strains.

Different classes of antibiotics targeting the cell envelope have been used against *S. aureus* infections like the fifth-generation cephalosporins (ceftaroline), carbapenems (imipenem), glycopeptides (vancomycin and teicoplanin), lipoglycopeptides (dalbavancin and telavancin), phosphonic acid (fosfomycin), and lipopeptide (daptomycin) (Vestergaard et al., 2019). The antibiotics vancomycin and daptomycin have been used as a key option to treat serious MRSA infections (Vestergaard et al., 2019). However, *S. aureus* has developed resistance against both of them. Vancomycin targets the cell wall synthesis by binding through hydrogen bonds to the D-alanyl-D-alanine pentapeptide moiety of the lipid II, preventing the cross-linking of the peptidoglycan (Zeng et al., 2016). A fully vancomycin resistant *S. aureus* strain (VRSA) was reported in 2002 (Howden et al., 2010) and the mechanism of resistance involved the replacement of the terminal D-alanine residue by either D-serine or D-lactate to which the antibiotic has reduced binding affinity (Zeng et al., 2016). In the case of daptomycin it targets the cell membrane causing its disruption and depolarisation, leading to cell death (Miller et al., 2016). It has been reported that an antimicrobial peptide present in human serum (LL-37) was able to induce daptomycin tolerance in *S. aureus* through two mechanisms: by increasing the amount of peptidoglycan in the cell wall and by increasing the amount of the phospholipid cardiolipin in the cell membrane (Ledger et al., 2022).

Amongst the classes of antibiotics that target nucleic acid biosynthesis in *S. aureus* we can find fluoroquinolones (ciprofloxacin, moxifloxacin) and rifamycins (rifampicin) that targets the DNA replication and transcription, respectively (Vestergaard et al., 2019). The molecular targets of fluroquinolones are the DNA gyrase and topoisomerase IV and the resistance against them is mediated by mutations leading to changes in the drug-binding site of the enzymes and by the overexpression of efflux pumps (Foster, 2017). It was reported that the resistance to ciprofloxacin was related to single or double point mutations identified in the genes *gyrA* (subunit A of the DNA gyrase) and *grlA* (subunit

A of the topoisomerase IV) that were identified in more than 50% of the analysed clinical strains (Tanaka et al., 2000). The resistance to fluoroquinolones mediated by the efflux pumps is associated with the overexpression of the pumps NorA, NorB or NorC responsible for the efflux of the drug (Foster, 2017). Rifampicin that targets the β subunit of RNA polymerase is used as an adjuvant agent against the bacteraemia or endocarditis caused by *S. aureus* and its resistance is mediated by mutations leading to changes in the drug binding site that reduces the affinity of the antibiotic for its target (Foster, 2017).

Finally, amongst the antibiotics that target enzymes involved in the metabolism of *S. aureus,* we can find trimethoprim (TMP)/sulfamethoxazole (SMX) that are recommended for the treatment of patients with skin and soft tissue infections caused by MRSA (Nathwani et al., 2008). These two antibiotics have a synergistic effect when used in combination and target both the dihydrofolate reductase (DHFR) and dihydropteroate synthase (DHPS) involved in the *de novo* synthesis of folic acid (Vestergaard et al., 2019). It was reported that in MRSA strains the resistance to TMP/SMX significantly increased in a 12-year period of time, from 2% to 13% (Khamash et al., 2019). The resistance is due to either, mutations in the genes coding the target enzymes or to the acquisition of variants of the gene *dfr* (*dfrA, dfrD, dfrK*) coding the DHFR, being the *dfrG* variant found globally distributed amongst the trimethoprim resistant strains (Nurjadi et al., 2015); both strategies resulting in a reduced affinity of the drugs for their targets.

Prontosil (sulfamido-chrysoidine) and bedaquiline are examples of drugs targeting bacterial metabolism. Prontosil is one of the few inhibitors of nutrient biosynthesis that targets the dihydropteroate synthase involved in the biosynthesis of folic acid and approved to be used in the clinic (Carfrae & Brown, 2023). Bedaquiline targets the bacterial adenosine triphosphate (ATP) synthase and has been used to treat mycobacterial infections (Murima et al., 2014). Thus, metabolic pathways hold promises as a resource of new antimicrobial drugs that should be considered when finding new targets.

1.5 New therapeutic strategies for the treatment of *S. aureus* infections

The period between 1940s and 1970s corresponds to the golden age of antibiotic discovery where nearly 40 new antimicrobial compounds were identified and introduced into the clinical practice (Altamirano & Barr, 2019). Since then, few new classes of antibiotics have been discovered resulting in the actual stagnancy in the discovery of new drugs, while a rapid increase in the rate of emergence of resistant strains has triggered research for new strategies to treat bacterial infections.

Amongst these strategies we can find the chemical modification of existing antimicrobials to improve its activity and overcome the resistance problem. As an example, Pavlović and colleagues developed a new class of macrolides after modifying ketolides (semisynthetic derivatives of erythromycin) by introducing a heteroaromatic side chain in the C-12 position of γ-lactone of an α-amino lactone derivative of clarithromycin, resulting in an enhanced *in vitro* antimicrobial activity against different pathogens including an inducible resistant *S. aureus* (Pavlović et al., 2014). One of the problems that can arise with this strategy where new molecules are synthesised after modifying the core structure of existing antibiotics, is that the appearance of resistance to the new antibiotic might be a matter of time. Another limitation could be the reduced chances to identify new compounds with new modes of action. When changing this conventional way of drug discovery other potential drug candidates might arise. In this context, Martin and colleagues identified the compound SCH-79797 after screening a 30,000 molecule library that showed bactericidal effect against Gram negative and Gram positive pathogens including *S. aureus* (Martin et al., 2020). They found that the compound had a dual mechanism of action that independently disrupted the membrane cell integrity and the folate biosynthesis (Martin et al., 2020), required for the synthesis of DNA and RNA, making it a good candidate to treat a broad spectrum of pathogens.

As an alternative to conventional antibiotic therapy, there is the phage-based therapy, which has also been used as a topical treatment against *S. aureus* infections (Vuong et

al., 2016). This therapy relies on the lytic cycle of a bacteriophage to destroy the target bacteria. Some advantages relative to the use of conventional antibiotics are its specificity, safety, reduced cost, its usage in patients with allergies to antibiotics, and that it is self-limited as the phage can exert its lytic activity only within the target bacteria (Altamirano & Barr, 2019). In 2014, it was reported that a phage cocktail was effective in the treatment of *S. aureus* bacterial sinusitis using a sheep model (Drilling et al., 2014). Another study showed that a cocktail of three bacteriophages from the Myoviridae family had a positive outcome in terms of safety and tolerability in the treatment of endocarditis and septic shock caused by *S. aureus*, although its effectiveness remains to be elucidated (Petrovic Fabijan et al., 2020). There is a phage cocktail in a phase II clinical trial (registration number NCT02664740) with 60 participants evaluating its effect on the topical treatment of diabetic foot ulcers in patients infected with *S. aureus*. There are also bacteriophage-coded proteins that are currently under clinical trials like: CF-301 (exebacase) and SAL200 (tonobacase) against *S. aureus* bloodstream infections and P128 (StaphTAME) against both, bacteraemia and nasal colonisation (Kesharwani et al., 2020).

Other alternative approach used to overcome the resistance problem is the antivirulence therapy, which focuses on the neutralisation of targeted virulence factors to treat an infection (Dickey et al., 2017). In the case of *S. aureus*, the following compounds have been developed as result of this approach that are under either, phase II or preclinical trials: MEDI4893 and AR-301 (targeting the α-toxin), ASN-100 (targeting α-toxin, PVL, LukED, LukGH and γ-hemolysin), 6e (targeting SrtA), and savarin (targeting the *agr*-quorum sensing system) (Dickey et al., 2017).

Antibody therapy has also been explored to target infections caused by high-priority pathogens. This strategy relies on the activation of the immune system (Kesharwani et al., 2020) and different monoclonal antibodies against different targets of *S. aureus* are in the clinical pipeline for its evaluation. Some examples of the antibody therapy are: 514G3 (targeting the cell wall SpaA protein), AR-301 (targeting the α-toxin), MEDI-4893

(targeting the α-toxin and ClfA), DSTA-4637S, which is an antibody-antibiotic conjugate that releases the conjugated antibiotic to the site of infection, and BT588 that is under the phase 2 clinical trial (WHO, 2020).

1.6 New targets for the treatment of *S. aureus* infections

The finding of new targets is another path researchers are following to develop new therapeutics to overcome the antimicrobial resistance crisis. In this context, the enzymes participating in the type II fatty acid synthetic (FASII) pathway of *S. aureus* have emerged as an important target to develop new drugs due to its role in the lipid synthesis needed for the bacterial cell wall biosynthesis. The enzymes participating in the elongation of the fatty acids are the Fab proteins FabG, FabZ, FabI and FabF and amongst the compounds used to target the enzymes involved in FASII pathway we can find triclosan derived compounds and Debio1452/afabicin, inhibiting FabI, and plantensimycin, inhibiting FabB (Foster, 2017). In an *in vitro* study it was reported that Debio1452 showed inhibitory effect against all *S. aureus* isolates tested (471 strains) and that it was even more active than daptomycin (64-fold) or vancomycin (128-fold) (Flamm et al., 2015). There were some concerns about the effectiveness of inhibiting FASII enzymes as a treatment since it was argued that bacteria might use exogenous fatty acids instead of *de novo* synthesis to produce phosphatidylglycerol (Brinster et al., 2009). However, those concerns were circumvented by Frank and colleagues who evaluated the effect of the inactivation of the FA kinase system on its virulence, which is the only system used by *S. aureus* to incorporate exogenous FAs, and finding no effect after shutting off the FA kinase system, thus demonstrating that FASII pathway is an effective drug target (Frank et al., 2020). The effectiveness of Debio1452/afabicin as a treatment for *S. aureus* infections including those caused by MRSA, has been demonstrated by Menetrey and colleagues after successfully completing a human phase II clinical trial in patients that

underwent surgery for hip replacement, showing good tolerance and penetration of the drug in the infection site (Menetrey et al., 2019).

Another potential target under study in the drug discovery research against *S. aureus* is the FtsZ enzyme responsible for the cell division that forms the Z ring in the mid-cell, recruits other proteins and finally leads to the division of the cell (Haydon et al., 2008). After the screening of more than 500 compounds derived from 3-methoxybenzamide, the compound PC190723, which targets the FtsZ protein, showed an inhibitory effect of cell division and had a potent and selective activity against *S. aureus* including MRSA and multidrug-resistant *Staphylococcus aureus* (MDRSA) strains (Haydon et al., 2008). It was also reported that this compound showed an effective activity when combined with β-lactams antibiotics using a murine infection model (Tan et al., 2012). However, the poor pharmacokinetics properties of this compound have triggered the improvement of its properties leading to the development of PC190723 derivatives with enhanced pharmaceutical properties like the compounds TXA709 and TXY541 (Kaul et al., 2015).

The biosynthesis of teichoic acids in *S. aureus* has also been explored as a potential target for the design of new antibiotics to treat staphylococcal infections due to its role in the cell viability, cell division, immune evasion, pathogenesis and resistance to β-lactam antibiotics (Pasquina et al., 2013). The teichoic acids (TAs) that are important for the physiology of the cell are the wall teichoic acids (WTAs) and lipoteichoic acids (LTAs), both having structural similarities but synthetised through different pathways (Pasquina et al., 2013). In this line, new compounds that target the TAs biosynthetic pathways have been discovered like the compound 1835F03 that targets the TarGH transporter that flips WTAs from the cytoplasm to the cell surface, thus specifically inhibiting WTA synthesis and producing a growth inhibition of *S. aureus* strains including MRSA (Swoboda et al., 2009). Although the compound showed good antibiotic activity against the strains tested, it was further optimised in order to improve its potency, obtaining an analogue to 1835F03 named targocil with 10-fold less mutational frequency and 10-fold more potency than the original compound (Lee et al., 2010). The early stages of the WTA biosynthesis

have also been targeted and compounds inhibiting the TarO enzyme, involved in the first step of the WTA synthesis, like tunicamycin or ticlopidine, have shown an effective inhibition of the enzyme with a concomitant resensitization of MRSA strains to β-lactams antibiotics (Campbell et al., 2011; Farha et al., 2013).

The synthesis of peptidoglycan (PG) remains an attractive target to develop new antibacterial drugs, focusing specifically on the enzymes involved in its synthesis. Bacterial PG intermediates are synthesised in the cytoplasm in a multistep process, from the uridine diphosphate N-acetylglucosamine (UDP-GlcNAc) to the final intermediate linked to the cytoplasmic side of the membrane, the lipid II (undecaprenyl-diphosphate-MurNAc-pentapeptideGlcNAc), by the Mur (MurA, MurB, MurC, MurD, MurE, MurF and MurI), MraY, and MurG enzymes (Bugg et al., 2011). The lipid II is further translocated to the outer side of the membrane by lipid II flippases MurJ or Amj (Meeske et al., 2015) and the lipid-linked oligosaccharide (GlcNAc-MurNAc-pentapeptide) it carries is incorporated into the growing chain of PG. High-throughput screens for potential inhibitors against the enzymes participating in PG synthesis have led to either the identification or design of PG synthesis inhibitors like: 2-aminotetralones or avenaciolide derivatives isolated from the fungus *Neosartorya fischethat* that inhibit the MurA (Chang et al., 2015; Dunsmore et al., 2008); 5- substituted tetrazol-2-yl acetamido inhibitors targeting the MurB (Hrast et al., 2018); feglymycin inhibiting MurC (Rausch et al., 2011); phenoxyacetohydrazide derivatives against MurD (Jupudi et al., 2021); 2-thioxothiazolidin-4-one based inhibitor targeting MurE (Azam et al., 2019); 4-methoxy-1-methyl-2-oxopyridine-3-carbamide targeting MurF (Swarupa et al., 2017); murgocil targeting MurG (Mann et al., 2013); rutin as a potential inhibitor of MraY (Rani et al., 2018); and humimycin 17S targeting MurJ as a potentiator of β-lactams antibiotics against *S. aureus* (Chu et al., 2018).

In the context of PG synthesis as target for new antibiotics, the lipid II is an important target for antibiotic development. Teixobactin, a compound that binds to the pyrophosphate-sugar motif of lipid II, was discovered in 2015 after screening extracts

from 10,000 isolates for antibacterial activity against *S. aureus* (Ling et al., 2015). This compound, obtained from the Gram negative bacterium, *Eleftheria terrae*, showed antibacterial effects against different Gram positive pathogens including MRSA strains, showing a better performance than vancomycin, and a failure to obtain resistant strains after 27 days serial passages with sub-MIC of the compound (Ling et al., 2015). Shortly after its discovery, it was reported that the bactericidal effect of teixobactin was due to its ability to inhibit simultaneously both, PG and TAs biosynthesis (Homma et al., 2016). Currently, there are several compounds targeting the lipid II structure under different developmental stages such as phase III or preclinical trials (Malin & De Leeuw, 2019).

Investigations looking for potential new drug targets in *S. aureus* had benefited from the creation of the Nebraska Transposon Mutant Library (NTML) (Fey et al., 2013). This library was created in the genetic background of the community-associated methicillin-resistant *S. aureus* (CA-MRSA) lineage USA300, strain LAC. This strain contained two plasmids that were cured obtaining the strain JE2 (wild-type) that was used to perform the mutagenesis through the insertion of the *bursa aurealis* transposon. The library contains 1,920 mutant strains, each of them with a transposon inserted within the coding sequence of non-essential genes and it is arranged into five 384-well plates (Fey et al., 2013). This library has been used in the genome-wide screen to identify genes involved in *S. aureus* cell death and pathogenesis, highlighting possible new drug targets (Yang et al., 2019; Yee et al., 2019).

1.7 Aim of the study

Methicillin-resistant *Staphylococcus aureus* (MRSA) remains a high priority pathogen according to the WHO since it has developed resistance to almost all ß-lactams (oxacillin, flucoxacillin, nafcillin) and cephalosporins used for its treatment, making it imperative to find new therapeutic targets. A number of studies have focused on the identification, on a genome scale, of *S. aureus* essential genes for growth under specific conditions, or for survival using different infection models to find new targets for the development of new antistaphylococcal drugs (Benton et al.,2004; Chaudhuri et al., 2009; Valentino et al., 2014). These investigations have led to the identification of essential genes required for *S. aureus* survival and growth identifying genes involved in protein and cell envelope biosynthesis, respiratory pathways, purine and pyrimidine biosynthesis, carbon metabolism, and amino acid metabolism as potential new targets. In this context, enzymes participating in the metabolism and specifically in the transamination process, which is key for the amino acid metabolism, might represent new targets for drug discovery. The aim of this project was to study three putative aminotransferases coded in the genome of *S. aureus* as potential new drug targets.

CHAPTER 2

Materials and Methods

2. Material and Methods

This chapter contains a general description of the materials and methods used in this work and the specific methods used for each of the following chapters are described at the beginning of the corresponding result chapter.

2.1 Media

The media used in this thesis was prepared with distilled water (dH_2O) and sterilized by autoclaving at 121°C at 15 pounds per square inch (psi) of pressure. The media used are listed in Table 2.1.

Table 2.1 Media used in this study

Medium/ Brand	Description
Tryptic Soy Broth/Sigma 30 g l^{-1}	For TSA agar plates preparation, it was mixed with bacteriological agar at 1.5 % (w/v) using agar No.1 (Oxoid).
Luria Bertani Broth/Sigma 20 g l^{-1}	For agar plates it was mixed with bacteriological agar at 1.5 % (w/v) using agar No.1 (Oxoid).
Brain Hearth Infusion/Oxoid 37 g l^{-1}	For broth preparation it was dissolved in the corresponding volume of dH_2O.
Mannitol Salt Agar/Oxoid 111 g l^{-1}	For agar plates it was dissolved in the corresponding volume of dH_2O.
Human Serum/Sigma (cat. n° H4522)	From human male AB plasma, USA origin.
RPMI-1640/Sigma (cat. n° R-8758)	Containing sodium bicarbonate and L-glutamine. Stored at 4°C before use.
RPMI-1640/Sigma (cat. n° R-0883)	With sodium bicarbonate, without L-glutamine. Stored at 4°C before use.

2.2 Antibiotics

The antibiotics and corresponding concentrations used in this study are listed in Table 2.2.

Table 2.2. Antibiotics used in this study

Antibiotic	Stock concentration (mg/mL)	Solvent	*S. aureus* working concentration (µg/mL)	*E. coli* working concentration (µg/mL)
Ampicillin	100	dH_2O	-	100
Chloramphenicol	10	100 % ethanol (v/v)	10	-
Erythromycin	5	100 % ethanol (v/v)	5	-

2.3 Bacterial strains and glycerol stocks

The *S. aureus* strains used in this study were obtained from the Nebraska Transposon Mutant Library (NTML) developed by the Nebraska Centre for Staphylococcal Research (CSR). The library was replicated using a pin replicator into five 384-well plates. The replicated library was maintained in TSB supplemented with 5 µg/mL erythromycin and 15% glycerol and kept at –70°C.

Bacterial stocks were prepared in TSB containing 15% glycerol (wild-type JE2 strain) and TSB containing 15% glycerol and 5 µg/mL erythromycin (mutant strains) and kept at –70°C. The JE2 strain was streaked out onto TSA plates while the mutant strains were streaked out onto TSA plates containing 5 µg/mL erythromycin and incubated at 37°C for 24 h.

The LS-1 *S. aureus* strains were provided by Dr. Sean Nair from the Department of Microbial Diseases, Eastman Dental Institute, UCL. The strains were streaked out onto LB plates with or without supplementation of 100 µg/mL ampicillin and incubated at 37°C for 24 h.

The *E. coli* strain carrying the plasmid pEAHISMRSA2028 was streaked out onto BHI plates supplemented with 100 µg/mL of ampicillin and incubated at 37°C for 24 h. All the strains used in this study are listed in Table 2.3.

Table 2.3. Bacterial strains and plasmids used in this study

Bacterial strain or plasmid	Relevant characteristics	Reference
S. aureus JE2	USA 300 LAC strain, methicillin resistant, and cured for the native plasmids.	(Fey et al., 2013)
S. aureus SAUSA300_1916	USA300 strain with a *Bursa aurealis* transposon insertion within the *aspB* gene coding a putative aspartate aminotransferase.	(Fey et al., 2013)
S. aureus SAUSA300_1614	USA300 strain with a *Bursa aurealis* transposon insertion within the *hemL1* gene coding a putative glutamate-1-semialdehyde aminotransferase.	(Fey et al., 2013)
S. aureus SAUSA300_1845	USA300 strain with a *Bursa aurealis* transposon insertion within the *hemL2* gene coding a putative glutamate-1-semialdehyde aminotransferase.	(Fey et al., 2013)
S. aureus SAUSA300_0605	USA300 strain with a *Bursa aurealis* transposon insertion within the *sarA* gene.	(Fey et al., 2013)
S. aureus LS-1	Strain isolated from a spontaneous septic arthritis in mice used to create a markerless gene deletion of the *hemL1* and *hemL2* genes.	(Bremell et al., 1990)
S. aureus LS-1 Δ *hemL1*	*S. aureus* LS-1 strain with a markerless gene deletion of *hemL1* predicted to code a putative glutamate-1-semialdehyde aminotransferase.	Nair Laboratory (Unpublished data)
S. aureus LS-1 Δ *hemL2*	*S. aureus* LS-1 strain with a markerless gene deletion of *hemL2* predicted to code a putative glutamate-1-semialdehyde aminotransferase.	Nair Laboratory (Unpublished data)

pEAHISMRSA2028	Plasmid containing Asp/Tyr/Phe pyridoxal-5'-phosphate-dependent aminotransferase from MRSA under the control of promoter T7.	Addgene, plasmid #97001
E. coli DH5alpha	Plasmid cloning host.	

2.4 Bacterial growth: spectrophotometric measurements and CFU quantification

2.4.1 Spectrophotometric measurements

The bacterial growth performed in broth was spectrophotometrically measured at 600 nm (OD_{600}) to quantify the bacterial yield. The samples were diluted 1:10 using fresh medium to allow measurements by using a SPECTROstar Nano absorbance plate reader.

2.4.2 CFU quantification

The direct cells count was performed after preparing 1:10 serial dilutions of the samples and plating 100 µL from each dilution onto agar plates. The agar plates were incubated at 37°C for 24 h and the colonies were quantified to determine the CFU/mL.

2.5 Centrifugation

The centrifuges used in this work are listed in the Table 2.4.

Table 2.4. Centrifuges used in this study

Brand - Model	Characteristics
Eppendorf microcentrifuge – 5415 D	With rotor F 45-24-11 for up to 2 mL centrifuge tubes. Maximum speed of 13,200 rpm or 16,110 × g.
Eppendorf centrifuge – 5804 R	With rotor A-4-44 with adapters for 15- or 50-mL conical tubes. Maximum speed of 5,100 rpm or 5,525 x *g*.

Sorvall centrifuge – RC5B Plus	Rotor used SLA 1500. Maximum speed of 14,500 rpm or 34,155 x *g*.

2.6 Enzymes

The enzymes used in this work are listed in the Table 2.5.

Table 2.5. Enzymes used in this study

Enzyme	Company/catalogue number	Characteristics
TEV protease	GenScript / Z03030	A site-specific cysteine protease found in the tags from fusion proteins. It recognizes the sequence Glu-Asn-Leu-Tyr-Phe-Gln-(Gly/Ser) [ENLYFQ(G/S)] and cleaves between Gln and Gly/Ser residues. Stored at -20°C
GOT	Sigma / G2751	Glutamic-oxalacetic transaminase type I isolated from the porcine heart. 200-500 units/mg protein. Stored at 4°C.
MDH	Sigma / M1567	Malic dehydrogenase isolated from the porcine heart. ≥600 units/mg protein. Stored at 4°C.
GDH	Sigma / G2626	Glutamate dehydrogenase type II isolated from the bovine liver. ≥35 units/mg protein. Stored at 4°C.
Taq polymerase	Bioline / BIO-25043	MyTaq™ Red Mix is a master mix containing the Taq DNA polymerase, a buffer system, and the red dye that has increased affinity for DNA. Stored at -20°C.
Proteinase K	Sigma / P4850	Proteinase K from *Tritirachium album* used for the proteolytic inactivation of nucleases during the isolation of DNA and RNA. Stored at -20°C.
RNase	Qiagen / 79254	RNase A catalyses the transphosphorylation and degradation of RNA. Stored at -20°C.

2.7 Amino acids and keto acids

The enzyme assays were performed using the following amino acids and keto acids listed in Table 2.6.

Table 2.6. Amino acids and keto acids used in this study

Amino acid or keto acid	Stock solution	Solvent	Storage conditions
L- aspartic acid	100 mM	0.1 M HCl	Freshly prepared
L- glutamic acid	100 mM	0.1 M HCl	Freshly prepared
L- glutamine	30 g/L	dH_2O	-20°C
Oxaloacetic acid	100 mM	dH_2O	-20°C
α-ketoglutarate	100 mM	dH_2O	-20°C

2.8 Buffers

The buffers used in this work were the following:

2.8.1 Elution buffer

PBS containing 500 mM imidazole, pH 8.0.

2.8.2 QIAGEN buffer AL (Lysis buffer)

Buffer used for cell lysis during DNA isolation supplied with the QIA quick kit. The details of its content were not specified by the manufacturer.

2.8.3 Lysis buffer for protein extraction

The buffer was prepared with 30 mL or 50 mL of B-PER complete bacterial protein extraction reagent (cat. n° 89822, Thermo Scientific), one tablet of protease inhibitor (cat. n° 04693159001, Roche), and either 20 µM of PMP or 30 µM of PLP.

2.8.4 Mobile phase buffer

The mobile phase buffer was prepared with potassium biphosphate at 13 mM and potassium dibasic at 1mM adjusted to pH 6.0 and mixed with methanol (97:3 v/v) after filtration using 0.22 µm filters.

2.8.5 Mops buffer

Mops, 1 M

pH 5.5

2.8.6 PBS

A tablet of PBS was dissolved in 200 mL of dH_2O and sterilized by autoclaving it at 121°C for 15 min at 15 psi. Once reconstituted, the solution components and concentrations were as follows:

NaCl, 137 mM

KCl, 2.7 mM

Phosphate buffer solution, 10 mM

pH 7.4

2.8.7 Potassium phosphate buffer

The buffer was prepared at a concentration of 2 M using dH_2O. The components and amount used for a volume of 100 mL are listed in Table 2.7.

Table 2.7. Potassium phosphate buffer components

Reagent	Company/cat. n°	Molecular weight (g/mol)	Amount weighted (g)
K_2HPO_4	Sigma/ 04248	174.18	34.8
KH_2PO_4	Sigma/ P0662	136.086	27.2

The preparation of 100 mL of 2M potassium phosphate buffer pH 8 was performed by mixing 94 mL of 2M K_2HPO_4 and 6 mL of 2M KH_2PO_4.

2.8.8 Protein loading buffer blue (2X)

Buffer solution from National Diagnostics (cat. n° EC-866) containing:

Tris-HCl, 0.5 M

SDS, 4.4% (w/v)

Glycerol, 20% (v/v)

2-mercaptoethanol 2% (v/v)

Bromophenol blue in dH_2O

2.8.9 TAE (1X working solution)

Tris acetate, 0.04 M

EDTA, 0.01 M

pH 8.0

2.8.10 Tricine buffer

Tricine, 0.1 M

pH 7.9

2.8.11 Tris-EDTA (1X working solution)

Tris, 10 mM

EDTA, 1 mM

pH 8.0

2.8.12 Reaction buffer

Phosphate buffer prepared at a concentration of 150 mM in dH_2O, pH 8.0.

2.8.13 Washing buffers

PBS containing 20 mM imidazole, pH 8.0

PBS containing 50 mM imidazole, pH 8.0

2.9 Stock solutions of reagents

The reagents used in this study are listed in the Table 2.8.

Table 2.8. Reagents used in this study

Reagent	Stock concentration	Working concentration	Solvent	Storage conditions
Acetic acid	30 % (v/v)	-	dH_2O	Room temperature
Adapalene	100 mM	0 – 100 µM	DMSO	-20°C
Alpha-ketobutyrate	100 µM	-	Reaction buffer	-20°C
Amino-oxyacetate	1 M	0 – 100 µM	dH_2O	-20°C
Crystal violet	1 % (w/v)	0.1 % (v/v)	dH_2O	Room temperature
D(+)- Glucose	20 % (w/v)	1% (w/v)	dH_2O	Room temperature
Gamma-acetylenic GABA	40 mM	0 – 10 mM	dH_2O	-20°C
Hesperetin	50 mM	0 – 0.12 mM	DMSO	-20°C
L-serine *O*-sulfate	100 mM	0 – 1 mM	dH_2O	-20°C
Lysostaphin	20 mg/mL	0.25 mg/mL	Molecular grade H_2O	-20°C

NADPH	12 mM	0.12 mM	0.1 M NaOH	-80°C
NaOH	3 M	-	dH_2O	Freshly prepared
NH_4Cl	31 mM	3.1 mM	dH_2O	Room temperature
PF-04859989	10 mM	0 – 100 µM	DMSO	-20°C
Phenylhydrazine	50 µM	-	Reaction buffer	Room temperature
PLP	0.5 mM	50 µM	dH_2O	-20°C
PMP	50 mM	20 – 50 µM	1 M HCl	-20°C
Trichloroacetic acid	50 % (w/v)	-	dH_2O	Room temperature
Vigabatrin	100 mM	0 – 100 µM	dH_2O	-20°C

2.9.1 Ehrlich's reagent

The reagent was prepared by dissolving 1 g of 4-(dimethylamino) benzaldehyde (cat. n°39070, Sigma) in 30 mL of glacial acetic acid following the addition of 8 mL of 70% perchloric acid and the volume was filled up to 50 mL with glacial acetic acid.

2.10 DNA manipulation

The procedures for DNA extraction, PCR amplification and agarose gel electrophoresis are described in the material and methods section of Chapter 3 Phenotypic characterisation of the strains having disrupted the genes *SAUSA300_1916*, *SAUSA300_1614* and *SAUSA300_1845* and evaluation of a planarian infection model to study survival and colonisation of *Staphylococcus aureus.*

2.11 Protein analysis

The protocols for the protein expression, purification, SDS-PAGE and Coomassie staining are described within the material and methods section of the chapters in which work has been done with proteins.

2.12 Statistical analysis

The data were presented as the mean ± standard deviation of the results. ANOVA one-way and mean comparison (Bonferroni/Tukey) tests were used to analyse the growth curve metrics, biofilm, and inhibitory activity of potential inhibitors against the enzymes. A normality test (Shapiro-Wilk) was used to determine if the data was normally distributed prior to perform the ANOVA test. Significance was as follows: *$P < 0.05$, **$P < 0.01$, ***$P < 0.001$, ****$P < 0.0001$.

The survival curves were analysed using the Kaplan-Meier estimator and compared using the log-rank equality test to determine significant differences in virulence between the strains in *Galleria mellonella* infection assays while the Mann-Whitney test was used to determine significant differences in survival/colonisation between the strains in planarians infection assays.

CHAPTER 3

Phenotypic characterisation of the strains having disrupted the genes *SAUSA300_1916*, *SAUSA300_1614* and *SAUSA300_1845* and evaluation of a planarian infection model to study survival and colonisation of *Staphylococcus aureus*

3. Phenotypic characterisation of the strains having disrupted the genes *SAUSA300_1916*, *SAUSA300_1614* and *SAUSA300_1845* and evaluation of a planarian infection model to study survival and colonisation of *Staphylococcus aureus*

3.1 Introduction

3.1.1 Overview of the role that the putative gene products of *SAUSA300_1916*, *SAUSA300_1614* and *SAUSA300_1845* have in the *S. aureus* metabolism

3.1.1.1 SAUSA300_1916 is predicted to code an aspartate aminotransferase

The biosynthetic precursors a bacterial cell requires for growth derives mainly from three metabolic pathways of the central metabolism: glycolysis, tricarboxylic acid (TCA) cycle, and pentose phosphate pathway (Somerville & Proctor, 2009).

The metabolism of *S. aureus* has a complete metabolic pathway for each of the three central metabolic routes but lacks a β-oxidation system and the glyoxylate shunt (GS) pathway, which is essential for fatty acid metabolism in bacteria (Halsey et al., 2017). Due to the impaired ability of *S. aureus* to metabolise lipids (phospholipids or triglycerides), its preferred carbon sources are carbohydrates that are metabolised through glycolysis and the pentose phosphate pathways.

Amongst the 13 biosynthetic intermediates that a bacterium needs to generate its macromolecules, 7 of them are derived from the glycolytic pathway: glucose-6-phosphate, fructose-6-phosphate, dihydroxyacetone phosphate, glyceraldehyde-3-phosphate, phosphoenolpyruvate, pyruvate, and acetyl-Coenzyme A (Richardson et al., 2015). In *S. aureus* the glucose (in its activated form of glucose-6-phosphate) is catabolized mainly through glycolysis by five enzymes coded by the genes *gap* (glyceraldehyde-3-phosphate dehydrogenase), *pgk* (phosphoglycerate kinase), *tpi*

(triosephosphate isomerase), *pgm* (phosphoglyceromutase), and *eno* (enolase) (Seidl et al., 2009). The products of the glycolysis are two molecules of pyruvate, two molecules of reduced NADH, and two molecules of ATP and the fate of pyruvate depends upon O_2 availability. *S. aureus* can grow under both, anaerobic and aerobic conditions, being the fate of pyruvate either, its fermentation with the excretion of lactate, acetate, formate, and ethanol or its decarboxylation with the production of acetyl coenzyme A (acetyl-CoA) and CO_2, respectively (Sadykov et al., 2013). The fate of acetyl-CoA depends on the growth conditions being shown that under excess of glucose and O_2, the phosphotransacetylase-acetate kinase (Pta-AckA) pathway, which hydrolyses acetyl-CoA to acetate, plays a key role in *S. aureus* to maintain the energy production during carbon overflow conditions (Sadykov et al., 2013).

The pentose phosphate pathway (PPP) provides three of the essential biosynthetic intermediates: D-ribose 5-phosphate, D-sedoheptulose 7-phosphate, and D-erythrose 4-phosphate (Potter et al., 2020). This pathway provides precursors for nucleotide and aromatic amino acids biosynthesis as wells as reducing molecules (NADPH) that helps bacteria to tolerate oxidative stress. In *Staphylococcus epidermidis* it has been shown that environmental conditions like iron deficiency, leads to an increase in the intracellular concentration of ribose, suggesting that the carbon flow occurs through the PPP activity (Sadykov et al., 2010). In *S. aureus*, three PPP-responsive regulators homologues to the RpiR repressor of the ribose 5-phosphate isomerase B (*rpiB*) found in *E. coli*, have been identified: RpiRA, RpiRB, and RpiRC (Zhu et al., 2011). The study found that both, RpiRB and RpiRC, had a regulatory effect in the PPP since the deletion of the genes coding for both regulators were linked to a decreased expression of two genes involved in the PPP, *rpiA* and *zwf,* coding for the enzymes ribose-5-phosphate isomerase A and glucose 6-phosphate dehydrogenase, respectively (Zhu et al., 2011). In the same study, a link between RpiRC and RNAIII expression was found in a strain that having inactivated the *rpiRC* gene showed a derepression in the transcription of RNAIII, a key regulator of the expression of *S. aureus* genes coding for different virulence factors.

In an effort to understand the role of PPP in *S. aureus* metabolism and persistence, a study showed that the inactivation of the transketolase (TKT), enzyme that participates in two main reactions of the nonoxidative branch of the PPP, caused a deregulation of the PPP leading to a change in the whole cell metabolomic profile with evident modifications in the TCA cycle activity (increased) and metabolism of aromatic amino acids (decreased) (X. Tan et al., 2019). The study also showed that in the Δ*tkt* mutant strain, the expression of the regulators RpiC and SigB was significantly down regulated while the expression of the RNAIII regulator was dramatically up regulated when compared with the wild-type strain, highlighting a new relationship between the PPP and the three regulators.

The TCA cycle provides the three remaining biosynthetic intermediates of the cell: oxaloacetate, α-ketoglutarate, and succinate or succinyl-CoA that are needed for the synthesis of amino acids and porphyrins (Richardson et al., 2015). It has been demonstrated in *S. aureus* that under nutrient-rich growth conditions the TCA cycle activity is repressed via the catabolite control protein A (CcpA), which is a global regulator in *S. aureus* that responds to changes in the intracellular concentration of carbohydrates. During the exponential growth phase and in absence of glucose, the genes coding TCA cycle enzymes: *citB* (aconitate hydratase), *citC* (isocitrate dehydrogenase), *citZ* (citrate synthase), *sdhB* (succinate dehydrogenase), and *sucCD* (succinyl-CoA synthetase) were down regulated in a CcpA dependent manner in *S. aureus* (Seidl et al., 2009). Upon glucose depletion from the media, the TCA cycle is activated in *S. aureus* by the catabolite control protein E (CcpE), which is a transcriptional regulator that modulates the TCA cycle activity mainly through the transcription of the gene encoding for aconitase, the first enzyme involved in the TCA cycle (Hartmann et al., 2013).

Under aerobic growth the oxidation of the dinucleotides produced during the metabolic reactions occurs mainly through the electron transport chain (ETC). The electrons are transferred to menaquinone and from menaquinone to oxidized cytochrome c to finally

been transferred to oxygen by the cytochrome c oxidase (Somerville & Proctor, 2009). During the process, a proton motive force (PMF) is generated and is used to produce ATP through the F_1F_0 ATPase complex. It has been demonstrated that under anaerobic conditions, the ATP synthase of *S. aureus* is used to extrude protons through the hydrolysis of ATP to maintain the PMF (Grosser et al., 2018). In *S. aureus*, a deficient ETC is associated with a small colony variant (SCV) phenotype that is linked to a reduced growth and an increased resistance to antibiotics (Kriegeskorte et al., 2014) as well as with an increased resistance to the host immune defences (Painter et al., 2017).

S. aureus can adapt its metabolism to prioritize the utilisation of primary carbon sources over secondary ones, and under nutrient conditions with limited glucose, the pathogen can catabolize different amino acids to generate central metabolism intermediates. Amongst 11 amino acids that are predicted to be catabolised by *S. aureus,* as it has the metabolic pathways coded in its genome, it has been shown that *S. aureus* catabolised 10 amino acids when growing in chemically defined medium lacking glucose (Halsey et al., 2017). The study carried out by Halsey and colleagues showed that together with others, the amino acids alanine and aspartate that fuels the synthesis of pyruvate and oxaloacetate, respectively were important for the growth of *S. aureus* in chemically defined medium. The key role of the putative aspartate aminotransferase in the central carbon metabolism relies on the linkage between the TCA cycle and the synthesis of both, aspartate-derived amino acids and purines (Figure 3.1). It has been shown that the aspartate metabolism is essential for the survival of *S. aureus* during osteomyelitis (Potter et al., 2020), which suggest that the aspartate aminotransferase would be a good target to develop new antibiotics against *S. aureus.* However, the activity of the SAUSA300_1916 or putative AspB has not been experimentally determined.

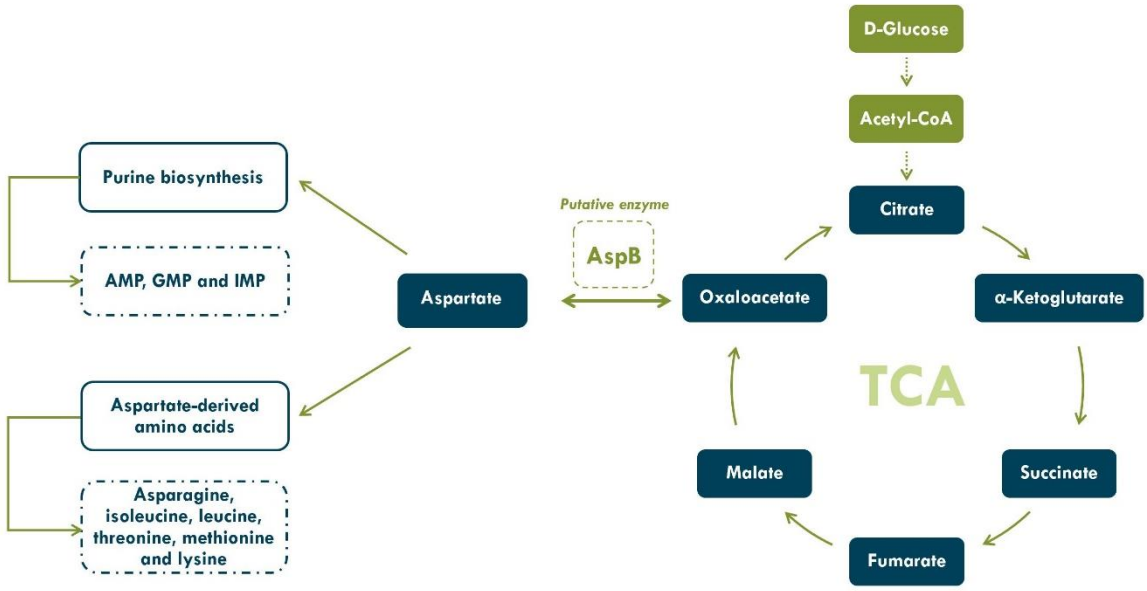

Figure 3.1 - Overview aspartate metabolism.

The aspartate aminotransferase links the TCA cycle with the synthesis of aspartate-derived amino acids and with the purine biosynthesis.

3.1.1.2 SAUSA300_1614 and SAUSA300_1845 are predicted to code glutamate-1-semialdehyde aminotransferases

The genes *SAUSA300_1614* and *SAUSA300_1845* are annotated as glutamate-1-semialdehyde aminotransferase, enzyme that participates in the metabolic pathway of haem biosynthesis, catalysing the formation of 5-aminolevulinic acid (ALA) from glutamate-1-semialdehyde (GSA) (Sinha et al., 2022).

Haem is a metalated tetrapyrrole complexed with iron that is widely distributed in nature (Dailey et al., 2017). The cells require haem for the correct function of proteins since it acts as a cofactor or prosthetic group in conserved enzymes like cytochrome peroxidase or oxygenase (L. Zhang, 2011). Haem is also important in different cellular processes such as cellular respiration due to its role as a cofactor in enzymes involved in the electron transport chain, cytochromes (Edwards et al., 2020), or terminal oxidases that are involved in the final step of aerobic respiration (Hammer et al., 2013). In *S. aureus* it has been demonstrated that haem is involved in the modulation of the expression of virulence factors (Torres et al., 2007).

The relevant role that haem plays in different cellular processes demands the development of an efficient mechanism of haem acquisition or a functional haem biosynthetic pathway to satisfy the intracellular requirements of this cofactor. In *S. aureus* the acquisition of haem, which is preferred as an iron source over transferrin (Skaar et al., 2004), depends on the lysis of erythrocytes by secreted haemolysins during infection (Hammer & Skaar, 2011), and on the iron-regulated surface determinant (Isd) system that allows the remotion of haem from the haemoglobin and its further incorporation and processing in the cytoplasm (Pishchany et al., 2014). Regarding the haem biosynthesis, most organisms have the metabolic pathway for its *de novo* synthesis, which in prokaryotes occurs through three different pathways (Dailey et al., 2017). The three pathways shares a common core which includes the conversion of ALA into uroporphyrinogen III (UROGEN) in a three-step enzymatic reactions performed by the enzymes porphobilinogen synthase (Pbgs), hydroxymethylbilane synthase (Hmbs), and uroporphyrinogen synthase (UroS) whose old abbreviations are HemB, HemC and HemD, respectively (Dailey et al., 2017).

The haem biosynthetic pathway requires the synthesis of the universal precursor ALA that can be synthetized through two different routes: the 4-carbon or the 5-carbon pathways (Layer et al., 2010). In the C_4 pathway, ALA is synthesised by the enzyme 5-aminolevulinic acid synthase (AlaS) from glycine and succinyl-CoA in a one-step reaction and it is commonly found in mammals and fungi while the C_5-pathway, used by *S. aureus*, is found mainly in bacteria, archaea, and plants (Layer et al., 2010). In *S. aureus* the synthesis of ALA starts with the synthesis of the precursor glutamyl-tRNA, which is converted into the intermediate glutamate-1-semialdehyde (GSA) by a glutamyl-tRNA reductase (GtrR or HemA), and further transformed into the universal precursor ALA by the enzyme glutamate-1-semialdehyde-2,1-aminomutase (GsaM or HemL) (Choby et al., 2018) (Figure 3.2).

Once the universal precursor ALA is formed, haem biosynthesis follows the common core pathway of three-step reactions leading to the formation of UROGEN, which is

further decarboxylated to coproporphyrinogen III. The synthesis of haem from coproporphyrinogen III can be achieved by two different pathways: classical and non-canonical (or coproporphyrin-dependent branch) (Dailey et al., 2015). In the classic pathway, which is present in Gram negative bacteria and eukaryotes, the intermediate coproporphyrinogen III is decarboxylated to protoporphyrinogen IX, further oxidized to protoporphyrin IX and finally converted into protoheme after the insertion of iron (Dailey et al., 2017). *S. aureus* synthesises haem by the non-canonical pathway that involves the oxidization of coproporphyrinogen III to coproporphyrin III by the enzyme coproporphyrinogen oxidase (CgoX or HemY), which is further transformed into coproheme III after the insertion of iron by the enzyme coproporphyrin ferrochelatase (CpfC or HemH), and finally transformed into protoheme following its decarboxylation by the enzyme coproheme decarboxylase (ChdC or HemQ) (Dailey et al., 2017).

In *S. aureus* has been reported that a proficient system of haem acquisition through the Isd system is essential for the colonisation of the pathogen in a murine model (Pishchany et al., 2010, 2014) and that a functional haem biosynthetic pathway is necessary for the development of infection, since a *hemA* mutant strain showed a reduced colonisation in both, heart and liver, using a murine infection model (Hammer et al., 2013). Thus, highlighting the haem synthesis as a biochemical pathway that could be a source of possible new druggable targets for *S. aureus* infections. In this context, the gene products of *SAUSA300_1614* (HemL1) and *SAUSA300_1845* (HemL2) seem to be good targets as the predicted coded enzymes are present in bacteria but not in humans, thus the determination of the glutamate-1-semialdehyde aminotransferase activity of HemL1 and HemL2 needs to be performed.

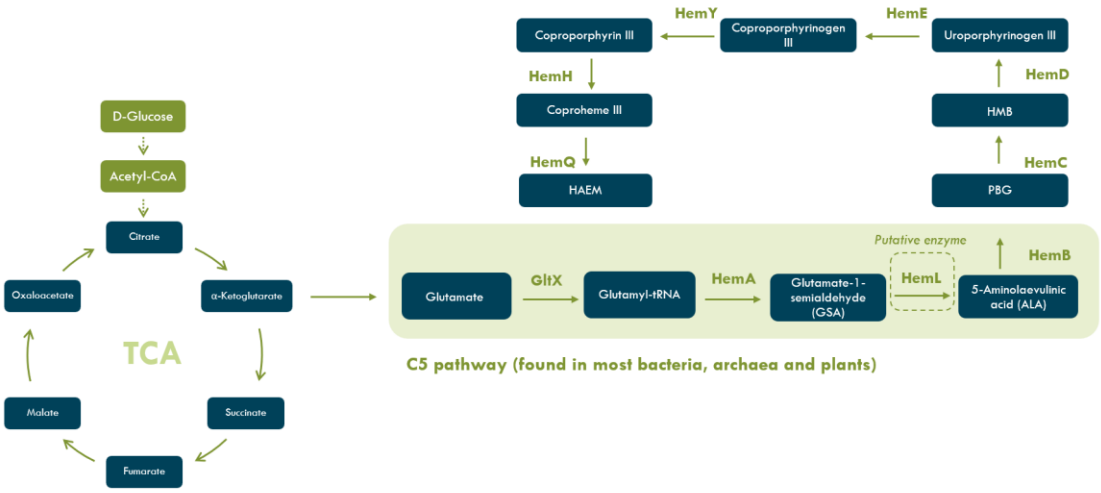

Figure 3.2 - Overview haem metabolism.

In *S. aureus* the synthesis of haem starts with the formation of glutamyl-tRNA from glutamate by GltX and further transformation into glutamate-1-semialdehyde (GSA) by HemA. The GSA is converted into the universal haem precursor 5-aminolaevulinic acid (ALA) by the enzyme HemL. The uroporphyrinogen III is formed from the ALA precursor after three consecutive enzymatic reactions where the enzymes HemB, HemC and HemD are involved. Haem is synthesised from uroporphyrinogen III after four consecutive enzymatic reactions where the enzymes HemE, HmY, HemH and HemQ are involved.

3.1.2 Biofilm formation by *S. aureus*

A biofilm corresponds to a microbial community in which cells are attached to a surface (biotic or abiotic), and to each other, encased in a self-produced extracellular matrix, and show a differentiated phenotype compared to their planktonic counterparts (Donlan & Costerton, 2002). In *S. aureus*, biofilm formation is associated with chronic infections and biofilm-associated infections on indwelling medical devices are one of the most common infections linked to *S. aureus* (Otto, 2008). Biofilm-related infection are more difficult to treat than those caused by planktonic cells due to the higher resistance to antimicrobial treatment (Manandhar et al., 2018), and to its capacity to evade the host immune system (Graf et al., 2019).

In *S. aureus* the biofilm formation was reported to occur in five successive steps: 1) attachment, 2) multiplication, 3) exodus, 4) maturation, and 5) dispersal that were defined after visualising the biofilm development using a microfluidics system and time-lapse microscopy (Moormeier et al., 2014). The *attachment* of the cells to proteins of the

extracellular matrix occurs through cell-wall anchored proteins like the MSCRAMMS (microbial surface components recognizing adhesive matrix molecules), NEAT motif family, the three-helical bundle family or G5-E repeat family of proteins (Paharik & Horswill, 2016). The *multiplication* stage occurs after the attachment of the cells to a surface and successive cell divisions while the *exodus* corresponds to an early release of the cells dependent on nuclease degradation of eDNA (Moormeier et al., 2014). The *maturation* corresponds to the formation of a microcolony-like structure with channels that allows nutrients flux and waste removal; and in the *dispersal* stage, the cells disseminate from the biofilm thanks to the activity of phenol-soluble modulins (PSMs) (Moormeier et al., 2014; Moormeier & Bayles, 2017).

Different studies have investigated the role of metabolism in the formation of *S. aureus* biofilms. It has been shown that the nutrients availability can influence the biofilm formation of *S. aureus* and that the supplementation of different complex media with glucose promoted its development (Seidl et al., 2008). It has also been reported that some metabolic pathways are important in the *S. aureus* biofilm formation. For example, a study aiming to identify metabolic pathways relevant for different stages during the *S. aureus* biofilm formation found that the expression levels of the genes coding for a formate-acetyltransferase-activating enzyme (*pflA*) and a formate acetyltransferase (*pflA*) were higher in the biofilm cells when compared with their expression in planktonic cells (Resch et al., 2005). Another example of genes involved in the *S. aureus* metabolism that were highly expressed in the biofilm cells than in their planktonic counterparts were the gene cluster coding urease (*ureD*, *ureF*, *ureB*, and *ureC*), and the genes coding an arginine deiminase (*arcA*) and a carbamate kinase (*arcC*) that participate in the arginine deaminase pathway (Resch et al., 2005). The methionine biosynthetic pathway has also been shown to be important for *S. aureus* biofilms as the cells showed a reduced capacity to form biofilms when this pathway was interrupted (Jochim et al., 2019). Genes involved in gluconeogenesis were also found to play a role in *S. aureus* biofilms as they inhibited a macrocolony formation (as an alternative biofilm

study model), while genes involved in purine biosynthesis activated its formation (Wermser & Lopez, 2018). Here, we aimed to evaluate the role that aspartate and haem metabolism might have in *Staphylococcus aureus* biofilm formation.

3.1.3 Utilisation of *Galleria mellonella* larvae model to study the virulence of *S. aureus*

G. mellonella is an insect belonging to the order Lepidoptera that has been used as an alternative model to vertebrate, like mice, and other invertebrate models, like the fruit fly, for the study of microbial infection, virulence, and drug discovery. The first time that *G. mellonella* was reported to be a useful model to study pathogenicity was in 2000, after a study showing this model to be able to successfully distinguish the pathogenicity between virulent and non-virulent yeast strains (Cotter et al., 2000). The *G. mellonella* model has been increasingly used, as reported by Cutuli and colleagues who showed that in 2016-2018, 292 scientific articles related with the topics *G. mellonella* and *microbiology* were published compared to 691 articles published during the previous 10 years (Cutuli et al., 2019).

G. mellonella, commonly known as the greater wax moth or the honeycomb moth, has the capacity to parasitize and destroy hives in its larval stage. Its life cycle consists of four stages: egg, larvae, pupa and adult (Kumar & Khan, 2018), and the larvae is used as a model organism in host-pathogen interaction studies. The size of *G. mellonella* larvae is about 3 cm in length and their weight between 0.3 and 0.5 g (Cutuli et al., 2019). As insects, *G. mellonella* do not have an adaptive immune response, and their innate immune system is their defence mechanism against invasion by foreign microorganisms. One of the main characteristics that makes *G. mellonella* suitable as an *in vivo* model to study microbial pathogenesis is its innate immune system, which in some respects is similar to that of mammals. For example, phagocytosis is carried out by neutrophils in mammals while in *Galleria* a similar function is performed by plasmatocytes, a type of haemocyte that circulates in the haemolymph of the insects (Browne et al., 2013). It was

also reported that the haemocytes of *G. mellonella* have two proteins homologs to the $p47^{phox}$ and $p67^{phox}$ proteins found in human neutrophils, which are needed for the generation of a functional NADPH oxidase complex required for microbial killing (J. Renwick et al., 2007), thus showing some similarities with the mammalian innate immune system.

Regarding the innate immune system of *G. mellonella,* it comprises two branches: cellular and humoral, and both branches are well-coordinated since the humoral response can affect the function of haemocytes and vice versa (Lavine & Strand, 2002). The cellular response is carried out by haemocytes, which are cells circulating freely in the haemolymph that recognize invasive microorganisms after recognition of pathogen-associated molecular patterns (PAMPs) and have phagocytic properties (Cutuli et al., 2019). In insects belonging to the order Lepidotera, five types of haemocytes have been reported: promehocytes, granular cells, plasmatocytes, spherulocytes, and oenocytoids (Lavine & Strand, 2002), being functionally characterized four of them: spherulocytes, plasmatocytes, granular cells, and oenocytoids. The latter three types have been shown to phagocytise *E. coli* cells (G. Wu et al., 2016). In the same study, a variation in the relative proportion of haemocytes was found at different stages of the larval development, which is a key characteristic to consider when performing assays with this organism since these variations might affect the reproducibility of the assay (Cutuli et al., 2019). A fifth type of haemocyte, the prohemocyte, was recognized during the characterization of the circulating haemocytes of *G. mellonella* after infection with strains of *Actinobacillus pleuropneumoniae* (Arteaga Blanco et al., 2017).

The humoral response of *G. mellonella* includes the synthesis of different effector molecules like antimicrobial peptides (AMPs), opsonins, and the melanisation of the haemolymph, amongst others. The AMPs have the ability to destabilize the bacterial cellular membrane and the identification of a wide range of AMPs in *G. mellonella* after infection with *E. coli* and *M. luteus* strains have been performed. Some of the AMPs detected after the infection with both pathogens were: lysozyme, moricin-like peptides,

cecropins, gloverin, Gm proline-rich peptides 1 and 2, Gm anionic peptides 1 and 2, galiomicin, gellerimycin, inducible serine protease inhibitor 2, 6 tox and heliocin-like peptide (Brown et al., 2009). Amongst the proteins that act as opsonins in *G. mellonella* can be found the multifunctional apolipophorin III (apoLp-III), peptidoglycan recognition proteins (PGRPs), the cationic protein 8 (Gm CP8), and hemolins (Tsai et al., 2016). The apoLp-III was reported to bind to lipopolysaccharides (LPS) (Dunphy & Halwani, 1997) and to teichoic acids (Halwani et al., 2000) of pathogenic bacteria. Additionally, it was reported to have antibacterial activity (Zdybicka-Barabas et al., 2014), stimulate phagocytosis of isolated plasmatocytes (Wiesner et al., 1997), and to bind to β-1,3 glucan released from the fungal cell wall as well as to the conidia (Whitten et al., 2004).

The melanisation process in *G. mellonella* includes a series of reactions that leads to the synthesis and accumulation of the pigment melanin on the site of the infection that starts with black spots on the larvae and might end up with a complete darkened and dead larvae (Tsai et al., 2016). The melanisation process requires the activation of the prophenoloxidase (proPO) system which is activated by PAMPs (i.e. LPS or β-1,3 glucan) that triggers a serine proteinase cascade that finally converts the inactivated form of the enzyme found in the haemocytes into an activated phenoloxidase leading to the production of melanin, together with the synthesis of cytotoxic compounds (Cerenius et al., 2008).

The *G. mellonella* model has some advantages that makes it suitable for the study of virulence of human pathogens apart from the similarities with the mammal innate immune system. These advantages include the wide range of temperature at which the larvae can be incubated, from 15°C (Réjasse et al., 2012) to 37°C (Purves et al., 2010) making it easy to mimic the conditions that pathogens can find in our body (37°C), its low cost in terms of acquisition and maintenance, the lack of ethical regulations, and the adequate larval size makes its manipulation easy.

In *S. aureus*, for example, the model has been used to discover proteins important for its virulence like the two homologous proteins with metabolic functions in glycolysis (GapA) and gluconeogenesis (GapB) (Purves et al., 2010). This model has also been used to evaluate the level of protection that the flavonoid myricetin confers to the host against *S. aureus* infection. The study found an increase in the survival rate of the larvae treated with either myricetin (50 mg/kg) or vancomycin (50 mg/kg) compared to untreated larvae (bacteria + 2% DMSO) (Silva et al., 2017). This model has proven to be useful in assessing the tolerance of *S. aureus* to antibiotics like vancomycin after treatment with LL-37, a human serum antimicrobial peptide that promotes tolerance to this antibiotic (Friberg et al., 2020), in the finding of combination therapies to treat *S. aureus* (Li et al., 2020), in characterising the development of *S. aureus* infection when the larvae were infected at doses ranging from 10^4 to 10^6 CFU larvae^{-1} (Sheehan et al., 2019), and in assessing the role of riboregulation during its infection (Ménard et al., 2021). Menard and colleagues found that the small regulatory RNAs (sRNAs), SprC and SprD, were increasingly expressed in the infected larvae with *S. aureus* (Ménard et al., 2021). Here, we used the *G. mellonella* model to evaluate the role of the genes *SAUSA300_1916*, *SAUSA300_1614* and *SAUSA300_1845* in the virulence of *S. aureus*.

3.1.4 Utilisation of the planarian *Dugesia japonica* to study survival and colonisation of *S. aureus*

Planarians are freshwater flatworms belonging to the Turbellaria class of the phylum Platyhelminthes that show bilateral symmetry (Newmark & Sánchez Alvarado, 2002) with a nervous system composed of a bi-lobed brain, formed by neural cells and two ventral nerve cords (Agata et al., 1998). The digestive system in planarians is formed by three branches (in the case of triclad planarians), one central and two ventral, and their intestine, connected to a pharynx, forms an extensible tube that function as a mouth and allow them to take food from the environment (Elliott & Sánchez Alvarado, 2013). They have light sensitive structures corresponding to a couple of eyes located in the head

region and chemoreceptors in the auricles, which are the triangular extensions seen in the head (Newmark & Sánchez Alvarado, 2002). These organisms are hermaphrodites and can reproduce sexually or asexually through splitting and regeneration (Newmark & Sánchez Alvarado, 2002).

Planarians are commonly known for their capacity to regenerate any part of their body and, even an entire new organism from a small tissue fragment, due to the presence of embryonic cells called neoblasts (Reddien & Sánchez Alvarado, 2004). These cells are undifferentiated pluripotent stem cells capable to regenerate tissues derived from the three germ layers (ectoderm, mesoderm and endoderm), which can migrate to the site of the wound and regenerate the damaged tissue or replace old tissues (Elliott & Sánchez Alvarado, 2013). Due to their remarkably regeneration capacity, planarians have been used as an *in vivo* model organism to study the genetic control of the tissue regeneration process (Reddien et al., 2005).

The defence mechanism in planarians relies on an innate immune system consisting of four main components: the epidermis, pharynx, intestines, and reticular cells (Gao et al., 2017). Their epidermis, which is a simple epithelium formed by ciliated and gland cells, secretes a viscous mucus from tubular structures called rhabdites (Hayes, 2017), and together with the pharynx are considered planarians first defence mechanism. The role of pharynx in immune response was identified when researchers investigating pharynx regeneration found that genes up regulated in this process are also involved in the immune response (Pang et al., 2017). In the study, Pang and colleagues found that a gene coding a placenta specific protein 8 (Plac8) of *Dugesia japonica* is up regulated during pharynx regeneration and shows antibacterial activity against two human pathogens, *Escherichia coli* and *Pseudomonas aeruginosa* (Pang et al., 2017).

Regarding the intestine of planarians and its role in immunity, the intestine is formed by one layer of cells consisting of three cell types: secretory goblet cells, basal cells, and phagocytes (Forsthoefel et al., 2020). Pathogens like *S. aureus*, *L. pneumophila* and *M.*

tuberculosis have been visualised within phagosomes, highlighting the role of phagocytes in bacterial elimination and planarian immunity (Abnave et al., 2014). The last components of planarian immunity, the reticular cells, have a similar function to that of macrophages from vertebrates that following bacterial recognition, this type of cell is able to mobilise through the body fluid, migrate to the site of infection, phagocytise and eliminate the bacteria (Morita, 1991; Peiris et al., 2014).

It has been reported that planarians have the ability to fight against Gram positive organisms (*S. aureus*, *L. monocytogenes*), *Mycobacterium* species *tuberculosis*, *avium*, and *marinum*, and against Gram negative organisms (*S. typhimurium* and *L. pneumophila*) when three different bacterial concentrations were used to fed planarians: 10^9, 10^7, and 10^5 CFUs per worm (Abnave et al., 2014), characteristic that can be helpful in the understanding of antibacterial resistance mechanisms. For example, in the study carried out by Abnave and colleagues they identified 18 genes involved in planarian clearance of two human pathogens, *L. pneumophila* and *S. aureus*, and half of those were orthologs to human genes. In addition, a human ortholog protein called Membrane Occupation and Recognition Nexus (MORN) repeat-containig-2 (MORN2) was shown to be involved in the elimination of all human pathogens tested (Abnave et al., 2014), thus uncovering immune factors previously unknown.

It has been shown that the immune response in planarians against *S. aureus* infection is regulated by the circadian rhythm (Tsoumtsa et al., 2017). In the study the authors identified in the genome of the planarians *Schmidtea mediterranea*, the presence of two genes homologs of the *Homo sapiens* circadian genes *(Hs)-arntl-1* and *Hs-tim*: *Smed-arntl-1* and S*med-tim*, respectively. They confirmed that the expression of the *Smed-tim* showed a 24 h expression cycle with a higher expression during the dark phase of a light and dark cycle. The study showed that *Smed-tim* is required for the clearance of *S. aureus* since planarians that had the gene silenced by interference RNA (RNAi) needed 3 extra days to eliminate the pathogen than the control group, thus linking the timeless

gene involved in the circadian clock with the clearance of *S. aureus* by planarians (Tsoumtsa et al., 2017).

Although the above mentioned studies have shown that planarians can efficiently clear the infection caused by some bacteria, those studies have focused on the understanding of the immune capacity of planarians to fight the infection. Here, we sought to use planarian model as an alternative model to the commonly used fruit flies, nematodes and mice, to study the virulence, survival and colonisation of *S. aureus.*

3.2 Aims of the work described in the chapter

- To determine the effect of the disruption of the genes *SAUSA300_1916*, *SAUSA300_1614*, and *SAUSA300_1845* on growth, virulence, and biofilm formation of *S. aureus*.
- To evaluate the planarian model to study survival and colonisation of *S. aureus*.

3.3 Materials and Methods

3.3.1 Detection of the transposon insertion within the genes *SAUSA300_1916*, *SAUSA300_1614* and *SAUSA300_1845 of S. aureus*

3.3.1.1 Genomic DNA extraction

A chemical extraction protocol was used to extract the genomic DNA from the *S. aureus* strains. For this purpose, a volume of 1.5 mL from a 16 h culture of the strains in BHI was pelleted down by centrifugation at 13,200 x *g* for 1 min. The supernatant was discarded and 160 µL of Tris-EDTA, Tris 10 mM and EDTA 1 mM pH 8.0, was added into each tube containing the pellets to resuspend the cells. Two µL of lysostaphin from a 20 mg/mL stock were added into each tube and incubated for 1 h at 37°C. Following the incubation period, 20 µL of RNase A from a 2 mg/mL stock were added into each

tube and incubated at 37°C for approximately 20 min. A volume of 8 µL of proteinase K from a 10 mg/mL stock was added into each tube and incubated at 56°C for 30 min. After the incubation period, a volume of 200 µL of Qiagen buffer AL (Lysis buffer) was added into each tube and vigorously mixed for 15 seconds and incubated at 56°C for 10 minutes. The DNA was precipitated by adding 1 mL of absolute ethanol into each tube. The tubes were centrifuged to pellet the DNA and the supernatant was removed. Finally, the DNA was washed twice with 200 µL of ice cold 70% ethanol. The pellet was air dried for 15 min and the DNA was resuspended into 100 µL of molecular grade water. The DNA concentration was quantified using a spectrophotometer (NanoDrop™ 1000, Termo Scientific, USA) and the integrity of the genomic DNA was checked on a 1% agarose gel.

3.3.1.2 DNA amplification

The PCR was performed using a Biometra 3000 thermocycler (Biometra, UK) in a 25 µL reaction volume containing 12.5 µL of MyTaq™ Red Mix, 4 ng/mL of DNA template, 1 µL of each primer (10 µM stock) and the total volume of the reaction was made up using molecular grade water (cat. n° W4502, Sigma). The primers, designed to anneal within a specific region of each gene, are listed in Table 3.1.

Table 3.1. Primers used to confirm the transposon insertion within the selected genes.

Gene identifier	Primer name	Sequence (5' → 3')	Primers used	Reference
SAUSA300_1916	*aspB*	ATGAATCCTTTAGCCCAAAG	*aspB* + Buster	This study
SAUSA300_1614	*hemL1*	AGAAGAAGCAATGAAGGTTG	*hemL1* + Buster	This study
SAUSA300_1845	*hemL2*	CGTTTACAACAACTTTCAAACG	*hemL2* + Buster	This study
	Buster	GCTTTTTCTAAATGTTTTTTAAGTAAATCAAGTAC	*Buster* + *gene specific primer*	NTML website
	Upstream	CTCGATTCTATTAACAAGGG	*Upstream* + *gene specific primer*	NTML website

These primers were used in combination with primers designed by the Nebraska group that anneal with a specific region of the transposon and can be found in the "Methods" section on their website under the "Confirmation of Mutations" subheading (https://app1.unmc.edu/fgx/methods.htmL). These transposon-specific primers are Buster (5'-GCTTTTTCTAAATGTTTTTTAAGTAAATCAAGTAC-3') and Upstream (5'-CTCGATTCTATTAACAAGGG-3') and their selection depends upon the orientation of the transposon insertion within the specific gene. If the transposon is inserted in the "plus" orientation within the gene, the Upstream primer should be used, whereas the Buster primer should be used if the transposon is inserted in the "minus" orientation within the gene. Each of those primers were used in combination with gene-specific primers and the expected product size corresponds to the length of the fragment between the annealing site of the gene-specific primer and the transposon-specific

primer, considering 464 bp distance to the transposon end when using the Upstream primer, and 133 bp distance to the transposon end when using Buster primer. The programme used to perform the PCR started with an initial denaturation at 95°C for 5 min followed by 30 cycles of i) denaturation at 94°C for 30 s, ii) annealing at 55°C for 1 min, iii) extension at 72°C for 1 min, and a final termination step at 72°C for 10 min. The PCR products were kept at 4°C overnight until agarose gel electrophoresis was performed.

The transposon insertion site and the details of its orientation within the genome, gene length, amongst other characteristics taken from the "Tn insertion map" section from the Nebraska group website (https://app1.unmc.edu/fgx/index.html), can be found in the tables below each of the figures depicting the gene sequence for each gene: putative aspartate aminotransferase *aspB* (Figure 3.3, Table 3.2), putative glutamate-1-semialdehyde aminotransferases *hemL1* (Figure 3.4, Table 3.3) and *hemL2* (Figure 3.5, Table 3.4). The expected PCR product size is included in each table and calculated as mentioned previously.

***SAUSA300_1916* (Gene ID: 3914404)**

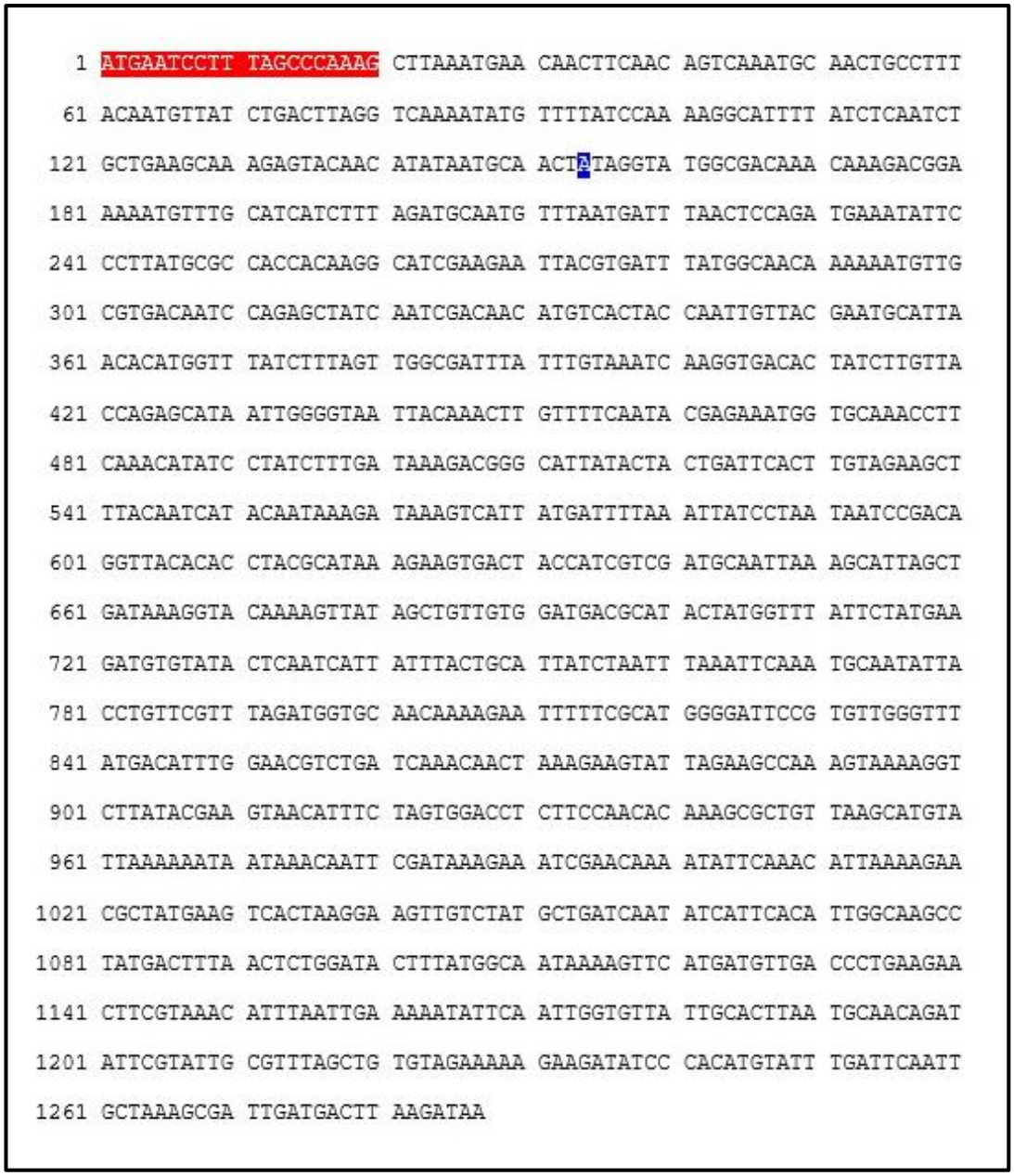

Figure 3.3 - Sequence of the gene coding a putative aspartate aminotransferase (*aspB*).

The sequence of the gene used for the design of the gene-specific primer is highlighted in red while the position of the transposon insertion within the gene is highlighted in blue.

Table 3.2. Genome and transposon insertion features within *SAUSA300_1916*

Feature	
DNA strand of the gene	Forward
Start position of the gene in the genome	2080435
End position of the gene in the genome	2081722
Length of the gene	1287 bp
Tn insertion position in the genome and orientation	2080588 – Reverse
Tn insertion relative to the start of the gene	154 bp
Suggested Tn specific primer	Buster
Expected PCR product size	133 bp + 154 bp = 287 bp

SAUSA300_1614 **(Gene ID: 3914650)**

Figure 3.4 - Sequence of the gene coding a putative glutamate-1-semialdehyde aminotransferase (*hemL1*).

The sequence of the gene used for the design of the gene-specific primer is highlighted in red while the position of the transposon insertion within the gene is highlighted in blue.

Table 3.3. Genome and transposon insertion features within *SAUSA300_1614*

Feature	
DNA strand of the gene	Reverse
Start position of the gene in the genome	1768844
End position of the gene in the genome	1767557
Length of the gene	1287 bp
Tn insertion position in the genome and orientation	1768561 – Forward
Tn insertion relative to the start of the gene	284 bp
Suggested Tn specific primer	Buster
Expected PCR product size	133 bp + 267 bp = 400 bp

SAUSA300_1845 **(Gene ID: 3913658)**

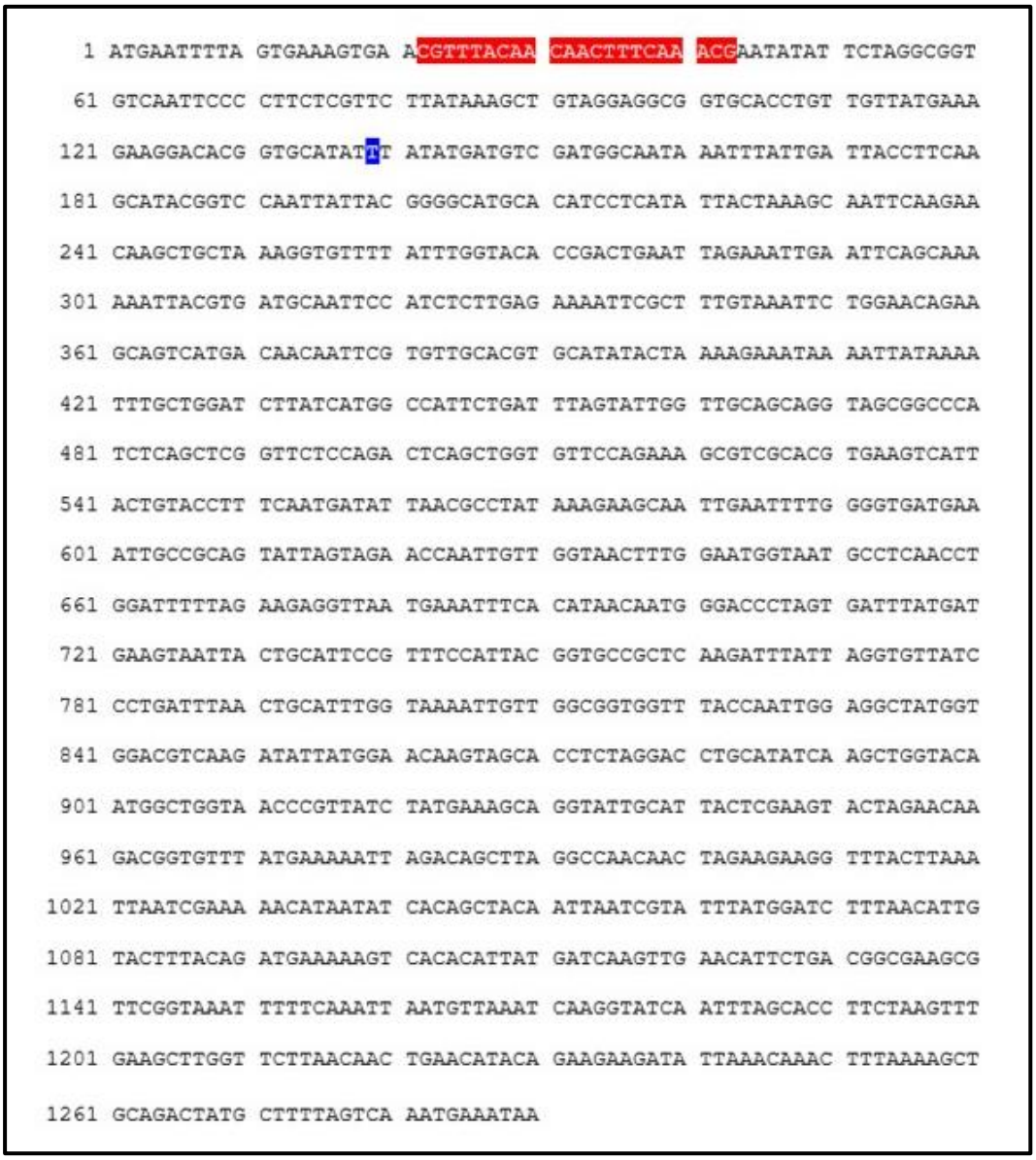

Figure 3.5 - Sequence of the gene coding a putative glutamate-1-semialdehyde aminotransferase (*hemL2*).

The sequence of the gene used for the design of the gene-specific primer is highlighted in red while the position of the transposon insertion within the gene is highlighted in blue.

Table 3.4. Genome and transposon insertion features within *SAUSA300_1845*

Feature	
DNA strand of the gene	Forward
Start position of the gene in the genome	2005499
End position of the gene in the genome	2006789
Length of the gene	1290 bp
Tn insertion position in the genome and orientation	2005637– Reverse
Tn insertion relative to the start of the gene	139 bp
Suggested Tn specific primer	Buster
Expected PCR product size	139 bp + 118 bp = 251 bp

3.3.1.3 Agarose gel electrophoresis

The PCR products were visualized by gel electrophoresis. For this purpose, 1% (w/v) agarose gels were prepared in 1X Tris acetate EDTA (TAE) electrophoresis buffer mixed with 2 µL of RedGel (10,000X stock) nucleic acid dye for DNA staining (cat. n° BT41003, Biotium). Before loading the wells, the samples were mixed with 1 µL of 6X loading dye (cat. n° B7025S, New England Biolabs) and a final volume of 3 µL was loaded. Two µL of Quick-Load 100 bp DNA ladder (cat. n° N0467S, New England Biolabs) were used as a marker. The gel electrophoresis was carried out in 1X TAE as a running buffer at 100 V for 1 h. The DNA bands were visualized under UV light using an Alpha Imager gel documentation system (Alpha InnoTech, UK).

3.3.2 Evaluation of the effect of the disruption of the genes *SAUSA300_1916*, *SAUSA300_1614* and *SAUSA300_1845* on the growth of *S. aureus* on human serum and RPMI1640

The growth curves were performed with human serum from male AB plasma (cat. n° H4522, Sigma). Since *S. aureus* is unable to grow in serum it was treated as follows before use, the serum was heat inactivated at 56°C for 30 min, centrifuged for 5 min and the clear zone was transferred into a centrifuge tube using a syringe with a 21G $1^{1/2"}$-Nr.2 (0.8 x 40mm) needle, and further filtered using a 0.22 µm filters. The RPMI-1640 complete formulation (cat. n° R8758, Sigma), RPMI-1640 without L-cystine and L-methionine (cat. n°R7513, Sigma), and RPMI-1640 without L-glutamine (cat. n° R0883, Sigma) were kept at 8°C and brought to room temperature before use.

Bacterial strains were streaked out from the glycerol stocks onto TSA plates containing the appropriate antibiotic. For *S. aureus* USA300 mutant strains the plates were supplemented with erythromycin at 5 µg/mL while no antibiotic supplementation was required for the growth of the *S. aureus* LS-1 strains, neither the wild-type nor the *hemL*(s) mutant strains.

A single colony was used to inoculate 10 mL of BHI broth in a 50 mL sterile centrifuge tube and the cultures were grown at 37°C for 16 h with shaking at 200 rpm. After the incubation period, the bacterial cultures were washed with sterile PBS twice and diluted to an OD_{600nm} of 0.05 in human serum or RPMI-1640 media (complete formulation and without the amino acids stated in the results section). A volume of 200 µL of the adjusted cultures was used to inoculate the wells of a non-tissue culture treated 96 wells plate (cat. n° 351172, Falcon). Wells inoculated with BHI were used as a control. Bacterial growth was monitored by measuring the optical density at 600 nm over either 24 h or 48 h every 30 min at 37°C using a SPECTROstar Nano absorbance plate reader. The experiment was performed in triplicate in three independent biological repeats. The absorbance readings were plotted against time using the OriginPro software and the analysis of the growth was performed by fitting the data to the logistic equation used in

the field of ecology and evolution ($N_t = K/1+(K-N_0/N_0)\ e^{-rt}$ where N_t= is the population size at time t; N_0= is the population size at the beginning of the growth; K = is the carrying capacity; r = is the growth rate of cells at certain time) using the *Growthcurver* package (Sprouffske & Wagner, 2016).

3.3.3 Evaluation of the effect of the disruption of the genes *SAUSA300_1916*, *SAUSA300_1614* and *SAUSA300_1845* on biofilm formation of *S. aureus*

3.3.3.1 Biofilm formation

All bacterial cultures were grown in BHI broth at 37°C for 16 h with shaking at 200 rpm. After incubation, the cultures were washed with sterile PBS and diluted into fresh BHI broth supplemented with 1% glucose to an OD_{600nm} of 0.05. A volume of 200 µL from each strain was added into the wells of a tissue culture treated plate (cat. n°833924, Sarstedt). The plate was covered with an AeraSeal™ breathable film (cat. n° A9224, Sigma) and the biofilm was allowed to form in static condition at 37°C for 24 h. Wells inoculated with BHI media were used as a blank control. The experiment was performed in three independent biological repeats.

3.3.3.2 Biofilm quantification

After the incubation period, the planktonic and biofilm phases were measured at 600 nm using a SPECTROstar Nano absorbance plate reader. Non adherent cells were discarded, and the wells gently washed twice with 100 µL of sterile distilled water. The plates were left to dry inverted in the oven at ~ 60°C for 1 h before the biofilm was stained. A volume of 100 µL of a 1% (v/v) crystal violet solution was added into each well containing the cells and the biofilm stained for 10 min. Excess stain was rinsed off and wells were washed three times with 200 µL of sterile distilled water. The crystal violet was solubilised with 200 µL of acetic acid 30 % (v/v), the plate incubated for 30 min in

shaking condition at 40 rpm and the biofilm quantified measuring the absorbance of the crystal violet at 590 nm using a plate reader. Before reading the stained wells were diluted 1:4 into 30% (v/v) acetic acid due to the high concentration of the dissolved crystal violet used. The results are shown as the mean ± standard deviation and the analysis of variance (ANOVA one-way) and mean comparison (Bonferroni/Tukey) tests were carried out by OriginPro. Significant differences were defined as $*P < 0.05$.

3.3.4 Evaluation of the effect of the disruption of the genes *SAUSA300_1916*, *SAUSA300_1614* and *SAUSA300_1845* on the virulence of *S. aureus* in a *Galleria mellonella* larvae model

The wax moth larvae of *G. mellonella* were acquired from Livefood UK Ltd. and they were kept at 10°C until use. For each experiment, 10 larvae weighing between 0.2 and 0.3 g were injected with *S. aureus* JE2 and the mutants for the genes *SAUSA300_1916*, *SAUSA300_1614*, and *SAUSA300_1845*. The *S. aureus* LS-1 background strains (wild-type and mutants LS-1Δ *hemL1* and LS-1Δ *hemL2*) were also used to infect the larvae. Bacterial cultures of the strains were prepared in BHI broth and incubated for 16 h at 37°C with shaking at 200 rpm. The cultures were washed with sterile PBS and adjusted to the required optical density depending on the strain (OD_{600nm} 0.1, 0.5 or 1). The adjusted bacterial suspensions were added into a 1 mL hypodermic syringe and 10 µL were injected in the hemocoel of each larva through the second left pro-leg using a single syringe pump (AL-1000HP, World Precision Instruments). The control larvae were injected with 10 µL of sterile PBS. After infection, the larvae were kept at 37°C and their mortality was checked every 24 h. Three independent experiments were performed, and the results were analysed by using the Kaplan-Meier survival analysis in the OriginPro software. Statistical differences were determined with a log-rank test.

3.3.5 Evaluation of a planarian model to study survival and colonisation of *S. aureus*

3.3.5.1 Planarian maintenance

Planarians belonging to the species *Dugesia japonica* were kept protected from light within containers with Deeside water without antibiotics at 22°C. Planarians propagation was performed once a month through two transverse amputations perpendicularly to the antero-posterior axis (Reddien & Sánchez Alvarado, 2004). For this purpose, planarians were transferred to a different container and the tail and head were removed. The fragments (head – trunk – tail) were left for regeneration for at least two weeks before mixing them again with the main colony. Planarian water was changed twice a week and the containers cleaned up using paper towels to eliminate mucus and debris that were stuck to their walls. Planarians were fed once every two weeks using organic ox liver, washed after feeding, and were starved for one week before each experiment.

3.3.5.2 Planarians fed with S. aureus strains

Planarians were fed with *S. aureus* strains mixed with ox liver following an adapted protocol of dsRNA infected planarians (Abnave et al., 2014). The wild-type and *SAUSA300_1916* mutant strains, stored in glycerol stocks, were grown on TSA plates alone or supplemented with 5 µg/mL erythromycin and incubated overnight at 37°C. A single colony of each strain was used to inoculate BHI broth, and the cultures were incubated at 37°C for 16 h with shaking conditions at 200 rpm. Bacterial cultures were spun down, washed with PBS, and resuspended in Deeside water at two bacterial concentrations ($1x10^9$ and $1x10^8$ CFU). Bacterial pellets were obtained after centrifugation at 13,000 x *g* for 5 min and were mixed with 300 µL of ox liver, 150 µL of ultra-low-gelling temperature agarose, and 7 µL of red food colouring using a tissue grinder. The mixture was allowed to solidify on ice for ~ 15 min and 100 µL of the mixture was added into Petri dishes containing a group of 20 planarians per strain. Planarians

fed with the mixture without bacteria were used as a control group. After 2 h feeding, planarians were gently washed with Deeside water, transferred into new Petri dishes, and left inside the incubator at 22°C during the experimentation period. The experiment was performed in three independent biological repeats.

3.3.5.3 Quantification of the colony forming units (CFUs)

The number of bacteria recovered from infected planarians (CFU/5 worms) was quantified at days 0 (2 h after feeding), 1, 2, and 4 post infection. A group of 5 planarians were retrieved from the incubator per each time point and homogenized in 25 µL of PBS using a tissue grinder. Serial dilutions of the homogenates were prepared and a volume of 25 µL was plated onto mannitol salt agar (MSA) plates (cat. n° CM0085, Oxoid). The plates were incubated at 37°C for 24 h and the number of colonies was recorded. As control, non-infected planarias were homogenised, serially diluted in PBS, and 25 µL of each dilution were plated out onto MSA plates. No bacterial growth was observed in the control group. The results were analysed using OriginPro software and the statistical differences were determined using the Mann-Whitney test.

3.3.5.4 Planarians infected with S. aureus strains

The *S. aureus* strains were introduced into the water containing planarians at different concentrations following a protocol aimed to evaluate tissue degeneration of planarians after bacterial infection (Arnold et al., 2016). Briefly, the wild-type and *SAUSA300_1916* mutant strains were grown in BHI for 16 h at 37°C in shaking conditions at 200 rpm. Bacterial suspensions at four different concentrations, between $1x10^9$ and $1x10^8$ CFU, were prepared by washing the cells with PBS and adjusting the OD_{600nm} to the concentrations required. A group of 20 planarians per bacterial strain was used for the experiment and they were separated from the main colony and added individually into the wells of a 24 wells plate at least three days before the day of infection to allow an

adjustment period to a small space prior the experiment. The selected group of planarians for the experiment was starved for one week, were similar in size, and did not show any visually lesion on their skin.

Planarians individually placed into each well were infected with the *S. aureus* wild-type and mutant strains by adding up to 1 mL of the bacterial strains resuspended in the water used to keep the planarian colony at the required concentration. Planarians resuspended into 1 mL of Deeside water, which was used to keep the colony, were used as a control group. The plates were left inside the incubator at 22°C and checked daily using a Zeiss Stemi 200 stereo microscope over a period for up to 20 days depending on the bacterial concentration used. Every 3 to 4 days planarians were gently washed with PBS and re-infected by adding freshly prepared bacterial cultures into new plates. The experiment was performed in three independent biological repeats.

3.4 Results

3.4.1 Detection of transposon insertion within the genes *SAUSA300_1916*, *SAUSA300_1614* and *SAUSA300_1845* by PCR

The transposon insertion within the genes *SAUSA300_1916* coding for a putative aspartate aminotransferase, *SAUSA300_1614* and *SAUSA300_1845*, both coding for putative glutamate-1-semialdehyde aminotransferases were detected by PCR using specific primers that annealed to the *bursa aurealis* transposon and to the sequence of the gene of interest.

The product size of the PCR amplification products detected the transposon inserted within the genes *SAUSA300_1916, SAUSA300_1614, and SAUSA300_1845* with the expected sizes of 287, 400, and 251 base pairs, respectively. The gel show the bands of the PCR products which are in good agreement with the size of the band expected for the insertion of the transposon within each gene, thus demonstrating that the transposon

was inserted within the genes *SAUSA300_1916*, *SAUSA300_1614*, and *SAUSA300_1845* (Figure 3.6) confirming the mutant clones were correct.

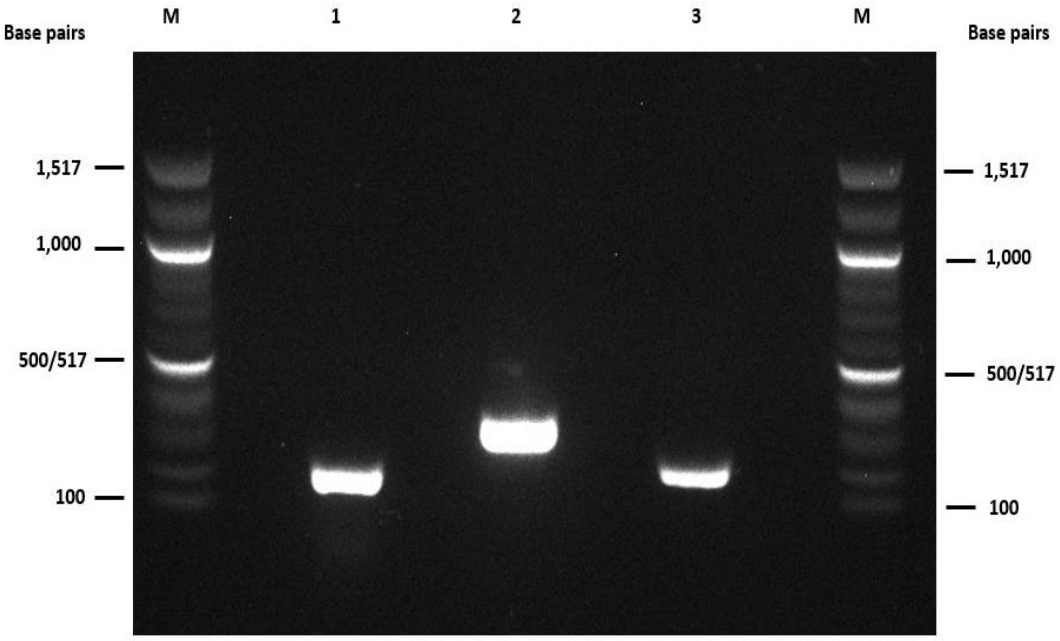

Figure 3.6 - Detection of transposon insertion within the genes *SAUSA300_1916*, *SAUSA300_1614* and *SAUSA300_1845* of *S. aureus*.

PCR products showing the presence of the transposon within the genes coding the putative aminotransferases of *S. aureus*. Lane M: 100 bp DNA ladder (New England BioLabs, UK); Lane 1: transposon presence within the gene *SAUSA300_1916* (putative aspartate aminotransferase), expected product size ~287 bp; Lane 2: transposon presence within the gene *SAUSA300_1614* (putative glutamate-1-semialdehyde aminotransferase), expected product size ~400 bp; and Lane 3: transposon presence within the gene *SAUSA300_1845* (putative glutamate-1-semialdehyde aminotransferase), expected product size ~251 bp.

3.4.2 Effect of the disruption of the genes *SAUSA300_1916*, *SAUSA300_1614* and *SAUSA300_1845* on the growth of *S. aureus* in human serum and RPMI1640

The nutrient availability that bacteria encounter once infecting a host is different from what they encounter when growing *in vitro*, and the composition between serum and rich medium varies, for example, in the presence of serum proteins (albumins, globulins), and ions (Oogai et al., 2011). The effect of the disruption within the gene *SAUSA300_1916* (coding for a putative aspartate aminotransferase), and within the genes *SAUSA300_1614* and *SAUSA300_1845* (both coding for a putative glutamate-1-semialdehyde aminotransferase) on the *S. aureus* growth was evaluated in human serum and RPMI medium in order to determine their essentiality in both conditions. Growth in rich medium (TSB) was determined to see if the mutants showed any growth defect in this medium compared to the wild-type strain.

The metabolism of aspartate is linked to the TCA cycle and nitrogen assimilation, and it has been shown that its disruption causes growth defects (Jansen et al., 2020). A small colony variant phenotype, which is associated with a slow growth feature, has been found in strains having mutations in genes participating in the haem biosynthetic pathway like *hemA* (Hubbard et al., 2020) or *hemB* (Roggenkamp et al., 1998) in *E. coli* and, for example, within *hemB* in *S. aureus* (Kriegeskorte et al., 2014). Since the gene products of *SAUSA300_1916*, *SAUSA300_1614* and *SAUSA300_1845* are predicted to be involved in the metabolism of both, aspartate and haem, it was hypothesised that the disruption within those genes would result in an impaired growth in both, serum and RPMI medium.

The results showed that in rich medium (TSB) no growth defect was observed in any of the strains tested, neither in the mutants created in the USA300 background nor in the LS-1 genetic background (Figure 3.7). These results were also analysed by the Growthcurver package, which showed no significant differences between the mutants and their respective wild-type strains in metrics like carrying capacity, growth rate, doubling time, or area under the curve, this latter considered as one of the most important

metrics given by Growthcurver since it summarizes the relevant metrics involved in a population growth (Sprouffske & Wagner, 2016) (Table 3.5 and Table 3.6).

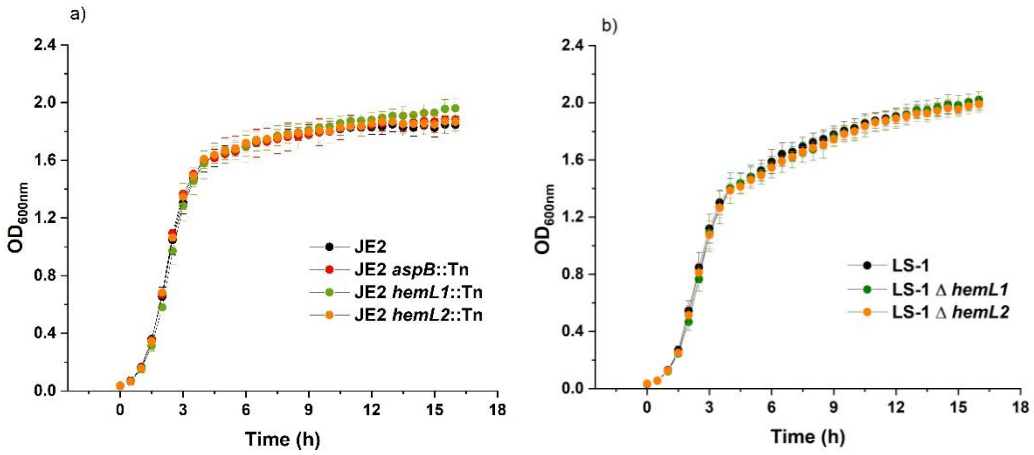

Figure 3.7 - Growth curves of the *S. aureus* strains in TSB.

The USA300 and LS-1 strains were grown in TSB in 96-well plates at 37°C and the OD_{600nm} readings measured over a 16-hour period. a) Growth curve of the USA300 strains and b) growth curve of the LS-1 strains. The data represents the average of the OD_{600nm} values ± standard deviation from three independent biological replicates.

Table 3.5. Comparison of the metrics obtained from Growthcurver for the *S. aureus* USA300 strains grown in TSB.

The growth curves were performed in TSB at 37°C for 16 h. The data were analysed by one-way ANOVA, Tukey post hoc test ($P < 0.05$) and expressed as the mean ± standard deviation of three independent experiments. No significant differences were found between the wild-type strain in comparison to each of the mutants evaluated.

Parameter	JE2	JE2 *aspB*::*Tn*	JE2 *hemL1*::*Tn*	JE2 *hemL2*::*Tn*
Initial population size (N_0)	0.05 ± 0.01	0.04 ± 0.02	0.05 ± 0.02	0.04 ± 0.01
Carrying capacity (k)	1.75 ± 0.05	1.76 ± 0.07	1.80 ± 0.04	1.75 ± 0.06
Growth rate (r)	1.52 ± 0.18/min	1.57 ± 0.23/min	1.45 ± 0.28/min	1.58 ± 0.14/min
Doubling time (dt)	0.46 ± 0.05	0.45 ± 0.08	0.49 ± 0.09	0.44 ± 0.04
Area under the curve (auc)	23.77 ± 0.59	23.97 ± 1.02	24.16 ± 0.70	23.87 ± 0.81

Table 3.6. Comparison of the metrics obtained from Growthcurver for the *S. aureus* LS-1 strains grown in TSB.

The growth curves were performed in TSB at 37°C for 24 h. The data were analysed by one-way ANOVA, Tukey post hoc test ($P < 0.05$) and expressed as the mean ± standard deviation of three independent experiments. No significant differences were found between the wild-type strain in comparison to each of the mutants evaluated.

Parameter	LS-1	LS-1 Δ*hemL1*	LS-1 Δ*hemL2*
Initial population size (N_0)	0.12 ± 0.02	0.11 ± 0.03	0.11 ± 0.03
Carrying capacity (k)	1.82 ± 0.04	1.83 ± 0.05	1.81 ± 0.07
Growth rate (r)	0.91 ± 0.15/min	0.93 ± 0.19/min	0.91 ± 0.16/min
Doubling time (dt)	0.78 ± 0.13	0.77 ± 0.14	0.78 ± 0.13
Area under the curve (auc)	23.50 ± 0.86	23.49 ± 0.70	23.28 ± 0.41

The growth of the strains in human serum showed a growth impairment in the mutant strains in the USA300 genetic background compared with the wild-type strain. The growth of *S. aureus* wild-type strain (JE2) in serum reached a maximum OD_{600nm} of 0.16 following 24 h of incubation while the JE2 *aspB*::*Tn* strain reached an OD_{600nm} of 0.11 showing a marked growth defect (Figure 3.8). These results were consistent with the data obtained from the analysis of the microbial growth curves using Growthcurver showing that the growth rate of this mutant was significantly lower than that of the wild-type strain (Table 3.7). As mentioned above, an important metric given by Growthcurver is the area under the curve which in a unique parameter integrates information about the initial population size, carrying capacity, and growth rate of a strain (Sprouffske & Wagner, 2016). The JE2 *aspB*::*Tn* strain showed a 1.6 times decrease in the area under the curve compared to the value obtained for the wild-type strain (Table 3.7). Similarly, the *hemL* mutants in the USA300 genetic background showed a growth defect in serum even though it was not as marked as in the JE2 *aspB*::*Tn* strain (Figure 3.8). Both strains,

JE2 *hemL1*::*Tn* and JE2 *hemL2*::*Tn*, showed a significant decrease in all the metrics obtained by Growthcurver compared to the wild-type strain (Table 3.7). The *hemL* mutants in the LS-1 genetic background did not show significant differences in comparison to the wild-type strain in any of the metrics obtained by Growthcurver (Table 3.8).

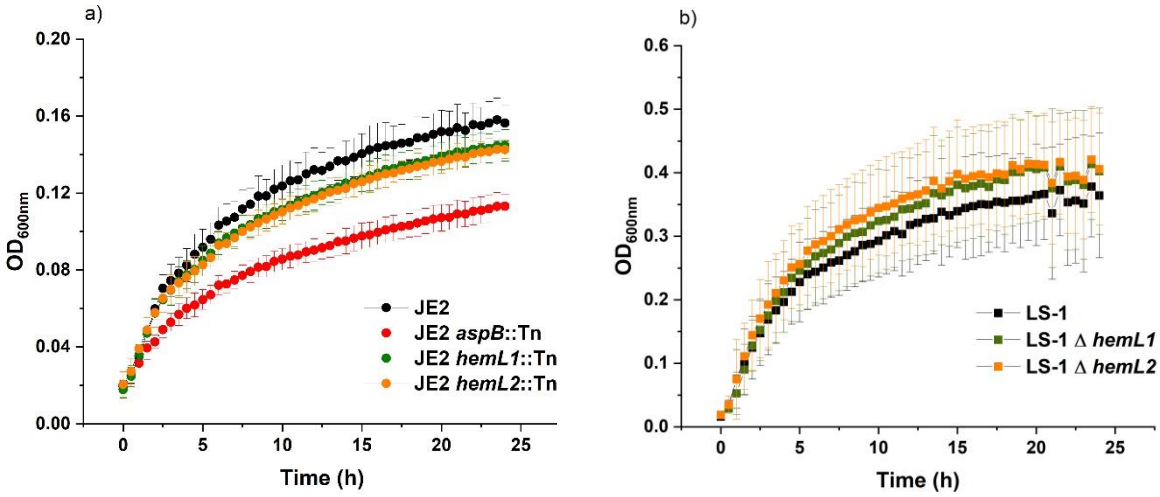

Figure 3.8 - Growth curves of the *S. aureus* strains in human serum.

The USA300 and LS-1 strains were grown in human serum in 96-well plates at 37°C and the OD_{600nm} readings measured over a 24-hour period. a) Growth curve of the USA300 strains and b) growth curve of the LS-1 strains. The data represents the average of the OD_{600nm} values ± standard deviation from three independent biological replicates.

Table 3.7. Comparison of the metrics obtained from Growthcurver for the *S. aureus* USA300 strains grown in human serum.

The growth curves were performed in human serum at 37°C for 24 h. The data were analysed by one-way ANOVA, Tukey post hoc test ($P < 0.05$) and expressed as the mean ± standard deviation of three independent experiments. Significance was as follows: *$P < 0.05$, **$P < 0.01$, ***$P < 0.001$, ****$P < 0.0001$ indicating the differences between the wild-type strain compared to each of the mutants evaluated.

Parameter	JE2	JE2 *aspB*::*Tn*	JE2 *hemL1*::*Tn*	JE2 *hemL2*::*Tn*
Initial population size (N_0)	0.02 ± 0.0	0.02 ± 0.0	0.02 ± 0.0	0.02 ± 0.0
Carrying capacity (k)	0.13 ± 0.01	0.09 ± 0.01*	0.12 ± 0.01*	0.12 ± 0.01*
Growth rate (r)	0.31 ± 0.02/min	0.26 ± 0.01*/min	0.29 ± 0.02*/min	0.28 ± 0.01*/min
Doubling time (dt)	2.23 ± 0.12	2.64 ± 0.12*	2.44 ± 0.14*	2.52 ± 0.08*
Area under the curve (auc)	2.42 ± 0.23	1.55 ± 0.09*	2.21 ± 0.13*	2.11 ± 0.10*

Table 3.8. Comparison of the metrics obtained from Growthcurver for the *S. aureus* LS-1 strains grown in human serum.

The growth curves were performed in human serum at 37°C for 24 h. The data were analysed by one-way ANOVA, Tukey post hoc test ($P < 0.05$) and expressed as the mean ± standard deviation of three independent experiments. No significant difference was found between the wild-type strain in comparison to each of the mutants evaluated.

Parameter	LS-1	LS-1 Δ*hemL1*	LS-1 Δ*hemL2*
Initial population size (N_0)	0.06 ± 0.03	0.06 ± 0.02	0.06 ± 0.03
Carrying capacity (k)	0.34 ± 0.07	0.37 ± 0.09	0.38 ± 0.08
Growth rate (r)	0.36 ± 0.07/min	0.37 ± 0.05/min	0.41 ± 0.09/min
Doubling time (dt)	1.98 ± 0.37	1.92 ± 0.27	1.78 ± 0.42
Area under the curve (auc)	6.42 ± 1.40	6.99 ± 1.85	7.34 ± 1.64

The results obtained from the growth curves of the strains in human serum showed that although the USA300 mutant strains had an impaired growth, the genes coding for a putative aspartate aminotransferase and a putative glutamate-1-semialdehyde aminotransferase, were not essential for the growth of *S. aureus* in this media under the assessed conditions.

The effect of the mutations in the genes *SAUSA300_1916*, *SAUSA300_1614* and *SAUSA300_1845* in growth was also assessed in the RPMI1640 medium, which is a synthetic medium that mimics the plasma composition. The JE2 *aspB*::*Tn* strain showed a total inhibition of growth in the complete formulation of RPMI following 24 h of incubation (Figure 3.9). The JE2 *hemL2*::*Tn* strain showed a similar growth pattern as that of the wild-type strain during the whole incubation period, while the JE2 *hemL1*::*Tn* strain started to show a growth impairment after ~ 8 h of incubation (Figure 3.9). These results are consistent with the metrics obtained from Growthcurver that shown a significant decrease in two out of the five parameters studied (carrying capacity and area under the curve) for the JE2 *hemL1*::*Tn* strain compared to those of the wild-type strain (Table 3.9). The *hemL* mutants in the LS-1 genetic background showed a similar growth pattern than that of the wild-type strain in the complete formulation of RPMI (Figure 3.9). Although the metrics obtained from Growthcurver for the LS-1 Δ *hemL1* mutant showed a significant increase in the parameter corresponding to the initial population size compared to the wild-type, it did not seem to affect the overall growth of the strain since the value for the metric area under the curve did not show any significant variation compared to that of the wild-type strain (Table 3.10).

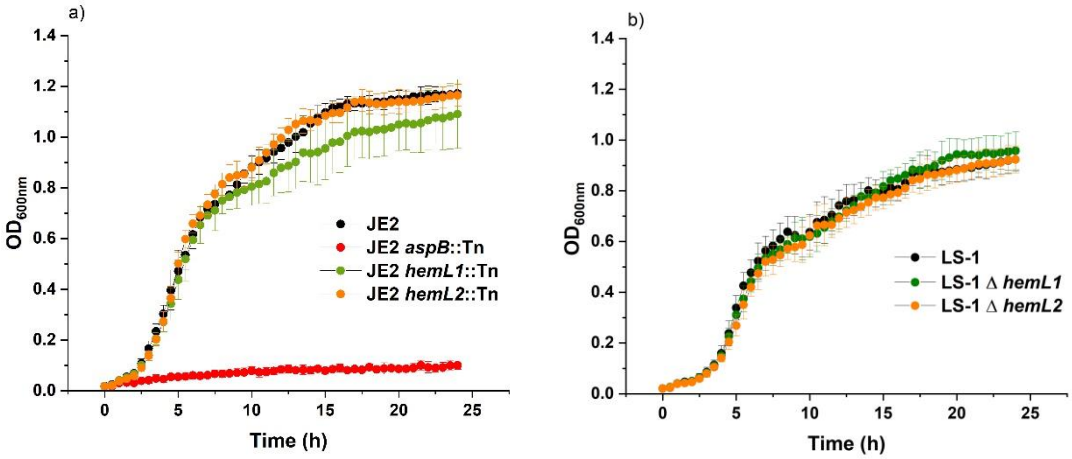

Figure 3.9 - Growth curves of the *S. aureus* strains in RPMI complete formulation.

The USA300 and LS-1 strains were grown in RPMI complete formulation in 96-well plates at 37°C and the OD_{600nm} readings measured over a 24-hour period. a) Growth curve of the USA300 strains and b) growth curve of the LS-1 strains. The data represents the average of the OD_{600nm} values ± standard deviation from three independent biological replicates.

Table 3.9. Comparison of the metrics obtained from Growthcurver for the *S. aureus* USA300 strains grown in RPMI complete formulation.

The growth curves were performed in RPMI complete formulation at 37°C for 24 h. The data were analysed by one-way ANOVA, Tukey post hoc test ($P < 0.05$) and expressed as the mean ± standard deviation of three independent experiments. Significance was as follows: *$P < 0.05$, **$P < 0.01$, ***$P < 0.001$, ****$P < 0.0001$ indicating the differences between the wild-type strain compared to each of the mutants evaluated.

Parameter	JE2	JE2 *aspB*::*Tn*	JE2 *hemL1*::*Tn*	JE2 *hemL2*::*Tn*
Initial population size (N_0)	0.07 ± 0.01	0.01 ± 0.001*	0.06 ± 0.02	0.06 ± 0.02
Carrying capacity (k)	1.12 ± 0.03	N/D	1.00 ± 0.11*	1.10 ± 0.03
Growth rate (r)	0.41 ± 0.04/min	N/D	0.46 ± 0.09*/min	0.48 ± 0.04/min
Doubling time (dt)	1.69 ± 0.18	N/D	1.55 ± 0.24	1.45 ± 0.13
Area under the curve (auc)	19.32 ± 0.65	N/D	17.69 ± 1.83*	19.51 ± 0.70

Table 3.10. Comparison of the metrics obtained from Growthcurver for the *S. aureus* LS-1 strains grown in RPMI complete formulation.

The growth curves were performed in RPMI complete formulation at 37°C for 24 h. The data were analysed by one-way ANOVA, Tukey post hoc test ($P < 0.05$) and expressed as the mean ± standard deviation of three independent experiments. Significance was as follows: *$P < 0.05$, **$P < 0.01$, ***$P < 0.001$, ****$P < 0.0001$ indicating the differences between the wild-type strain compared to each of the mutants evaluated.

Parameter	LS-1	LS-1 Δ*hemL1*	LS-1 Δ*hemL2*
Initial population size (N_0)	0.04 ± 0.01	0.06 ± 0.01*	0.05 ± 0.01
Carrying capacity (k)	0.85 ± 0.04	0.90 ± 0.05*	0.85 ± 0.04
Growth rate (r)	0.46 ± 0.09/min	0.35 ± 0.03*/min	0.39 ± 0.06*/min
Doubling time (dt)	1.59 ± 0.36	2.00 ± 0.17*	1.82 ± 0.31
Area under the curve (auc)	14.53 ± 0.92	14.55 ± 0.94	13.97 ± 0.87

The JE2 *aspB*::*Tn* strain showed a growth inhibition in the complete formulation of RPMI and to examine which could be the amino acid responsible for this effect, if any, growth curves in RPMI without cystine, methionine and glutamine were performed as a starting point. No growth recovery was observed in the JE2 *aspB*::*Tn* mutant in RPMI medium without cystine or methionine (Figure 3.10). Glutamine provides metabolic intermediates for the synthesis of macromolecules and its metabolism includes the formation of glutamate with the concomitant production of ammonium (NH_4^+) that can be used for the synthesis of purine and pyrimidines (D. C. de Oliveira et al., 2016).

The glutamine concentration in the complete formulation of RPMI (Cat. N°8758, Sigma) is 0.3 g/L while the concentration of glutamate is 0.02 g/L, and it was hypothesised that the excess of glutamine in this medium might prevent the growth of the cell without a functional aspartate aminotransferase that would allow nitrogen assimilation.

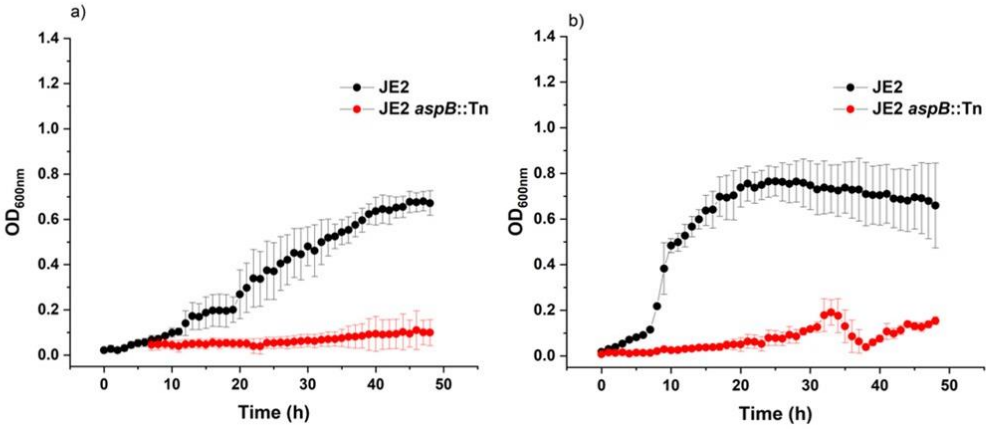

Figure 3.10 - Growth curves of *S. aureus* JE2 and JE2 *aspB*::*Tn* strains in RPMI without cystine and without methionine.

The wild-type and mutant strains of *S. aureus* were grown in RPMI without cystine (a) and without methionine (b) in 96-well plates at 37°C and the OD_{600nm} readings measured over a 48-hour period. The data represents the average of the OD_{600nm} values ± standard deviation from three independent biological replicates.

In fact, the removal of glutamine allowed the growth of the JE2 *aspB*::*Tn* mutant strain, which was able to grow to the JE2 wild-type level (Figure 3.11). Although the initial population size of this mutant obtained by Growthcurver was significantly lower than that of the wild-type strain (0.03 ± 0.01 and 0.07 ± 0.01 respectively), their corresponding metrics for the area under the curve did not show any significant difference when compared to those of the wild-type strain (Table 3.11). Similar to what was observed in the growth of the JE2 *hemL* mutants in the complete formulation of RPMI, the JE2 *hemL1*::*Tn* strain showed a growth impairment in RPMI medium without glutamine (Figure 3.11). The lack of glutamine in the medium gave a lower value for the metric of initial population (N_0) for the JE2 *hemL* mutants compared to the wild-type strain (Table 3.11) and compared to those values obtained for the growth in complete RPMI. It is worth mentioning that all strains were adjusted to the same values of optical densities at the beginning of the experiment. These discrepancies between the initial population size of the mutants grown in RPMI complete formulation and RPMI lacking glutamine were not observed for the JE2 strain, since the values for its metric were the same (0.07 ± 0.01)

in both media, implying that the lack of glutamine in the medium was affecting that metric for the *hemL* mutants only. By contrast, the LS-1 Δ *hemL1* and LS-1 Δ *hemL2* mutants had a similar growth pattern compared to the LS-1 wild-type strain (Figure 3.11) with no significant difference in metrics like growth rate, doubling time or area under the curve (Table 3.12).

The results obtained from the growth curves of the strains in RPMI complete formulation showed that the disruption of the gene coding a putative aspartate aminotransferase leads to growth inhibition, which can be reverted by removing the amino acid glutamine from the medium.

Although there were differences in the growth pattern between the JE2 *hemL*(s) mutant strains grown in RPMI complete formulation and RPMI without glutamine, the genes coding for a putative glutamate-1-semialdehyde aminotransferase were not essential for the growth of *S. aureus* in these media.

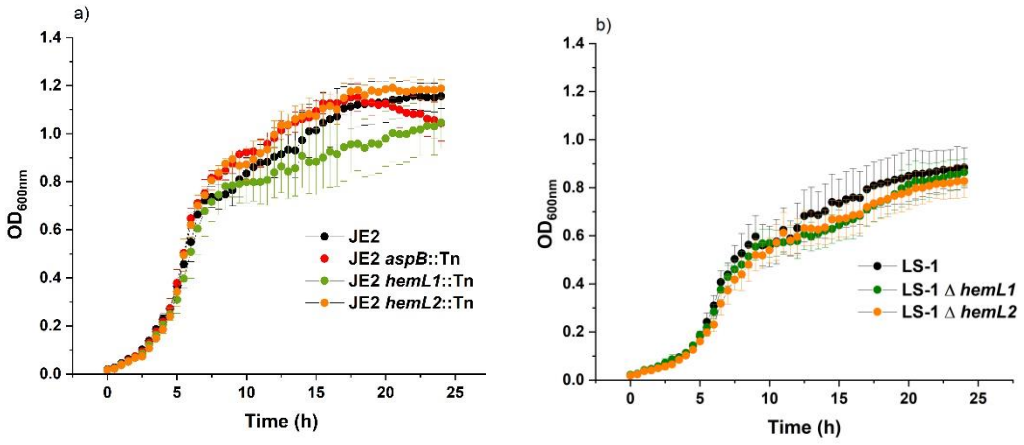

Figure 3.11 - Growth curves of the *S. aureus* strains in RPMI lacking glutamine.

The USA300 and LS-1 strains were grown in RPMI lacking glutamine in 96-well plates at 37°C and the $OD_{600\ nm}$ readings measured over a 24-hour period. a) Growth curve of the USA300 strains and b) growth curve of the LS-1 strains. The data represents the average of the OD_{600nm} values ± standard deviation from three independent biological replicates.

Table 3.11. Comparison of the metrics obtained from Growthcurver for the *S. aureus* USA300 strains grown in RPMI lacking glutamine.

The growth curves were performed in RPMI lacking glutamine at 37°C for 24 h. The data were analysed by one-way ANOVA, Tukey post hoc test ($P < 0.05$) and expressed as the mean ± standard deviation of three independent experiments. Significance was as follows: *$P < 0.05$, **$P < 0.01$, ***$P < 0.001$, ****$P < 0.0001$ indicating the differences between the wild-type strain compared to each of the mutants evaluated.

Parameter	JE2	JE2 *aspB*::*Tn*	JE2 *hemL1*::*Tn*	JE2 *hemL2*::*Tn*
Initial population size (N_0)	0.07 ± 0.01	0.03 ± 0.01*	0.03 ± 0.01*	0.04 ± 0.01*
Carrying capacity (k)	1.09 ± 0.08	1.07 ± 0.06	0.93 ± 0.12*	1.12 ± 0.05
Growth rate (r)	0.40 ± 0.04/min	0.60 ± 0.07*/min	0.58 ± 0.05*/min	0.51 ± 0.02*/min
Doubling time (dt)	1.77 ± 0.19	1.18 ± 0.13*	1.20 ± 0.11*	1.36 ± 0.06*
Area under the curve (auc)	18.42 ± 1.49	19.05 ± 0.69	16.53 ± 2.04*	19.51 ± 0.82

Table 3.12. Comparison of the metrics obtained from Growthcurver for the *S. aureus* LS-1 strains grown in RPMI lacking glutamine.

The growth curves were performed in RPMI lacking glutamine at 37°C for 24 h. The data were analysed by one-way ANOVA, Tukey post hoc test ($P < 0.05$) and expressed as the mean ± standard deviation of three independent experiments. Significance was as follows: *$P < 0.05$, **$P < 0.01$, ***$P < 0.001$, ****$P < 0.0001$ indicating the differences between the wild-type strain compared to each of the mutants evaluated.

Parameter	LS-1	LS-1 Δ*hemL1*	LS-1 Δ*hemL2*
Initial population size (N_0)	0.04 ± 0.01	0.05 ± 0.01	0.03 ± 0.01
Carrying capacity (k)	0.82 ± 0.08	0.78 ± 0.06	0.76 ± 0.06*
Growth rate (r)	0.37 ± 0.07/min	0.33 ± 0.06/min	0.39 ± 0.05/min
Doubling time (dt)	1.93 ± 0.43	2.16 ± 0.39	1.83 ± 0.29
Area under the curve (auc)	13.03 ± 1.60	12.10 ± 1.01	11.90 ± 1.19

3.4.3 Effect of the disruption of the genes *SAUSA300_1916*, *SAUSA300_1614* and *SAUSA300_1845* on biofilm formation of *S. aureus*

Biofilm formation allows bacteria to resist the antimicrobial treatment and to evade the host defences and *S. aureus* has the capacity to form biofilms that are stimulated by the addition of glucose into the media (E. O'Neill et al., 2008). Genes coding aminotransferase enzymes involved in the central metabolism such as a putative 4-aminobutyrate aminotransferase and a putative aspartate aminotransferase have been shown to be overexpressed during *S. aureus* biofilm formation (Beenken et al., 2004) indicating that those enzymes might have a role during the development of the biofilm. The role of haem metabolism in the biofilm formation of *S. aureus* is not well understood, however, a study showed that a *hemL* mutant strain had an altered morphology of the macrocolony of *S. aureus* when compared to that of the wild-type strain (Wermser & Lopez, 2018). This suggests that the enzymes involved in the metabolic pathway of haem might have a role in the biofilm formation of *S. aureus*. In this context, the role of the proteins coded by the genes *SAUSA300_1916*, *SAUSA300_1845* and *SAUSA300_1614* in the biofilm formation of *S. aureus* was evaluated in BHI medium supplemented with 1% glucose under static conditions and quantified using the crystal violet staining method.

The disruption in *aspB* (*SAUSA300_1916*) coding for a putative aspartate aminotransferase showed no difference in the biofilm formation between the wild-type and the mutant strains under the conditions evaluated (Figure 3.12). Similarly, the disruption in *hemL1* (*SAUSA300_1614*) and *hemL2* (*SAUSA300_1845*), both coding putative glutamate-1-semialdehyde aminotransferases did not show a significant difference in the capacity to form biofilm compared to the wild-type strain (Figure 3.12) in BHI medium supplemented with glucose. The same assay was performed using the mutant strains for the *hemL1* and *hemL2* genes created in the LS-1 genetic background to detect if the deletion of those genes would have an effect in the biofilm formation capacity of *S. aureus*. The results showed a significant decrease in the biofilm capacity of the LS-1 Δ*hemL1* ($P < 0.05$) and no difference in the biofilm capacity of LS-1 Δ*hemL2* when compared to the wild-type strain (Figure 3.13). The results of the biofilm assays showed that the disruption in the genes *SAUSA300_1916*, *SAUSA300_1614* and

SAUSA300_1845 had no effect in the biofilm formation of the *S. aureus* USA300 strain under the conditions tested.

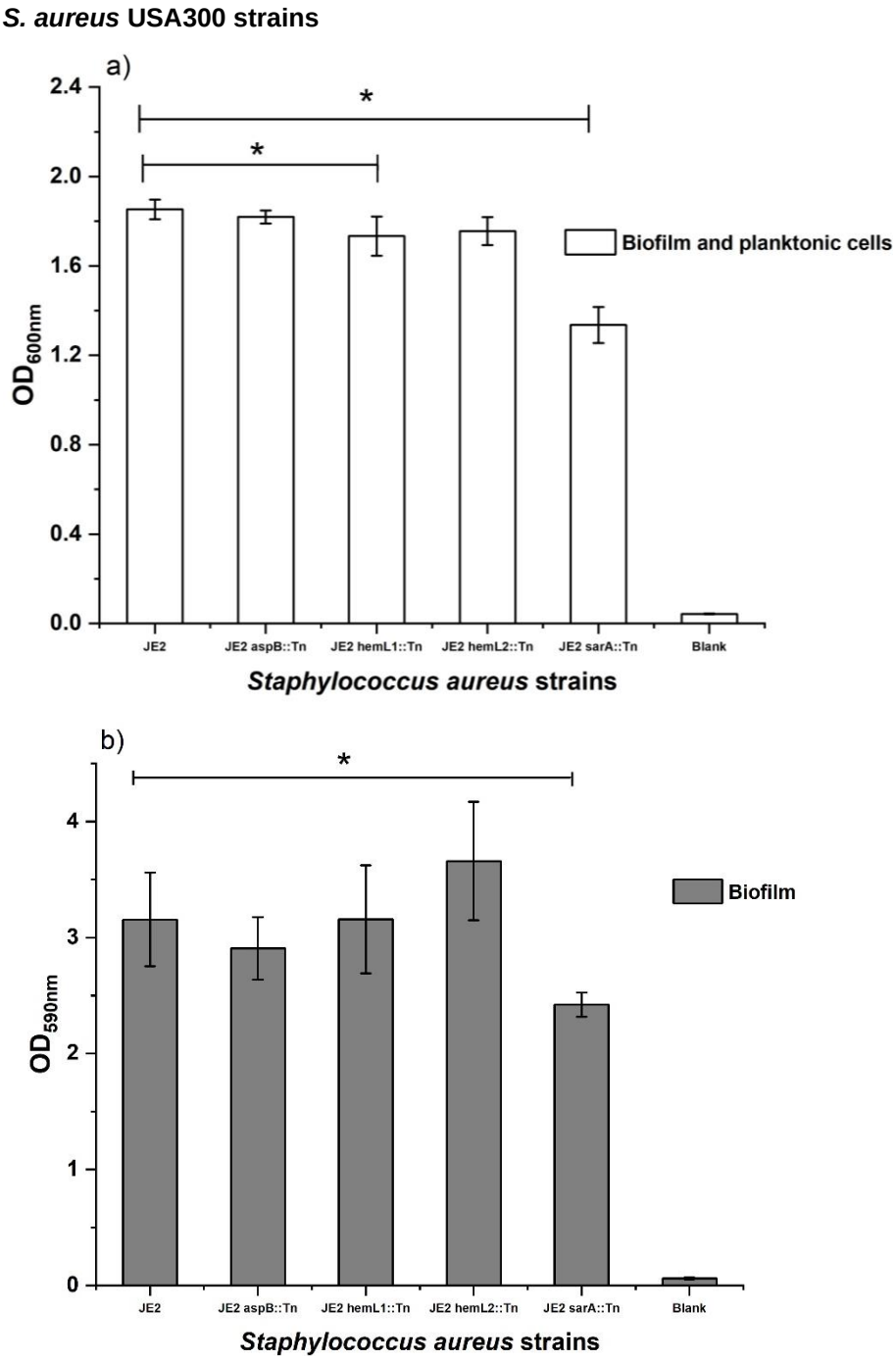

Figure 3.12 - Biofilm formation by *S. aureus* USA300 strains.

The biofilm formation was evaluated after 24 h of static incubation in BHI + 1% glucose at 37°C. The OD of the planktonic and biofilm phases was measured at 600 nm (a). The biofilm quantification was performed using the crystal violet staining method and its measurement was performed at 590 nm (b). The data was analysed by one-way ANOVA, Bonferroni post hoc test ($P < 0.05$) and expressed as the mean ± standard deviation of three independent experiments.

***S. aureus* LS-1 strains**

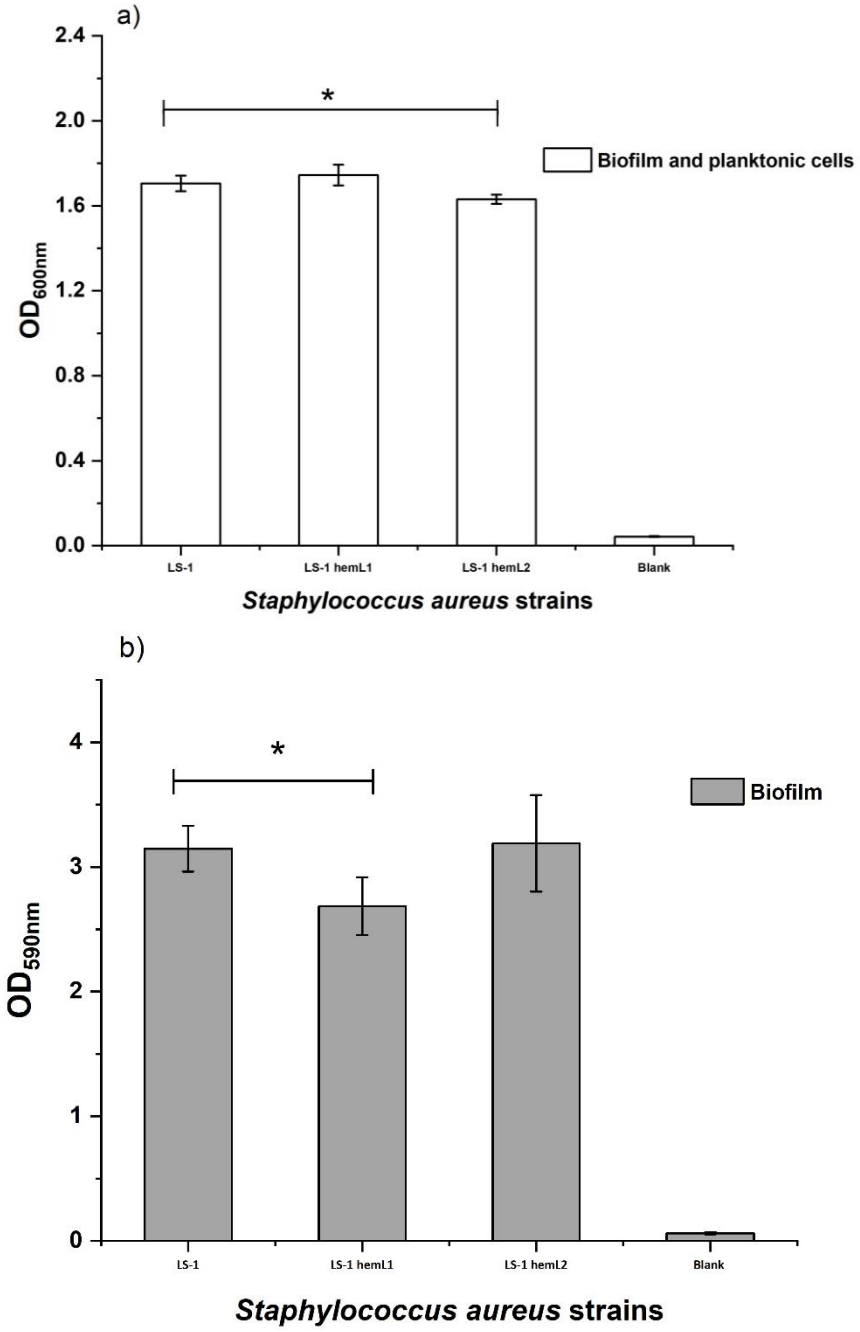

Figure 3.13 - Biofilm formation by *S. aureus* LS-1 strains.

The biofilm formation was evaluated after 24 h of static incubation in BHI + 1% glucose at 37°C. The OD of the planktonic and biofilm phases was measured at 600 nm (a). The biofilm quantification was performed using the crystal violet staining method and its measurement was performed at 590 nm (b). The data was analysed by one-way ANOVA, Bonferroni post hoc test ($P < 0.05$) and expressed as the mean ± standard deviation of three independent experiments.

3.4.4 Effect of the disruption of the genes *SAUSA300_1916*, *SAUSA300_1614* and *SAUSA300_1845* on virulence of *S. aureus* in a *Galleria mellonella* larvae model

The importance of a putative aspartate aminotransferase for the virulence of *S. aureus* was published in a study after screening a transposon mutant library to identify essential genes for virulence in a murine model of systemic infections. The study found a 1,000-fold reduction in the virulence in a competitive infection assay (mutant strain mixed with the wild-type strain) of a strain that had disrupted the gene coding for a putative aspartate aminotransferase (*aspB*) (Benton et al., 2004). This finding was supported by another study where the authors identified the gene coding for a putative aspartate aminotransferase (*SAOUHSC_02158*) as essential for its fitness in a murine infection model (Valentino et al., 2014).

It has also been described that a putative glutamate-1-semialdehyde aminotransferase (coded by *SAOUHSC*_02000, corresponding to *SAUSA300_1845* in USA300_FPR3757) was essential for the fitness of *S. aureus* in a murine abscess model (Valentino et al., 2014), which suggests that the strains having disruptions in the genes *SAUSA300_1614* and *SAUSA300_1845*, coding a putative glutamate-1-semialdehyde aminotransferase, would be important for the virulence of the pathogen.

The role in virulence of the strains having disrupted the genes *SAUSA300_1916*, *SAUSA300_1614* and *SAUSA300_1845* was evaluated using a *G. mellonella* infection model. The larvae were inoculated with 10^5 CFU/larvae through parenteral injection, incubated at 37°C, and their survival was monitored over a period of either 4 or 7 days depending on the strain. The survival rates of the larvae infected with the strains showed a decrease in virulence of the strain with the transposon inserted within the gene *SAUSA300_1916* (JE2 *aspB*::*Tn*) coding for a putative aspartate aminotransferase (AspB) when compared to the wild-type strain (Figure 3.14), thus showing a decreased virulence in this model, similar to what was found with the mutant strain for a putative aspartate aminotransferase in the murine model mentioned above. Similarly, the

disruption of the genes *hemL1* (*SAUSA300_1614*) and *hemL2* (*SAUSA300_1845*) showed a significant decrease in virulence when compared to the wild-type strain (Figure 3.15). After 1 day of incubation all the larvae infected with the wild-type strain were found dead, while 100% larval death was observed after 2 days for the *SAUSA300_1614* (JE2 *hemL1*::*Tn*) strain and after 4 days for the *SAUSA300_1845* (JE2 *hemL2*::*Tn*) strain. The effect of the disruption of the *hemL* genes in the virulence of *S. aureus* was also evaluated in the LS-1 genetic background giving similar results to those observed in the USA300 genetic background (Figure 3.16). The larvae infected with both, LS-1 Δ*hemL1* and LS-1 Δ*hemL2* showed a 100% killing after 4 days of infection while the LS-1 wild-type showed a 100% larval death after 2 days of infection. Taken together these results highlight the importance of the three putative aminotransferases for *S. aureus* virulence in the *G. mellonella* infection model.

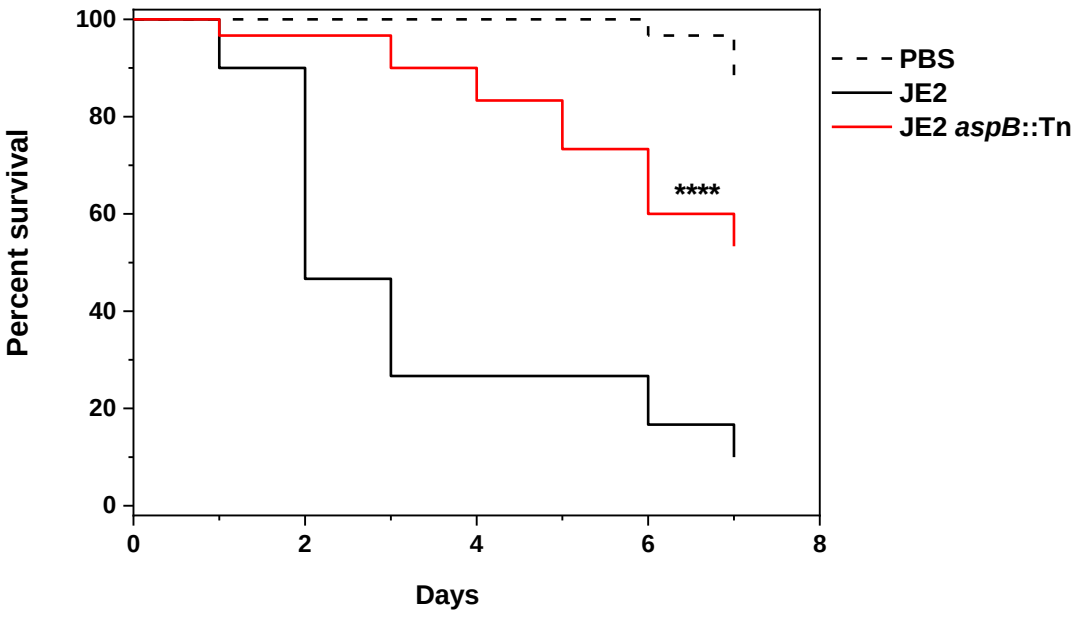

Figure 3.14 - Effect of the disruption within the gene *aspB* coding a putative aspartate aminotransferase in the virulence *of S. aureus* in *G. mellonella* model.

The Kaplan-Meier plot indicates the viability of *Galleria* larvae over a period of 7 days after infection with the wild-type (JE2) and mutant (JE2 *aspB*::*Tn*) strains at 10^5 CFU/larva. PBS injected larvae were included as negative control. The data are derived from three independent experiments with groups of 10 larvae (n = 30). *, P < 0.05; **, P < 0.01; ***, P < 0.001; and ****, P < 0.0001 as determined by log-rank test when comparing the survival of the larvae infected with the wild-type and the mutant strains.

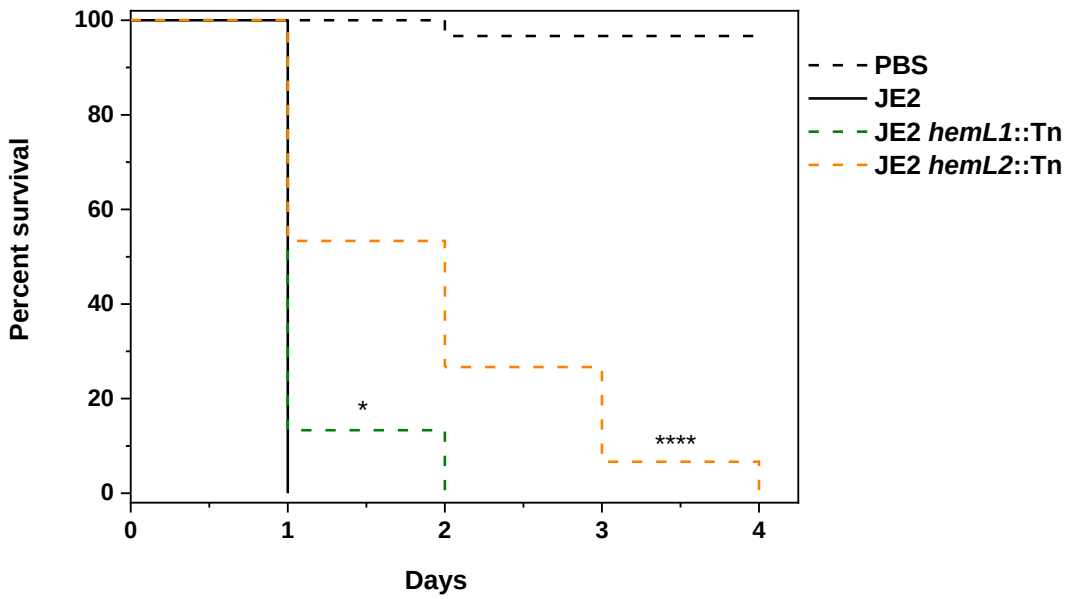

Figure 3.15 - Effect of the disruption within the genes *hemL1* and *hemL2* coding putative glutamate-1-semialdehyde aminotransferases in the virulence of *S. aureus* in *G. mellonella* model.

The Kaplan-Meier plot indicates the viability of Galleria larvae over a period of 4 days after infection with the wild-type (JE2) and mutants for *hemL1* (JE2 *hemL1*::*Tn*) and for *hemL2* (JE2 *hemL2*::*Tn*) strains at 10^5 CFU/larva. PBS injected larvae were included as negative control. The data are derived from three independent experiments with groups of 10 larvae (n = 30). *, P < 0.05; **, P < 0.01; ***, P < 0.001; and ****, P < 0.0001 as determined by log-rank test when comparing the survival of the larvae infected with the wild-type and each of the mutant strains.

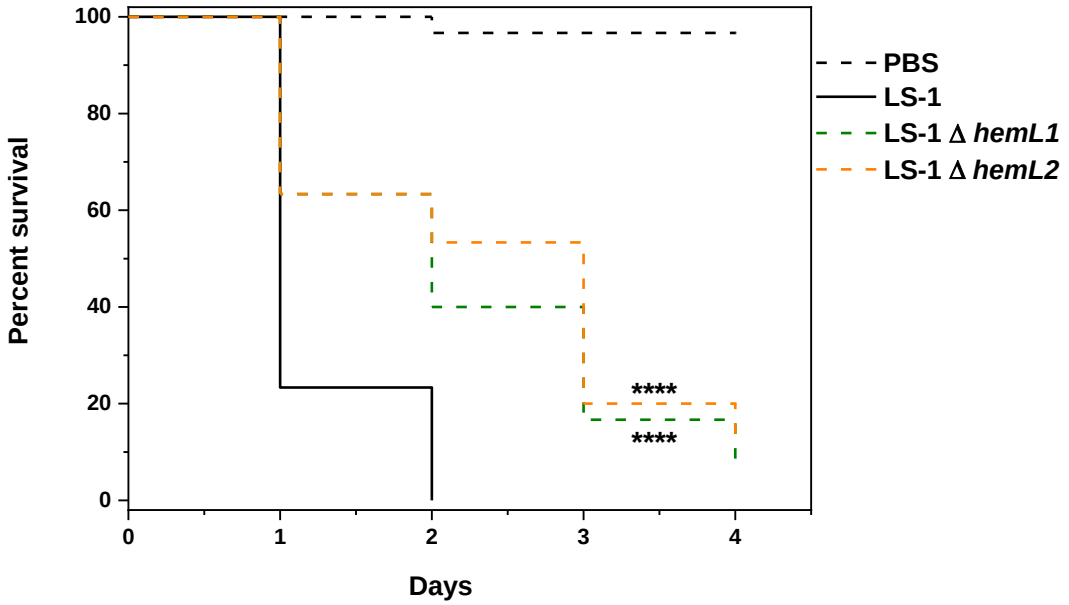

Figure 3.16 - Effect of the gene deletion of *hemL1* and *hemL2* coding putative glutamate-1-semialdehyde aminotransferases in the virulence of *S. aureus* in *G. mellonella* model.

The Kaplan-Meier plot indicates the viability of *Galleria* larvae over a period of 4 days after infection with the wild-type (LS-1) and mutant for *hemL1* (LS-1 Δ*hemL1*) and for *hemL2* (LS-1 Δ*hemL2*) strains at 10^5 CFU/larva. PBS injected larvae were included as negative control. The data are derived from three independent experiments with groups of 10 larvae (n = 30). *, P < 0.05; **, P < 0.01; ***, P < 0.001; and ****, P < 0.0001 as determined by log-rank test when comparing the survival of the larvae infected with the wild-type and each of the mutant strains.

3.4.5 Evaluation of planarians as a model to study survival and colonisation of *S. aureus*

Planarians have been used as a model organism to study mainly the molecular basis of tissue regeneration, but other phenomenon like host-pathogen interaction, specifically the mechanisms involved in bacterial clearance, and the function and assemble of motile cilia have also been studied using planarian models. In this study, the feasibility of a planarian model to study colonisation and survival of *S. aureus* was evaluated by challenging planarians through bacterial feeding and media infections.

The *S. aureus* strain selected to evaluate this model was the strain having a disruption in the gene *SAUSA300_1916*, which codes a putative aspartate aminotransferase, since it has been reported that mutants defective for the gene coding this putative enzyme in *S. aureus* showed growth attenuation in a mouse model (Benton et al., 2004) and a survival defect in a murine osteomyelitis infection model (Potter et al., 2020), which makes it suitable to test it in this this model for defectiveness in colonisation and survival.

Firstly, planarians were infected by mixing their food with a bacterial pellet adjusted to either 10^8 or 10^9 CFU/group. Planarians fed with 10^8 CFU/group showed similar bacterial burden at the start of the experiment, and an average of $4.1x10^7$ CFU/5 worms and $4.9 x10^7$ CFU/5 worms were determined for those infected with the wild-type strain and the mutant strain, respectively (Figure 3.17). From day 1 onwards, a difference in bacterial loads could be seen between the wild-type and the mutant strains infected groups, with a steady decline in the bacterial loads resulting in a significant difference between the strains at the end of the experiment (4 dpi). The bacterial burden decreased by 1.5 $\log_{10}$ in the wild-type infected planarians and 2.2 $\log_{10}$ in the mutant strain for the *aspB* gene infected group, showing a significant defect in survival and colonisation compared with the wild-type strain. However, this difference could not be observed when planarians were fed with bacteria at 10^9 CFU/group (Figure 3.18). It is worth mentioning that no bacterial growth was observed from the non-infected group of planarians after plating out the homogenates of planarians onto mannitol salt agar plates.

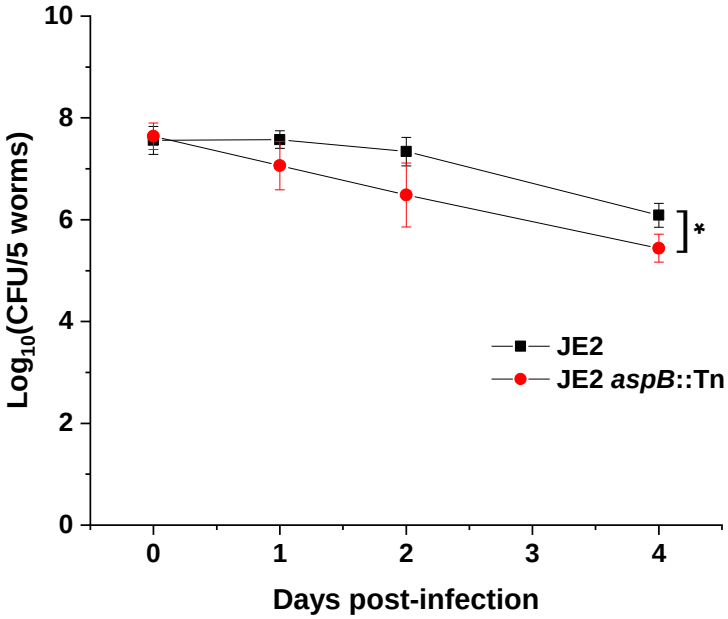

Figure 3.17 - Effect of the disruption within the *aspB* gene coding a putative aspartate aminotransferase in the colonisation of *S. aureus* in planarians.

A group of planarians belonging to *D. japonica* were infected through the food with the wild-type (JE2) and *aspB* mutant (JE2 *aspB*::*Tn*) strains at 10^8 CFU/group. CFU quantification was performed over a period of 4 days. PBS fed planarians were included as control. The data are derived from three independent experiments with groups of 20 planarians (n = 60). *, $P < 0.05$ as determined by the Mann-Whitney test in comparison to the planarians infected with the wild-type strain at day 4.

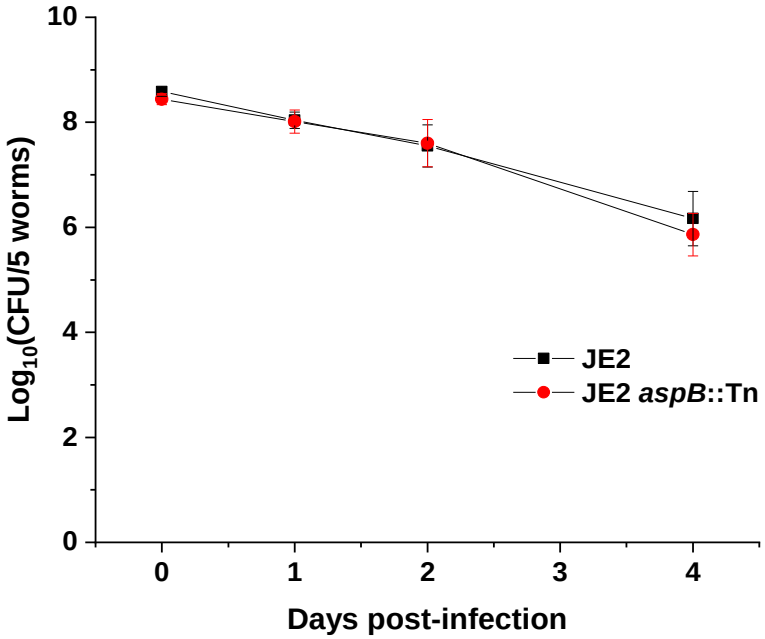

Figure 3.18 - Effect of the disruption within the *aspB* gene coding a putative aspartate aminotransferase in the colonisation of *S. aureus* in planarians.

A group of planarians belonging to *D. japonica* were infected through the food with the wild-type (JE2) and *aspB* mutant (JE2 *aspB*::*Tn*) strains at 10^9 CFU/group. CFU quantification was performed over a period of 4 days. PBS fed planarians were included as control. The data are derived from three independent experiments with group of 20 planarians (n = 60). No significant difference was determined by the Mann-Whitney test in comparison to the planarians infected with the wild-type strain at day 4.

Secondly, and in order to visualise differences in the survival of planarians or in the pathological progression of the infection between the strains, planarians were infected by adding specific bacterial numbers into their media with re-infection steps every 3 to 4 days and visually monitored over a determined period of time. The results showed a significant difference in survival between the planarians infected with the wild-type strain and the mutant strain for the gene coding a putative AspB when infected with 10^8 CFU/mL (Figure 3.19). No significant differences in survival were observed when planarians were infected with an inoculum of 10^9 CFU/mL of both strains (Figure 3.20). It is worth noticing that a highest bacterial concentration used to infect planarians led to a faster decrease in survival, but no significant differences were found between the worms infected with both strains.

According to Arnold and colleagues, planarians showed declining health after infection with *Vogesella*, *Chryseobacterium*, and *Pseudomonas* exhibiting a progression of clinical signs from posterior and anterior legions, head regression, partial lysis and finally a full lysis of the organism (Arnold et al., 2016). However, in this study no such progression could be observed after the infection of planarians with *S. aureus*. Although, different clinical signs of the infection were noticed according to the classification made by Arnold and colleagues, like anterior lesion, head regression (Figure 3.21) or full lysis, a clear and consistent pattern in the progression of the infection from normal to fully lysed planarians could not be observed.

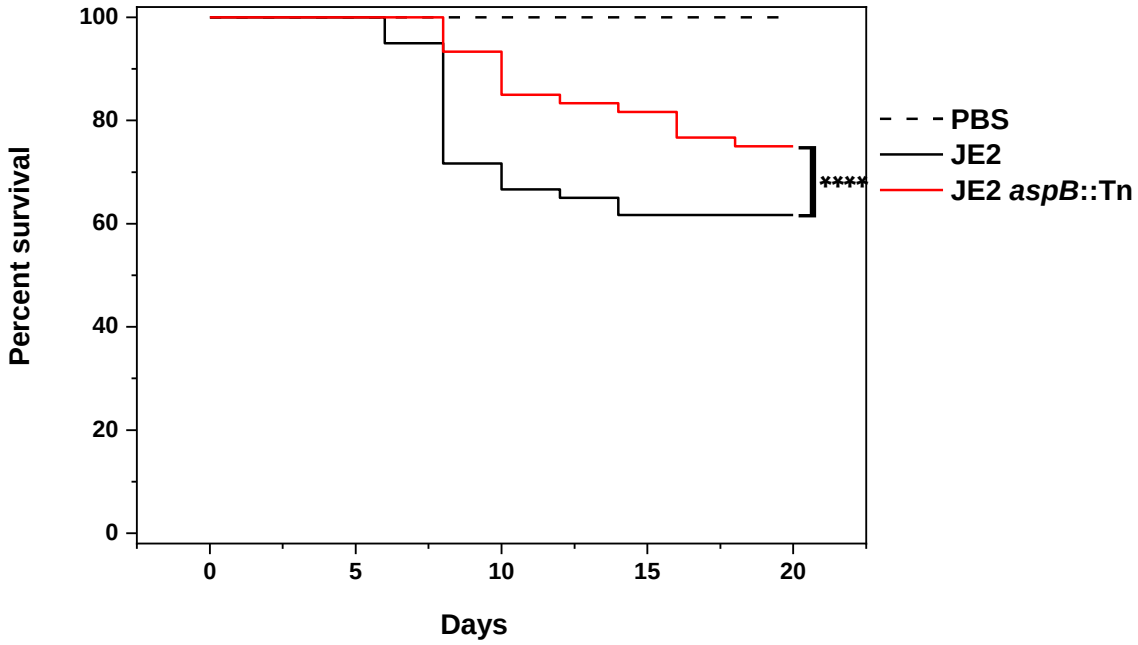

Figure 3.19 - Effect of the disruption of the *aspB* gene coding a putative aspartate aminotransferase in *S. aureus* in planarians survival.

A group of planarians belonging to *D. japonica* were infected with the wild-type strain (JE2) at 6.7 x10^8 CFU/mL or with the mutant strain for the *aspB* gene (JE2 *aspB::Tn*) at 5.9 x10^8 CFU/mL. The Kaplan-Meier plot indicates the viability of planarians over a period of 20 days post-infection. Planarian exposed to PBS were included as control group. The data are derived from three independent experiments with groups of 20 planarians (n = 60) monitored over a period of 20 days. ****, $P < 0.0001$ as determined by the log-rank test when comparing the survival of the planarians infected with JE2 *aspB*::*Tn* and the wild-type strain.

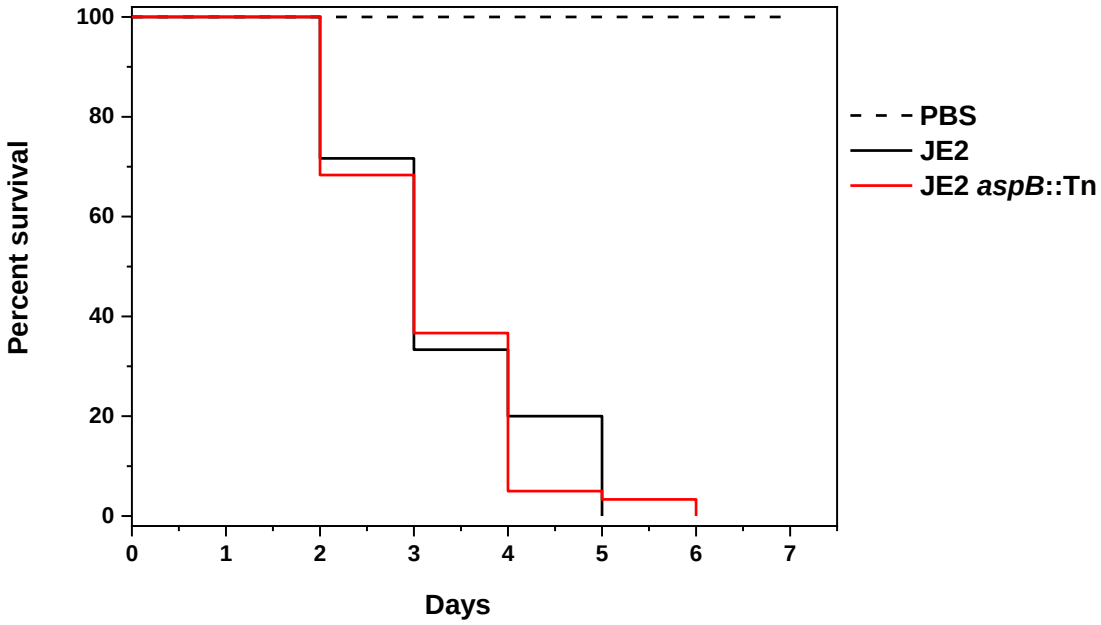

Figure 3.20 - Effect of the disruption of the *aspB* gene coding a putative aspartate aminotransferase in *S. aureus* in planarians survival.

A group of planarians belonging to *D. japonica* were infected with the wild-type strain (JE2) at 2.7 x10^9 CFU/mL and with the mutant strain for the *aspB* gene (JE2 *aspB::Tn*) at 2.4 x10^9 CFU/mL. The Kaplan-Meier plot indicates the viability of planarians over a period of 7 days post-infection. Planarians exposed to PBS were included as control group. The data are derived from three independent experiments with groups of 20 planarians (n = 60) monitored over a period of 7 days. No significant difference was determined by the log-rank test between the planarians exposed to JE2 *aspB*::*Tn* and the wild-type strain.

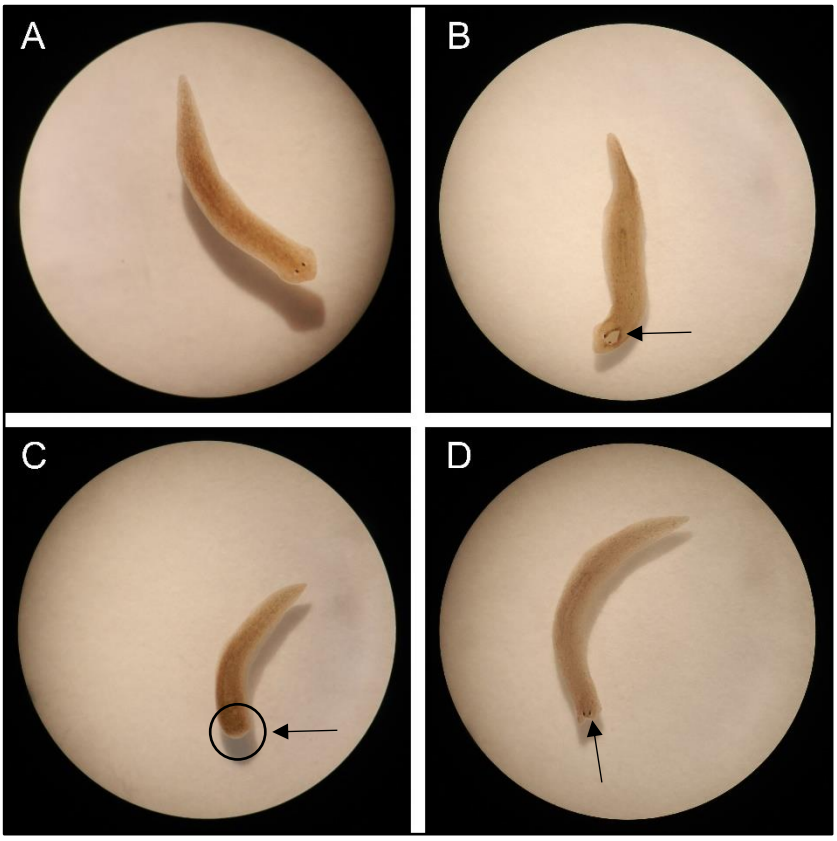

Figure 3.21 - Planarians showing different lesions after infection with *S. aureus* strains.

Planarians were infected with either 10^8 or 10^9 CFU/mL with the wild-type strain or mutant strain for the *aspB* gene. The appearance of clinical lesions on their body were observed using a stereo microscope. Planarians kept in PBS were used as a control. A) normal planarian without any lesion or tissue damage, B) planarian showing an anterior lesion at 3 days after infection with the wild-type strain, C) planarian showing head regression at 8 days after infection with the wild-type strain, and D) planarians showing an anterior lesion at 4 days after infection with the mutant strain for the *aspB* gene. Pictures were taken using a Nikon camera.

3.5 Discussion

In order to identify new candidates for drug development against *S. aureus*, three putative aminotransferases (AspB, HemL1 and HemL2) were selected to assess their potential as new antimicrobial targets as in our laboratory there was an interest in the study of this type of enzymes. Although the predicted functions of the genes annotated as *aspB* and *hemL(s)* are aspartate aminotransferase (AspB) and glutamate-1-semialdehyde aminotransferases (HemL1 and HemL2) respectively, their enzymatic activities have not been experimentally determined yet.

Growth assays

To evaluate the essentiality of the putative enzymes for the growth of *S. aureus* in different media, strains having disrupted the genes coding the three putative aminotransferases were grown in serum and RPMI and compared to the growth of the wild-type strain. These media were chosen to mimic the nutrient environment that the pathogen may encounter during an infection. It has been shown that *S. aureus* mutant strains for two genes coding enzymes involved in the purine biosynthesis pathway (*purA* and *purB)* had a reduced growth phenotype compared to the wild-type strain in serum (human and bovine) (Connolly et al., 2017). In *S. aureus* it has been shown that the purine biosynthetic pathway depends on a functional aspartate aminotransferase (Potter et al., 2020), work that was published while doing this PhD, and that may explain why the JE2 *aspB*::*Tn* strain had a growth impairment in serum (Figure 3.8).

In the case of the strains having disruptions in the *hemL* genes (JE2 *hemL1*::*Tn* and JE2 *hemL2*::*Tn*) a slight growth defect could be seen in serum when compared to the wild-type strain (Figure 3.8). This growth impairment in serum by the *hemL* mutant strains was also reflected in the metrics obtained by Growthcurver that showed a significant decrease in parameters like carrying capacity, growth rate, and area under the curve compared to those obtained for the wild-type strain (Table 3.7). In order to determine if the phenotype shown in serum by the *hemL* mutants in the USA300 genetic background

was observed in other *S. aureus* strains, mutants for the *hemL* gene created in the LS-1 genetic background were included. The mutants in the LS-1 strains were generated by gene deletion and were available in Prof. Nair laboratory (unpublished data). The *hemL1* and *hemL2* mutants in the LS-1 genetic background did not show significant differences in growth in serum compared to the wild-type strain (Figure 3.8). The differences in growth observed in the *hemL* mutants between the USA300 and the LS-1 genetic background in serum might be explained by the differences in the mechanism of mutation used: transposon insertion (USA300) disruption and markerless gene deletion (LS-1). This type of discrepancy has been described in a study comparing the phenotype of a *M. tuberculosis* strain with mutation in the *rv1248c* gene coding a 2-hydroxy-3-oxoadipate synthase (HOAS) that was created by either, transposon insertion or gene deletion (Maksymiuk et al., 2015). The authors found a growth inhibition in the gene deleted mutant while an impaired growth was observed in the transposon insertion mutant.

Seif and colleagues developed a computational manually reconstructed *S. aureus* JE2 genome-scale model of metabolism in order to elucidate its metabolic response to the nutrient availability of the environment. This model predicted the essentiality, amongst others, of genes participating in the haem biosynthetic pathway, specifically *hemA*, *hemB*, *hemE*, and *hemY* for the growth of *S. aureus* in different chemically defined media (CDM), like synthetic nasal extract (SNM3), CDM + glucose, CDM + galactose, and RPMI (Seif et al., 2019). Our results showed that the genes coding a putative HemL enzyme, *hemL1* and *hemL2*, were not essential for the growth of *S. aureus* in the complete formulation of RPMI or in serum as the strains having disrupted the genes coding a putative glutamate-1-semialdehyde aminotransferase were able to grow in both media. The growth phenotypes of the assessed strains in RPMI medium are in line with what Seif and colleagues predicted as no essentiality of the *hemL* gene was reported for the growth of *S. aureus* in RPMI by using the genome-scale model.

The model also predicted the essentiality of a gene coding a putative aspartate aminotransferase for the growth of *S. aureus* in SNM3 but not in TSB, RPMI, or CDM supplemented with either glucose or galactose (Seif et al., 2019). Our results are not in line with what was predicted by Seif and colleagues as the strain having disrupted the gene coding a putative aspartate aminotransferase, *aspB*, showed a growth inhibition in the complete formulation of RPMI. Although in serum, this strain showed a significant growth defect compared to the wild-type strain, this gene would not be essential for the growth of *S. aureus* in that medium.

Aminotransferases catalyse the reversible reaction between amino acids and α-keto acids and are key enzymes in the distribution of nitrogen from amino acids. Although the metabolism of aspartate is not the main source of nitrogen for the cell, it has been estimated that ~27% of the nitrogen available comes from aspartate (Reitzer, 2004). In this regard, it has been specifically shown that an aspartate aminotransferase mediates the nitrogen metabolism in *M. tuberculosis* (Jansen et al., 2020), thus highlighting the importance of this type of enzymes for the distribution of nitrogen within the cell. As the amino acids glutamate and glutamine are the main nitrogen donors, which is used for example, for the synthesis of purines and pyrimidines, it was sought that their availability might affect the growth of the strain having disrupted the gene coding for the putative *aspB*. We observed that the mutant strain was not able to grow in the complete formulation of RPMI and demonstrated that glutamine was affecting the growth of the mutant strain since the lack of glutamine in the medium restored the growth defect of the mutant strain to levels similar to those of the wild-type strain. It is possible that the RPMI medium that does not contain glutamine, but has glutamate as the major nitrogen source, led to a redirection of the metabolism of the cell that allowed the strain to grow when lacking a functional putative aspartate aminotransferase. However, this is an untested assumption as no further assays were performed to elucidate the effect of the availability of glutamine in the growth of the strain having disrupted the gene coding a putative aspartate aminotransferase.

The *hemL* mutants in the LS-1 genetic background had an overall similar growth pattern to that of the wild-type strain in both RPMI media. However, some differences in the growth pattern could be seen between *hemL1* and *hemL2* mutants in the USA300 genetic background grown in RPMI lacking glutamine (Figure 3.11), which might be strain-specific.

Further assays to evaluate the effect of the disruption within the genes coding a putative aspartate aminotransferase (*aspB*) and putative glutamate-1-semialdehyde aminotransferases (*hemL1* and *hemL2*) on the biofilm formation and virulence of *S. aureus* were performed in order to assess the potential of their gene products as antimicrobial targets.

Biofilms

Beenken and colleagues showed that amongst 580 genes differentially expressed in the biofilm of a clinical isolate of *S. aureus*, the genes involved in the intermediary metabolism, *N315-SA2397* and *N315-SA1749,* coding a putative PLP-dependent aminotransferase and a putative aspartate aminotransferase, respectively were overexpressed in the biofilm compared to their expression in the planktonic phase (Beenken et al., 2004). Although the authors did not quantify the biofilm formation of the strain with mutations in those genes, it was considered that a disruption within the gene coding a putative aspartate aminotransferase in *S. aureus* might result in an impaired capacity to form biofilm. However, our results indicated that the mutant strain coding a putative AspB enzyme did not show a significant decrease in its capacity to form biofilm compared to the wild-type strain (Figure 3.12). Regarding the biofilm formation capacity of the strains having disrupted the genes coding a putative glutamate-1-semialdehyde aminotransferase (GSA-AT), no significant differences were found in the mutants in the USA300 genetic background compared to the wild-type strain (Figure 3.12). In the case of the mutants in the LS-1 genetic background, a significant decrease in the biofilm

formation capacity was found in the LS-1 Δ*hemL1* mutant strain compared to the wild-type strain (Figure 3.13). Although the link between biofilm formation and haem metabolism in *S. aureus* has not been elucidated, a study focused on the identification of *S. aureus* genes important for the formation of microcolonies, as an alternative biofilm model to the crystal violet assay, identified a *hemL* mutant strain with an altered morphology of the microcolony (Wermser & Lopez, 2018), thus suggesting that a functional haem biosynthetic pathway may be needed for *S. aureus* to form biofilms. However, under the assay conditions tested it was not possible to demonstrate if a functional putative GSA-AT would be required for the biofilm formation of *S. aureus*. As the strains having disrupted the genes coding the putative GSA-ATs did not show a significant growth defect compared to the wild-type strain in serum, this medium could be used in further assays to evaluate if the putative enzymes would be required for the biofilm formation of *S. aureus*.

Virulence

The effect that the disruption of the gene coding a putative aspartate aminotransferase had in the virulence of *S. aureus* was tested by using the *Galleria mellonella* model. The mutant strain showed a significant decrease in virulence in this model compared to the wild-type strain (Figure 3.14). Potter and colleagues found that the putative aspartate aminotransferase was essential for the *S. aureus* survival in a murine osteomyelitis infection model as the mutant strain experienced a survival defect as early as one day post-infection when compared with the wild-type strain and showed this survival defect in different tissue types including kidneys, liver, and heart (Potter et al., 2020). Our results add to the body of existent evidence that the aspartate biosynthesis would be needed for the infection of *S. aureus*, thus representing a good metabolic pathway to be targeted in the fight against *S. aureus* infections.

It was reported that the genes *SAUSA300_1845* and *SAUSA300_1618*, both predicted to be involved in the haem biosynthetic pathway codes a putative enzyme HemL and

HemX, respectively were important for *S. aureus* fitness during infection (Valentino et al., 2014). Since the two genes under study in this project, *SAUSA300_1614* and *SAUSA300_1845*, are predicted to code a putative glutamate-1-semialdehyde aminotransferase (HemL1 and HemL2), it was decided to evaluate the effect of the disruption within both genes in the virulence assays. The mutant strains for the genes *SAUSA300_1614* and *SAUSA300_1845* showed a significant attenuation in virulence when compared to the wild-type strain. These results suggest that the putative glutamate-1-semialdehyde aminotransferase would be required for the virulence of *S. aureus* and both gene products could be used as targets in the design of new antimicrobials against this pathogen.

Planarians

The suitability of planarians as a model organism to study survival and colonisation of *S. aureus* was evaluated in this thesis. This model would have allowed us to visualize and quantify bacteria in the cells of planarians by using, for example *S. aureus* cells fluorescently labelled and electron microscopy techniques. Although this model has been used mainly for the study of the genetic mechanisms involved in the tissue regeneration process (Atabay et al., 2018; Reddien et al., 2005; Sikes & Newmark, 2013), it has emerged as a model organism to study host-pathogen interactions (Abnave et al., 2014; Hamada et al., 2016; Jordan et al., 2020; Maciel et al., 2019). In this work, the strain having disrupted the gene coding a putative aspartate aminotransferase that was proven to be less virulent in the *G. mellonella* model was chosen to assess planarians as a model organism to study the survival and colonisation capacities of *S. aureus*. Two different ways of administering bacteria were tested: by feeding planarians with the bacteria mixed in the food and by exposing planarians to the bacteria introduced into planarian water where they were kept during the length of the experiment. Planarians administered through the food with the strain having disrupted the gene coding a putative aspartate aminotransferase showed a significant decreased in the bacterial burden at

the end of the experiment in comparison to the wild-type strain (Figure 3.17). Although planarians exposed to the *S. aureus* strain having disrupted the gene *aspB* showed a decreased survival after 20 days compared to the wild-type strain (Figure 3.19), no clear pattern in the progression of the infection was observed. It was described by Arnold and colleagues that the infection of planarians belonging to the species *Schmidtea mediterranea* with bacteria from their own microbiome (i.e. *Vogesella*, *Chryseobacterium*, and *Pseudomonas*), resulted in a progressive tissue degeneration pattern consisting in the appearance of lesions either in the posterior or anterior region, a severe anterior lesion would lead to a head regression, and a fully lysis of planarians would be followed after head regression (Arnold et al., 2016). This pattern was not visualised in the planarians infected with *S. aureus* strains over the experimentation period, which suggest it may be elicited by specific bacterial species and not be a common infection progression pattern in planarians. If further analysis will be performed using this model, the best way of infection would be by feeding planarians with bacteria mixed in their food since significant differences can be seen in a shorter period of time compared to the time needed to visualise significant differences in planarians exposed to bacteria in the environment. Although in this study, planarians did not completely clear the infection when fed with bacteria, it has been reported that *S. aureus* can be cleared after six days by the planarian species *D. japonica* when fed with bacterial concentrations of 10^9, 10^7, and 10^5 CFU/worm (Abnave et al., 2014). Those findings indicated that it would be possible to get results within a reasonable time-period, thus optimising the experimentation time when using this model.

In summary, we were able to determine the following:

- The genes predicted to code a putative aspartate aminotransferase (*SAUSA300_1916*) and putative glutamate-1-semialdehyde aminotransferases (*SAUSA300_1614* and *SAUSA300_1845*) were not essential for the *in vitro* growth of *S. aureus* in rich media (tryptic soy broth) nor in human serum. The putative aspartate aminotransferase (AspB) was essential for the growth of *S.*

aureus in RPMI complete formulation, and its growth was restored to the wild-type levels when the medium lacked glutamine.

- The deficiency of the three putative aminotransferases (AspB, HemL1 and HemL2) showed a significant decrease in the virulence of *S. aureus* in a *Galleria mellonella* model and did not decrease the biofilm formation capacity of the *S. aureus* strains.
- The planarian animal model was suitable to test the colonisation of *S. aureus* strains but had the limitation that was not possible to easily administered the bacterial inoculum without a microinjection system.

CHAPTER 4

Determination of aspartate aminotransferase activity of SAUSA300_1916

4. Determination of aspartate aminotransferase activity of SAUSA300_1916

4.1 Introduction

4.1.1 Aminotransferases and pyridoxal 5'-phosphate dependent enzymes

Aminotransferases are a group of enzymes involved in transamination reactions that catalyse the reversible transference of an amino group from an amino donor to a keto acid or aldehyde acceptor. Aminotransferases are dependent on pyridoxal 5'-phosphate (PLP), which is perhaps one of the most versatile cofactors found in nature (Percudani & Peracchi, 2003).

PLP is an essential cofactor and one of the six derivatives of the vitamin B6 (pyridoxal, pyridoxine, pyridoxamine, pyridoxal 5'-phosphate, pyridoxine 5'-phosphate and pyridoxamine 5'-phosphate), that has a key function as a protein cofactor in a wide range of enzymes (Mehta & Christen, 2000; Percudani & Peracchi, 2009). The variety of reactions catalysed by PLP-dependent enzymes include transamination (e.g. aspartate aminotransferase, tyrosine aminotransferase), racemization (e.g. alanine racemase), decarboxylation (e.g. ornithine decarboxylase), α-elimination and replacement (e.g. serine hydroxymethyltransferase), β-replacement (tryptophan synthase), β-elimination (serine dehydratase), γ-replacement (cystathionine γ-synthase), and γ-elimination (cystathionine γ-lyase) (Eliot & Kirsch, 2004). Due to the versatility of reactions catalysed by PLP-dependent enzymes they are found in all organisms participating in the biosynthesis of amino acids and amino acid derived metabolites, interconversion between L- and D- amino acids, and also have been involved in the biosynthesis of amino sugars (Percudani & Peracchi, 2003).

PLP-dependent enzymes were initially classified into five-fold types (I to V) depending on the information available on sequence similarity, three-dimensional structure and biochemical properties of the enzymes (Grishin et al., 1995). Two more-fold types (VI and VII) were added to the classification after hidden Markov models (HMM) used in

computational biology were constructed based on the homology of the enzyme sequences deposited in the B6 database, which contains biochemical and molecular information of B6-dependent enzymes (Percudani & Peracchi, 2009). Transaminases are found in the categories of fold-types I and IV and based on sequence homology they can be sub classified into different groups or subclasses (Berglund et al., 2012). Aspartate aminotransferases belong to the fold type I, subgroup I that has been further subdivided into three categories, Ia, Ib and Ic (Oshima et al., 1996; Son & Kim, 2016). The latter described category, Ic, contains aspartate aminotransferases present in bacteria but not in humans (Jansen et al., 2020).

In the transaminase reaction carried out by PLP-dependent enzymes, the cofactor is found covalently bound to the enzyme through a Schiff base linkage formed between the aldehyde group of the cofactor and the amine group of the lysine residue in the active site of the enzyme. The Schiff base, also called an internal aldimine, is the resting state of the PLP-dependent enzymes and is the starting point for all those reactions catalysed by PLP-dependent enzymes (Mehta & Christen, 2000; Toney, 2005).

In the first step of the reaction, the amine group from the amino donor replaces the lysine from the internal aldimine to form a new Schiff base between the cofactor and the amino acid (Figure 4.1). At this point in the reaction the amino acid is covalently bound to the PLP forming an intermediate called an external aldimine. Following proton transfer steps between the amine of the lysine group of the enzyme and the intermediate, a ketimine is formed. After hydrolysation of the intermediate, the keto acid is released, and the pyridoxamine 5’-phosphate (PMP) form of the cofactor is formed. In the second half of the reaction, the PMP forms a ketimine intermediate with a keto acid that acts as the amino acceptor. Following proton transfer steps, the amino acid is released and the Schiff base between the amino group of the lysine residue of the enzyme and the cofactor is regenerated (Berglund et al., 2012; Mehta & Christen, 2000).

It has been reported that 1.5% of the genome of prokaryotes code for PLP-binding proteins highlighting the importance of this type of enzymes in the metabolism of the organisms due to the wide range of biochemical reactions they are involved in (Percudani & Peracchi, 2009). The enzyme commission has systematically classified enzymes according to the mechanism of action and the first digit of the enzyme code (EC) refers to a different mechanism, e.g. EC 1., reductases, EC 2., transferases, EC 3., hydrolases, EC 4., lyases, EC 5., isomerases, and EC 6., ligases (Komoda & Matsunaga, 2015). Remarkably, amongst the six general enzyme reaction mechanism groups, PLP-dependent enzymes are representative in five of them (Percudani & Peracchi, 2003).

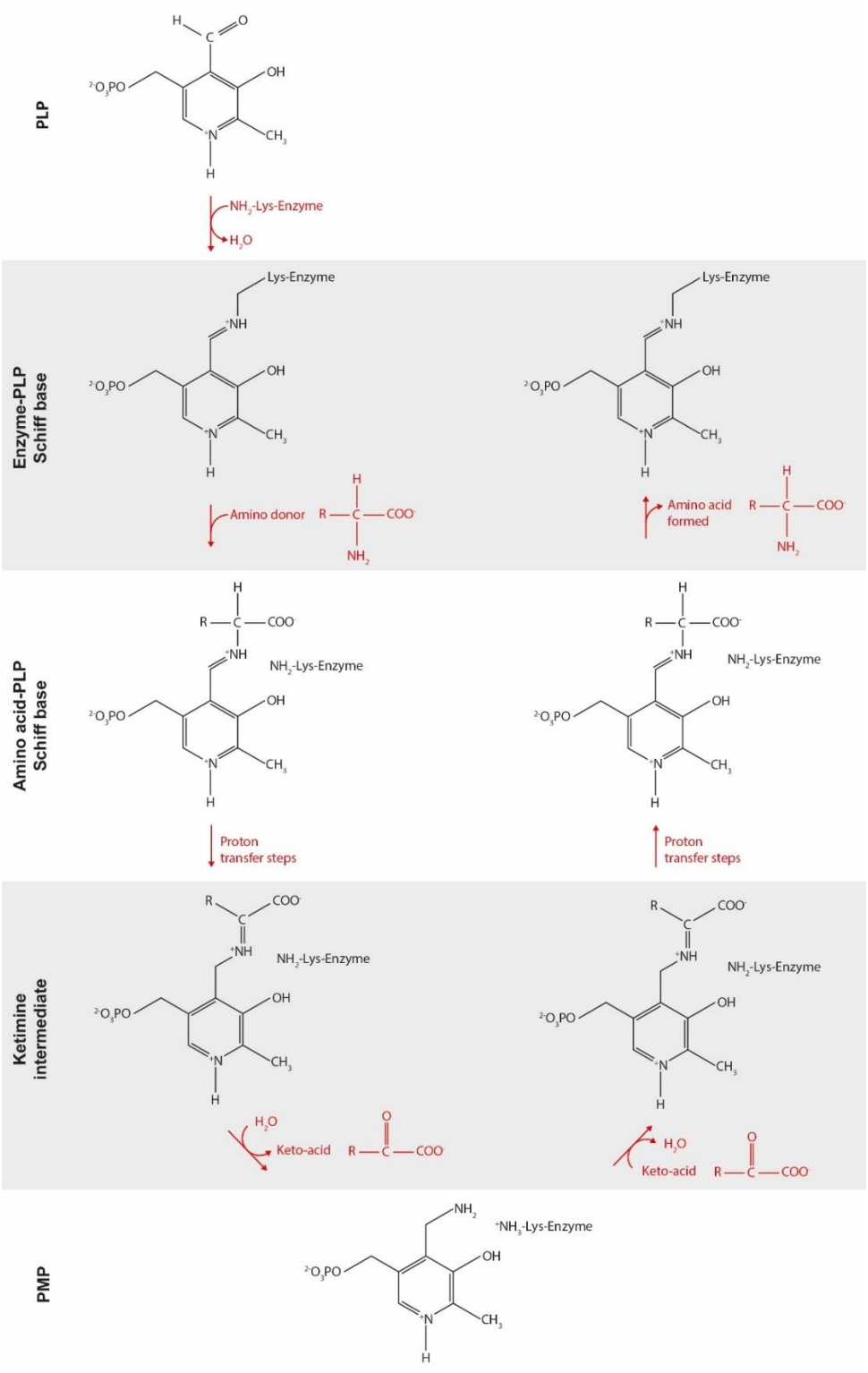

Figure 4.1 - Scheme showing the steps involved in the transamination reaction catalysed by PLP-dependent enzymes.

The reaction starts with the cofactor bound to the enzyme through the formation of a Schiff base between them. As a result of the first half of the transamination reaction, a pyridoxamine 5'-phosphate (PMP) molecule is formed while the ketoacid product is released and the enzyme can be found free. In the second half of the reaction, the PMP molecule reacts with the second keto acid to form an intermediate ketimine to finally release the amino acid product and the enzyme-PLP complex is regenerated. The scheme is based on the illustrations from (Berglund et al., 2012) and (Liang et al., 2019).

4.1.2 Characteristics of the inhibitors used in the experiments described in this chapter: 1) Amino-oxyacetate, 2) L-serine *O*-sulfate, 3) Hesperetin, 4) PF-04859989, 5) Vigabatrin, and 6) Adapalene

4.1.2.1 Amino-oxyacetate

Amino-oxyacetate (AOA or AOAA) (Figure 4.2), is a compound that has shown inhibitory activity against different PLP-dependent enzymes. The inhibition of these types of enzymes by AOA is caused by an attack of the acid to the Schiff base linkage formed between the cofactor and the enzyme (Beeler & Churchich, 1976).

Amino-oxyacetate has been used as an inhibitor of kynurenine aminotransferase, an enzyme involved in the metabolism of tryptophan, catalysing the synthesis of kynurenic acid (KYNA), a substance that has neuroprotective properties since in abnormal levels it has been associated with neurological disorders like schizophrenia (Nadvi et al., 2017). In a study performed by Nadvi and colleagues, AOA was shown to inhibit the human kynurenine aminotransferase I with an IC_{50} of 13.1 μM through formation of an irreversible oximine (=N-OH) with the PLP linked to the enzyme, thus preventing the formation of the Schiff base between the cofactor and the enzyme leading to an inhibition of the catalytic activity.

In cancer, the targeting of specific metabolic pathways has emerged as an alternative for drug design. For example, the glutamine metabolic pathway has become a potential target for control of carcinogenic cells (Korangath et al., 2015; Qin et al., 2010). It has been shown that in breast cancer cells the overexpression of the *c-myc* gene, that codes an important transcription factor, is linked to changes in the metabolism of glutamine, leading to an increase in the amino acid uptake and a shift of the glutamine metabolic pathway from the canonical to a non-canonical pathway to keep both, a redox homeostasis and a stable intracellular ATP levels for the cells to proliferate (Korangath et al., 2015; Thornburg et al., 2008). In this context, AOA has been used to target enzymes involved in the glutaminolytic pathway in breast cancer cells showing that the

compound was able to inhibit the growth of the cells by supressing the catabolism of glutamine, which suggest that the compound was inhibiting transaminases involved in the metabolism of that amino acid (Korangath et al., 2015).

AOA has been shown to have inhibitory activity against an aspartate aminotransferase showing that 0.1 mM of AOA caused more than a 97% of inhibition of the rat brain aspartate aminotransferase (Fitzpatrick et al., 1983), and another study showed complete inhibition of an aspartate aminotransferase by 5 mM of AOA when trying to understand if glutamate was transformed into α-KG by either, transamination (catalysed by aspartate aminotransferase), or oxidative deamination (catalysed by glutamate dehydrogenase) in astrocytes (A. C. Yu et al., 1982).

AOA has also proven to have potent inhibitory effects against a mitochondrial aspartate aminotransferase and pig heart alanine aminotransferase (Moreno-Sánchez et al., 2017). The compound has also been used as a positive control for the inhibition of a human glutamate-oxaloacetate transaminase 1 (GOT 1) when successful inhibitors against KAT2 and γ-aminobutyric acid (GABA) aminotransferases were tested against GOT 1 in a study aiming to evaluate the selectivity of different inhibitors against the growth of pancreatic ductal adenocarcinoma cell lines as potential drugs against this type of cancer (T. Yoshida et al., 2020).

4.1.2.2 L-serine O-sulfate

L-serine *O*-sulfate (L-SOS) (Figure 4.2) is an acid sulphur-containing amino acid (SAA), structural analogue to glutamate, that has been included within the group of toxic compounds to glial cells known as gliotoxins (McBean, 2007). The term gliotoxin refers to the toxic effect shown by excitatory amino acids against astrocytes including changes in their morphology, leading to cell death after incubation with different concentrations of the amino acids (Bridges et al., 1992).

Brennan and colleagues shown that L-SOS resulted to be toxic for astrocytes and its toxicity was caused by the disruption of different metabolic pathways where the activities of alanine aminotransferase (53% reduction) and aspartate aminotransferase (67% reduction) were affected by L-SOS. That study also showed a 27% reduction in the *de novo* synthesis of the cellular antioxidant glutathione, thus suggesting that the toxicity mechanism of L-SOS on the astrocytes was the result of a disruption in the metabolism of glucose and alanine as well as a reduction in the intracellular concentration of glutathione (Brennan et al., 2006).

The aspartate aminotransferase can catalyse either, a transamination or β-elimination reaction after its interaction with L-SOS as a substrate. In the occurrence of a β-elimination reaction, the sulphate group of the compound is lost, leading to the formation of aminoacrylate that can be finally converted into pyruvate and ammonia, or it can react with the enzyme, leading to an irreversible inactivation of the aspartate aminotransferase activity (Birolo et al., 1995).

The inhibitory effect of L-SOS against aminotransferases has been used to inhibit aminotransferases purified from parasitic protozoa showing a slight inhibition against the aspartate aminotransferase from *Trypanosoma vaginalis* (~25%) and *Giardia intestinalis* (~30%) when the enzymes were incubated in the presence of a final concentration of 1 mM of L-SOS (Berger et al., 2001). This compound was included in the list of potential inhibitors as it might also show inhibitory activity against the aspartate aminotransferase from *S. aureus*.

4.1.2.3 Hesperetin

Hesperetin (Figure 4.2) is a type of flavonoid, which are secondary plant metabolites that have a wide range of biological activities. The conserved carbon structure, common to all flavonoids is formed by a flavan nucleus of 15 carbon atoms (C6-C3-C6) arranged in two aromatic rings (A and B rings) linked through a three-carbon structure that forms the

C ring (Isoda et al., 2014; Pietta, 2000). Flavonoids are classified into six major subclasses: flavonols, isoflavonoids, flavones, flavanones, chalcones, and anthocyanins based on the oxidation of the C ring and the position at which the B ring is attached to the C ring (Panche et al., 2016).

Hesperetin (3′,5,7-trihydroxy-4′-methoxy-flavanone) belongs to the flavanone class of flavonoids and can be found in the form of hesperidin mainly in citrus fruits like oranges, mandarins, lemons, grapefruits and bergamots (Barreca et al., 2017). Amongst the wide range of pharmacological activities of flavanones, and specifically of hesperetin or hesperidin are their antioxidant properties (Elavarasan et al., 2012), anticancer effect (Alshatwi et al., 2013; Aranganathan et al., 2008; Banjerdpongchai et al., 2016), anti-inflammatory activity (Rotelli et al., 2003), and lowering cholesterol effects (Mollace et al., 2011; Wilcox et al., 2001).

In the context of enzyme inhibition, and as an example, the inhibitory activity of the flavanones hesperidin and hesperetin has been assessed against the enzymes alanine and aspartate aminotransferases by Zaarei and colleagues. Their study showed that both compounds successfully inhibited the enzymatic activities of both aminotransferases by preventing the reaction between the PLP-enzyme complex with the substrate of the enzyme as the inhibitor interacts with the enzyme residues located at the entrance cavity of the active site (Zareei et al., 2017). The docking simulation analysis showed that in the inhibition of the aspartate aminotransferase by hesperetin, the active site residues Trp140 and Gly38 interacted with the inhibitor through hydrogen bonds, while the residues Lys258, Phe360, Arg386, Pro195, Asn194 as well as the cofactor PLP were key in the binding of hesperetin to the enzyme by hydrophobic interactions (Zareei et al., 2017). It can be assumed that hesperetin will have a potent inhibitory activity against the aspartate aminotransferase purified from *S. aureus*.

4.1.2.4 PF-04859989

The compound PF-04859989 or (3S)-3-amino-1-hydroxy-3,4-dihydroquinolin-2(1H)-one (Figure 4.2) was discovered in 2012 by a research group of the Neuroscience Chemistry division at Pfizer, in a project aimed to discover new drugs for neurogenerative diseases like schizophrenia (Dounay et al., 2012). The aim of the study was to find novel selective and brain penetrant compounds able to inhibit the brain enzyme kynurenine aminotransferase II (KAT II). This enzyme has PLP as a cofactor and it is involved in the biosynthesis of kynurenic acid (KYNA) by catalysing the conversion of L-kynurenine into KYNA. It has been shown that pharmacologically elevated levels of KYNA in the central nervous system are related with psychiatric and neurological disorders like schizophrenia (Erhardt et al., 2007; Linderholm et al., 2012) or bipolar disorder (Olsson et al., 2010) when comparing the KYNA levels to healthy controls. The researchers performed a high-throughput screening of a compound library they had, finding an aminodihydroquinolone 6 as a potential candidate, but after synthesis of this compound, it had no inhibitory activity against KAT II and it was discarded (Dounay et al., 2012). Following a series of chromatographic separations and re-synthesis methods from the original sample from the chemical library, they identified the compound PF-04859989, which showed inhibitory activity against KAT II (IC_{50} = 23 nM) (Dounay et al., 2012). The compound also showed selectivity for KAT II, which is known to be the major enzyme involved in KYNA biosynthesis, over other KAT enzymes isoforms (KAT I, KAT III and KAT IV). The *in vivo* tests performed in rats showed that after 1 h of subcutaneous injection of a dose of 10 mg/kg of the compound, the KYNA levels decreased by 50% of the basal concentrations returning to their baseline 20 h after injection, thus showing a prolonged duration of the effect (Dounay et al., 2012).

The X-ray structure of the KAT II bound to PF-04859989 showed that the compound was covalently attached to the PLP cofactor in the active site of the enzyme and that this linkage was irreversible having the advantage to be used at low doses and to avoid potential toxic side effects (Dounay et al., 2012). Since its discovery, the compound has

been used as a template molecule for the design and improvement of new irreversible inhibitors against the human KAT II enzyme (Dounay et al., 2013; Tuttle et al., 2013), and as a control to compare the inhibitory properties of potential new inhibitors against KAT II to determine if the selected compounds are able to bind to the cofactor of the enzyme in the same way as PF-04859989 (Y. Yoshida et al., 2019).

PF-04859989 has also been tested against other aminotransferases, like a glutamate-oxaloacetate transaminase (GOT 1) (T. Yoshida et al., 2020). The study aimed to test previously described KAT II and GABA aminotransferase inhibitors against GOT as a starting point for the design of novel drugs against pancreatic ductal adenocarcinoma (PDA). In the inhibition assays, the compound showed a 16% inhibition of GOT 1 when the enzyme was pre-incubated with both, cofactor and inhibitor for 15 min, and a 96% of inhibition when the preincubation step was longer (24 h) (T. Yoshida et al., 2020). The authors also found that the compound impaired the growth of two PDA cell lines, PATU-8988T and PATU-8902, in a GOT 1 inhibition dependent way (T. Yoshida et al., 2020).

4.1.2.5 Vigabatrin

Once established that γ-aminobutyric acid (GABA) was an inhibitory neurotransmitter in the brain, the finding of selective inhibitors against the GABA aminotransferase (GABA-AT), enzyme responsible for the catalysis of GABA, was a major task for researchers to understand the role of the neurotransmitter in the central nervous system.

In this context, finding the structural analogues of the substrate of an enzyme was an approach that researchers followed to find new and selective inhibitors, and vigabatrin, an analogue of GABA, was discovered as a selective inhibitor of the GABA-AT (Lippert et al., 1977).

Vigabatrin (4-amino-hex-5-enoic acid or γ-vinyl GABA) (Figure 4.2) was found to inhibit the rat brain GABA-AT, a PLP-dependent enzyme, when tested at 0.1 mM in an

irreversible manner since only between 5% and 10% of the control enzyme activity was recovered after four days of dialysis with buffer (Lippert et al., 1977). After peripheral administration to rats, the compound was able to inhibit the GABA-AT in a dose dependent manner accompanied by an increase in the brain concentration of GABA, thus demonstrating the *in vivo* effect of the inhibitor (Jung et al., 1977).

The irreversible inhibition of GABA-AT shown by vigabatrin was due to an adduct formed between the compound, the Lys329 residue of the enzyme, and the PLP cofactor as shown in a study when comparison between the crystal structure of the enzyme in the native form and after vigabatrin treatment was performed (Storici et al., 2004).

Vigabatrin was approved in Europe in the 1980s and for the first time approved in the United Kingdom in 1989 as an antiepileptic drug (Waterhouse et al., 2009). Since its approval it has been used as an anticonvulsant agent due to its inhibitory activity against GABA-AT leading to an increase in the concentration of the GABA neurotransmitter in the brain and diminishing the convulsions caused when a below threshold concentrations of GABA in the brain is found (Waterhouse et al., 2009).

The inhibitory effect of vigabatrin has also been evaluated against other aminotransferases, such as a glutamic oxaloacetic aminotransferase (T. Yoshida et al., 2020), showing that after 15 min and 24 h of pre-incubation of the enzyme with its cofactor and the inhibitor, a 1.4% of enzyme inhibition was found, thus suggesting this compound might show inhibitory activity against the aspartate aminotransferase purified from *S. aureus*.

4.1.2.6 Adapalene

Adapalene or (6-[3-(1-adamantyl)-4-methoxyphenyl]-2-naphthoic acid (Figure 4.2) (Bernanrd, 1993), is the result of molecular modifications of the retinoic acid skeleton in

an effort to overcome limitations shown by other derivatives of retinol used for the topical treatment of acne vulgaris (Weiss, 1997).

Adapalene has been tested as an anticancerogenic compound and its effect on cell proliferation has been evaluated in different cell lines, for example, it has been shown an *in vitro* antiproliferative effect on HeLa cells derived from a cervical carcinoma after the treatment of the cells for 4 days with different retinols including adapalene (Shroot et al., 1997).

Although the adapalene has shown antiproliferative activity against different cancer cell lines, its mechanism of action is not completely understood. To better understand the target of adapalene for its anti-tumour effect, a study investigating the effect of the compound on ovarian cancer cells (ES-2) was performed. The study showed that adapalene inhibited the enzymatic activity of glutamate oxaloacetic aminotransferase (GOT 1) in a non-competitive way against the substrate α-ketoglutarate, and that the compound was able to directly bind to an hydrophobic pocket of the enzyme located at the back of the active site (Q. Wang et al., 2019). The molecular docking performed demonstrated that adapalene and GOT1 interacted through hydrophobic and hydrogen bonds. The key hydrophobic interactions were between the residues Pro314 and the adamantine part of the compound and between Phe317 and the benzene ring of the compound, while the hydrogen linkage was predicted to be between the Asn233 residue and adapalene (Q. Wang et al., 2019).

The selective inhibition shown by adapalene on the GOT 1 enzyme, suggests it could be a good candidate to inhibit the *S. aureus* aspartate aminotransferase, AspB.

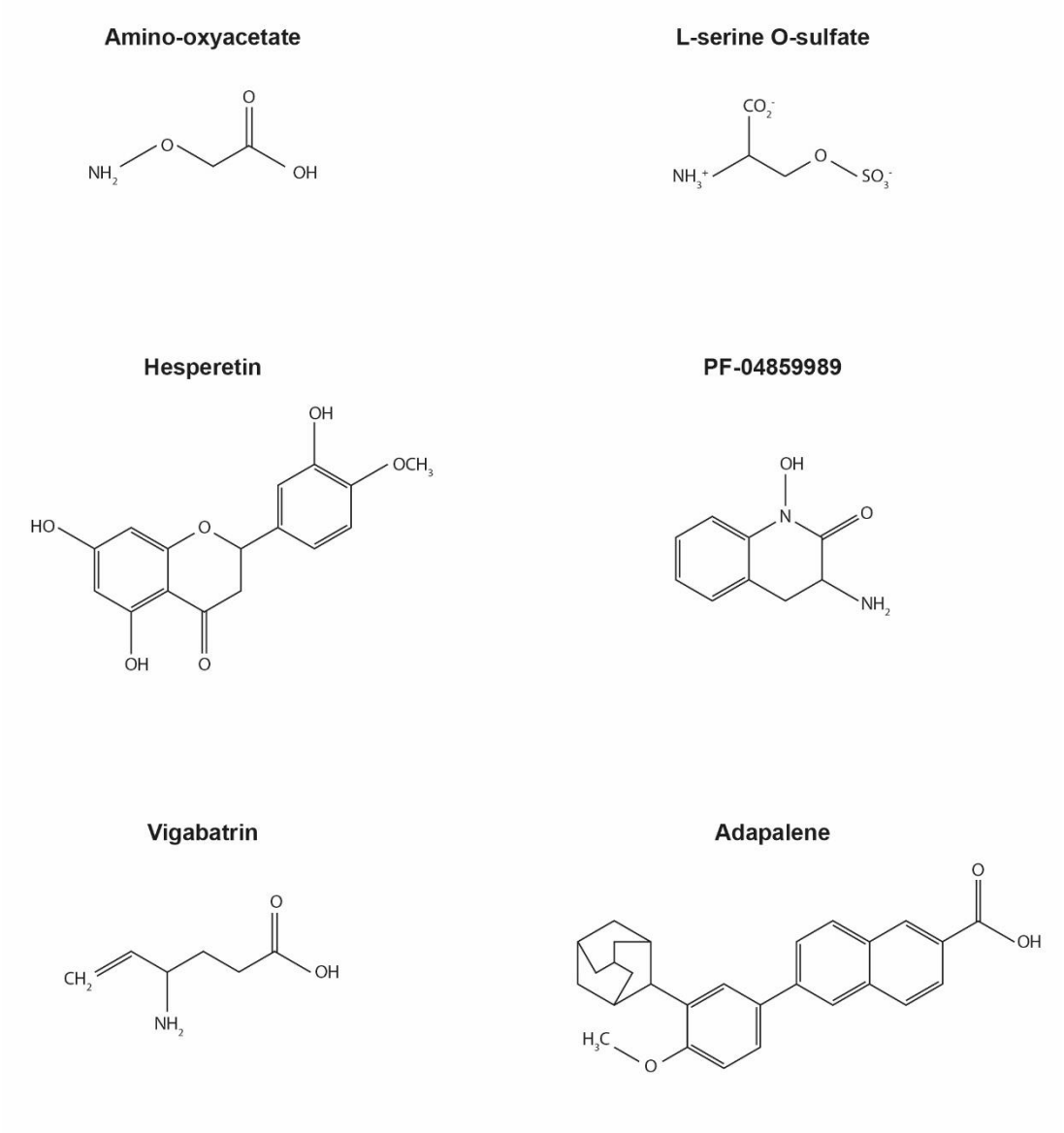

Figure 4.2 - Molecular structure of the aminotransferase inhibitors used.

4.2 Aims of the work described in the chapter

- To determine the capacity of SAUSA300_1916 to act as an aspartate aminotransferase.
- To determine the kinetics of SAUSA300_1916.
- To evaluate the inhibition of SAUSA300_1916 by aminotransferase inhibitors.
- To determine the effect of the selected inhibitor(s) in the virulence of *S. aureus* by using *Galleria mellonella* model.

4.3 Materials and Methods

4.3.1 Plasmid, enzymes, and chemicals used

The gene coding the hypothetical AspB enzyme inserted into the plasmid pEAHISMRSA2028 was a gift from Huanting Liu & James Naismith (Addgene plasmid #97001; http://n2t.net/addgene:97001; RRID:Addgene_97001). The gene coding the putative aspartate aminotransferase was amplified from the genome DNA of *S. aureus* strain MRSA252, cloned into the plasmid pDEST14 and transformed into *E. coli* BL21 (DE3) by the authors (Seetharamappa et al., 2007). The *S. aureus* gene *sar2028,* which codes the putative aspartate aminotransferase*,* was not codon optimised for *E. coli*. The Tobacco Etch Virus protease (TEV) used to remove the His-tag from the protein was bought in GenScript (TEV protease, His, cat. n° Z03030).

The enzymatic assays were performed with the following enzymes obtained from Sigma: glutamic-oxalacetic transaminase from porcine heart type I (cat. n° G2751), malic dehydrogenase from porcine heart (cat. n° M1567), and L-glutamic dehydrogenase from bovine liver type II (cat. n° G2626).

The amino acids L-glutamic acid and L-aspartic acid were obtained from Sigma (cat. n° G8415 and A9256, respectively). The cofactors pyridoxal 5'-phosphate (cat. n° P9255)

and reduced β-nicotinamide adenine dinucleotide, NADH, (cat. n°43420) were purchased from Sigma as well as the co-substrates oxaloacetic acid, OAA, (cat. n° O4126) and α-ketoglutaric acid, α-KG, (cat. n° 75890).

4.3.2 Expression of the recombinant His-tagged hypothetical AspB in *E. coli*

The *E. coli* BL21(DE3) strain containing the plasmid pEAHISMRSA2028 was grown in LB plates supplemented with ampicillin (100 µg/mL) at 37°C for 24 h. A starter culture of 5 mL was prepared by inoculating LB broth containing 100 µg/mL ampicillin with a single colony of *E. coli* DE3. The cell cultures were incubated at 37°C for 16 h in shaking condition at 200 rpm.

The expression of the putative AspB protein was induced by using the commercial autoinduction medium MagicMedia™ from Invitrogen. The content of one pouch (*component A*) of MagicMedia™ was dissolved into 950 mL of dH_2O in a 1 L flask, dispensed into 1 L bottles containing 100 mL of media and autoclaved prior to use. Each bottle containing the media was supplemented with 100 µg/mL of ampicillin and immediately before the inoculation with the starter culture, the *component B* of the MagicMedia™ was added. The cultures were grown at 37°C for 24 h in shaking condition at 200 rpm. After incubation, the cells were harvested by centrifugation at 11,800 x *g* at 4°C for 15 min. The supernatant was discarded, and the pellets were kept at -20°C until further use.

4.3.3 Purification of the recombinant hypothetical AspB protein

The cell pellets were thawed on ice and resuspended in lysis buffer containing 50 mL of B-PER™ complete bacterial protein extraction reagent (Thermo Scientific), one tablet of protease inhibitor His-tag compatible (Roche), and 30 µM of the cofactor PLP. The tubes were left in a tube rotator and the cells were lysed at 4°C for 90 min. The crude lysate was clarified by centrifugation at 13,000 x *g* at 4°C for 20 min.

The putative AspB protein was purified by using Ni^{2+}-nitrilotriacetic acid metal-chelating affinity chromatography (Qiagen). For this purpose, the crude lysate was mixed with the resin by shaking them for 1 h at 4°C. After they were mixed, the Ni-NTA agarose beads and the proteins were added into an empty gravity flow column and washed with at least 10 column volumes of washing buffer (phosphate-buffered saline containing 20 mM imidazole). The putative AspB protein was eluted with two column volumes of elution buffer (phosphate-buffered saline buffer containing 500 mM imidazole). The fractions containing the eluted proteins were desalted by gel filtration chromatography using disposable chromatography EconoPAC 10DG columns (cat. n° 732-2010, Bio-Rad) into a buffer solution containing 50 mM Tris buffer (pH 7.5). The purified enzyme was kept at 4°C for short term storage.

4.3.4 Removal of His-tag from the purified hypothetical AspB and second step purification

The His-tag was removed by incubating the putative AspB protein with the Tobacco Etch Virus protease (TEV) at 33.2 IU of TEV per 1 mg of protein for 16 h at 22°C. The second step of purification was performed by using a Ni-NTA agarose column and the storage buffer was replaced with 50 mM Tris buffer pH 7.5 before loading the column with the TEV treated protein. The mixture was incubated for 10 min before collecting the fractions containing the cleaved proteins. The uncleaved proteins and His-tags were removed using elution buffer (phosphate-buffered saline buffer containing 500 mM imidazole). The purity of the proteins was checked through SDS-PAGE gel and the purified putative AspB was kept at -20°C for long term storage.

4.3.5 Protein determination and SDS-PAGE analysis

The concentration of the purified putative AspB protein was determined spectrophotometrically by measuring the UV absorption at 280 nm wavelength. The

extinction coefficient of the putative AspB (50310 M^{-1} cm^{-1}) was estimated by ExPASy ProtParam tool (https://web.expasy.org/protparam).

The protein samples (10 µL) were mixed with the same volume of protein loading buffer (cat. n° EC-886, National Diagnostics) and heated at 95°C for 5 min using the heat block. The samples were left at room temperature to cool down before loading the gel.

The SDS-PAGE was carried out using a 12% polyacrylamide resolving gel which allows a separation size range between 20 – 120 kDa. For this purpose, a 20 mL volume of the gel was prepared by adding 6.6 mL of distilled water, 8 mL of 30% (w/v) acrylamide, ProtoGel (cat. n°A2-0072, National Diagnostics), 5 mL of 1.5 M Tris buffer pH 8.8 (cat. n° BP152-1, Fisher Chemical), 0.2 mL of 10% SDS, 0.2 mL of 10% ammonium persulfate (cat. n° 401165000, Acros Organics) and 8 µL of TEMED (cat. n° T9281, Sigma). The solution was poured into the glass plates previously mounted in the casting stand and a layer of butan-1-ol was added to remove bubbles and flatten the surface of the gel. After polymerisation, the alcohol was drained off and the gel rinsed with distilled water. The components of the stacking gel were mixed in a final volume of 5 mL by adding 3.4 mL of distilled water, 0.83 mL of 30% (w/v) acrylamide, ProtoGel, 0.63 mL of 1 M Tris buffer pH 6.8, 50 µL of 10% SDS, 50 µL of 10% ammonium persulfate and 5 µL of TEMED. The stacking gel was poured on top of the resolving gel and the comb inserted immediately. The gel was allowed to polymerise for 1 h before adding the protein samples.

After polymerisation of the stacking gel, the comb was removed, and the glass plates mounted into the cassette and inserted inside the tank. The chamber was filled with freshly prepared 1X running buffer (Tris/Glycine/SDS) diluted from a 10X buffer Tris/Glycine/SDS electrophoresis grade (0.25 M Tris -1.92 M glycine – 1% SDS) (cat. n° EC-870, National Diagnostics) using distilled water. The samples were loaded into the wells of the gel and 5 µL of unstained protein standard broad range (10 – 200 kDa) marker was used (cat. n° P7704, New England Biolabs) to determine the relative molecular weight size. The gel was run at a current of 60 mA until the dye reached the

bottom of the stacking gel and then at a current of 40 mA until the dye reached the bottom of the resolving gel. The gels were stained with Brilliant Blue (cat. n° B2025, Sigma) for 30 minutes and de-stained overnight with distilled water.

4.3.6 Determination of aspartate aminotransferase activity through HPLC

4.3.6.1 Enzymatic reaction

The enzymatic reactions to determine the aspartate aminotransferase activity of AspB were performed in 250 mM potassium phosphate buffer at pH 7.52 and at 37°C as those mimic the pH and temperatures conditions that *S. aureus* encounters within the host. The reaction mixture contained the buffer, PLP (50 µM), the pair of substrates, L-glutamic acid (10 mM) and OAA (10 mM), and the reaction was initiated by adding the purified AspB at a final concentration of 0.625 mg/mL in a total reaction volume of 100 µL. The enzyme reaction was carried out at 37°C and samples were taken every 20 s for up to 120 s. The reaction was stopped by adding 50 µL of trichloroacetic acid (TCA 50%) and the samples were kept at -20°C until analysis. As a control, the reaction was set up as previously described but without the addition of AspB. As a positive control, 2.5 µL of GOT at a final concentration of 0.2 mg/mL in a total volume of 100 µL were added to the reaction mixture and samples were taken every 20 s over a period of 120 s.

4.3.6.2 Sample preparation and HPLC analysis

The samples were prepared following a method described to simultaneously determine the concentrations of different oxoacids in the plasma or tissues by reversed-phase HPLC column (Lange & Mályusz, 1994). For this purpose, 50 µL of sodium hydroxide (NaOH, 3 M) were added into the tubes containing the thawed samples (containing 100 µL of the enzyme reaction and 50 µL of TCA) followed by the addition of 100 µL of reaction buffer (150 mM of phosphate buffer, pH 8) and 10 µL of internal standard (100

µM of 2-oxobutyrate in reaction buffer). The content of the tubes was transferred into a Costar Spin-X centrifuge tube filter (cat. n° 8161, Fisher) and the precipitated protein was removed by centrifugation at 3,000 x *g* for 2 min. A volume of 100 µL of the supernatant was transferred into a microcentrifuge tube and 5 µL of a phenylhydrazine solution (50 µL of phenylhydrazine dissolved in 1 mL of reaction buffer) were added into the tube to start the derivatization. The samples were incubated at 37°C for 15 min with shaking and diluted 1:10 in potassium phosphate buffer (pH 6)-methanol (97:3, v/v) before manually loading 1 µL onto the HPLC system using a 10 µL Microlitre™ syringe (cat. n° 549-1139, VWR). The oxoacids standard solution was prepared by adding the same components for the enzyme reaction, but the amino acid was replaced by α-KG and OAA at a final concentration of 10 mM. The treatment of the standards was the same as that for the samples before loading 1 µL onto the system.

An Adept Cecil HPLC system was used, consisting of a Cecil CE 4405 UV-visible detector, a Cecil CE 4402 binary pump, and a Merit operating software. The separation was conducted using a reversed-phase HPLC column, 50 mm length x 2.1 mm width and 2.6 µm particle size (Accucore, Thermofisher) and run at room temperature with a flow rate of 0.8 mL/min with a 13 mM potassium biphosphate and 1 mM potassium dibasic (pH 6)-methanol (97:3, v/v) mobile phase. The separation of the phenylhydrazine-derivatized 2-oxoacids was detected by UV spectrophotometry at 324 nm 5 min after injection of the sample.

4.3.7 Determination of the kinetics of the AspB enzyme

To determine the kinetic parameters, maximum velocity (V_{max}), Michaelis-Menten constants (K_m), catalytic constant (K_{cat}), and catalytic efficiency (K_{cat}/K_m) of the enzymes for the substrates of the forward (L-aspartic acid and α-KG) and reverse (L-glutamic acid and OAA) reactions, the aminotransferase activity was coupled with a second reaction

catalysed by either, malic dehydrogenase (MDH) or glutamic dehydrogenase (GDH), depending on the reaction.

The MDH enzyme catalyses the formation of malate from OAA in the presence of NADH, thus indirectly allowing the measurement of AspB activity by spectrophotometrically monitoring the decrease in absorbance of NADH at 340 nm. In the forward reaction the aminotransferase activity was coupled with 2 units of MDH in a 1 mL final volume using UV-vis cuvettes (cat. n° 10663852, Fisher Scientific). The assay reaction contained a final concentration of 250 mM potassium phosphate buffer (pH 87.2), 50 µM of PLP, 0.12 mM NADH, a fixed concentration of α-KG (10 mM) and L-aspartic acid in final concentrations ranging from 0 to 2 mM for the $K_m^{L\text{-}asp}$ of AspB, while a range of concentrations between 0 and 6 mM was used for the $K_m^{L\text{-}asp}$ of GOT. All the reactions were initiated by adding 0.01 mg/mL of the AspB or GOT enzymes (obtained by dilution of the stock solution with 200 mM potassium phosphate buffer pH 8) and performed at 37°C. To determine the $K_m^{\alpha\text{-}KG}$ of AspB and GOT, a range of concentrations between 0 and 2 mM of α-KG was tested at a fixed concentration of L-aspartic acid (10 mM).

The kinetic parameters for the pair of substrates of the reverse reaction, L-glutamic acid and OAA, were determined by coupling the aminotransferase activity with GDH. This enzyme catalyses the formation of L-glutamate from α-KG in the presence of NADH and ammonium (NH_4^+). The enzyme assay contained the buffer and cofactor at the concentrations previously mentioned, a final concentration of 3.1 mM ammonium chloride (NH_4Cl), 0.12 mM NADH, a fixed concentration of OAA (1 mM) and L-glutamic acid in final concentrations ranging from 0 to 5 mM for the $K_m^{L\text{-}glu}$ of AspB, while a range of concentrations between 0 and 3.75 mM was used for the $K_m^{L\text{-}glu}$ of GOT. The reactions were initiated by adding 0.01 mg/mL of the enzyme and the assay performed at 37°C. To determine the K_m^{OAA} of AspB, the assay was performed at a fixed concentration of L-glutamic acid (10 mM) and OAA in a final concentration ranging from 0 to 0.28 mM for K_m^{OAA} of AspB, while a range of concentrations between 0 and 0.36 mM was used for K_m^{OAA} of GOT. Every reaction was performed in three independent experiments in

triplicate and the results were reported as the average ± standard deviation of the data. Reactions in which the volume of the enzyme was replaced by potassium phosphate buffer were used as control. The absorbance of NADH at 340 nm (ε = 6.22 mM^{-1} cm^{-1}, 340 nm) was monitored every 5 s for up to 5 min using a SPECTROstar Nano absorbance reader. The enzyme rates were determined from the slopes obtained from the linear phase of the reaction at each substrate concentration tested. The V_{max} and K_m values were determined from the plot of the initial velocities versus substrate concentration after fitting the data to the Michaelis-Menten equation ($y = V_{max} * [S] / (K_m + [S])$. The specific activities of the enzymes were calculated from the V_{max} value for all of the substrates tested and expressed as µmol min^{-1} mg^{-1} of protein. The values of the turnover number (K_{cat}) and catalytic efficiency (K_{cat}/K_m) were determined for the reactions with all of the substrates.

4.3.8 Inhibition of the aspartate aminotransferase activity of the AspB enzyme

4.3.8.1 Aminotransferase inhibitors tested

Amino-oxyacetate (cat. n° C13408, Sigma), vigabatrin (cat. n° AB 446916, abcr GmbH) and L-serine *O*-sulfate potassium salt (cat. n° sc-235478, ChemCruz) were dissolved in distilled water. Hesperetin (cat. n° H4125, Sigma), PF-04859989 (cat. n° PZ0250, Sigma), and adapalene (cat. n° A7486, Sigma) were dissolved in dimethyl sulfoxide (DMSO) and kept at -20°C until use.

4.3.8.2 Inhibition assays

The inhibitory activity of the selected compounds against AspB was evaluated using the aminotransferase activity assay coupled to MDH described in previous section. The coupled assays were performed in a final concentration of 250 mM of potassium

phosphate buffer (pH 8), 50 µM of PLP, 4 mM of L-aspartic acid, 0.20 mM of α-KG, 2 units of MDH, 0.12 mM NADH, and different concentrations of the inhibitors. High concentration stocks of adapalene, PF-04859989, and vigabatrin were prepared in their respective solvents and serially diluted (1:10) to evaluate a range of final concentrations between 0 – 100 µM in the assays. In the case of amino-oxyacetate, L-serine *O*-sulfate and hesperetin the range of final concentrations tested was 0 -10 mM, 0 - 50 mM, and 0 - 0.12 mM, respectively.

Each enzyme reaction was initiated by adding a final concentration of 0.01 mg/mL of GOT or AspB into the cuvette and performed at 37°C using a SPECTROstar Nano absorbance reader. The decrease in the absorbance of NADH was spectrophotometrically measured at 340 nm every 5 s for up to 5 min. Enzyme assays with no inhibitor were performed to estimate the total enzyme activity.

Pre-incubation steps of 1 h and 24 h before the assay were included for the potential inhibitors PF-04859989 and vigabatrin while a 1 h pre-incubation step was included for L-serine *O*-sulfate. Following the pre-incubation step, the enzyme reactions were initiated by adding an aliquot from the mixture containing the inhibitor, enzyme, and cofactor, into the cuvette containing all the rest of components of the reaction at the concentrations mentioned above. The assays were performed at 37°C and monitored spectrophotometrically by measuring the decrease in the absorbance of NADH at 340 nm using the plate reader.

Enzyme assays to evaluate the effect of the compounds against MDH were performed under the same conditions as those for GOT and AspB at 5 mM of OAA and 0.12 mM of NADH as substrates in order to discriminate if the inhibitory activity of the active compounds against either GOT or AspB was due to the inhibition of the aminotransferases and not due to the inhibition of MDH.

The enzyme rates were determined from the slopes obtained from the linear phase of the reaction after plotting the data using the Origin(Pro) software version 2019. The

percent of enzyme inhibition was plotted against each inhibitor concentration tested and the IC_{50} values were calculated by fitting the data to the DoseResponse function in Origin(Pro).

4.3.9 Effect of the inhibitor PF-04859989 in *S. aureus* infection using *Galleria mellonella* model

The *Galleria* larvae were bought from Live Foods Direct, United Kingdom, kept on woodchips in the dark at 10°C until use. The larvae were used as a model organism to study any potential effect of the inhibitor PF-04859989 on the virulence of *S. aureus*.

The *S. aureus* strains were streaked out onto TSA plates (wild-type) and TSA plates supplemented with 5 µg/ml of erythromycin (JE2 *aspB*::*Tn*) and incubated at 37°C for 24 h. A single colony of each strain was used to inoculate 10 mL of BHI broth and incubated at 37°C for 16 h in shaking conditions (200 rpm). The overnight cultures were washed with PBS and the bacterial concentration adjusted to inoculate the larvae with 10^5 CFU/larva. For each experiment, 5 larvae weighing between 0.2 and 0.3 g were infected with 10 µL of *S. aureus* wild-type (JE2) alone or in combination with two different final concentrations of the inhibitor PF-04859989 in the larvae (0.01 mM and 0.1 mM). The injection was performed into the hemocoel of each larva through the second left pro-leg using a hypodermic syringe and an automated syringe pump. Larvae infected with the mutant strain JE2 *aspB*::*Tn* alone and in combination with two different final concentrations of the inhibitor in the larvae (0.01 mM and 0.1 mM) were included as well as larvae injected with PBS and with the inhibitor alone as controls. The larvae were left in the dark, inside Petri dishes covered with foil at 37°C and their survival monitored daily over a 5-day period. The larvae were recorded as dead when no mobility response was observed after touching them with a plastic inoculation loop. Three independent experiments were performed using a total of 15 larvae per condition and the results were analysed using the Kaplan-Meier survival analysis in the OriginPro software version 2021b. Statistical differences were determined with a log-rank test using the same software.

4.4 Results

4.4.1 Purification and detection of aspartate aminotransferase activity of the putative AspB

The gene coding a putative aspartate aminotransferase (AspB) from *S. aureus* was cloned into the plasmid pEAHISMRSA2028 and transformed into the *E. coli* BL21 (DE3) host strain by Liu & Naismith. It was successfully expressed and purified by Ni-NTA affinity. The 6xHis-tag was cleaved from the enzyme using a viral endoprotease (TEV) to obtain the native amino acid sequence of the enzyme. The molecular mass of the AspB calculated from the nucleotide sequence was estimated to be 48 kDa by the ProtParam tool and it was reported to be 48 168 Da by Seetharamappa and colleagues (Seetharamappa et al., 2007), which is in good agreement with the band size observed in the eluted samples after the 6xHis-tag removal (Figure 4.3). The enzyme shows an absorbance maximum at 280 nm and a peak at ~350 nm that corresponds to the PLP bound to the enzyme (Figure 4.4). The concentration of the purified protein was determined spectrophotometrically at 280 nm using the extinction coefficient estimated by ProtParam tool from ExPASy (50310 M^{-1} cm^{-1} at 280 nm, measured in water) giving a concentration of 5.7 mg/mL. The AspB enzyme had a specific activity of 12 µmol min^{-1} mg^{-1}, which is half of the activity shown by Cj0762, an aspartate aminotransferase from *Camplylobacter jejuni* that showed an activity of 21.9 µmol min^{-1} mg^{-1} (see Table 4.1). The specific activity shown by the *S. aureus* AspB was more than 10 times lower than the specific activity shown by the aspartate aminotransferase from *P. haloplanktis* when purified with the strong anion exchange resin Poros HQ (137,7 µmol min^{-1} mg^{-1}); 18 times lower than the specific activity showed by the purified aspartate aminotransferase from *B. subtilis* (220 µmol min^{-1} mg-1) after treatment with protamine sulfate that, according to the authors, it could have removed inhibitory compounds from the cells extracts (Sung et al., 1990); and nearly 17 times lower than the activity shown by the aspartate aminotransferase purified from *E. coli* (200 µmol min^{-1} mg^{-1}), see Table 4.1 .

Table 4.1. Specific activities reported for aspartate aminotransferases purified from different microorganisms.

Aspartate aminotransferase source	Specific activity per purification step (µmol min^{-1} mg^{-1})		Reference
Pseudoalteromonas haloplanktis	Cell lysate	4.1	(Birolo et al., 2000)
	$(NH_4)_2SO_4$ 35%	4.5	
	DEAE-Sepharose	22.1	
	$(NH_4)_2SO_4$ 82%	22.6	
	Superdex 200	61.7	
	POROS HQ	137.7*	
Methanococcus aeolicus	Cell extract	0.3	(Xing & Whitman, 1992)
	$(NH_4)_2SO_4$	0.6	
	Phenyl Sepharose	3.6	
	DEAE-Cellulose	6.8	
	S-300 Sephacryl	5.7	
	Hydroxyapatite	5.8	
Phormidium lapideum	$(NH_4)_2SO_4$	0.15	(Kim et al., 2003)
	Heat Treatment	0.9	
	Butyl-Toyopearl	18.5	
	DEAE-Toyopearl	107	
	TSK G-3000SW	221	
***Bacillus* sp**.	Crude extract	0.15	(Sung et al., 1990)
	Protamine sulphate	0.30	
	DEAE-Toyopearl	1.78	
	DEAE- 5PW	3.16	
	Butyl-Toyopearl	120	
	Phenylsuperose	218	
	Hydroxyapatite	220*	

Escherichia coli	Crude extract	0.9	(Yagi et al., 1985)
	Ammonium sulfate fractionation	1.3	
	1st DEAE-Cellulose chromatography	3.7	
	Sephacryl S-200	11.3	
	2nd DEAE-Cellulose chromatography	67.2	
	Hydroxyapatite	200*	
Pseudomonas aeruginosa	Crude extract	1.7	(Gu et al., 1998)
	DEAE-Cellulose	3.5	
	Hydroxylapatite		
	Gradient	11.9	
	Wash	24.5	
	Superdex 75	32.1	
Campylobacter jejuni	Cj0762	21.9*	(Guccione et al., 2008)

* Values used for comparison

To further determine whether the putative AspB enzyme might act as an aspartate aminotransferase, HPLC analyses were performed. For this purpose, the aminotransferase catalysed reaction was assessed at 37°C in a reaction containing L-glutamic acid as an amino donor and oxaloacetic acid as an amino acceptor, and the detection of one of the oxo acids formed during the reaction (KG) was performed through HPLC.

Figure 4.5 shows HPLC chromatograms at UV 324 nm of the derivative keto acids present in the sample after performing the enzyme assay with the putative AspB using L-glutamic acid and OAA as the pair of substrates. The chromatogram on the top of the figure (A) shows the peaks corresponding to OAA, KG, and internal standard (IS) whose elution times were at 276, 555, and 931 seconds after injection, respectively. In the chromatogram of the bottom of the figure (B), a peak can be seen at 540 seconds

corresponding to that of the retention time of the phenylhydrazine derivative of α-KG that eluted at 555 s after injection in the standard sample. The peak corresponding to the derivative of OAA showed a decreased height after 60 seconds from the start of the enzyme reaction and no degradation of this compound was observed during the assay. The results showed that AspB was able to transfer the amino group from L-glutamic acid onto OAA thus showing aminotransferase activity.

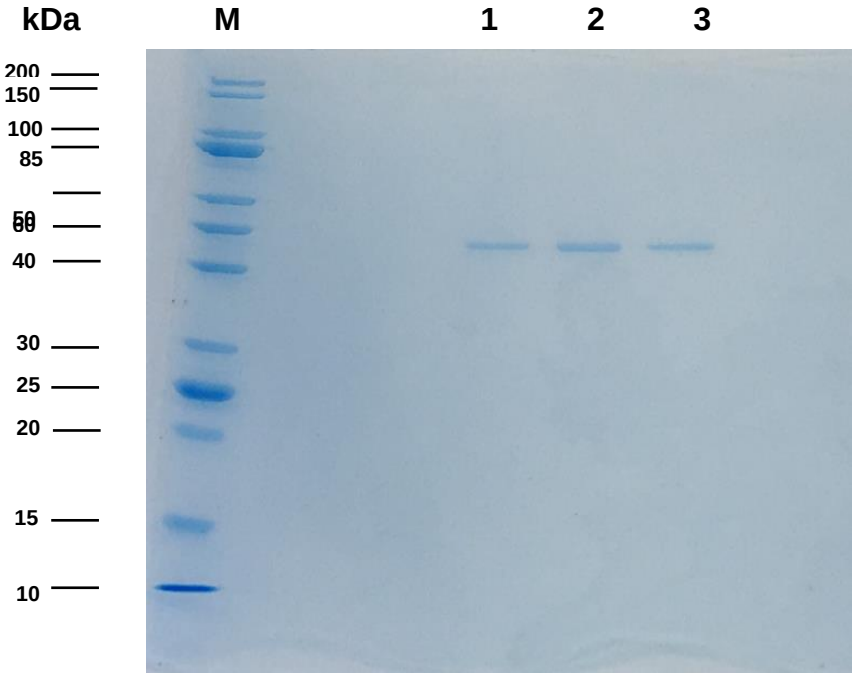

Figure 4.3 - SDS-PAGE of *S. aureus* AspB purification fractions on a 12% polyacrylamide gel.

Lanes: M. Protein marker (10 – 200 kDa), 1 – 3. Three different fractions of the purified AspB protein after TEV treatment with a molecular weight of 48 kDa.

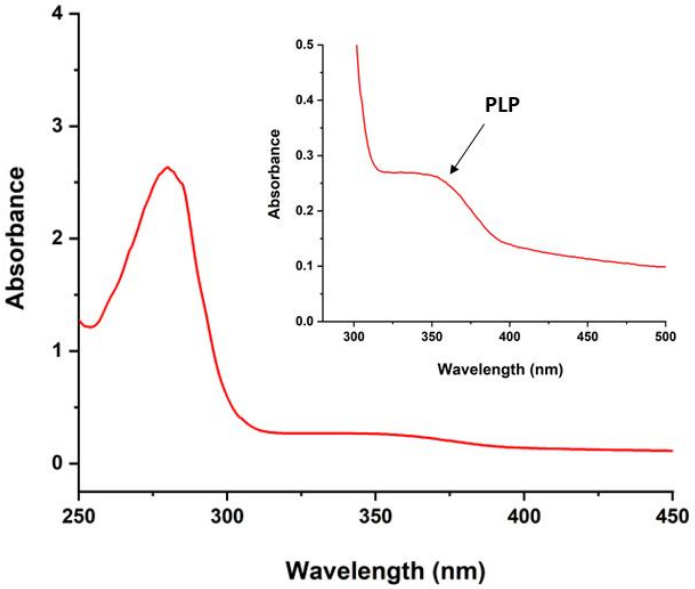

Figure 4.4 - UV-visible spectra of AspB purified from *E. coli*.

The spectrum was recorded in 50 mM Tris buffer containing 0.5 M NaCl, pH 7.5

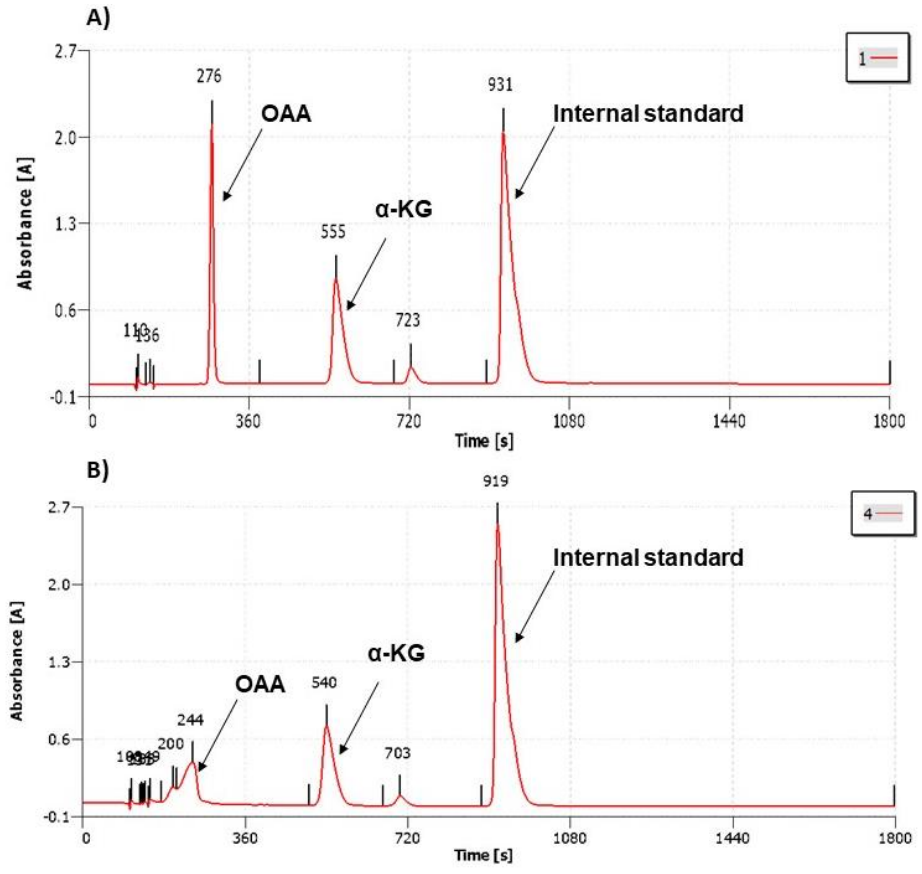

Figure 4.5 - High-performance liquid chromatography (HPLC) analysis on the reaction products of the AspB with L-glutamic acid and oxaloacetic acid as the pair of substrates.

A) Chromatogram corresponding to the standards consisting of α-KG, OAA, and the internal standard (2-oxobutyrate). B) Chromatogram corresponding to the reaction products of the enzyme reaction at 37°C after 60 s of enzyme reaction. The absorption of the derivatized oxoacids was measured at 324 nm.

4.4.2 Determination of the enzyme kinetics of AspB

To further characterise the AspB enzyme, coupled enzymatic assays were performed to determine the kinetics for the pair of substrates of the forward and reverse reactions. Parameters such as maximum velocity (V_{max}), Michaelis-Menten constants (K_m), turnover rate (k_{cat}), and catalytic efficiency (k_{cat}/K_m) were determined and compared to those obtained for the porcine glutamic-oxaloacetic transaminase (GOT) (Table 4.2).

The kinetic parameters for the pair of substrates of the forward reaction were assayed using a coupled enzyme assay with malate dehydrogenase (MDH) (Figure 4.6).

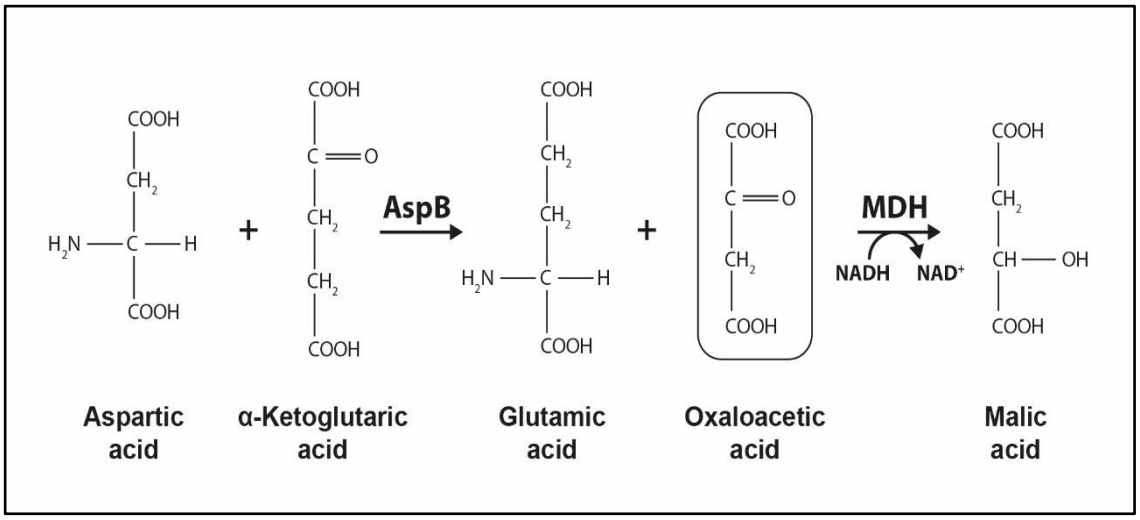

Figure 4.6 - A schematic diagram of the MDH coupled enzyme assay.

The aminotransferase reaction catalysed by AspB produces L-glutamic acid and oxaloacetic acid which is reduced by MDH in the presence of the cofactor NADH. The coupled enzyme assay generates NAD^+ that is detected by the absorbance decrease at 340 nm.

Using a varied concentration of L-aspartic acid and a fixed concentration of α-KG, the $K_m^{L\text{-}asp}$ were determined to be 3.88 mM for GOT (Figure 4.7) and 1.36 mM for AspB (Figure 4.9) with a turnover rate (k_{cat}) of 2,498.84 min^{-1} and 573.20 min^{-1}, respectively (Table 4.2). The GOT enzyme displayed nearly 1.5 times higher catalytic efficiency (k_{cat}/K_m) for L-aspartic acid than the AspB enzyme (Table 4.2). The K_m values shown by AspB for aspartate were compared with those reported for other aminotransferases from different microorganisms (Table 4.3) and the AspB enzyme from *S. aureus* showed higher affinity for aspartate than almost all the other aspartate aminotransferases used

for comparison, except for *Lactobacillus brevis,* that had the highest affinity for aspartate ($K_m^{L\text{-}asp}$ = 0.65 mM).

For the corresponding keto acid evaluated at a fixed L-aspartic acid concentration, the $K_m^{\alpha\text{-}KG}$ was determined to be similar for both enzymes with values of 0.2 mM for GOT (Figure 4.8) and 0.26 mM for AspB (Figure 4.10) with turnover rates (k_{cat}) of 2,126.06 min^{-1} and 506.61 min^{-1}, respectively (Table 4.2). The GOT enzyme displayed 5.4-fold higher catalytic efficiency with α-KG than the AspB (Table 4.2).

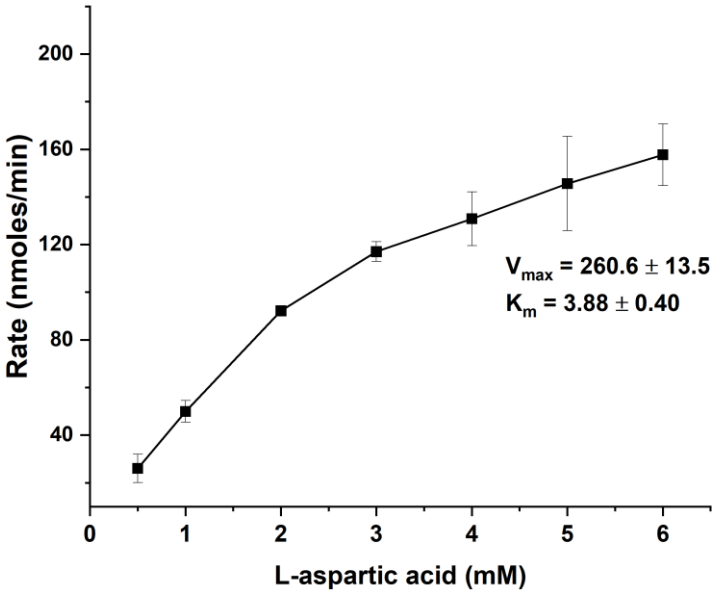

Figure 4.7 - Kinetic parameters of Glutamic-oxaloacetic transaminase (GOT) for L-aspartic acid.

The GOT activity was coupled with 2 U of malate dehydrogenase (MDH) and a range between 0 – 6 mM of L-aspartic acid concentrations was evaluated at a fixed concentration of α-ketoglutarate (10 mM). The reaction was performed at 37°C and pH 7.2. The kinetic parameters were obtained by fitting the data to the Michaelis-Menten equation. The data represent the mean ± standard deviation of three independent experiments performed in triplicate (r^2= 0.996).

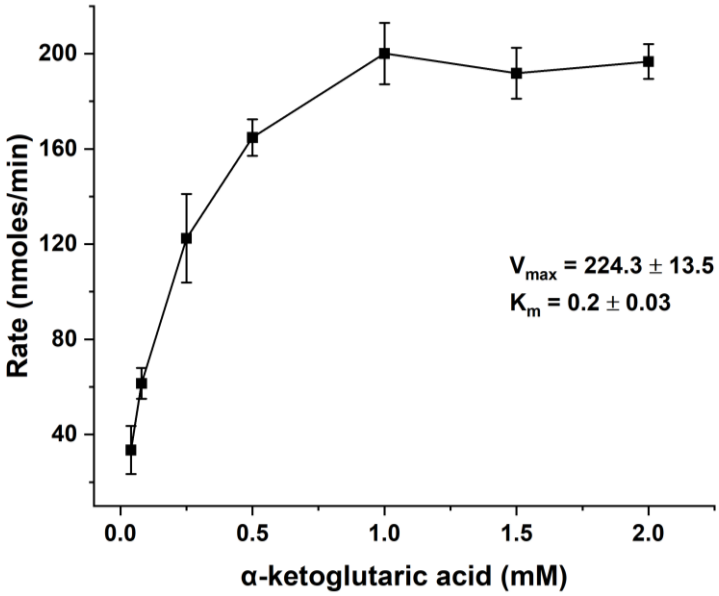

Figure 4.8 - Kinetics parameters of Glutamic-oxaloacetic transaminase (GOT) for α-ketoglutaric acid.

The GOT activity was coupled with 2 U of malate dehydrogenase (MDH) and a range between 0 – 2 mM of α-ketoglutaric acid concentrations was evaluated at a fixed concentration of L-aspartic acid (10 mM). The reaction was performed at 37°C and pH 7.2. The kinetic parameters were obtained by fitting the data to the Michaelis-Menten equation. The data represent the mean ± standard deviation of three independent experiments performed in triplicate (r^2= 0.989).

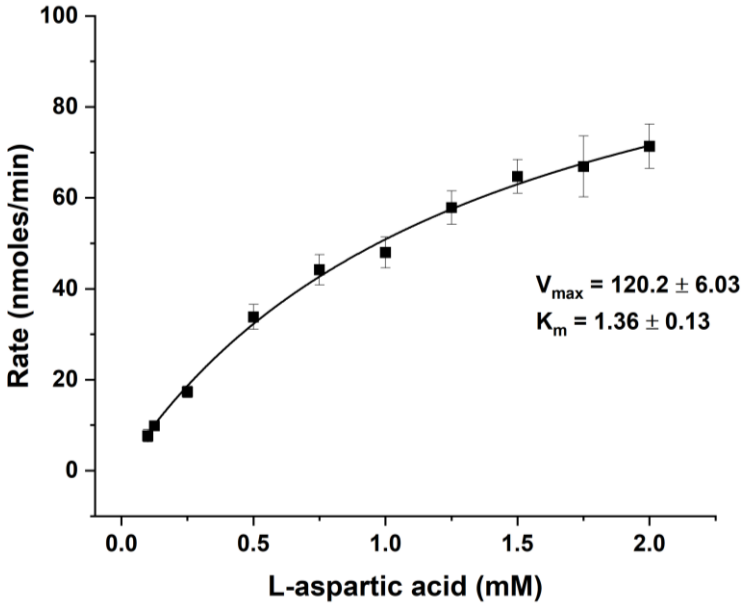

Figure 4.9 - Kinetic parameters of the recombinant aspartate aminotransferase (AspB) from *S. aureus* for L-aspartic acid.

The AspB activity was coupled with 2 U of malate dehydrogenase (MDH) and a range between 0 – 2 mM of L-aspartic acid concentrations was evaluated at a fixed concentration of α-ketoglutarate (10 mM). The reaction was performed at 37°C and pH 7.2. The kinetic parameters were obtained by fitting the data to the Michaelis-Menten equation. The data represent the mean ± standard deviation of three independent experiments performed in triplicate (r^2= 0.996).

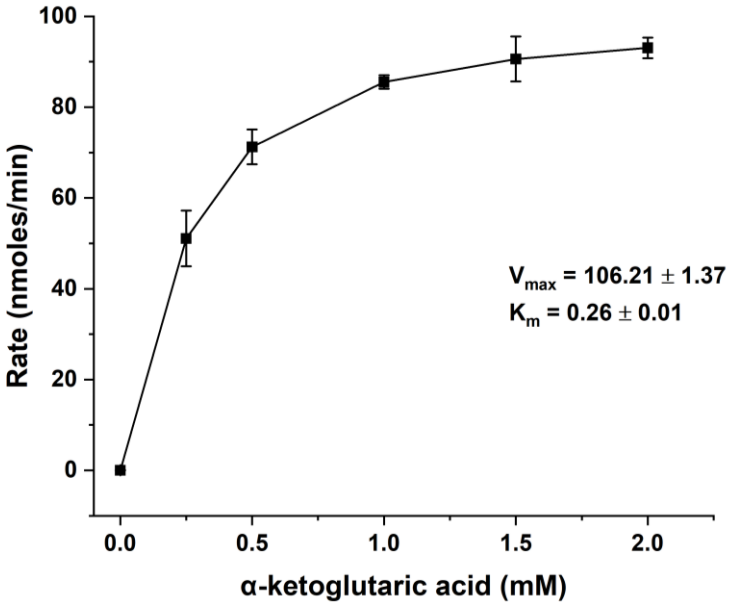

Figure 4.10 - Kinetic parameters of the recombinant aspartate aminotransferase (AspB) from *S. aureus* for α-ketoglutaric acid.

The AspB activity was coupled with 2 U of malate dehydrogenase (MDH) and a range between 0 – 2 mM of α- ketoglutaric acid concentrations was evaluated at a fixed concentration of L-aspartic acid (10 mM). The reaction was performed at 37°C and pH 7.2. The kinetic parameters were obtained by fitting the data to the Michaelis-Menten equation. The data represent the mean ± standard deviation of three independent experiments performed in triplicate (r^2= 0.999).

The kinetic parameters for the pair of substrates of the reverse reaction were assayed using a couple enzyme assay with glutamate dehydrogenase (GDH) (Figure 4.11). With different L-glutamic acid concentrations and a fixed concentration of OAA, the $K_m^{L\text{-}glu}$ was determined to be similar for both enzymes, with values of 1.44 mM for GOT (Figure 4.12) and 1.18 mM for AspB (Figure 4.14) and with a turnover rate (k_{cat}) of 1,143.15 min^{-1} and 156.14 min^{-1}, respectively (Table 4.2). Similarly, to what was described for L-aspartate, the catalytic efficiency (k_{cat}/K_m) for L-glutamic acid was 6.17 times higher with GOT than with AspB (Table 4.2).

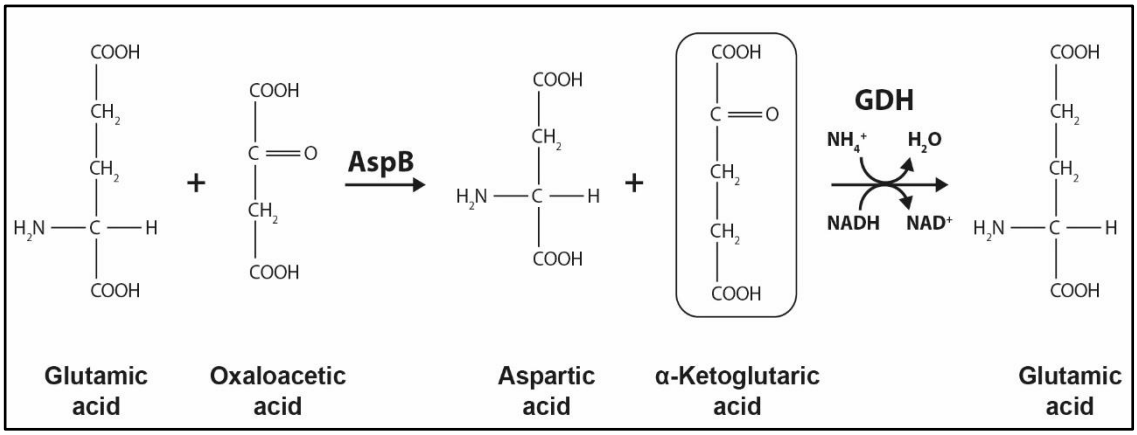

Figure 4.11 - A schematic diagram of the GDH coupled enzyme assay.

The aminotransferase reaction catalysed by AspB produces L-aspartic acid and α-ketoglutaric acid which is reduced by GDH in the presence of the cofactor NADH. The coupled enzyme assay generates NAD^+ that is detected by the absorbance decrease at 340 nm.

For the OAA substrate assayed at a fixed L-glutamic acid concentration, the K_m^{OAA} was similar for the two enzymes with values of 0.23 mM for GOT (Figure 4.13) and 0.20 mM for AspB (Figure 4.15) with turnover rates (k_{cat}) of 1,258.15 min^{-1} and 286.89 min^{-1}, respectively (Table 4.2). The catalytic efficiency (k_{cat}/K_m) for OAA was 5.14 times higher with GOT than with AspB (Table 4.2).

The results showed that both enzymes had higher catalytic efficiency (k_{cat}/K_m) for the keto acids substrates assayed at fixed amino acids concentrations than for the amino acids assayed at fixed keto acid concentrations. For all the substrates assayed, GOT enzyme showed better catalytic efficiency (between 1.5 and 6.2 times higher) than the efficiency showed by AspB.

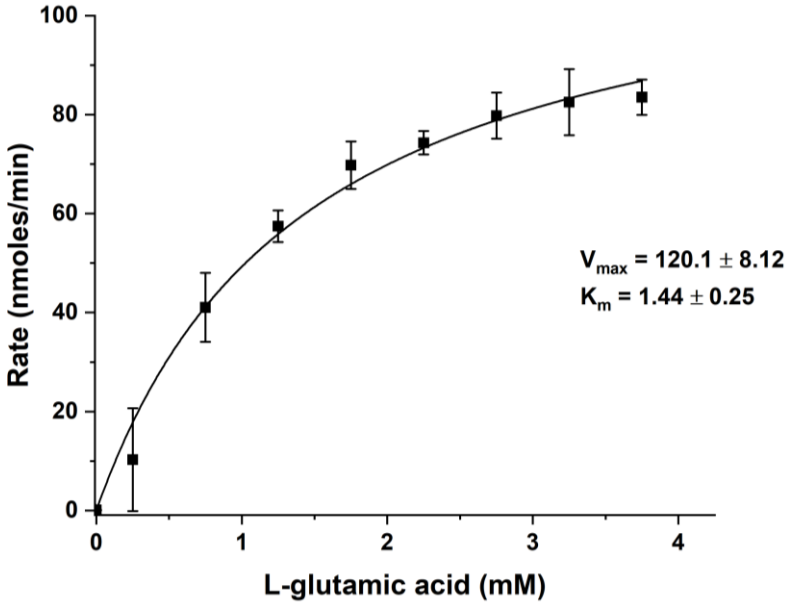

Figure 4.12 - Kinetics parameters of Glutamic-oxaloacetic transaminase (GOT) for L-glutamic acid.

The GOT activity was coupled with 5 U of glutamate dehydrogenase (GDH) and a range between 0 – 3.75 mM of L-glutamic acid concentrations was evaluated at a fixed concentration of oxaloacetic acid (1 mM). The reaction was performed at 37°C and pH 7.45. The kinetic parameters were obtained by fitting the data to the Michaelis-Menten equation. The data represent the mean ± standard deviation of three independent experiments performed in triplicate (r^2= 0.988).

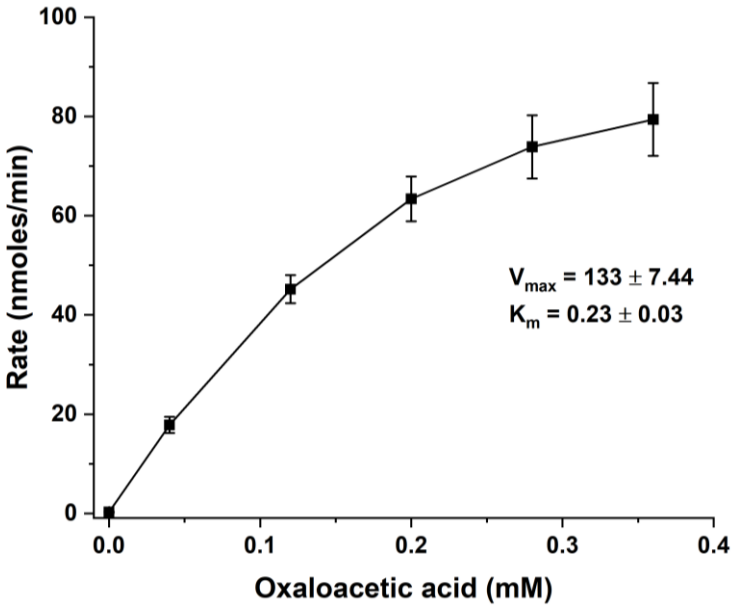

Figure 4.13 - Kinetic parameters of Glutamic-oxaloacetic transaminase (GOT) for oxaloacetic acid (OAA).

The GOT activity was coupled with 5 U of glutamate dehydrogenase (GDH) and a range between 0 – 0.36 mM of OAA concentrations was evaluated at a fixed concentration of L-glutamic acid (10 mM). The reaction was performed at 37°C and pH 7.2. The kinetic parameters were obtained by fitting the data to the Michaelis-Menten equation. The data represent the mean ± standard deviation of three independent experiments performed in triplicate (r^2= 0.998).

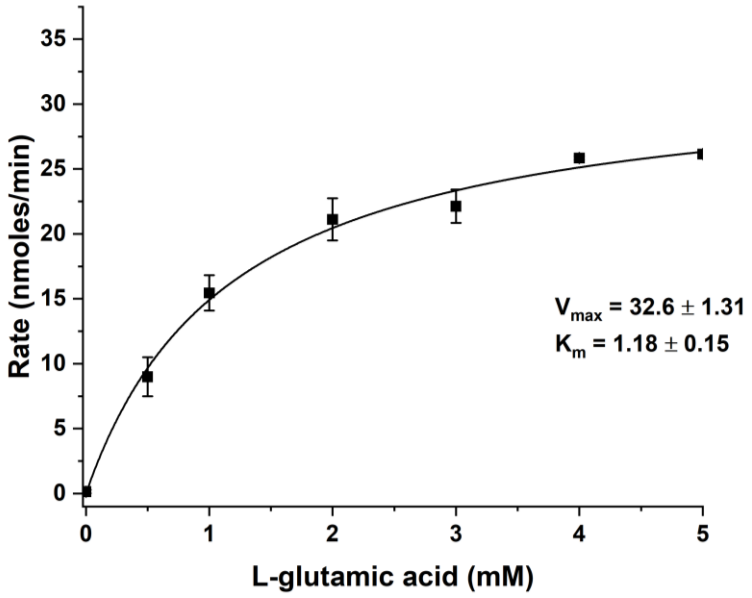

Figure 4.14 - Kinetic parameters of the recombinant aspartate aminotransferase (AspB) from *S. aureus* for L-glutamic acid.

The AspB activity was coupled with 5 U of glutamate dehydrogenase (GDH) and a range between 0 – 5 mM of L-glutamic acid concentrations was evaluated at a fixed concentration of oxaloacetic acid (1 mM). The reaction was performed at 37°C and pH 7.2. The kinetic parameters were obtained by fitting the data to the Michaelis-Menten equation. The data represent the mean ± standard deviation of three independent experiments performed in triplicate (r^2= 0.993).

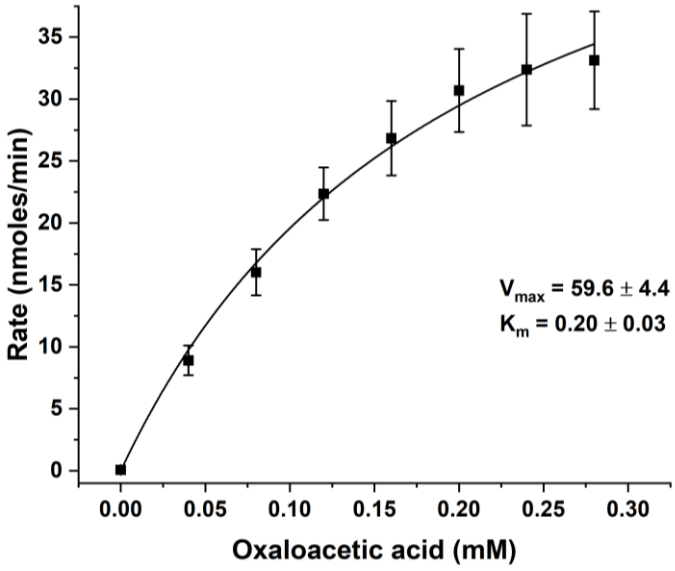

Figure 4.15 - Kinetic parameters of the recombinant aspartate aminotransferase (AspB) from *S. aureus* for oxaloacetic acid (OAA).

The AspB activity was coupled with 5 U of glutamate dehydrogenase (GDH) and a range between 0 – 0.28 mM of OAA concentrations was evaluated at a fixed concentration of L-glutamic acid (10 mM). The reaction was performed at 37°C and pH 7.2. The kinetic parameters were obtained by fitting the data to the Michaelis-Menten equation. The data represent the mean ± standard deviation of three independent experiments performed in triplicate (r^2= 0.994).

Table 4.2. Kinetic parameters of *S. aureus* purified AspB and the control enzyme glutamic-oxaloacetic transaminase type I (GOT).

The V_{max} and Michaelis-Menten constant (K_m) values represent averages from three independent experiments performed in triplicate ± standard deviations**.**

Enzyme	Substrate Pair (Varied, fixed)	V_{max} (nmoles/min)	K_m (mM)	K_{cat} (min^{-1})	K_{cat}/K_m (mM^{-1} min^{-1})
AspB	**Asp/KG**	120.2 ± 6.03	1.36 ± 0.13	573.20 ± 50.76	421
GOT	**Asp/KG**	260.6 ± 13.5	3.88 ± 0.40	2,498.84 ± 470.22	636
AspB	**KG/Asp**	106.21 ± 1.37	0.26 ± 0.01	506.61 ± 17.33	2,006
GOT	**KG/Asp**	224.3 ± 13.5	0.2 ± 0.03	2,126.06 ± 194.08	10,874
AspB	**Glu/OAA**	32.6 ± 1.31	1.18 ± 0.15	156.14 ± 9.52	133
GOT	**Glu/OAA**	120.1 ± 8.12	1.44 ± 0.25	1,143.15 ± 168.83	821
AspB	**OAA/Glu**	59.6 ± 4.4	0.20 ± 0.03	286.89 ± 45.76	1,380
GOT	**OAA/Glu**	133 ± 7.44	0.23 ± 0.03	1,258.15 ± 161.90	7,092

Table 4.3. Michaelis-Menten (K_m) values determined for aspartate aminotransferases from different microbial sources.

	K_m (mM)				
Source	**Aspartate**	**α-ketoglutarate**	**Glutamate**	**Oxaloacetate**	**Reference**
Phormidium lapideum	5.0	0.2	5.7	0.032	(Kim et al., 2003)
Lactobacillus brevis CGMCC 1306	0.65	0.06	ND	ND	(Hu et al., 2017)
Bacillus subtilis B3	6.7	0.3	8.0	0.6	(H. J. Wu et al., 2011)

Crithidia fasciculata	5.0	6.78	11.34	ND	(Berger et al., 2001)
Trypanosoma brucei brucei	10.38	6.96	8.93	ND	
Giardia intestinalis	11.30	5.44	10.94	ND	
Plasmodium falciparum	5.48	1.26	8.90	ND	
Methanococcus aeolicus	3.7	0.5	ND	ND	(Xing & Whitman, 1992)
Bacillus sp.	3.0	2.6	ND	ND	(Sung et al., 1990)
Thermus thermophilus	1.5	1.7	ND	ND	(Oshima et al., 1996)
Campylobacter jejuni	12.8	ND	ND	ND	(Guccione et al., 2008)
Mycobacterium tuberculosis	2.34	ND	ND	ND	(Jansen et al., 2020)
E. coli	1.4	0.15	4.5	0.02	(Köhler et al., 1994)
S. aureus	1.36	0.26	1.18	0.20	This study

ND: Not determined.

4.4.3 Determination of aspartate aminotransferase inhibition by aminotransferase inhibitors

A total of six compounds were selected as potential inhibitors based upon their reported capacity to inhibit different PLP-dependent aminotransferases. All the compounds tested were assayed at similar concentration ranges as those reported as effective against their targets.

The inhibitor amino-oxyacetate (AOA) was chosen as a positive control due to its reported success inhibiting aminotransferases, like alanine, aspartate, and kynurenine aminotransferases. A concentration of 0.1 µM of AOA inhibited GOT activity by more than 50%, while 1 mM was required for similar inhibitory activity on AspB (Figure 4.16). The half-maximal inhibitory concentration (IC_{50}) values of AOA for GOT and AspB were determined to be 5.1 $x10^{-5}$ mM and 0.24 mM, respectively (Figure 4.17). Similar IC_{50} values have been reported for the inhibition of a human aspartate aminotransferase (IC_{50}= 0.52 mM) (Thornburg et al., 2008) while a concentration of 4.5 mM of AOA were needed to decrease the activity of an hepatic aspartate aminotransferase from *Sparus aurata* by more than 50% (González et al., 2012).

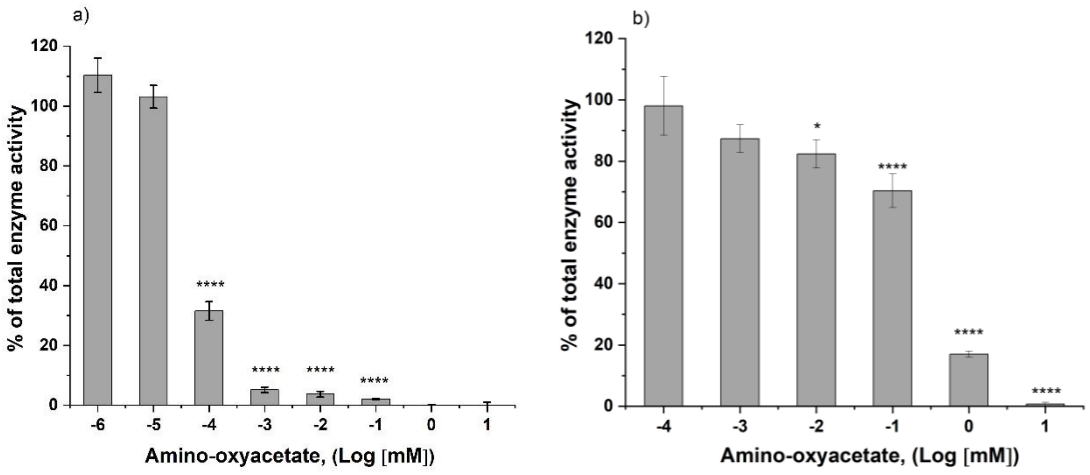

Figure 4.16 - Percent inhibition of aminotransferase activity by amino-oxyacetate (AOA).

The inhibition assays were performed at 37°C in 250 mM potassium phosphate buffer pH 7.2 using a wide range of AOA concentrations. The enzyme activity was measured by monitoring the decrease in absorbance of NADH at 340 nm over time. a) Corresponds to the AOA activity on GOT while b) on AspB. The data are presented as the mean ± standard deviation of n = 3 determinations.

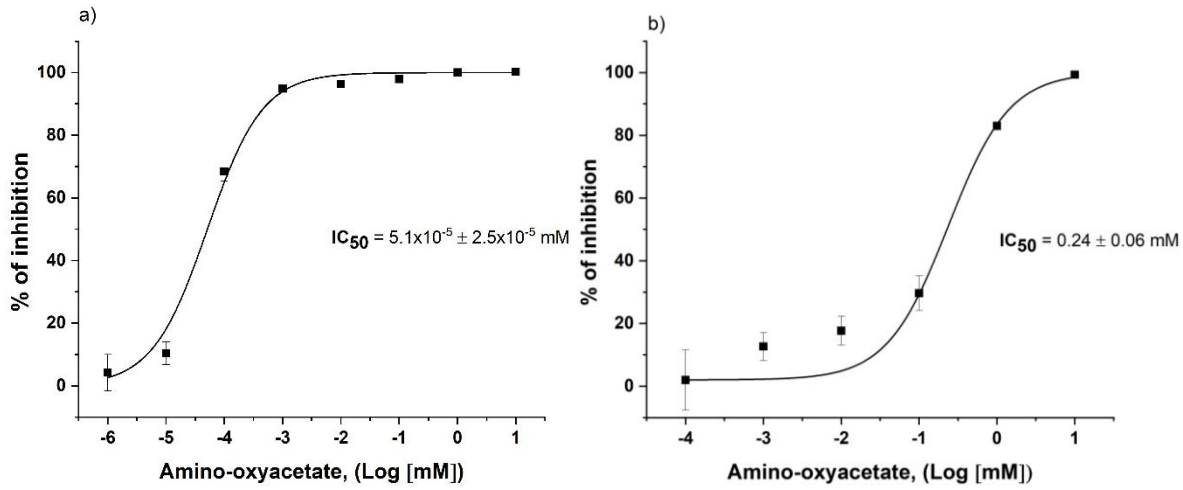

Figure 4.17 - Representative dose-response curve used to determine IC_{50} values of amino-oxyacetate (AOA) on the aminotransferase activity.

The inhibition assays were carried out at 37°C in 250 mM potassium phosphate buffer pH 7.2. The GOT and AspB activities were measured by monitoring the decrease in absorbance in NADH at 340 nm over time. The IC_{50} values of AOA on GOT (a) and on AspB (b) were determined by fitting the data to the dose response equation in OriginPro and represent the mean ± standard deviation of n = 3 determinations.

PF-04859989, an inhibitor with activity against kynurenine aminotransferase II, showed an obvious inhibitory effect on both enzymes with the most potent inhibitory activity against AspB amongst the compounds tested. It has been reported that this compound needed a pre-incubation step with the enzyme and cofactor to be effective showing a time-dependent inhibitory activity against GOT 1 (T. Yoshida et al., 2020). To determine both, its inhibitory activity, and the effect of the length of pre-incubation time on the activity, two different pre-incubation time conditions were evaluated, 1 h and 24 h. The results showed that the length of the pre-incubation time did not have an effect in the inhibitory activity of PF-04859989 against both, GOT (Figure 4.18) and AspB (Figure 4.19). The IC_{50} values of the compound on GOT were 5.61 ± 1.74 µM and 5.56 ± 1.08 µM after 1 h and 24 h of pre-incubation, respectively (Figure 4.20). Meanwhile, a two-fold higher potency was shown by the compound on inhibiting the AspB enzyme, compared to GOT, with IC_{50} values of 2.6 ± 0.15 µM and 2.5 ± 0.2 µM after 1 h and 24 h of pre-incubation, respectively (Figure 4.21).

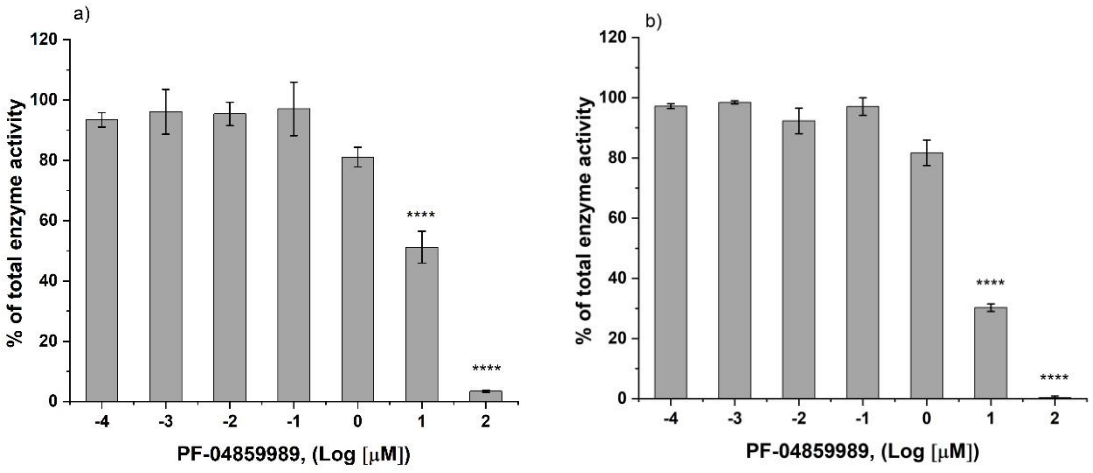

Figure 4.18 - Percent of inhibition of GOT activity by PF-04859989.

The inhibition assays were performed at 37°C in 250 mM potassium phosphate buffer pH 7.3 using a wide range of PF-04859989 concentrations. The enzyme activity was measured by monitoring the decrease in absorbance of NADH at 340 nm over time. a) PF-04859989 activity on GOT after 1 h of pre-incubation while b), after 24 h of pre-incubation. The data are presented as the mean ± standard deviation of n = 3 determinations.

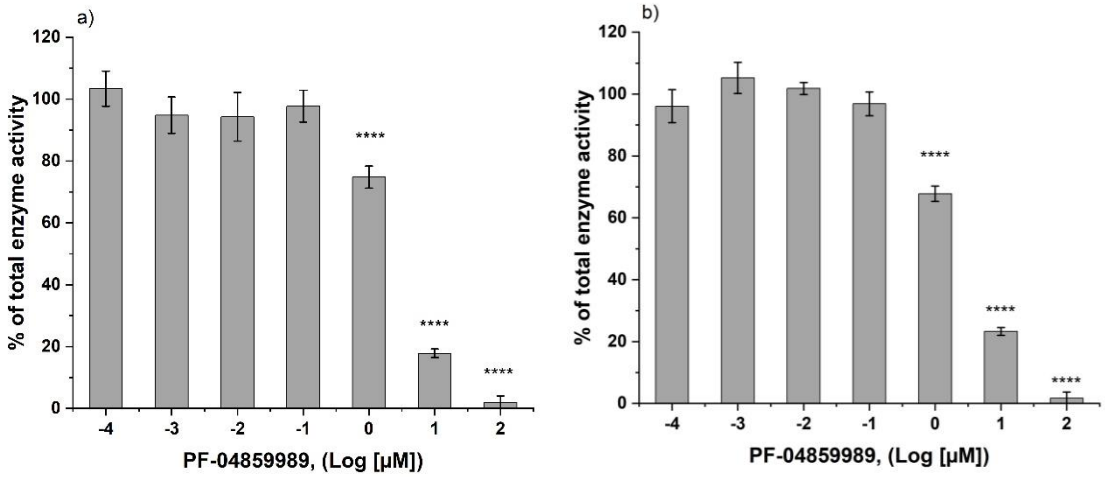

Figure 4.19 - Percent inhibition of AspB activity by PF-04859989.

The inhibition assays were performed at 37°C in 250 mM potassium phosphate buffer pH 7.25 using a wide range of PF-04859989 concentrations. The enzyme activity was measured by monitoring the decrease in absorbance of NADH at 340 nm over time. a) PF-04859989 activity on AspB after 1 h of pre-incubation while b), after 24 h of pre-incubation. The data are presented as the mean ± standard deviation of n = 3 determinations.

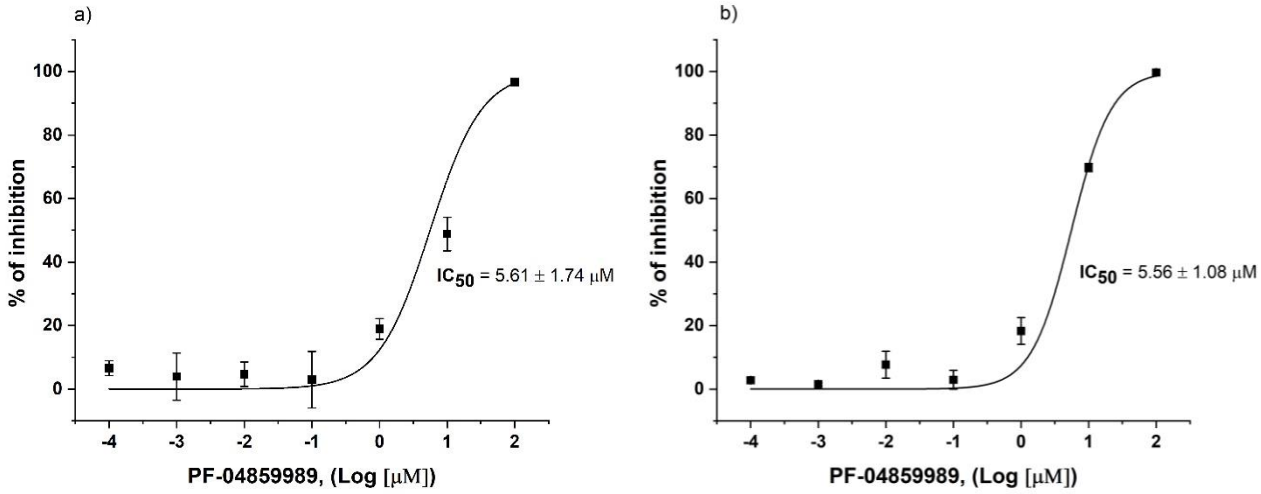

Figure 4.20 - Representative dose-response curve used to determine IC_{50} values of PF-04859989 on the GOT activity.

The inhibition assays were carried out at 37°C in 250 mM potassium phosphate buffer pH 7.3. The GOT activity was measured by monitoring the decrease in absorbance in NADH at 340 nm over time. The IC_{50} values of PF-04859989 on GOT after 1 h pre-incubation (a) or 24 h pre-incubation (b) were determined by fitting the data to the dose response equation in OriginPro and represent the mean ± standard deviation of n = 3 determinations.

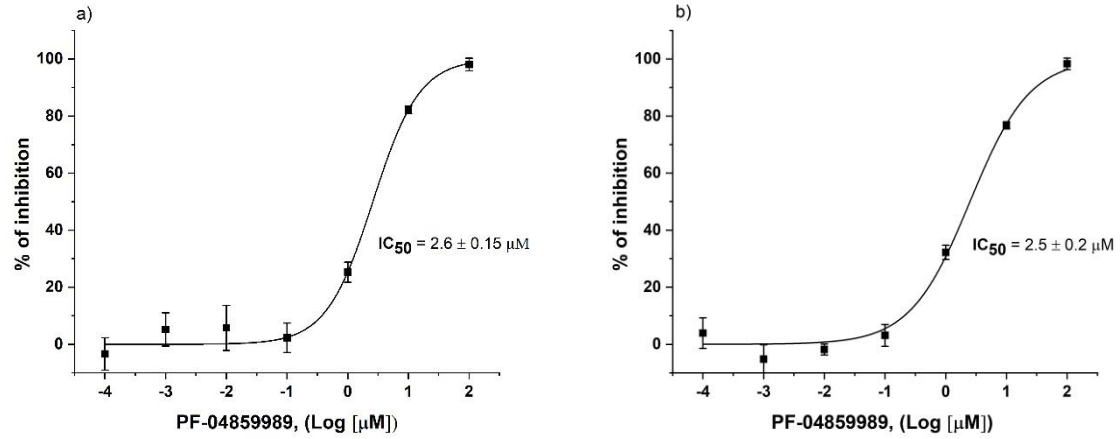

Figure 4.21 - Representative dose-response curve used to determine IC_{50} values of PF-04859989 on the AspB activity.

The inhibition assays were carried out at 37°C in 250 mM potassium phosphate buffer pH 7.25. The AspB activity was measured by monitoring the decrease in absorbance in NADH at 340 nm over time. The IC_{50} values of PF-04859989 on AspB after 1 h pre-incubation (a) or 24 h pre-incubation (b) were determined by fitting the data to the dose response equation in OriginPro and represent the mean ± standard deviation of n = 3 determinations.

The reported non-competitive inhibitor of GOT 1, adapalene, currently used for the treatment of acne vulgaris, was also included as a possible AspB inhibitor. Adapalene, unlike PF-04859989, is not reported to require prior incubation with the enzyme and cofactor since the compound binds to a pocket located at the back of the active site of the enzyme (Q. Wang et al., 2019). The results show that this compound was able to significantly reduce (≥ 50% of inhibition) the activity of both enzymes at a concentration of 10 µM (Figure 4.22) with an IC_{50} value of 4.61 ± µM on GOT and 5.45 ± µM on AspB (Figure 4.23).

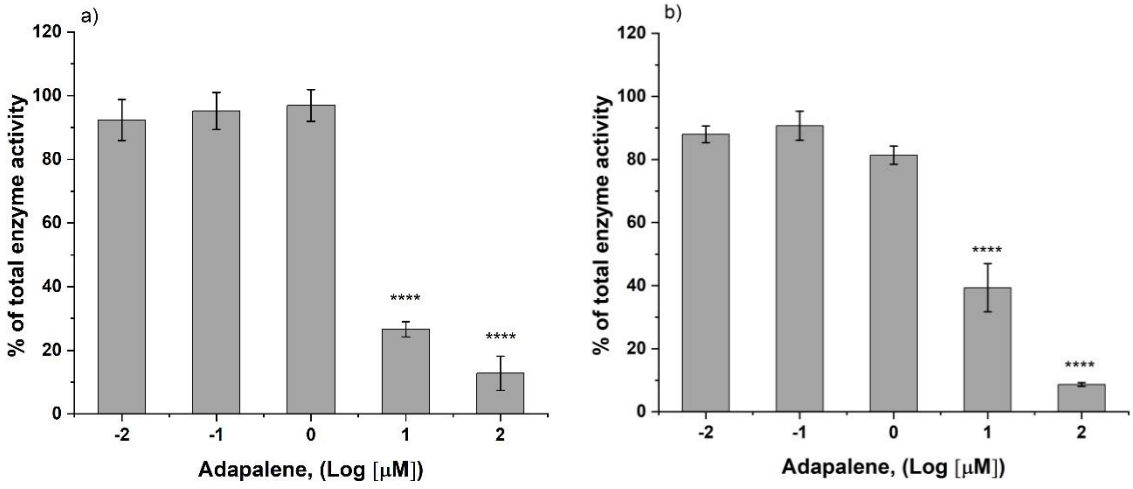

Figure 4.22 - Percent inhibition of aminotransferase activity by adapalene.

The inhibition assays were performed at 37°C in 250 mM potassium phosphate buffer pH 7.2 using a range of adapalene concentrations. The enzyme activity was measured by monitoring the decrease in absorbance of NADH at 340 nm over time. a) Adapalene activity on GOT while b), on AspB. The data are presented as the mean ± standard deviation of n = 3 determinations.

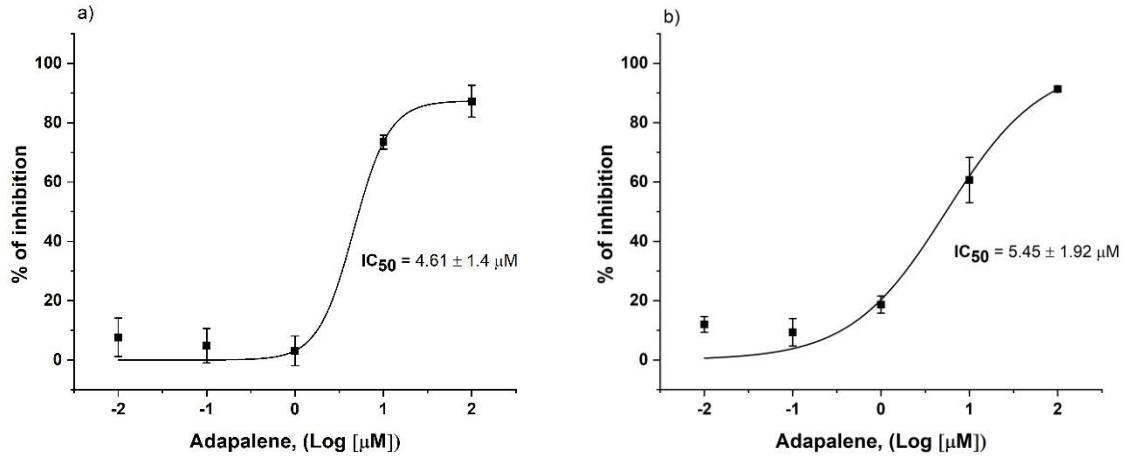

Figure 4.23 - Representative dose-response curve used to determine IC_{50} values of adapalene on the aminotransferase activity.

The inhibition assays were carried out at 37°C in 250 mM potassium phosphate buffer pH 7.2. The GOT and AspB activities were measured by monitoring the decrease in absorbance in NADH at 340 nm over time. The IC_{50} values of adapalene on GOT (a) and on AspB (b) were determined by fitting the data to the dose response equation in OriginPro and represent the mean ± standard deviation of n = 3 determinations.

The glutamate analogue, L-serine *O*-sulfate (L-SOS), has been reported to reduce the activity of an aspartate aminotransferase by 67% (Brennan et al., 2006) and it was chosen as a potential candidate to inhibit the AspB enzyme. A wide range of concentrations of the compound was used ($1x10^{-4}$ mM – 100 mM) in order to test assay concentrations that give inhibitory activity at least two points below the lower bend point and two points above the upper bend point of the curve (Sebaugh, 2011). The compound was pre incubated with the enzyme and cofactor for 1 h before the enzyme assays were performed. The results shown that L-SOS was able to completely inhibit both enzymes at 10 mM showing a higher activity on AspB since more that 50% of the enzyme activity was inhibited at 0.1 mM while a similar effect on GOT was obtained at 1 mM (Figure 4.24). The compound showed a 20-fold selectivity for the bacterial aspartate aminotransferase over the control enzyme with IC_{50} values of 0.44 ± 0.18 mM for GOT and 0.021 ± 0 mM for AspB (Figure 4.25).

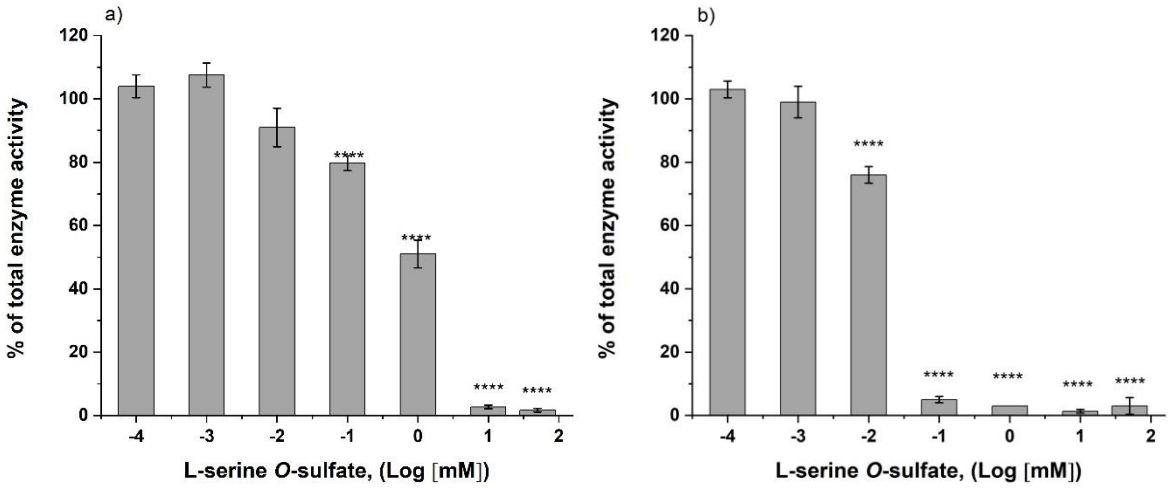

Figure 4.24 - Percent inhibition of aminotransferase activity by L-serine *O*-sulfate (L-SOS).

The inhibition assays were performed at 37°C in 250 mM potassium phosphate buffer pH 7.4 using a wide range of L-SOS concentrations. The enzyme activity was measured by monitoring the decrease in absorbance of NADH at 340 nm over time. a) L-SOS activity on GOT while b), on AspB. The data are presented as the mean ± standard deviation of n = 3 determinations.

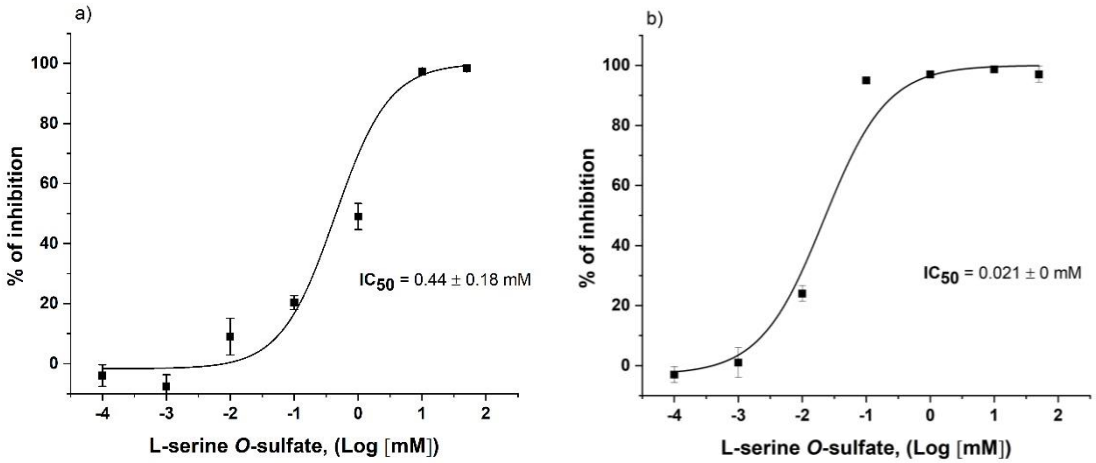

Figure 4.25 - Representative dose-response curve used to determine IC_{50} value of L-serine *O*-sulfate on the aminotransferase activity.

The inhibition assays were carried out at 37°C in 250 mM potassium phosphate buffer pH 7.4. The GOT and AspB activities were measured by monitoring the decrease in absorbance in NADH at 340 nm over time. The IC_{50} values of L-SOS on GOT (a) and on AspB (b) were determined by fitting the data to the dose response equation in OriginPro and represent the mean ± standard deviation of n = 3 determinations.

Vigabatrin, an inhibitor of GABA-AT, was also assayed for its ability to inhibit the bacterial aminotransferase. As shown in Figure 4.26, it did not exert any effect on the activity of GOT, neither after 1 h or 24 h of pre-incubation with the enzyme and cofactor. A decrease in the activity of AspB was observed when the compound was tested at 100 μM after 1 h of preincubation and no further improvement of the inhibitory activity of the compound was observed after a longer pre-incubation time, even showing a decrease in its inhibitory effect after 24 h of pre-incubation (Figure 4.27). In the case of hesperetin, no significantly inhibitory activity was found with either of the aminotransferases at the concentrations tested (Figure 4.28).

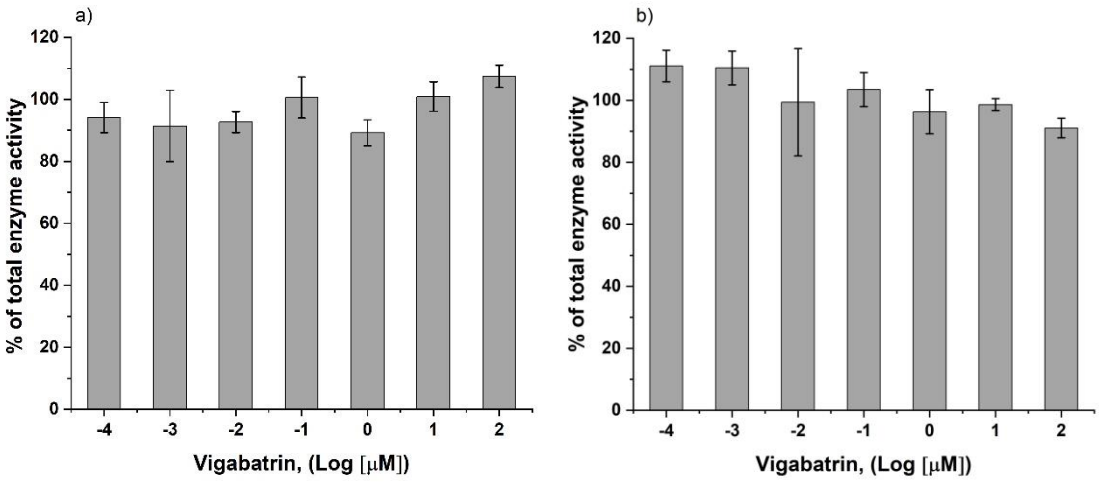

Figure 4.26 - Percent inhibition of GOT activity by vigabatrin.

The inhibition assays were performed at 37°C in 250 mM potassium phosphate buffer pH 7.4 using a wide range of vigabatrin concentrations ($1x10^{-4}$ μM – 100 μM). The enzyme activity was measured by monitoring the decrease in absorbance of NADH at 340 nm over time. a) Vigabatrin activity on GOT after 1 h of pre-incubation while b), after 24 h of pre-incubation. The data are presented as the mean ± standard deviation of n = 3 determinations.

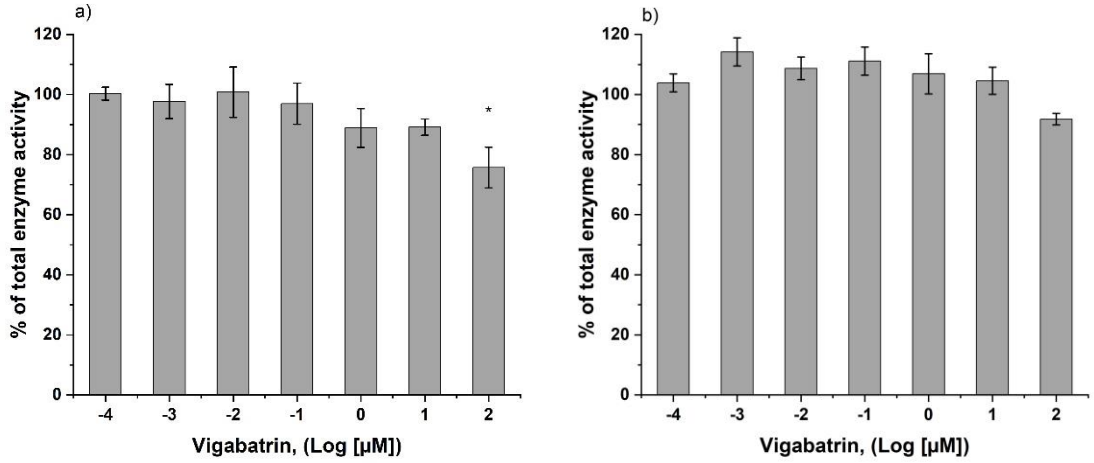

Figure 4.27 - Percent inhibition of AspB activity by vigabatrin.

The inhibition assays were performed at 37°C in 250 mM potassium phosphate buffer pH 7.4 using a wide range of vigabatrin concentrations ($1x10^{-4}$ µM – 100 µM). The enzyme activity was measured by monitoring the decrease in absorbance of NADH at 340 nm over time. a) Vigabatrin activity on AspB after 1 h of pre-incubation while b), after 24 h of pre-incubation. The data are presented as the mean ± standard deviation of n = 3 determinations.

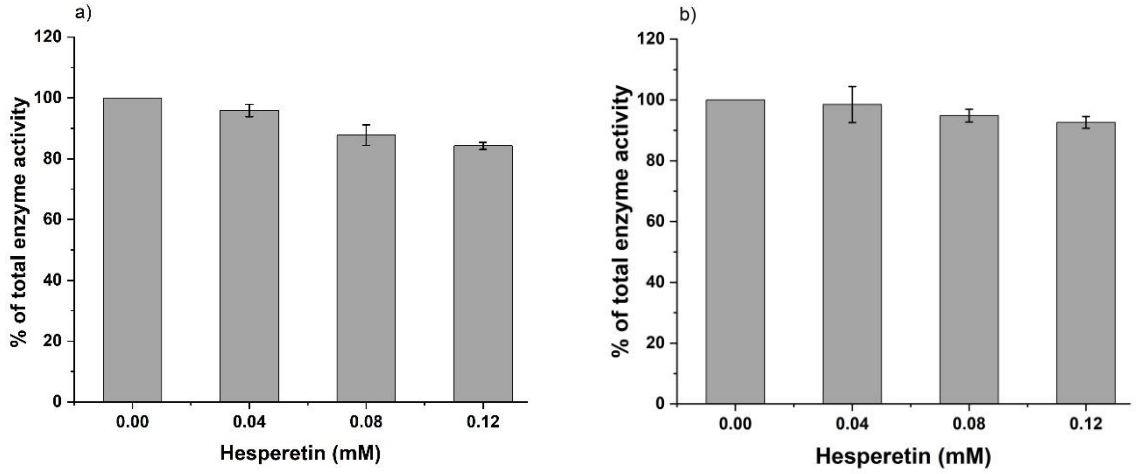

Figure 4.28 - Percent inhibition of aminotransferase activity by hesperetin.

The inhibition assays were performed at 37°C in 250 mM potassium phosphate buffer pH 7.3 using a hesperetin concentrations between 0 and 0.12 mM. The enzyme activity was measured by monitoring the decrease in absorbance of NADH at 340 nm over time. The left plot corresponds to the hesperetin activity on GOT while the right plot, on AspB. The data are presented as the mean ± standard deviation of n = 3 determinations.

To rule out that the inhibitory effect of the compounds was due to the inhibition of the aminotransferases and not of the malic dehydrogenase (MDH), which is coupled to either GOT or AspB, inhibitory assays on MDH were performed. Neither AOA nor PF-04859989 showed activity on MDH (Figure 4.29). L-SOS started to show a decrease in the enzyme activity of MDH at 50 mM, which is 5 times higher than the concentration needed to completely inhibit both aminotransferases (Figure 4.30). In the case of adapalene, a concentration of 100 µM was required to inhibit more than 70% of MDH activity, that is 10 times higher the concentration needed to show similar results with the aminotransferases (Figure 4.30). These results demonstrated that the activity of the compounds was due to the inhibition of both aminotransferases rather than their inhibition on MDH.

In summary, the data showed that PF-04859989 proved to be a potent inhibitor of the AspB with the lowest IC_{50} value amongst the compounds tested, followed by adapalene and L-SOS. Meanwhile, the potential inhibitors vigabatrin and hesperetin did not lead to the inhibition of the aminotransferases at the concentrations tested.

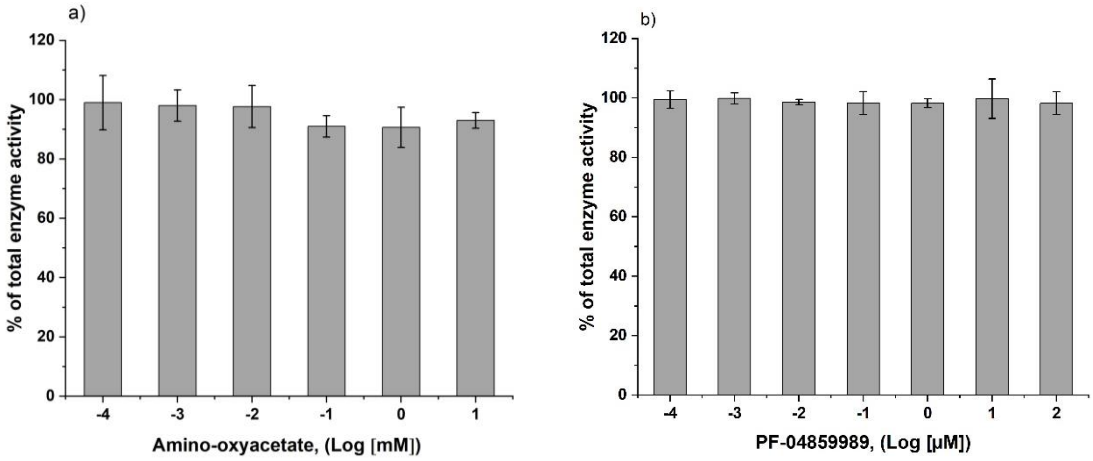

Figure 4.29 - Percent inhibition of MDH activity by amino-oxyacetate (AOA) and PF-04859989.

The inhibition assays were performed at 37°C in 250 mM potassium phosphate buffer with the inhibitors AOA and PF-04859989 at pH 7.2 and 7.5, respectively. The inhibitor concentrations assessed were the same as those assessed in the aminotransferase inhibition assays. The enzyme activity was measured by monitoring the decrease in absorbance of NADH at 340 nm over time. a) AOA activity on MDH and b) PF-04859989 activity on MDH. The data are presented as the mean ± standard deviation of n = 3 determinations.

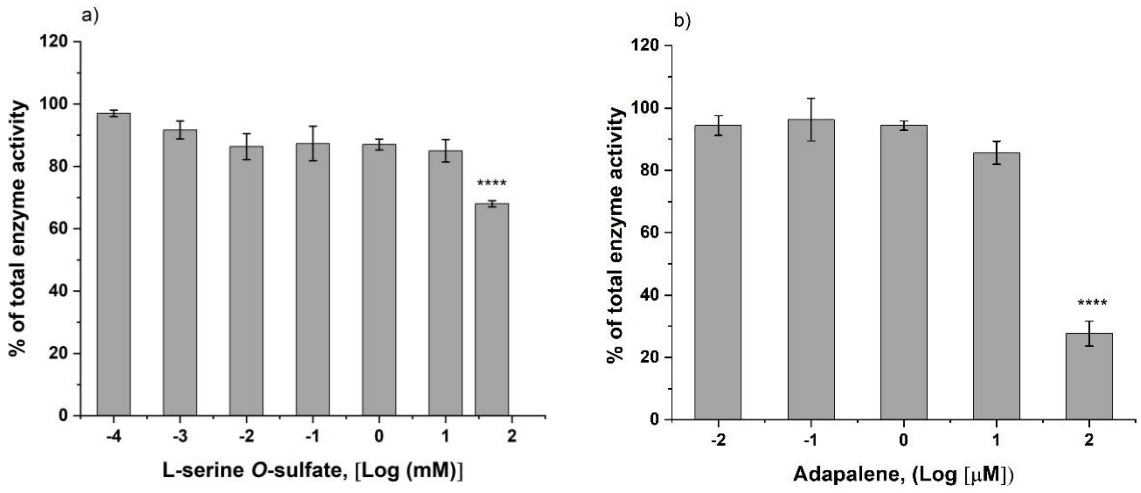

Figure 4.30 - Percent inhibition of MDH activity by L-serine *O*-sulfate (L-SOS) and adapalene.

The inhibition assays were performed at 37°C in 250 mM potassium phosphate buffer with the inhibitors L-SOS and adapalene at pH 7.2 and 7.4, respectively. The inhibitor concentrations assessed were the same as those assessed in the aminotransferase inhibition assays. The enzyme activity was measured by monitoring the decrease in absorbance of NADH at 340 nm over time. The left plot corresponds to the L-SOS activity on MDH while the right plot corresponds to the adapalene activity on MDH. The data are presented as the mean ± standard deviation of n = 3 determinations.

Table 4.4. The IC_{50} values of the inhibitors tested against the aminotransferases.

The values correspond to the average and the standard deviation of n = 3 determinations.

Compound	IC_{50} GOT (μM)	IC_{50} AspB (μM)
Amino-oxyacetate (AOA)	0.051 ± 0.025	240 ± 60
PF- 04859989 (1 h pre-incubation)	5.61 ± 1.74	2.6 ± 0.15
PF-04859989 (24 h pre-incubation)	5.56 ± 1.08	2.5 ± 0.2
Adapalene	4.61 ± 1.4	5.45 ± 1.92
Vigabatrin (1 h pre-incubation)	ND	ND
Vigabatrin (24 h pre-incubation)	ND	ND
L-serine *O*-sulfate (L-SOS)	440 ± 180	21 ± 0
Hesperetin	ND	ND

ND: Not Determined

4.4.4 Effect of the inhibitor PF-04859989 on *S. aureus* infection of *Galleria mellonella*

Amongst the inhibitors tested against the purified aspartate aminotransferase from *S. aureus* (AspB), the compounds PF-04859989 and adapalene showed the highest inhibitory activity with IC_{50} values of 2.6 and 5.5 μM, respectively. Both compounds seemed to be good candidates to test if any protective effect was given by the inhibitors to the larvae infected with the wild-type strain of *S. aureus*. Although the water solubility of adapalene is reported to be $4.0x10^{-6}$ g/L (Wishart et al., 2022), it was not possible to dissolve it in water at the concentration required. Other reported solvents of adapalene are tetrahydrofuran and ethanol (Piskin & Uzunali, 2007), but we used dimethyl sulfoxide (DMSO) instead as it was used to dissolve adapalene when performing the enzyme inhibition assays. However, DMSO resulted to be toxic for the larvae when preliminary assays were performed by injecting the larvae with 10 μL of different concentrations of DMSO (data not shown). For this reason, adapalene was not used in the assays, instead PF-04859989 was tested at two different final concentrations in the larvae in order to assess if any protective effect against *S. aureus* infection was given by this compound. PF-04859989 is water soluble, and it was dissolved in sterile PBS to avoid any potential killing of the larvae caused by injecting distilled H_2O. It is worth mentioning that this compound was able to completely inhibit the purified AspB at 0.1 mM in the inhibitory assays and showed similar IC_{50} values when pre-incubated for either 1 or 24 h with the enzyme and cofactor, with values of 2.6 and 2.5 μM, respectively. Taking into consideration that these values inhibited completely (0.1 mM) or half (2.5 μM) the enzymatic activity, it was decided to test two different final concentrations of the inhibitor in the larvae: 0.01 mM and 0.1 mM as these concentrations were 5- and 50-fold higher than the IC_{50} value determined for the purified AspB. The results show that at a final concentration of 0.01 mM of the PF-04859989 in the larvae, no protective effect was given by the inhibitor against the infection with the wild-type strain of *S. aureus* as no significant differences were observed between the larvae infected with the wild-type

strain alone or in combination with the inhibitor (Figure 4.31). Similar results were observed when the inhibitor was assessed at 0.1 mM final concentration in the larvae as no significant differences in the virulence of the wild-type strain were determined for the larvae infected with *S. aureus* JE2 alone or in combination with the inhibitor (Figure 4.32).

These results suggest that higher concentration of the inhibitor in the larvae should be tested to visualize any protective effect against *S. aureus* infection, or that the inhibitor is not entering the bacterial cells thus it is not reaching its target. Another possibility is that the inhibitor is being metabolised/degraded by the larvae, thus no protective effect against the infection could be observed.

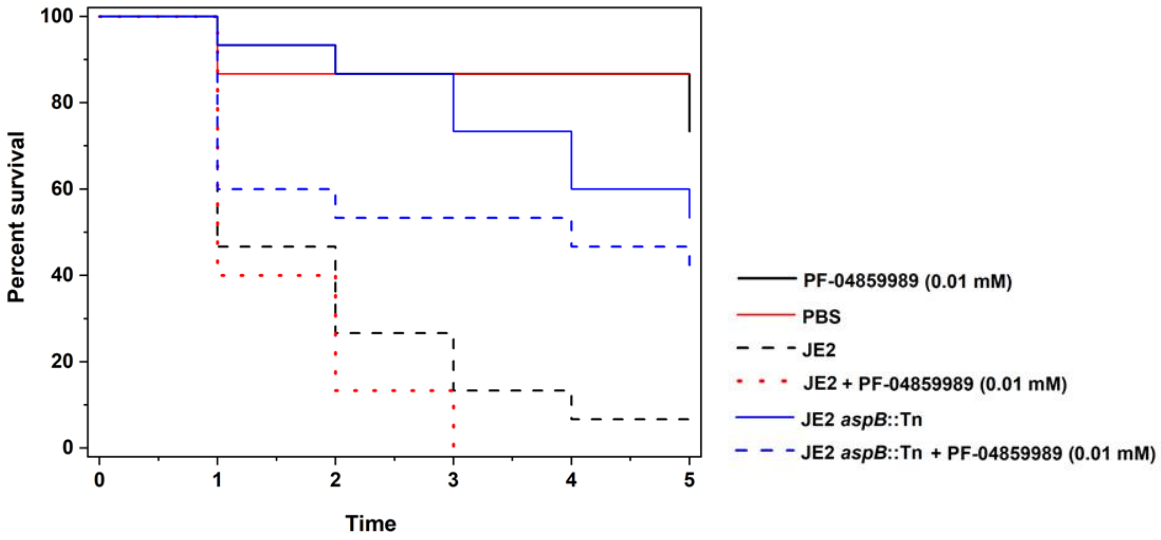

Figure 4.31 - Effect of the inhibitor PF-04859989 (0.01 mM) on the virulence of *S. aureus* in *G. mellonella* model.

The Kaplan-Meier plot indicates the viability of *Galleria* larvae over a period of 5 days after infection with the wild-type strain (JE2) alone (black-dashed line) or in combination with 0.01 mM of PF-04859989 (red-dashed line) at 10^5 CFU/larva. The inhibitor alone administered to the larvae (black-straight line) as well as PBS injected larvae (red-straight line) were included as controls together with the larvae infected with the mutant strain for the AspB alone (JE2 *aspB*::*Tn*) (blue-straight line) or in combination with 0.01 mM of PF-04859989 (blue-dashed line). The data are derived from three independent experiments with groups of 5 larvae each (n = 15).

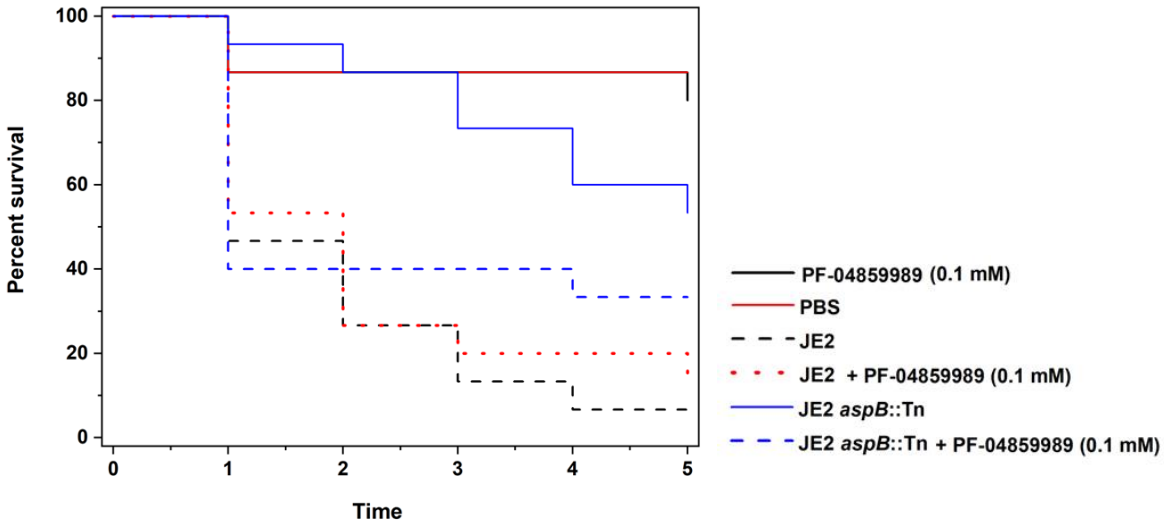

Figure 4.32 - Effect of the inhibitor PF-04859989 (0.1 mM) on the virulence of *S. aureus* in *G. mellonella* model.

The Kaplan-Meier plot indicates the viability of *Galleria* larvae over a period of 5 days after infection with the wild-type strain (JE2) alone (black-dashed line) or in combination with 0.1 mM of PF-04859989 (red-dashed line) at 10^5 CFU/larva. The inhibitor alone administered to the larvae (black-straight line) as well as PBS injected larvae (red-straight line) were included as controls together with the larvae infected with the mutant strain for the AspB alone (JE2 *aspB*::*Tn*) (blue-straight line) or in combination with 0.1 mM of PF-04859989 (blue-dashed line). The data are derived from three independent experiments with groups of 5 larvae each (n = 15).

4.5 Discussion

The gene *SAUSA300_1916* is bioinformatically predicted to code an aspartate aminotransferase in *S. aureus*, however its enzymatic activity has not been yet experimentally determined.

The difficulty in functionally characterising all the genes and their protein products identified in a genome leads to the use of computational tools to try and predict function and to annotate genes (Ellens et al., 2017). Computational functional prediction relies on algorithms developed to analyse the sequence homology between unknown or novel sequences and those deposited in public databases. However, it has been proposed that genomic enzymology and postgenomic approaches should be considered when determining a protein/enzymatic function (Saghatelian & Cravatt, 2005). Some authors have suggested predicting the function of a new sequence based on its homology to an experimentally determined protein function (Kasif & Roberts, 2020). With a more rigorous approach, others have suggested a protein to be annotated as having an unknown function until both, its biological and molecular properties are determined (Ellens et al., 2017).

It has been estimated that nearly half of the predicted coding sequences are wrongly annotated, unannotated or code extra functions (Ellens et al., 2017) and that less than 0.01% of the prokaryotic genes are assigned to functions that have traceable experimental support (Law et al., 2021). As an example of this protein annotation gap, Jansen and colleagues highlighted this problem when studying the gene *rv3722c* of *Mycobacterium tuberculosis,* which was annotated as an unknown protein and at the same time it was predicted to code a wide variety of functions: PLP-binding enzyme, serine hydrolase, secreted protein, and a member of the GntR family of transcription factors (Jansen et al., 2020). These authors studying aminotransferases found two types of misannotation in their study: 1) two genes, *rv0337c* and *rv3565,* of *M. tuberculosis* were erroneously annotated as coding for aspartate aminotransferases after the authors

experimentally demonstrated that those genes products had alanine and alanine-valine transaminase activity, respectively; and 2) the actual aspartate aminotransferase coded by the gene *rv3722c* was unannotated (Jansen et al., 2020). In this context, it seemed essential to experimentally determine if the predicted function of the *S. aureus* gene *SAUSA300_1916* was an aspartate aminotransferase.

In the present work, reversed-phase HPLC was employed to identify one of the substrates consumption (OAA) of the enzyme activity of SAUSA300_1916, this technique was chosen due to its ability to determine directly and simultaneously both, substrate consumption and product formation, as well as due to its high resolution, accuracy, and automatization. The determination of the enzyme activity was performed using the reverse reaction (glutamate + oxaloacetate → aspartate + ketoglutarate), and the formation and consumption of ketoglutarate and oxaloacetate, respectively were monitored over a time period when the oxaloacetate, which is chemically unstable and degrades with time to pyruvate (L. Yu & Sivitz, 2020), was proven to remain stable. In this study, it has been determined that the product of the gene *SAUSA300_1916* of *S. aureus* acts as an aspartate aminotransferase and it was thus characterised at a functional level for the first time.

In this study, the catalytic activity of the enzyme was determined at pH 7.2 and at 37°C, but the influence of both pH and temperature on the enzyme activity was not determined. It has been reported that aspartate aminotransferases (Asp-ATs) from different organisms show variable optimal pH and temperature, for example, the maximum catalytic activity for an Asp-AT purified from *L. brevis* was observed at 25°C (Hu et al., 2017), while higher temperatures were observed for the enzymes purified from *B. subtilis* (45°C) (H. J. Wu et al., 2011), *P. haloplanktis* (64°C), and *E. coli* (75°C) (Birolo et al., 2000). The lower catalytic activity observed for the *S. aureus* aminotransferase compared to that of the enzymes isolated from other sources, might be explained due to variations in the optimal temperature and pH at which the enzyme activities were determined. A limitation of the results of this study is that the effect of those factors on

the enzyme activity were not investigated, suggesting that the catalytic activity of the enzyme might not have been determined under its optimal conditions of pH and temperature. However, these are the conditions that the enzyme would experience within *S. aureus*. Another factor that can influence the maximum catalytic activity shown by an enzyme is the buffer system used in the reaction as slight changes in pH might affect the enzyme activity through the interaction between hydrogen ions and the negatively charged residues of the active site of the enzyme. It was reported that an Asp-AT purified from *L. brevis* showed its highest catalytic activity when using Tris-HCl, but nearly 60% of that activity when using potassium phosphate buffer (Hu et al., 2017). In this study, all the enzyme assays were performed using potassium phosphate buffer and the effect of other buffers like HEPES, MOPS, Tris-HCl, or sodium phosphate on the enzyme activity was not determined. It would have been advantageous to check the folding of the protein through analysis of its circular dichroism spectra to determine if the purified protein had any conformational changes that could have explained the weaker enzymatic activity compared with other reported activities.

Table 4.2 presents a comparison of the values of kinetic parameters determined in this study for the aminotransferases GOT and AspB. The K_m values determined for all the substrates involved in both, forward and reverse, reactions revealed that the *S. aureus* Asp-AT had more affinity for the amino acceptors than for the amino donors, similar to what was found for the control enzyme GOT. This higher affinity shown by the enzyme for its amino acceptors has also been reported in Asp-ATs from different microorganisms, like *B. subtilis* (Sung et al., 1990; H. J. Wu et al., 2011), *P. lapideum* (Kim et al., 2003), and *E. coli* (Köhler et al., 1994), as well as for Asp-ATs isolated from plants, like *Arabidopsis thaliana* (Wilkie & Warren, 1998), and *Pinus pinaster* (De La Torre et al., 2009).

Compared with other enzymes from different microorganisms, the *S. aureus* Asp-AT showed high affinity for its substrates: for instance, the K_m value for aspartate (1.36 mM) is about 2-fold lower than the value reported for an Asp-AT from *Bacillus sp*. (3.0 mM),

almost 5-fold lower than that reported for an Asp-AT from another *B. subtilis* strain (6.7 mM), and close to those reported for the Asp-AT from *E.coli* (1.4 mM) and *T. thermophilus* (1.5 mM) (Table 4.3).

Once experimentally determined that the putative aspartate aminotransferase isolated from *S. aureus* had aspartate aminotransferase activity, we examined whether the AspB activity of *S. aureus* could be blocked by potential inhibitors of aminotransferases or PLP-dependent enzymes. For this purpose, the following compounds were assessed as potential inhibitors: PF-04859989, adapalene, L-serine *O*-sulfate, vigabatrin, hesperetin, and as a broad range inhibitor of PLP-dependent enzymes, the compound amino-oxyacetate (AOA) was included.

AOA has been used to inhibit different PLP-dependent enzymes and it has proven to be effective against different enzymes, like kynurenine aminotransferase I (Nadvi et al., 2017), glutamine aminotransferase (Thornburg et al., 2008), alanine aminotransferase (González et al., 2012), and both, human and bacterial cystathionine γ-lyase (CSE) (Shatalin et al., 2021). In the latter study, the authors determined the mechanism of inhibition of AOA by resolving the crystal structure of the complex formed between the *S. aureus* CSE and the inhibitor. The X-ray crystal structure showed that AOA interacted with the PLP cofactor and prevented the formation of the external aldimine between the cofactor and the enzyme that is needed for the catalytic activity of the enzyme (Shatalin et al., 2021). As this inhibitor can interact with the cofactor, it might affect the activity of other PLP-dependent enzymes involved in different metabolic routes. As expected, the aminotransferases GOT and AspB were inhibited by AOA but with different potencies. While the IC_{50} value for GOT was 0.051 µM, the IC_{50} value for AspB was 240 µM, which is within the ranges of AOA concentrations reported to be effective against other aminotransferases, like kynurenine aminotransferase 1 (KAT1) (IC_{50} = 13.1 µM) (Nadvi et al., 2017) or a human aspartate aminotransferase (IC_{50} = 515 µM) (Thornburg et al., 2008), and even against the *S. aureus* CSE, which is a PLP-dependent enzyme (IC_{50} = 24.35 µM) (Shatalin et al., 2021).

Amongst the compounds tested, PF-04859989 showed the highest inhibitory effect. This compound was discovered as a result of investigations aimed to find novel and selective inhibitors against the KAT2 to treat schizophrenia and other psychiatric conditions (Dounay et al., 2012).

Both inhibitors, PF-04859989 and AOA, are reported to interact with the PLP cofactor of the enzyme (Dounay et al., 2012; Nadvi et al., 2017), but their obtained IC_{50} values for the AspB aminotransferase were very different. PF-04859989 showed a high potency against the *S. aureus* aminotransferase with an IC_{50} value nearly 100-times lower than that obtained with AOA. Regarding the activity of PF-04859989 for the aspartate aminotransferases, the IC_{50} values of this compound for a previously reported aminotransferase (GOT 1) and for the *S. aureus* AspB were similar. The latter enzyme was inhibited by PF-04859989 with an IC_{50} value of 2.5 µM after a 24 h period of pre-incubation, while GOT 1 was reported to be inhibited by the same compound with an IC_{50} of 8.0 µM after the same period of the pre-incubation step (T. Yoshida et al., 2020).

While Yoshida and colleagues found that the PF-04859989 inhibited the human GOT 1 in a time dependent manner, no significant differences in the inhibitory activity of the *S. aureus* aminotransferase by the compound were found when enzyme, cofactor and inhibitor were pre-incubated for 1 h or 24 h. Similar results were found for the control enzyme used in this study (GOT).

The second most potent inhibitor of AspB was adapalene. This compound has been used in the treatment of acne vulgaris, and it has been under research as a potential drug for cancer treatments (Rusu et al., 2020; Q. Wang et al., 2019). Here, it was found that this compound could inhibit both aminotransferases to a similar extent with IC_{50} values of 4.61 ± 1.4 µM for GOT and 5.45 ± 1.92 µM for AspB.

An advantage in the potential use of adapalene over PF-04859989 against *S. aureus* infections might be that adapalene was reported to be a non-competitive inhibitor of the aminotransferase GOT 1 (Q. Wang et al., 2019). This would be advantageous as the

increased substrate concentration due to the inhibition of the metabolic route might not overcome the inhibitory effect of the compound (Cornish-Bowden, 1986; Holdgate et al., 2018), which might be the case if adapalene would have been reported as a competitive inhibitor.

Wang and colleagues elucidated the binding mode of adapalene with GOT 1 finding that the compound interacted with hydrophobic amino acids located in an allosteric site of the enzyme. Although more studies need to be done to determine the mechanism of inhibition by which adapalene inhibits the AspB, these preliminary results and the fact that it is already used in humans for the treatment of acne and proven to be safe, suggest that adapalene could be a good candidate as a leading compound to design specific drugs against the *S. aureus* AspB. In this regard, it would be advantageous to solve the structure of the enzyme to determine at what fold type subgroup of aminotransferases the AspB belongs to: Ia, Ib or Ic. The latter subgroup was described in 2016 while studying an aspartate aminotransferase from *Corynebacterium glutamicum* (CgAspAT) (Son & Kim, 2016), and it includes the members of the family Pfam P12897 where aspartate aminotransferases from bacteria but not from humans can be found (Jansen et al., 2020). If the AspB belongs to this subgroup it would be advantageous to use it as a possible antimicrobial target against *S. aureus* infections.

Another compound tested, the L-serine *O*-sulfate (L-SOS), was an effective inhibitor of both aminotransferases, it was nearly 21-times more effective against AspB than against GOT, with IC_{50} values of 21 µM and 440 µM, respectively. This inhibitory effect on the enzymes could be due to the fact that L-SOS is an structure analogue of one of the substrate of the enzymes, L-glutamate, and it has been reported that this compound is able to disrupt the metabolism of rat astrocytes by targeting the activity of both, alanine and aspartate aminotransferases (Brennan et al., 2006). Brennan and colleagues tested subtoxic concentration of L-SOS in cultures of astrocytes cells, which was determined to be 400 µM, and we have determined that the IC_{50} value of L-SOS that inhibited the activity of AspB (21 µM) was nearly 20-times less than the subtoxic concentration tested

by those authors. This compound was also assessed as a substrate inhibitor of the glutamate transporter (GluT) resulting in the blockage of the access of glutamate inside an osteoblast lineage cell line with a concomitant extracellular accumulation of the amino acid (Xie et al., 2016).

The differences in the potency that PF-04859989 and L-SOS exhibited against the aminotransferases being a 2-fold (PF-04859989) and ~21-fold (L-SOS) more active against AspB than GOT, might rely upon differences in the catalytic sites of the enzymes that can be resolved to develop specific inhibitors against AspB.

The compound vigabatrin, which is an analogue of the inhibitory neurotransmitter gamma-aminobutyric acid (GABA) found in the central nervous system, was selected to evaluate its potential inhibitory activity against the aspartate aminotransferase as it has been shown that it can irreversible inhibit other aminotransferases (Lippert et al., 1977). Vigabatrin has been reported to inhibit the GABA aminotransferase (GABA-AT), an enzyme responsible for GABA degradation (H. Lee et al., 2015) and has been used as an antiepileptic drug (Camposano et al., 2008). The inactivation of GABA-AT by vigabatrin leads to an increase in GABA concentrations in the brain with a concomitant anticonvulsant effect. The resolved crystal structure of the GABA-AT with vigabatrin showed that the compound forms a covalent adduct with the residue Lys329 located in the active site of the enzyme and the PLP-cofactor (Storici et al., 2004). For this reason, and similar to the conditions of the assays performed with PF-04859989, vigabatrin was pre-incubated with the enzyme and cofactor for 1 h and 24 h before the enzyme assays were performed. The results showed no inhibitory effect on GOT regardless of the length of the pre-incubation step and in the case of the *S. aureus* AspB, a slight inhibition was showed after 1 h of pre-incubation with 100 µM of vigabatrin. The concentrations tested in this study were 10-times lower than those reported to inhibit GABA-AT (De Biase et al., 1991), or 100-times lower than those used to study the mechanism of inhibition of vigabatrin against GABA-AT (Storici et al., 2004), and 10-times lower than the concentration tested using analogues of vigabatrin that inhibited more than 50% of the

activity of GABA-AT (Pinto et al., 2016). It is possible that the inhibition of the aspartate aminotransferases can be achieved at higher concentrations of vigabatrin that were not evaluated in this study.

The possible inhibitory effect of the flavanone hesperetin was also assessed on AspB activity. This compound was chosen due to its reported inhibitory activity against two aminotransferases present in the liver, alanine and aspartate aminotransferases (Zareei et al., 2017). In this study, the inhibitor was tested at concentrations of 40, 80, 100, and 120 µM in the assays without showing any inhibitory effect on either of the two aminotransferases evaluated, GOT and AspB. Results reported by Zareei and colleagues, showed that the aspartate aminotransferase activity from the rat liver tissue started to decrease at a concentration of 50 µM of hesperetin, reaching a complete inhibition at 160 µM with an IC_{50} value of 85.29 µM (Zareei et al., 2017). In this study the highest concentration of hesperetin tested was 120 µM and it is possible that an inhibitory effect would have been seen at higher concentrations of hesperetin.

Overall, amongst the compounds assessed the most effective inhibitors against the *S. aureus* AspB were PF-04859989, adapalene, and L-serine *O*-sulfate with no significant inhibitory activity of hesperetin or vigabatrin on the enzymes activities at the concentrations tested.

The potential protective effect against *S. aureus* infection of the most effective inhibitor of the AspB enzyme, PF-04859989, was assessed in the *Galleria mellonella* model. The compound was dissolved in the solvent carrier PBS and two different final concentrations in the larvae were evaluated (0.01 and 0.1 mM). None of the concentrations tested showed significant differences in the virulence between the larvae infected with the wild-type strain alone or in combination with the inhibitor (Figure 4.31 and Figure 4.32). Some of the possible explanations why PF-04859989 was not giving any protective effect against *S. aureus* infection could be that 1) the evaluated concentrations of the inhibitor were too low to see any protection in the larvae, 2) the inhibitor was not reaching the

bacterial cell thus, it was not reaching the target enzyme. This could have been evaluated by assessing the effect of different concentrations of the inhibitor on the viability of *S. aureus in vitro*, and 3) the larvae could degrade the inhibitor once it was injected into the haemolymph. It would have been advantageous to test the protective effect that the inhibitor adapalene gives to the infected larva, as adapalene was the second most potent inhibitor against the purified AspB enzyme. However, we did not test this inhibitor as the solvent used to dissolved it (DMSO) resulted toxic for the larvae. Allegra and colleagues evaluated the effect of different solvents including DMSO on *G. mellonella* larvae finding that larvae infected with 80% (v/v) DMSO were completely killed after the injection while a lower concentration (50% v/v) of the solvent was better tolerated by the larvae (Allegra et al., 2018). If adapalene will be tested in furthers studies, it can be dissolved in DMSO but at a solvent concentration not exceeding 50% (v/v) in the larvae.

Further studies need to be done to determine what could be the reason(s) behind the lack of a protective effect given by PF-04859989 against *S. aureus* infection. Improvements in the assay like the measurements of the concentration of the inhibitor in the larvae over time or refreshing the protection daily, as well as to determine other characteristics of the inhibitor like its stability, antimicrobial activity, ability to select resistant mutants, etc. would be needed to determine if the inhibitor is a good candidate to be used as a therapeutic agent to treat *S. aureus* infections.

In summary, we were able to determine the following:

- The enzyme coded by *SAUSA300_1916* had the annotated aspartate aminotransferase activity.
- The kinetic parameters of maximum velocity (V_{max}) and Michaelis-Menten (K_m) constants were determined for the substrates of the forward (L-aspartic acid and α-ketoglutarate) and reverse (L-glutamic acid and oxaloacetate) reactions.
- The aspartate aminotransferase (AspB) was inhibited by the compounds PF-04859989, adapalene, amino-oxyacetate, and L-serine *O*-sulfate.

- The inhibitor PF-04859989 did not confer any protection to the *Galleria mellonella* larvae against the *S. aureus* infection under the conditions tested.

CHAPTER 5

Determination of glutamate-1-semialdehyde aminotransferase activity of SAUSA300_1614 and SAUSA300_1845

5. Determination of glutamate-1-semialdehyde aminotransferase activity of SAUSA300_1614 and SAUSA300_1845

5.1 Introduction

In the metabolic route of tetrapyrrole biosynthesis a key step, considered to be rate-limiting, involves the synthesis of 5-aminolevulinic acid (ALA) from glutamate-1-semialdehyde (GSA) (Sinha et al., 2022). The tetrapyrrole biosynthetic route in *S. aureus* starts with glutamyl-tRNA, which is reduced to GSA by the enzyme glutamyl-tRNA reductase (GtrR, formerly known as HemA). Then, the GSA is converted into ALA by the activity of the enzyme glutamate-1-semialdehyde aminotransferase (HemL). In the *S. aureus* genome, there are two genes annotated as glutamate-1-semialdehyde aminotransferases: *SAUSA300_1614 (hemL1)* and *SAUSA300_1845 (hemL2)*. The genetic contexts where those genes are located are shown in Figure 5.1.

The gene *SAUSA300_1614* (*hemL1*) is located in a genetic locus where genes coding enzymes participating in the haem biosynthetic pathway are found, like *hemB* which codes the aminolaevulinic acid dehydratase, an enzyme that converts ALA into porphobilinogen, or *hemD* that codes the uroporphyrinogen III synthase that participates in the formation of uroporphyrinogen III. The *hemL1* gene in *S. aureus* is found within the *hemAXCDBL* gene cluster that contains the genes coding the enzymes that participate in the pyrrole biosynthesis (Choby et al., 2018).

The gene *SAUSA300_1845* (*hemL2*), also annotated as glutamate-1-semialdehyde aminotransferase is found adjacent to the gene *SAUSA300_1844* coding a putative bacterioferritin comigratory protein on one side and to the gene *SAUSA300_1846* coding a hypothetical protein on the other side, in a region of genes coding proteins that are not known to be involved in the synthesis of tetrapyrroles. Amongst the genes found in that region can be found *SAUSA300_1843* and *SAUSA300_1842* coding a putative D-isomer

specific 2-hydroxyacid dehydrogenase family protein and a putative FUR family transcriptional regulator, respectively.

SAUSA300_1614 (*hemL1)* is 1,287 bp, while *SAUSA300_1845* (*hemL2*) is 1,290 bp. As a consequence, their products also differ in size, SAUSA300_1614 (HemL1) has 428 amino acids, while SAUSA300_1845 (HemL2) has 429 amino acids. Although the protein sequences show a similarity of 69.2% and an identity of 47.1% (Figure 5.2), this is not indicative of differences in their activity. For example, the amino acid sequence identity between the proven GSA-ATs from *B. subtilis* and *Synechococcus* shares a 58% identity (Lv et al., 2006). Moreover, a comparison of the amino acid sequence between the GSA-AT from *Synechococcus* and *E. coli* showed a 56% identity and the analysis of the primary structure of the enzymes suggested that the putative pyridoxamine phosphate binding site is conserved in the enzymes from both bacteria (Grimm et al., 1991).

Since the gene products of *SAUSA300_1614* and *SAUSA300_1845* are bioinformatically predicted to have glutamate-1-semialdehyde aminotransferase activity but this has not been experimentally determined, we hypothesised that the two genes code products with different activities. Thus, the main objective of this chapter was to detect any glutamatate-1-semialdehyde aminotransferase activity in the gene products of *SAUSA300_1614* and *SAUSA300_1845*.

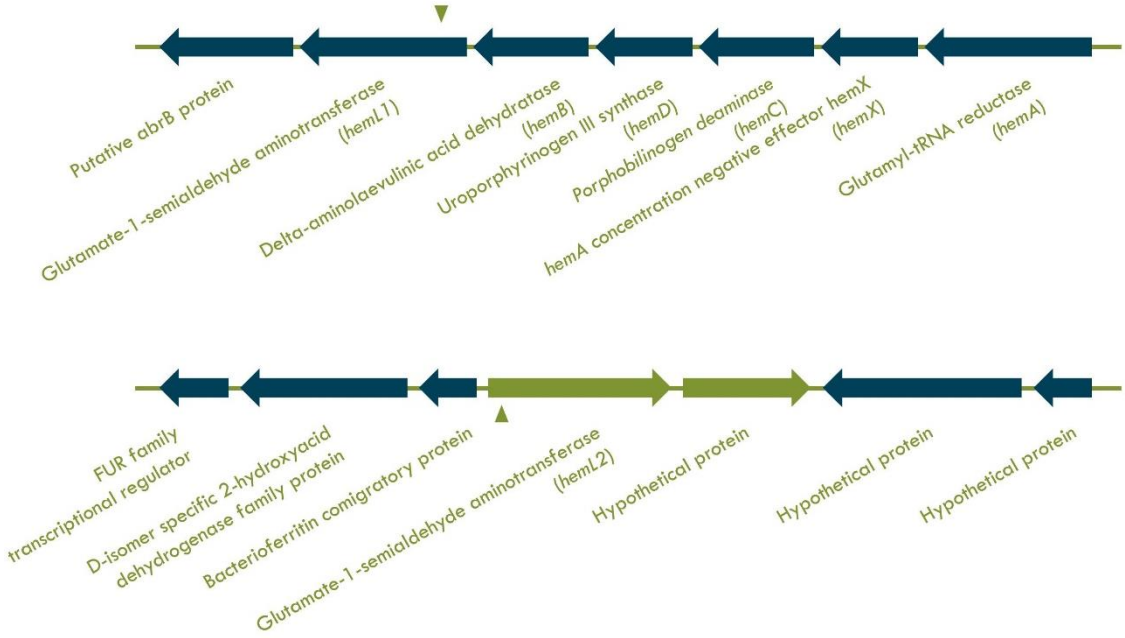

Figure 5.1 - Genetic context of the genes annotated as glutamate-1-semialdehyde aminotransferases in *S. aureus*.

The figure shows the genes surrounding *SAUSA300_1614* (*hemL1*) (top) and *SAUSA300_1845* (*hemL2*) (bottom), both annotated as glutamate-1-semialdehyde aminotransferases. The green triangle indicates the transposon insertion within each mutant of the Nebraska Transposon Mutant Library (NTML) for the genes *hemL1* and *hemL2* used in this study.

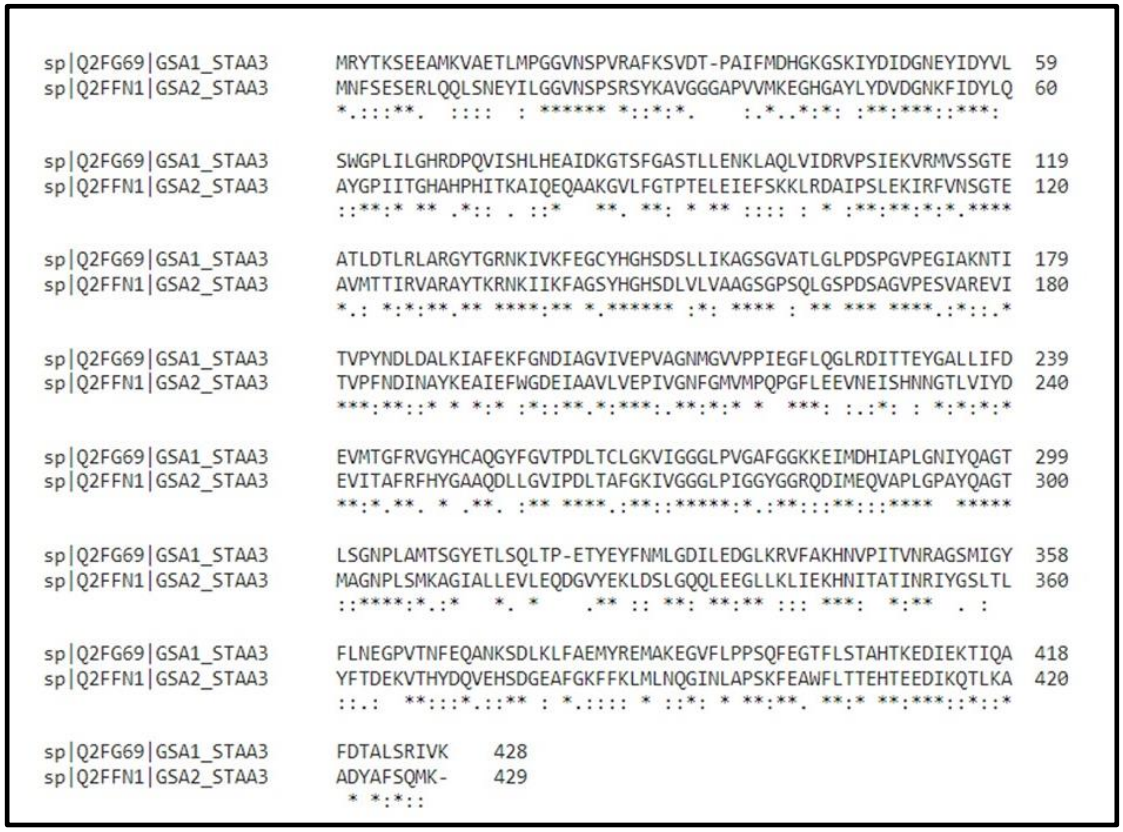

Figure 5.2 - **Protein sequence alignment of the putative glutamate-1-semialdehyde aminotransferases of *S. aureus*.**

Sequence alignment of the putative glutamate-1-semialdehyde aminotransferases HemL1 (GSA1) and HemL2 (GSA2) coded in the genome of *S. aureus*. The GenBank accession numbers are ABD22302.1 (HemL1) and ABD22077.1 (HemL2). The sequences were aligned by using the ClustalW software. The asterisks correspond to absolutely conserved residues, while the colons and dots corresponds to highly conserved and semiconserved residues, respectively.

5.2 Aims of the work described in the chapter

- To determine the capacity of the hypothetical proteins SAUSA300_1614 and SAUSA300_1845 of *S. aureus* to act as glutamate-1-semialdehyde aminotransferases.
- To determine the kinetics and inhibition of the protein showing glutamate-1-semialdehyde aminotransferase activity.
- To determine the effect of the selected inhibitor in the virulence of *S. aureus* using *Galleria mellonella* model.

5.3 Materials and Methods

5.3.1 Synthesis of glutamate-1-semialdehyde

The synthesis of the substrate of the putative enzyme, glutamate-1-semialdehyde (GSA), was performed by ozonolysis of vigabatrin in the Chemistry Department at UCL under the guidance and supervision of Dr. Helen Allan. For this purpose, 10 g of a Dowex 50W-X8, 200-400 mesh resin, H^+-form (Cat. n° 44519, Sigma) were washed with 1 M NaOH using a sintered funnel. The resin was then washed with distilled H_2O until the eluent showed a neutral pH when using the pH-indicator strips. The resin was washed with 100 mL of 50 mM HCl, resuspended in 50 mM HCl and degassed it. Finally, it was poured into a 1 x 5 cm column, washed with 5 column volumes of 50 mM HCl and stored until use.

The GSA was synthesised by ozonolysis from vigabatrin following the protocol described by (Pugh et al., 1991) with slight modifications. For this purpose, 50 mg of the enantiopure material (S)-4-aminohex-5-enic acid (cat. n° AB446916, abcr GmbH) were resuspended in 2 mL of 1 M HCl and kept at -20°C overnight before performing the ozonolysis. On the day of the ozonolysis, the sample was allowed to melt and kept at 0°C inside a bucket with ice and NaCl. The ozone at a rate of 0.56 mmol/min was bubbled through the sample using an ozone generator (OZ500/2, Fisher) at a rate of 25 litres/h for 11 min and 37 s. The resulted ozonide was diluted with 20 mL of ice-cold deionised water, applied to the Dowex column, and allowed to drain. The column was eluted first

with 25 mL of 0.1 M HCl, and the GSA was eluted with 55 mL of 0.5 M HCl. A total of 10 fractions of 5.5 mL each were collected and kept at -20°C until analysis.

The detection of the presence of the compound in the collected fractions was performed using the 3-methyl-2-benzothiazolinone (MBTH) hydrazone test (Sawicki et al., 1961). For this purpose, one drop (either 1 µL or 5 µL volume) of the fractions collected was mixed with a same volume drop of 3-methyl-2-benzothiazolinone hydrazone (cat. n° 129739, Sigma). After 2 min of incubation, the same volume drop of iron (III) chloride (cat. n° 157740, Sigma) was added. The presence of aldehyde in the sample was identified due to the appearance of a blue colour in the mixture. The samples containing the GSA were freeze-dried and the purity and amount of product obtained was determined by NMR analysis.

5.3.2 Protein expression and purification

The *E. coli* BL21 strains containing the plasmids carrying each of the genes coding the putative glutamate-1-semialdehyde aminotransferases *(hemL1* and *hemL2*) were available at Nair's laboratory. The presence of the fragments of interest within the pET-15b vector was confirmed by colony PCR using the T7 forward (5'-TAATACGACTCACTATAGGGG-3') and T7 reverse (5'-TAGTTATTGCTCAGCGGTGG-3') primers and also by the digestion with the restriction enzymes NdeI and XhoI, and visualization on an agarose gel. Following a plasmid extraction step, the competent *E. coli* strains were transformed with each plasmid containing the *hemL1* and *hemL2* genes and the transformants were plated onto LB plates supplemented with 100 µg/mL of ampicillin and grown for 24 h at 37°C. Once the transformants were confirmed (data not shown), glycerol stocks were prepared in LB medium supplemented with 100 µg/mL of ampicillin and kept at -80°C until use.

The *E. coli* BL21 strains containing the plasmids with the genes coding for the putative GSA-ATs were streaked out onto LB plates supplemented with 100 µg/mL of ampicillin

and incubated at 37°C for 24 h. A single colony of each strain was used to inoculate 5 mL of LB broth supplemented with 100 µg/mL of ampicillin in 15 mL centrifuge tubes and incubated at 37°C for 16 h in shaking conditions (180 rpm). A total of five tubes were used to prepare the overnight cultures per each strain. After the incubation time, a volume of 95 mL of LB broth supplemented with 100 µg/mL of ampicillin in a 1 L container was inoculated with the 5 mL of overnight cultures. A total of five 1 L containers containing 100 mL of culture were prepared for each strain (500 mL in total per strain) and incubated at 37°C for 2 h until the OD_{600nm} reached between 0.7 and 0.8. The expression of the proteins was induced by adding 400 µM of isopropyl ß-D-1-thiogalactopyranoside (IPTG) into the medium in the presence of 20 µM of the enzyme cofactor pyridoxamine 5'-phosphate (PMP) for 3 h at 37°C in shaking conditions (180 rpm). The cells were pelleted down by centrifugation at 11,800 x *g* at 4°C for 15 min, the supernatant was discarded, and the pellets kept at -20°C until use.

Cell lysis was performed by incubating the pellets with lysis buffer prepared by mixing 30 mL of B-PER™ complete bacterial protein extraction reagent (cat. n° 89822, Thermo Scientific) with one tablet of protease inhibitor (cat. n° 04693159001, Roche), and 50 µM of the cofactor PMP in a proportion of 5 mL of lysis buffer per 1 g of cell pellet for 90 min in a tube rotator at 4°C. The crude lysate was obtained after centrifugation at 13,000 x *g* at 4°C for 20 min and mixed with the Ni^{2+}-nitrilotriacetic acid metal-chelating affinity agarose (Ni-NTA, cat. n° 1018240, Qiagen) in a proportion of 1 mL of Ni-NTA per 6 mL of lysate for 1 h at 4°C in a tube rotator. The mixture was added into an empty gravity flow column and washed with 20 mL of the washing buffer (phosphate-buffered saline containing 20 mM imidazole) followed by a second washing step with 30 mL of the phosphate-buffered saline containing 50 mM imidazole. The proteins were eluted with 6 mL of the elution buffer (phosphate-buffered saline buffer containing 500 mM imidazole) and the fractions collected into 1.5 mL centrifuge tubes. The fractions containing the proteins were pooled and desalted by gel filtration chromatography using disposable chromatography EconoPAC 10DG columns (cat. n° 732-2010, Bio-Rad) into a buffer

solution containing 0.1 M tricine buffer, pH 7.9. The purified proteins were kept at -20°C until use. The proteins were visualised by SDS-PAGE and quantified spectrophotometrically by measuring the UV absorption at 280 nm wavelength. The extinction coefficient of the putative HemL1 (29465 M^{-1} cm^{-1}) and HemL2 (37820 M^{-1} cm^{-1}) were estimated by ExPASy ProtParam tool (https://web.expasy.org/protparam).

5.3.3 Detection of glutamate-1-semialdehyde aminotransferase activity of SAUSA300_1614 and SAUSA300_1845

The purified putative glutamate-1-semialdehyde aminotransferases (GSA-AT) (15 µg) were pre-incubated with tricine buffer (0.1 M, pH 7.9), Mops buffer (1 M, pH 5.5) and 10 µM of the cofactor PMP for 5 min at 37°C to allow temperature equilibration. The Mops buffer was added to lower the pH of the reaction to 6.7. The enzyme reaction was initiated by adding the substrate GSA (50 µM) and allowed to occur for 10 min at 37°C in a final reaction volume of 150 µL. The reaction was stopped by adding 3 µL of trichloroacetic acid. The Ehrlich's test was performed to detect the presence of 5-aminolaevulinic acid. For this purpose, 130 µL of the supernatant obtained after centrifugation of the enzyme reaction were transferred into screw-cap tubes and treated with 80 µL of 4 M sodium acetate buffer, pH 4.6 and 25 µL of ethyl acetate at 95°C for 20 min to allow pyrrole formation. Then, a volume of 235 µL of Ehrlich's solution was added into each tube and the OD_{553nm} measured after 15 min using a spectrophotometer. Control assays containing all the components of the reaction but without the enzymes were included in order to subtract the absorbance values given by the spontaneous transformation of GSA into 5-aminolevulinic acid from the absorbance values given by the enzyme activity. The pyrrole of the aminolaevulinic acid formed was quantified by Ehrlich's reagent considering an extinction coefficient of ε_{553} = 53200 M^{-1} cm^{-1} (Friedmann et al., 1992).

5.3.4 Determination of the kinetics of the glutamate-1-semialdehyde aminotransferase

The enzyme assays were performed as follows, 15 µg of the enzyme were pre-incubated with the buffers tricine (0.1 M, pH 7.9), Mops (1 M, pH 5.5) and cofactor PMP (10 µM) at 37°C for 5 min. The reaction was initiated by adding 12.5 µL of the substrate GSA at different final concentrations (0 – 25 – 50 – 75 – 100 – 125 µM) in a final reaction volume of 150 µL at pH 6.7. The enzyme assays were allowed to occur at 37°C for 1, 2, 3 and 4 minutes and the reaction stopped by adding 3 µL of trichloroacetic acid. The samples were kept on ice until the Ehrlich's test was performed on all the samples as described in the section 5.3.3. Due to the spontaneous formation of ALA from GSA, controls containing all the components of the mixture except the enzymes were included in order to subtract the values of the absorbance at 553 nm produced by the system without enzyme from the value obtained from the enzymatic activity.

The kinetics parameters of the GSA-AT, maximum velocity (V_{max}) and Michaelis-Menten constants (K_m), were determined by calculating the rate of the enzyme from the slopes of the linear part of the reaction at each of the different substrate concentrations tested followed by fitting the data of the plot of enzymatic rate against GSA concentration to the Michalis-Menten function using the Origin(Pro) software version 2021b.

5.3.5 Investigation of glutamate-1-semialdehyde aminotransferase inhibition by potential aminotransferase inhibitors

The following inhibitors were tested against the enzyme showing GSA-AT activity: amino-oxyacetate (AOA) (cat. n° C13408, Sigma), gamma-acetylenic GABA (sc-295002A, Santa Cruz Biotechnology) and gamma-vinyl GABA or vigabatrin (cat. n° V8261, Sigma). The stocks were prepared in distilled water and kept at -20°C until use.

The inhibitory activity of the selected compounds against the GSA-AT activity was determined by performing enzymatic assays with different concentrations of each compound. For this purpose, 15 µg of the enzyme were pre-incubated with the buffers

tricine (0.1 M, pH 7.9), Mops (1 M, pH 5.5) and cofactor PMP (10 µM) and a range of nine different concentrations of each inhibitor (0-10 mM) with a ten-fold dilution starting with 10 mM at 37°C for 5 min. The enzymatic reactions were initiated by adding the substrate GSA at a final concentration of 8.6 µM in a total reaction volume of 150 µL. The reaction was allowed to occur at 37°C for 3 min and 3 µL of trichloroacetic acid were added to stop the reaction. Enzyme assays with no inhibitor were performed to estimate the total enzymatic activity. The quantification of the aminolaevulinic acid formed was performed with the Ehrlich's test considering an $\varepsilon_{553} = 53200\ M^{-1}\ cm^{-1}$ (Friedmann et al., 1992). The percent of enzyme inhibition was plotted against each inhibitor concentration tested and the IC_{50} values were calculated by fitting the data to the DoseResponse function in Origin(Pro) software version 2021b.

5.3.6 Evaluation of the activity of the inhibitor gamma-acetylenic GABA in a *S. aureus* infection model using *Galleria mellonella*

Galleria mellonella larvae were obtained from Live Foods Direct, United Kingdom, kept on woodchips in the dark at 10°C and used within the first week from delivery.

The *S. aureus* strains were streaked out onto TSA plates (wild-type strain) and TSA plates supplemented with 5 µg/mL of erythromycin (JE2 *hemL1*::*Tn*) and incubated at 37°C for 24 h. A single colony of each strain was used to inoculate 10 mL of TSB broth and incubated at 37°C for 16 h in shaking conditions (200 rpm). The overnight cultures were washed with PBS and the bacterial concentration adjusted to inoculate the larvae with 10^5 CFU/larva. For each experiment, 10 larvae weighing between 0.2 and 0.3 g were infected with 10 µL of *S. aureus* wild-type (JE2) (10^5 CFU/larva) alone or combined with two different final concentrations of the inhibitor gamma-acetylenic GABA in the larvae (0.8 mM and 1.6 mM). The injection was performed into the hemocoel of each larva through the second left pro-leg using a hypodermic syringe and an automated syringe pump. Larvae infected with the mutant strain JE2 *hemL1::Tn* alone and in combination with two different final concentrations of the inhibitor in the larvae (0.8 and

1.6 mM) were also included as well as larvae injected with PBS and with the inhibitor alone as controls. The larvae were left in the dark, inside Petri dishes covered with foil at 37°C and their survival monitored daily over a 5-day period. The larvae were recorded as dead when no mobility was observed after stimulating them with a plastic inoculation loop. Three independent experiments were performed using a total of 30 larvae per condition and the results were analysed by using the Kaplan-Meier survival analysis in the OriginPro software version 2021b. Statistical differences were determined with a log-rank test using the same software.

5.4 Results

5.4.1 Synthesis of glutamate-1-semialdehyde

The substrate of the enzyme was produced by ozonolysis of the enantiopure material (S)-4-aminohex-5-enic acid. The compound eluted in the first fraction collected after adding 0.5 M HCl (5.5 mL) and the presence of the aldehyde was detected by the bluish colour formed following its reaction with the reagent 3-methyl-2-benzothiazolone hydrazone (Figure 5.3). The sample was lyophilized for 24 h, until completely dry, and NMR analysis performed. The proton NMR spectrum of the sample is shown in appendix 1. The amount of GSA in the lyophilized sample was determined by using $2.58x10^5$ M of maleic acid as a reference standard. The GSA was found to be in its hydrate form (relative molecular mass of 185.60 g) and an amount of 1.1 mg of GSA was quantified in the sample.

Figure 5.3 - Aldehyde-specific test.

The fractions containing the glutamate-1-semialdehyde were initially detected by its reaction with the reagent 3-methyl-2-benzothiazolone hydrazone and the appearance of a bluish colour. V = vigabatrin; 1 – 10 = 10 fractions collected after eluting the Dowex column with 55 mL of 0.5 M HCl (5.5 mL each).

5.4.2 Determination of the capacity of the hypothetical proteins SAUSA300_1614 and SAUSA300_1845 of *S. aureus* to act as glutamate-1-semialdehyde aminotransferases

The putative glutamate-1-semialdehyde aminotransferases were successfully expressed and purified from *E. coli*. The molecular masses of the HemL1 and HemL2 proteins were estimated to be 46388.08 and 46756.07 Da, respectively by the ProtParam tool. The predicted size of both proteins is in agreement with the bands visualised in the SDS-PAGE gel that are in the molecular weights of ~43 and ~45 kDa for the HemL1 and HemL2 proteins, respectively (Figure 5.4). The protein yields obtained of HemL1 and HemL2 were 3 mg/mL (1.5 g of protein per 500 mL of culture) and 5.5 mg/mL (2.75 g of protein per 500 mL of culture), respectively and their absorption spectrums showed two peaks at ~ 330 nm and ~410 nm corresponding to the enzyme cofactor in the form of PMP and PLP, respectively (Figure 5.5).

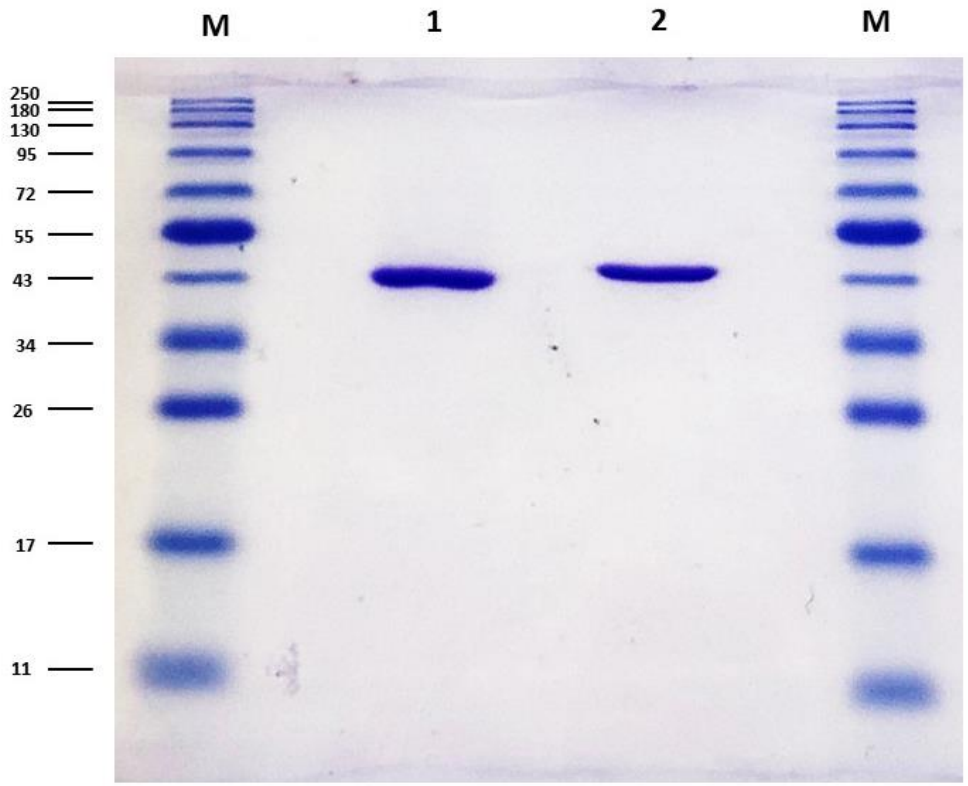

Figure 5.4 - SDS-PAGE of the HemL1 and HemL2 purified proteins on a 12% polyacrylamide gel.

Lanes: **M.** Protein standard (11 – 250 kDa), **1.** Purified HemL1 protein, and **2.** Purified HemL2 protein.

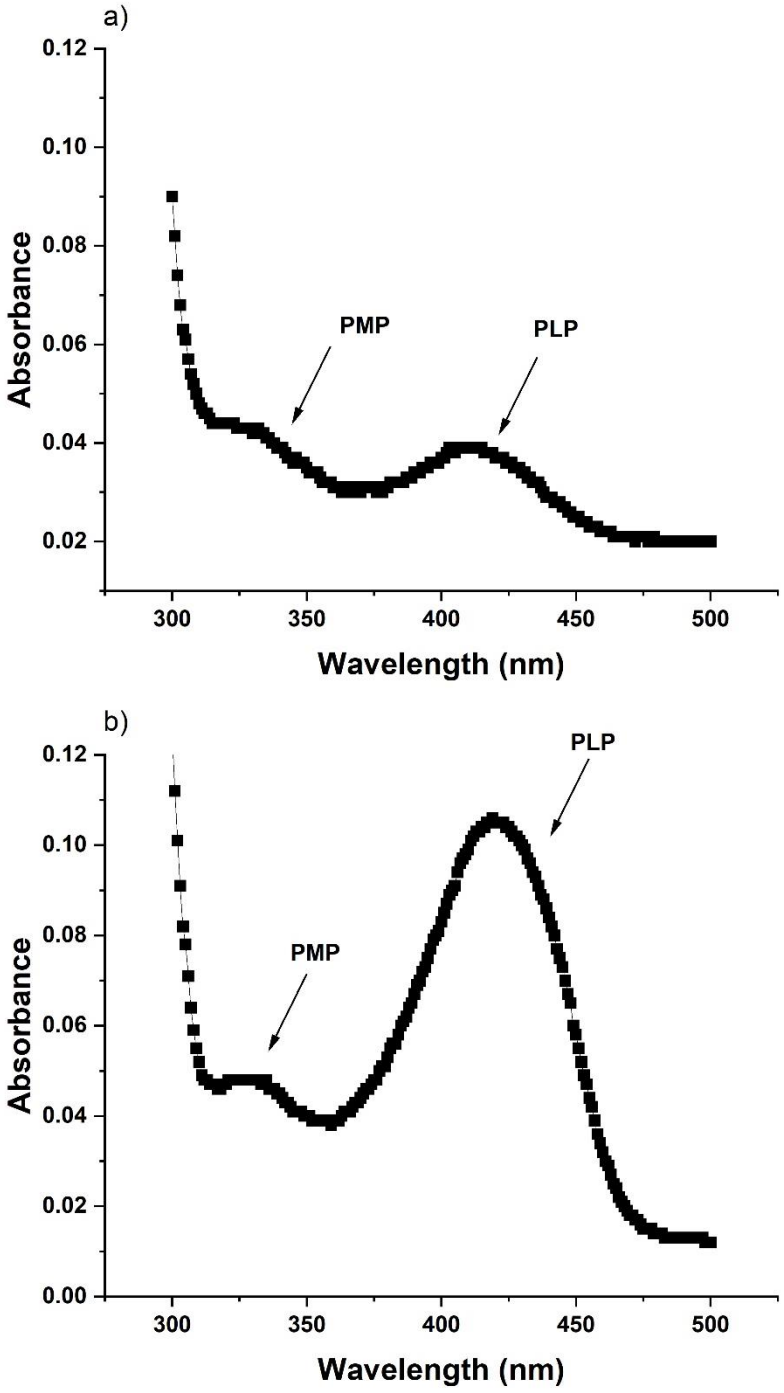

Figure 5.5 - Absorption spectrums of the purified HemL1 and HemL2 proteins.

UV-visible spectra of HemL1 (a) and HemL2 (b) purified from *E. coli*. The protein concentrations were 1.2 mg/mL in 0.1 M tricine buffer at pH 7.9. The peaks are indicated by the arrows and correspond to the pyridoxamine 5'-phosphate (PMP) bound to the enzyme (~330 nm) and to the pyridoxal 5'-phosphate (PLP) bound to the enzyme (~400 nm).

The glutamate-1-semialdehyde aminotransferase activity (GSA-AT) was detected for the protein SAUSA300_1614 annotated as HemL1 but not detected for SAUSA300_1845 annotated as HemL2 (Figure 5.6) after 10 min of incubation at 37°C in the presence of 15 µg of protein.

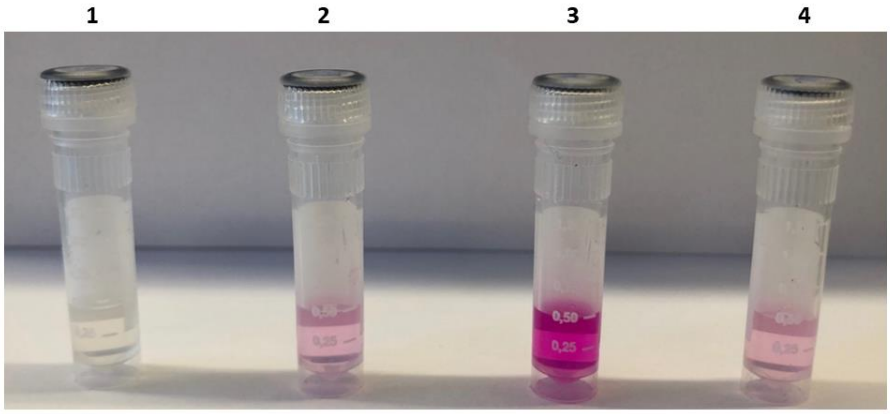

Figure 5.6 - Detection of glutamate-1-semialehyde aminotransferase (GSA-AT) activity.

The detection of GSA-AT activity was performed by incubating the putative HemL1 and HemL2 enzymes (15 µg) with 0.1 M tricine buffer pH 7.9, 1 M Mops buffer pH 5.5, in the presence of the enzyme cofactor PMP (10 µM) and the substrate GSA (50 µM) for 10 min at 37°C. The enzyme product, 5-aminolaevulinic acid (ALA), can be detected by the appearance of a pink colour after performing the Ehrlich's test. Tubes 1 = blank; 2 = control for the spontaneous transformation of GSA into ALA (the mixture contains everything except the enzyme); 3 = enzymatic reaction containing the putative HemL1; and 4 = enzymatic reaction containing the putative HemL2. No enzymatic activity was detected for the putative HemL2 enzyme at the assay conditions evaluated.

The increase in absorbance at 553 nm due to the enzymatic activity of HemL1 was determined to be 0.83 ± 0.09 SD (n = 6) after subtracting the value corresponding to the spontaneous transformation of GSA into ALA by this assay system (0.25 ± 0.03 SD (n = 6)). The concentration of ALA produced by HemL1 after 10 min at 37°C was determined to be 15.6 µM. The specific enzyme activity of HemL1 was determined to be 93.6 nmol min^{-1} mg^{-1}. No increase in the absorbance at 553 nm compared to the control of the spontaneous transformation of GSA into ALA was found for the putative HemL2 enzyme.

The GSA-AT activity of HemL1 at different time points showed that future assays in the presence of 15 µg of the enzyme and 50 µM of substrate should occur within the first four min of reaction as the amount of ALA formed starts to stabilise after that period of time (Figure 5.7).

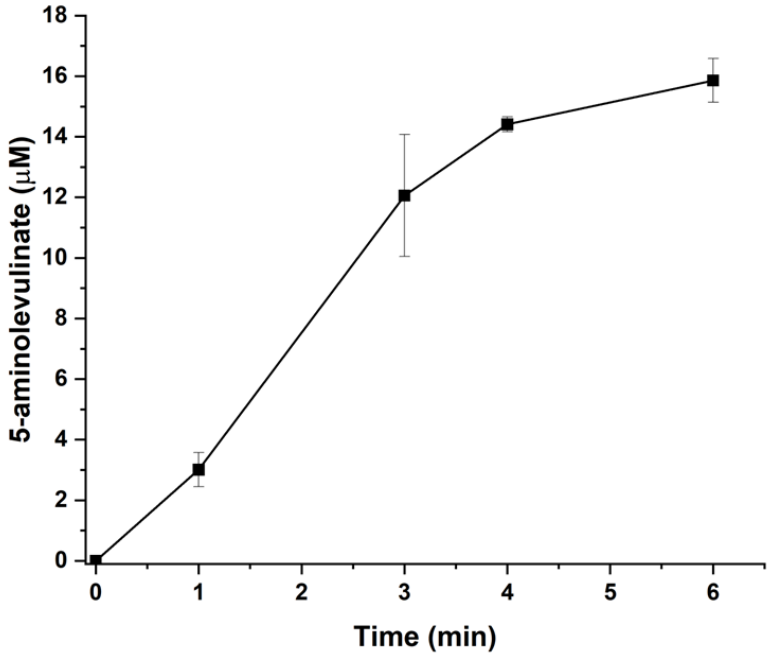

Figure 5.7 - Glutamate-1-semialdehyde aminotransferase activity of HemL1 at different time points.

The formation of 5-aminolevulinate (ALA) from a concentration of 50 µM of glutamate-1-semialdehyde was detected by Ehrlich's test in the supernatants of enzymatic assays performed in the presence of 15 µg of the enzyme, 10 µM of the enzyme cofactor (PMP) in 0.1 M tricine buffer and 1 M Mops buffer in a final volume of 150 µL reaction at pH 6.7 and at 37°C at different time points. The data represent the mean ± standard deviation of three replicates.

5.3.3 Determination of the kinetic parameters of HemL1, inhibition, and effect of gamma-acetylenic GABA on *S. aureus* infection of *Galleria mellonella*

The kinetics parameters of GSA-AT for the enzyme substrate, glutamate-1-semialdehyde, V_{max} and K_m were determined to be 0.9 ± 0.07 nmoles/min and 8.6 ± 2.9 µM, respectively (Figure 5.8).

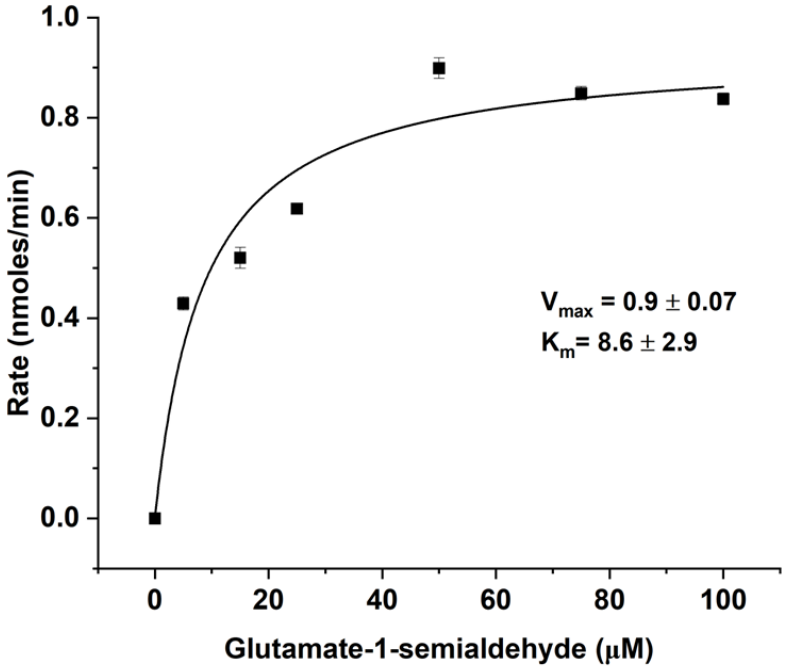

Figure 5.8 - Kinetic parameters of the glutamate-1-semialdehyde aminotransferase (HemL1) from *S. aureus*.

The GSA-AT activity was performed in 0.1 M tricine buffer, 1 M Mops buffer, 10 µM of the enzyme cofactor (PMP), a range of different substrate (GSA) concentrations in the presence of 15 µg of enzyme. The reaction was performed at 37°C and pH 6.7. The kinetic parameters were obtained by fitting the data to the Michaelis-Menten equation. The data represent the mean ± standard deviation of three replicates (r^2= 0.941).

Although this is the first time that GSA-AT activity has been described for *S. aureus*, other GSA-ATs have been studied and characterized in different organisms which allow for comparison of the results obtained in this study.

A GSA-AT purified from *Synechococcus* had a K_m value for the substrate GSA of 12 µM when the cofactor was in the PMP-form and 37 µM when it was in the PLP-form (Smith et al., 1991). The K_m value of the *S. aureus* GSA-AT for its substrate was 1.4-fold higher than that of the PMP-form of the enzyme purified from *Synechococcus*. The GSA-AT from barley showed a high affinity for its substrate, GSA, with an estimated K_m of 3 µM (Grimm et al., 1991), which is 2.87 times lower than the K_m calculated for the GSA-AT from *S. aureus* (8.6 µM).

Once GSA-AT activity and important kinetics parameters of the enzyme had been determined, the next step was to find inhibitors able to block the GSA-AT activity of HemL1. For this purpose, three compounds were tested as possible GSA-AT inhibitors. The compound amino-oxyacetate (AOA) was included as it is known as an inhibitor of PLP-dependent enzymes as well as a non-specific enzyme inhibitor. AOA inhibited GSA-AT activity with an IC_{50} value determined to be 41.8 ± 8.4 µM (Figure 5.9).

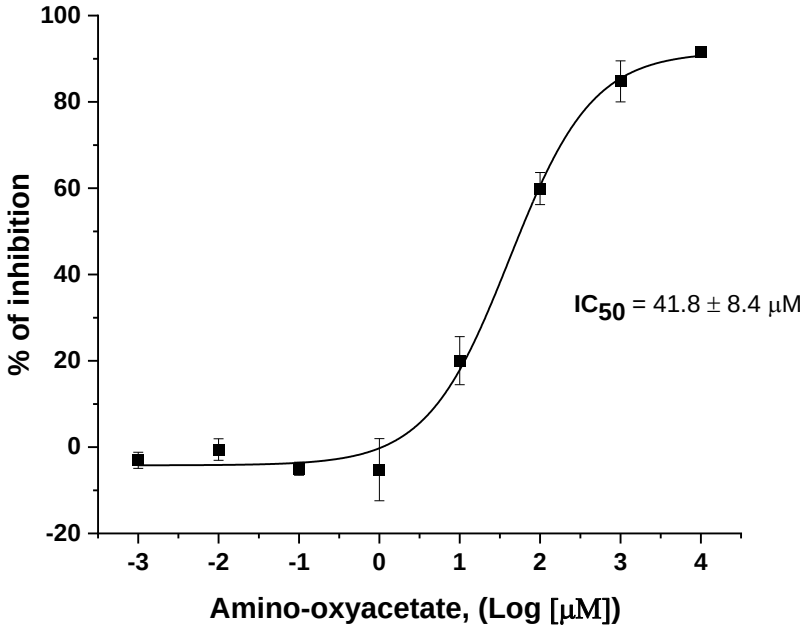

Figure 5.9 - Representative inhibitor dose curve used to determine the IC_{50} value of amino-oxyacetate on glutamate-1-semialdehyde aminotransferase.

The inhibition assays were carried out at 37°C in 0.1 M tricine buffer at pH 6.7. The GSA-AT activity was determined by quantifying the pyrrole formed with the Ehrlich's reagent. The IC_{50} value of AOA on the GSA-AT was determined by fitting the data to the dose response equation in OriginPro and corresponds to the mean ± standard deviation of n = 3 determinations.

Another potential inhibitor of the GSA-AT tested was the substrate used for ozonolysis from which the GSA was synthesised, the compound vigabatrin. The racemic mixture was used instead of the enantiopure material as it was much cheaper and it was reported to act as an inhibitor of aminotransferases, specifically GABA-AT. This compound was also tested as a potential inhibitor of the *S. aureus* aspartate aminotransferase studied in the previous chapter but it did not show any capacity to inhibit that enzyme. Vigabatrin was able to inhibit *S. aureus* GSA-AT by more than a 50% of the enzyme activity when tested at a concentration of 10 mM in the assay (Figure 5.10)

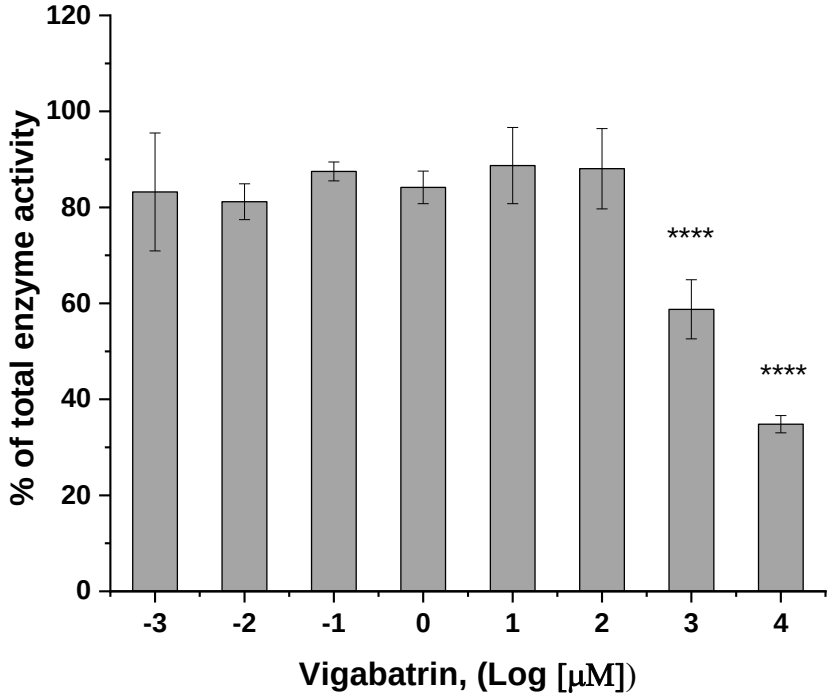

Figure 5.10 - Percent inhibition of glutamate-1-semialdehyde aminotransferase by vigabatrin.

The inhibition assays were carried out at 37°C in 0.1 M tricine buffer at pH 6.7. The GSA-AT activity was determined by quantifying the pyrrole formed with the Ehrlich's reagent. The data are presented as the mean ± standard deviation of n = 3 determinations.

The compound gamma-acetylenic GABA is a known inhibitor of GABA-aminotransferase, an enzyme participating in GABA metabolism (Löscher, 1980), and it has shown inhibitory activity against a GSA-AT purified from peas (Nair, unpublish data). In this study it was determined that gamma-acetylenic GABA was able to inhibit the *S. aureus* GSA-AT with an IC_{50} value of 54.5 ± 16.97 µM (Figure 5.11), which is slightly similar to what was found for the inhibition of GSA-AT by the unspecific inhibitor AOA.

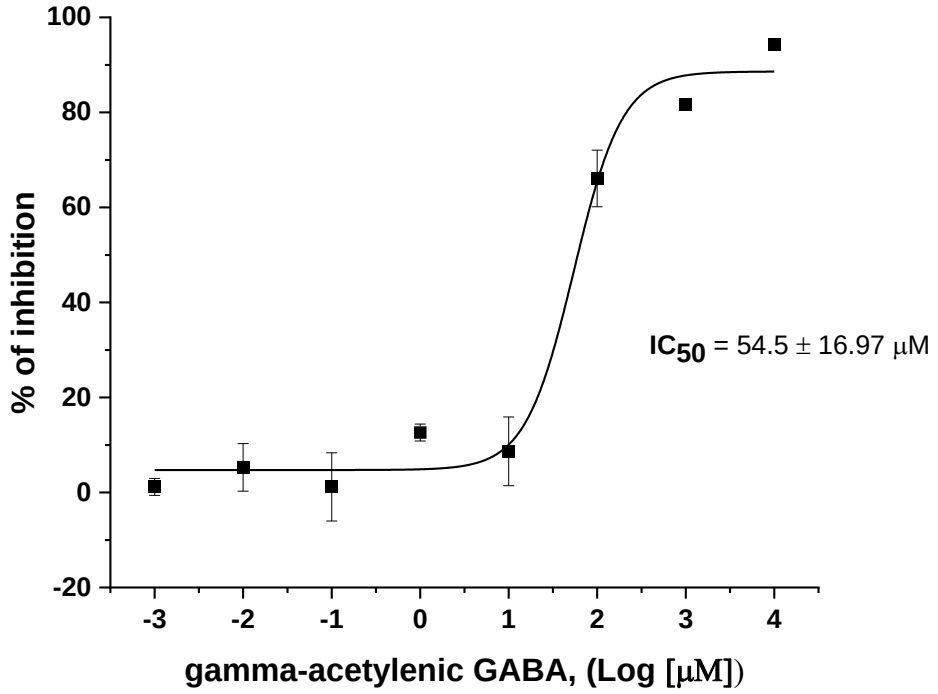

Figure 5.11 - Representative inhibitor dose curve used to determine the IC_{50} value of gamma-acetylenic GABA on glutamate-1-semialdehyde aminotransferase.

The inhibition assays were carried out at 37°C in 0.1 M tricine buffer at pH 6.7. The GSA-AT activity was determined by quantifying the pyrrole formed with the Ehrlich's reagent. The IC_{50} values of gamma-acetylenic GABA on GSA-AT activity were determined by fitting the data to the dose response equation in OriginPro and represent the mean ± standard deviation of n = 3 determinations.

Amongst the two inhibitors that showed the highest inhibitory effect against GSA-AT activity, amino-oxyacetate and gamma-acetylenic GABA, the latter was chosen to evaluate if any protective effect against the *S. aureus* infection was given by using the *Galleria mellonella* larvae model. The inhibitor amino-oxyacetate was ruled out as it is a non-specific inhibitor that might affect the aminotransferases present in the *Galleria* and result toxic for them.

For this purpose, larvae weighing an average of 0.25 g were used to test two different final concentrations of gamma-acetylenic GABA in each larvae: 0.8 mM and 1.6 mM. It is worth noticing that this inhibitor showed an IC_{50} = 54.5 µM against the *S. aureus* GSA-AT. In *Galleria* larvae the estimated final concentration of the inhibitor was 16- and 32-times higher than the concentration of the inhibitor that achieved 50% inhibition of the purified enzyme.

The results show that, although the inhibitor on its own was not toxic to the larvae, no decrease on the virulence of the wild-type strain was observed either when administered together with 0.8 mM (Figure 5.12) or with 1.6 mM (Figure 5.13) final concentrations of gamma-acetylenic GABA in the larvae. It is possible that higher concentrations of the inhibitor might be needed to observe a protective effect against *S. aureus* infection in this model.

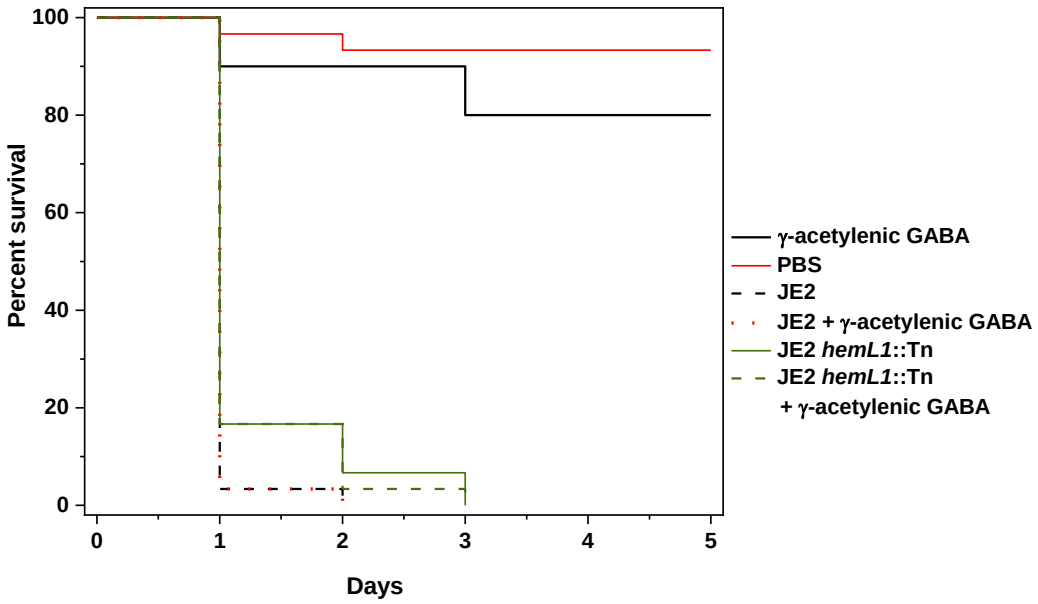

Figure 5.12 - Effect of the inhibitor gamma-acetylenic GABA (0.8 mM) on the virulence of *S. aureus* in *G. mellonella* model.

The Kaplan-Meier plot indicates the viability of *Galleria* larvae over a period of 5 days after infection with the wild-type strain (JE2) alone or in combination with 0.8 mM of gamma-acetylenic GABA at 10^5 CFU/larva. The inhibitor alone administered to the larvae as well as PBS injected larvae were included as controls together with the larvae infected with the mutant for the GSA-AT alone (JE2 *hemL1::Tn*) or in combination with 0.8 mM of gamma-acetylenic GABA. The data are derived from three independent experiments with groups of 10 larvae each (n = 30).

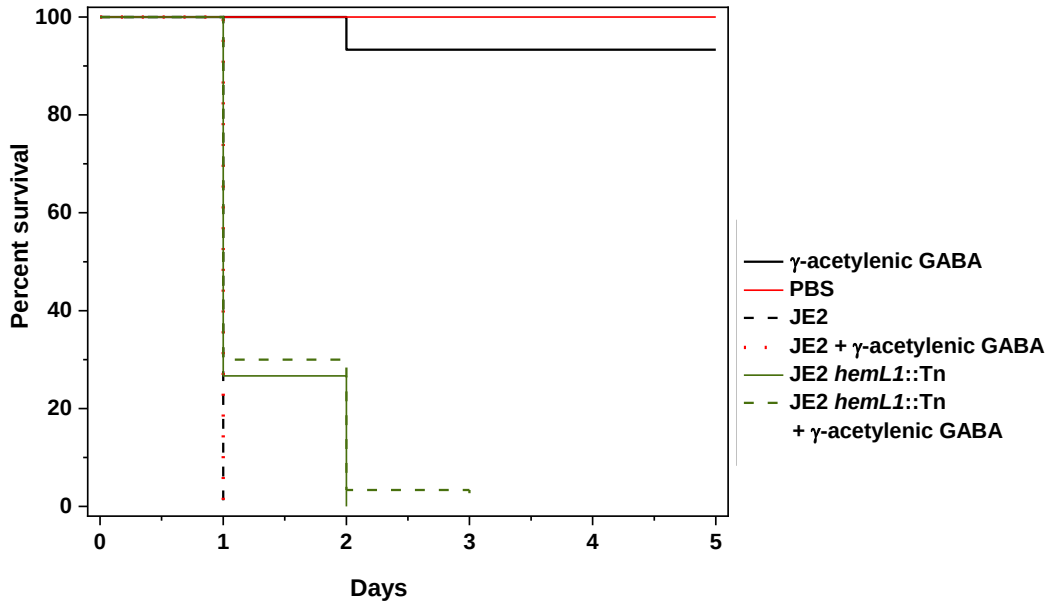

Figure 5.13 - Effect of the inhibitor gamma-acetylenic GABA (1.6 mM) on the virulence of *S. aureus* in *G. mellonella* model.

The Kaplan-Meier plot indicates the viability of *Galleria* larvae over a period of 5 days after infection with the wild-type strain (JE2) alone or in combination with 1.6 mM of gamma-acetylenic GABA at 10^5 CFU/larva. The inhibitor alone administered to the larvae as well as PBS injected larvae were included as controls together with the larvae infected with the mutant for the GSA-AT alone (JE2 *hemL1::Tn*) or in combination with 1.6 mM of gamma-acetylenic GABA. The data are derived from three independent experiments with groups of 10 larvae each (n = 30).

5.4 Discussion

The main objective of this chapter was to detect glutamate-1-semialdehyde aminotransferase activity in the products of the genes *SAUSA300_1614* and *SAUSA300_1845* coded in the genome of *S. aureus*. In order to detect their enzymatic activity, the synthesis of the enzyme substrate, glutamate-1-semialdehyde (GSA), was an important task. This compound could not be synthesised by a number of commercial services as it is very unstable. One vendor suggested including a protective group within the compound to stabilise it but could not guarantee we could deprotect it and end up with GSA. My supervisor, Dr. Nair had previous experience at synthesising the GSA by different methods including ozonolysis. Therefore, the compound was synthesised in the laboratory following the ozonolysis protocol described by Pugh and colleagues with slight modifications. A higher amount of the starting material (0.387 mmoles instead of 0.1 mmoles) and a higher amount of 0_3 (5.6 mmoles instead of 1.68 mmoles) were used. The GSA was successfully synthesized and purified by the ozonolysis of the enantiopure material (S)-4-aminohex-5-enic acid. A mass of 1.1 mg of GSA was synthesised from the ozonolysis of 50 mg of starting material. The amount and purity of the GSA obtained were enough to perform the enzymatic assays to detect if the gene products SAUSA300_1614 and SAUSA300_1845 had GSA-AT activity.

It is worth mentioning that *S. aureus* is not the only organism predicted to code for two GSA-AT in its genome. Although not a bacterium, the plant *Arabidopsis thaliana*, has two isoforms of the gene coding the GSA-AT, *gsa1* and *gsa2*, that share 90% sequence identity and have a divergent expression in different organs. For example, the gene *gsa1* was highly expressed in dry seeds, roots and senescent leaves while *gsa2* was found to be highly expressed in developmental aerial organs like green leaves and shoots (Sinha et al., 2022). However, according to the authors, the reason for keeping both genes in *A. thaliana* is still not clear. In the genome of S. *aureus*, there are two genes predicted to code for glutamate-1-semialdehyde aminotransferases, *SAUSA300_1614* and *SAUSA300_1845.* However, only the gene *SAUSA300_1614* is located within the

hemAXCBDL operon that comprises six genes coding enzymes involved in the haem biosynthetic pathway, operon that has been described for different bacteria including *B. subtilis* and *S. aureus* (Choby et al., 2018; Hansson et al., 1991). In *S. aureus* it has been reported that HemA (glutamyl-tRNA reductase) is a key regulator of haem synthesis, and it is under control of both, haem abundance and the membrane protein HemX (Choby et al., 2018). Furthermore, it has been described in *A. baumannii* that a stable complex between HemA and HemL is formed when both proteins were co-expressed and co-purified (Nardella et al., 2019). This complex formed between the two enzymes suggests the channelling of the unstable GSA formed by the catalytic activity of HemA directly into the active site of HemL for the synthesis of the tetrapyrrole precursor 5-aminolaevulinic acid (Nardella et al., 2019). The above mentioned reports on the coordinated functions of the enzymes coded within the *hemAXCBDL* operon suggests that *hemL* genes would not be located in different loci as their expression might not be regulated in this way. The *S. aureus SAUSA300_1845* or *hemL2* gene is located outside the *hemAXCBDL* operon in a region between a gene coding a putative bacterioferritin comigratory protein (*SAUSA300_1844*) and a gene that has not an assigned function and it is annotated as coding for a hypothetical protein (*SAUSA300_1846*).

In order to distinguish if the two putative GSA-ATs coded by *hemL1* and *hemL2* show the predicted enzymatic activity, both proteins (HemL1 and HemL2) were successfully expressed and purified from *E. coli* and their UV-vis absorption spectrums analysed (Figure 5.5). The enzyme HemL1 showed two peaks at ~330 and ~410 nm corresponding to the absorption of PMP and PLP, respectively. The enzyme HemL2 showed a minor band corresponding to PMP (at ~330 nm) and a larger band that corresponds to the PLP (at ~410 nm) bound to the enzyme, suggesting that both enzymes might have different activities. It has been reported that GSA aminotransferases in solution can be found in the two forms (PMP- and PLP-bound) (Song et al., 2016) and that the GSA-ATs are purified mainly in their pyridoxamine form (Grimm et al., 1992), which is not what is seen in the HemL2 absorbance spectrum in

this work as it appeared to be purified in its PLP-form. In this work, GSA-AT activity was detected for the gene product of *SAUSA300_1614* (HemL1), while no activity was detected for the gene product of *SAUSA300_1845* (HemL2). The results agree with the hypothesis that both gene products have different enzymatic activities. It was expected that HemL1, whose gene is located within the *hemAXCBDL* operon, would have GSA-AT activity. The SAUSA300_1845 has also been tested for ω-transaminase activity by Felix Vega, a PhD student at our laboratory working with PLP-dependent enzymes (data not shown), however none was found under the conditions tested and its activity remains to be elucidated.

In order to characterise the GSA-AT from *S. aureus*, enzyme assays at different time points were performed to determine its specific activity. The enzyme showed a specific enzyme activity of 93.6 nmol min^{-1} mg^{-1}, which is 9.6 times lower than that of the specific GSA-AT activity of the enzyme from peas chloroplasts reported by Nair and colleagues, which was 900 nmol min^{-1} mg^{-1} and 15 times lower than the estimated specific activity of the pure enzyme reported by the authors, which was 1400 nmol min^{-1} mg^{-1} (Nair et al., 1991).

The kinetics parameters of the HemL1 enzyme for GSA, V_{max} and K_m, were determined to be 0.9 ± 0.07 nmol/min and 8.6 ± 2.9 µM, respectively. The K_m value is slightly similar to those obtained for the K_m of GSA for the PMP-form of a GSA-AT purified from *Synechococcus,* which was 12 µM, while the PLP-form of the enzyme showed a 3.1-fold higher K_m for GSA (37 µM) compared to that of the PMP-form of the enzyme (Smith et al., 1991).

The effect of three potential inhibitors of GSA-AT were investigated in this work. The compound amino-oxyacetate (AOA) was effective in inhibiting the GSA-AT from *S. aureus* with an IC_{50} of 41.8 ± 8.4 µM. This compound was also tested against the purified aspartate aminotransferase (AspAT) from *S. aureus* in previous chapter and showed a higher inhibitory activity against the GSA-AT (IC_{50}= 0.042 mM) than against the purified

AspAT (IC_{50}= 0.24 mM). The inhibitor gamma-acetylenic GABA was chosen as it was effective in inhibiting a GSA-AT from peas (Nair, unpublished data) and it has also been tested against aminotransferases, showing to be a potent and non-toxic irreversible inhibitor of the enzyme GABA-aminotransferase (Löscher, 1980). Gamma-acetylenic GABA showed an inhibitory activity with an IC_{50} of 54.6 ± 16.97 µM against the *S. aureus* GSA-AT. Another potential inhibitor of the GSA-AT used in this work was gamma-vinyl GABA (vigabatrin), which has proven to be effective against GABA-AT. In the case of this inhibitor, it was not efficacious enough to allow the determination of the IC_{50} under the range of concentrations tested as the highest concentration assessed (10 mM) inhibited the GSA-AT activity by 65%.

Studies *in vivo* were performed by using the inhibitor gamma-acetylenic GABA in the larvae of *Galleria mellonella* to analyse its effect on the virulence of the *S. aureus*. For this purpose, two different concentrations of the compound in the larvae were used: 0.8 mM and 1.6 mM in order to see if any protective effect against *S. aureus* infection was conferred by this compound.

The results showed that the larvae administered at final concentrations of either, 0.8 or 1.6 mM of gamma-acetylenic GABA in combination with *S. aureus,* did not show significant differences in their survival rate when compared with the larvae infected with the wild-type strain alone.

These results might suggest the possibility that higher concentrations of the inhibitor are needed to decrease the virulence of *S. aureus* in this model. Although the highest concentration of the inhibitor used in the larvae (1.6 mM) corresponds to a dose of 200 mg/kg, which is 4 times higher than the dose found to inhibit the activity of the aminotransferase GABA-AT in the cerebral cortex and cerebellum of rats by this inhibitor (van der Laan et al., 1985), this concentration was not enough to observe a reduction in the virulence of *S. aureus* in the larvae. Another reason behind the absence of protection given by the compound against *S. aureus* infection might be due to the lack of penetration

of the inhibitor to the site where the pathogen is found within the host. It has been reported that *S. aureus* induced nodules formation in the perimeter of the larvae haemocoel after 6 hours of infection and single cells of the pathogen were found within those nodules at 24 h post-infection (Sheehan et al., 2019), being possible that the structure of the nodules could be impermeable to the inhibitor. Lastly, it might be possible that the metabolic activity of the larvae induced changes in some properties of the compound like its absorption rate or distribution, that prevents the inhibitor to exert any protective effect against *S. aureus* infection. Although this inhibitor has the potential to be used against *S. aureus* infections as it inhibited the HemL1 enzyme and did not result to be toxic to the larvae, further experiments need to be performed to detect an effective dose or to improve its delivery within the larvae in order to observe a reduction in the virulence of *S. aureus* in this model.

In summary, we were able to determine the following:

- The enzyme coded by *SAUSA300_1614* (HemL1) had the annotated glutamate-1-semialdehyde aminotransferase activity.
- The kinetic parameters of maximum velocity (V_{max}) and Michaelis-Menten (K_m) constants were determined for the substrate of the HemL1 enzyme, glutamate-1-semialdehyde.
- The glutamate-1-semialdehyde aminotransferase, HemL1, was inhibited by the compounds amino-oxyacetate, gamma-acetylenic GABA, and gamma-vinyl GABA.
- The inhibitor gamma-acetylenic GABA did not confer any protection to the *Galleria mellonella* larvae against the *S. aureus* infection under the conditions tested.

CHAPTER 6

General discussion and future work

6. General discussion and future work

6.1 General discussion

It was estimated that nearly 50 million people will die annually by 2050 due to infections caused by antimicrobial resistant pathogens (Murray et al., 2022). *Staphylococcus aureus* is one of the six pathogens associated to antimicrobial resistance deaths, together with *Escherichia coli*, *Klebsiella pneumoniae*, *Streptococcus pneumoniae*, *Acinetobacter baumannii,* and *Pseudomonas aeruginosa* (Murray et al., 2022). *S. aureus* can acquire resistance to most antibiotics currently in use and it is considered as a high priority pathogen by the World Health Organisation, which makes an urgent task to find new ways of treatment. One approach to fighting antimicrobial resistance is finding new drug targets. In this thesis, the bacterial metabolism of *S. aureus* was explored as a source of potential new targets by identifying enzymes that can be used to either develop new antimicrobials or inhibit their activity. Three enzymes participating in two metabolic pathways were chosen as potential targets for drug development against *S. aureus* infections. One of them, (SAUSA300_1916) is predicted to have an aspartate aminotransferase activity and participates in the central carbon metabolism, specifically in the synthesis of aspartate. The other two enzymes (SAUSA300_1614 and SAUSA300_1845) are predicted to act as glutamate-1-semialdehyde aminotransferases that are involved in the metabolic route leading to the biosynthesis of the cofactor haem.

Although metabolic pathways have not been considered as good candidates for drug development since they are not all specific for bacteria (Murima et al., 2014), their therapeutic potential have been highlighted in the fight against the rise in antimicrobial resistance (Murima et al., 2014; Yelamanchi & Surolia, 2021). Some examples of drugs targeting the bacterial central metabolism include trimethoprim, that showed selective inhibition against the microbial dihydrofolate reductase (DHFR) when compared with the human DHFR; prontosil, that targets dihydropteroate synthase (DHPS), enzyme that

participates in the synthesis of folic acid; and bedaquiline, used against *M. tuberculosis* that inhibits the bacterial ATP synthase (Murima et al., 2014).

It is known that *S. aureus* is a metabolically versatile pathogen that encounters unique environmental conditions at different infection sites. For example, higher oxygen levels and lower pH on the skin than in the deep tissues, which results in an adaptation of its metabolism to overcome tissue-specific nutritional requirements to successfully colonise those tissues (Richardson, 2019). The link between *S. aureus* metabolism and its virulence have been previously reported (Kaiser et al., 2015; Nuxoll et al., 2012; Spahich et al., 2016; Vitko et al., 2015), highlighting the possibility that metabolic pathways might be good source of novel therapeutic targets against *S. aureus* infections.

The enzyme chosen that participates in carbon central metabolism was a putative aspartate aminotransferase (AspB), that might have structural characteristics that could be exploited further to design new and specific drugs against *S. aureus*. To determine whether this enzyme is a potential drug target, a transposon mutant strain from the NTM library with disruption in the gene coding a putative aspartate aminotransferase was selected to evaluate its role in different aspects of the physiology of *S. aureus* such as fitness and virulence. The mutant strain for the putative AspB enzyme did not show any growth defect in rich media compared to the wild-type strain (Figure 3.7). However, it did show an impaired growth in serum compared to the growth of the wild-type strain (Figure 3.8). To rule out that any human factor present in the serum could be responsible for this growth defect, a medium mimicking serum conditions was chosen to confirm previous results (RPMI-1640). In this medium, the mutant for the putative AspB enzyme was not able to grow (RPMI-1640, complete formulation) (Figure 3.9) and this phenomenon was overcome when glutamine was removed from the medium (Figure 3.11), suggesting that this amino acid might prevent the bacterial growth when the cell lacks of a functional aspartate aminotransferase.

The effect of the disruption in the putative aspartate aminotransferase activity in biofilm and virulence was also investigated in this project, finding that the lack of a functional putative aspartate aminotransferase did not affect the biofilm formation capacity of the strain (Figure 3.12) but it did affect its virulence in the larvae model used (Figure 3.14). Here, we used the SAUSA300_1916 strain from the NTML having disrupted the gene coding for a putative AspB to evaluate a planarian model as a model organism to study the survival and colonisation of *S. aureus*. Previous research has found that the synthesis of aspartate is essential for the survival of *S. aureus* in an osteomyelitis (Potter et al., 2020) and it has also been reported that the virulence of a *S. aureus* mutant strain for the putative AspB enzyme was reduced by 2,000-fold in comparison to the wild-type strain in an abscess infection model (Benton et al., 2004). Thus, it has been sought that the suitability of planarian model to study the survival and colonisation capacities of *S. aureus* could be assessed by comparing those capacities between the mutant strain having disrupted the gene coding for the putative AspB and the wild-type strain. We showed that although a significant difference in the colonisation of *S. aureus* was observed between the wild-type and mutant strains in this model, those differences were not as marked as the differences found on the virulence between both strains when using the *G. mellonella* infection model. For that reason, planarians model was not used for further analysis and *G. mellonella* model was used instead.

The decrease in the virulence observed in the mutant strain having disrupted the gene coding a putative AspB of *S. aureus* in the *G. mellonella* model is in line with reports that show virulence attenuation due to the lack of a functional aspartate aminotransferase (Jansen et al., 2020). Due to the evidence of the role that the disruption in the aspartate metabolic pathway has in pathogenicity and virulence in *S. aureus* and due to the key role aspartate aminotransferase has in 1) nitrogen assimilation, 2) aspartate-derived amino acids biosynthesis (lysine, isoleucine, methionine, threonine, and asparagine), and 3) linkage between amino acid synthesis and the TCA cycle, it has been proposed

that aspartate metabolism could be a good target for drug development against *S. aureus* infections (Yelamanchi & Surolia, 2021).

Although the predicted function of the putative AspB enzyme is an aspartate aminotransferase, its activity has not been experimentally determined yet. It has been shown that 40% of the prokaryotic coding sequences have not been empirically characterised and less than 0.01% of the genes in the UniProt database have experimental support (Law et al., 2021). For example, as high as the 78% of the functional annotations of a S-2-hydroxyacid oxidases class of enzymes are misannotated (Rembeza & Engqvist, 2021) and as another example, Girardi and colleagues corrected the misannotation of two genes, one from *Shewanella spp.* (WP_088211966.1) and the other one from *Pseudomonas congelans* (WP_096244125.1) that were annotated as L-methionyl-tRNA transferases but both were determined to have N-formyltransferase activity (Girardi et al., 2020). Therefore, one of the aims of this project was to experimentally determine the activity of the protein coded by the gene *SAUSA300_1916* of *S. aureus*.

The results show that the enzyme has aspartate aminotransferase activity (Table 4.2), confirming the bioinformatically predicted activity of this enzyme. It showed kinetic parameters such as K_m similar to those reported for aspartate aminotransferases from different microorganisms (Table 4.3). It is worth mentioning that the substrate range of the AspB enzyme was not determined in this study, hence it cannot be ruled out that the enzyme might have affinity for other pair of substrates that were not evaluated.

Once aspartate aminotransferase activity was proven for the AspB enzyme of *S. aureus*, both PLP-dependent enzyme and aspartate aminotransferase inhibitors were assessed to identify compounds with high inhibitory activity against the AspB enzyme that could be used to evaluate their potential as therapeutics in *S. aureus* infection *in vivo*. Amongst the six compounds evaluated (amino-oxyacetate, PF-04859989, adapalene, L-serine *O*-sulfate, vigabatrin, and hesperetin), the compounds PF-04859989 and adapalene

showed the highest inhibitory activity against the AspB enzyme. It has been reported that PF-04859989 forms a covalent linkage with the PLP cofactor of the GOT 1 enzyme (T. Yoshida et al., 2020), and that adapalene binds to a pocket of the GOT 1 enzyme located at the back of its active site (Q. Wang et al., 2019), suggesting that both inhibitors might bind to the AspB enzyme. Because the inhibitor adapalene had poor aqueous solubility, while PF-04859989 was water-soluble and showed the highest potency against the purified AspB, we focused further on assessing the *in vivo* efficacy of this compound. However, no significant differences were observed between the larvae infected with the wild-type strain alone and the larvae infected with the wild-type strain in combination with the inhibitor PF-04859989 at the concentrations tested. This could imply that other factors might play a role in the lack of protection observed in this model by PF-04859989, for example, the concentration of inhibitor used, the possibility that the larvae are degrading the compound or that the bacterial inoculum was too high to evaluate the efficacy of the compound in this model. All are factors that need to be considered for further assays.

The other two enzymes chosen in this project to evaluate their potential use as new drug targets were SAUSA300_1614 and SAUSA300_1845, both predicted to act as putative glutamate-1-semialdehyde aminotransferases (GSA-ATs). These enzymes are involved in the conversion of glutamate-1-semialdehyde (GSA) to the universal haem precursor 5-aminolaevulinic acid (ALA) leading to the synthesis of the cofactor haem. This cofactor is critical for the correct function of bacterial proteins such as the nitric oxide synthases or catalases that are important for its pathogenesis, as well as for the correct function of the electron transport chain (Choby et al., 2018). The particularity of these enzymes is that they participate in the C5 metabolic pathway for the synthesis of ALA, which involves the three following steps: glutamate conversion to glutamyl-tRNA by the enzyme glutamate-tRNA ligase (GltX), transformation of the latter product into GSA by the enzyme glutamyl-tRNA reductase (GtrR, formerly known as HemA), and conversion of GSA into ALA by the GSA aminotransferase (GsaM, formerly known as HemL) (Choby

et al., 2018). In humans, as well as in fungi and purple non-sulphur bacteria, the synthesis of ALA occurs via the C4 pathway in a one-step reaction through the condensation of succinyl-coenzyme A with glycine by the enzyme ALA synthase (Sinha et al., 2022; J. Zhang et al., 2015). The C5 pathway has been found in most bacteria, archaea and plants but not in humans (Sinha et al., 2022). This makes the enzymes participating in this pathway a specific drug target against microbial infections.

It has been reported that endogenous haem biosynthesis in *S. aureus* is needed for colonisation and establishment of a systemic infection in a murine model (Hammer et al., 2013) and that haem-deficient mutant strains showed a decreased energy production and a non-spreading phenotype, thus affecting the motility of the strain that is important for the pathogenesis of the bacteria (C. C. Liu & Lin, 2020). *S. aureus* codes two putative glutamate-1-semialdehyde aminotransferases (GSA-ATs) in its genome, HemL1 and HemL2, but their activities have not been experimentally determined, this is the reason why they were selected for further analysis.

To assess the effect of the putative GSA-ATs on the fitness and different aspects of *S. aureus* pathogenesis such as biofilm formation and virulence, mutants for both genes (*hemL1* and *hemL2*) in the USA300 and LS-1 genetic backgrounds were used.

The mutant strains for the genes *hemL1* and *hemL2* did not show any growth defect in rich medium (TSB) when compared to the wild-type strain, regardless of their genetic background (USA300 or LS-1). However, a significant growth defect ($P < 0.05$) in serum was observed for both mutants in the USA300 genetic background compared to the wild-type strain. Although both mutants (*hemL1* and *hemL2*) showed a similar growth pattern in TSB, significant differences ($P < 0.05$) in the parameters of carrying capacity and area under the curve between *hemL1* and *hemL2* mutant strains were observed in both, RPMI complete formulation and RPMI without glutamine. These significant differences in both RPMI media were only observed in the mutants created in the USA300 but not in the LS-1 genetic background. These discrepancies could be explained by the differences in the

method by which the mutants were created. Maksymiuk and colleagues compared the phenotype of *M. tuberculosis* mutant strains for the gene *rv1248c* encoding a 2-hydroxy-3-oxoadipate synthase that were created in the same genetic background but by two different methods: transposon mutagenesis and deletion, finding phenotypic discrepancies in the growth between the mutants created by these two methods (Maksymiuk et al., 2015). In this study the *hemL(s)* mutant strains used were created by transposon insertion (USA300 background) and by gene deletion (LS-1 background), thus the discrepancy in the growth observed in RPMI between the two *hemL* mutations may be partially explained by the differences in the mutagenesis method used. Bioinformatic analysis of the genome sequence of the mutants created in the USA300 and LS-1 genetic backgrounds for the *hemL* gene through transposon insertion and gene deletion, respectively could have been performed to confirm that no frameshifts occurred after the genes were mutated that could have led to the expression of truncated proteins. This could also have been checked by performing reverse transcription-quantitative polymerase chain reaction (RT-qPCR) analysis to compare the level of expression of the *hemL* genes between the strains.

To determine if these differences between the *hemL*(s) mutants could be observed in other characteristics of *S. aureus*, their role in biofilm was assessed. The USA300 mutant strain for the *hemL1* gene did not show any biofilm formation defect when compared to the wild-type strain (Figure 3.12), while a significant decrease ($P < 0.05$) in the biofilm formation was observed in the mutant for the *hemL1* gene created in the LS-1 genetic background (Figure 3.13). The role of haem biosynthesis in *S. aureus* has been proven to be key in colony spreading (C. C. Liu & Lin, 2020) and specifically, a mutant for the *hemL* gene (*SAUSA300_1614* or *hemL1*) in *S. aureus* was found to form a macrocolony with a minimal surface wrinkling compared to the colony formed by the wild-type strain, which was wrinkled and correlated with a biofilm forming phenotype (Wermser & Lopez, 2018). In the latter study the authors used the same *hemL1* mutant strain in the USA300 genetic background from the NTML as the strain used in this project, and no significant

differences were found in that study in the biofilm formation assay between the *hemL* mutant and the wild-type strain. It is worth noticing that those authors performed the biofilm assay using TSB supplemented with magnesium and/or TSB supplemented with 0.5% glucose and 3% NaCl and we used BHI supplemented with 1% glucose. Our results showed no significant differences in the biofilm formation assay between the mutant strains for the *hemL2* gene and their respective wild-type strains regardless of their genetic background (Figure 3.12 and Figure 3.13).

The characteristic of *S. aureus* that was significantly affected by the disruption of the *hemL1* gene was its virulence. In the case of the USA300 strain, complete killing of the *G. mellonella* larvae was observed the day after the infection by the wild-type strain, while the mutant strain showed a complete killing after 2 days of the infection. The differences were highly marked in the LS-1 genetic background were *G. mellonella* larvae were completely killed after 2 days of infection by the wild-type strain and after 4 days post infection by the *hemL1* mutant strain. In *S. aureus* is known that the haem homeostasis, which is regulated by the two-component system HssRS and HrtAB, modulates its virulence (Torres et al., 2007). It has also been shown that a double mutant for the haem transport proteins (IsdE and HtsA) had a significant reduction in the bacterial load in the heart, kidneys and lungs of mice compared to the wild-type strain in a systemic murine infection model (Mason & Skaar, 2009). Virulence defects have been reported for mutants of the genes *isdBH* and *htsB* that codes a haem transport apparatus (Torres et al., 2006) and haem transport system (Skaar et al., 2004), respectively. The role of haem biosynthesis has been found to be linked to the occurrence of a persister phenotype in *S. aureus* when mutants for the *hemA* and *hemB* genes were assessed for their capacity to form a persister state (X. Wang et al., 2021). The authors found that the persister level of both mutant strains were lower than those of the wild-type strain under different stress conditions: heat (57°C), acid (pH =3), oxidative stress (50 mM H_2O_2), and ciprofloxacin stress (400 µg/mL) (X. Wang et al., 2021). The above-mentioned references are examples of the extensive supporting evidence of the role that haem

biosynthesis or transportation have in the virulence and survival of *S. aureus* during the infection.

The effect of the mutation of the *hemL2* gene on *S. aureus* virulence was also assessed in this study, finding a significant defect in virulence in this mutant strain compared to the wild-type strain, regardless of the genetic background (USA300 or LS-1). The differences observed in virulence and in the growth phenotype observed in RPMI-1640 media between the *hemL1* and *hemL2* mutant strains created in the USA300 genetic background, might suggest that both genes code proteins that might have different activities. Moreover, the gene coding the putative HemL1 enzyme is located within the operon where enzymes participating in the haem metabolic pathway are coded, while the gene coding the putative HemL2 enzyme is located outside this operon in a different loci between genes coding a putative bacterioferritin comigratory and a hypothetical protein. To elucidate whether the two enzymes show the annotated function of GSA-AT, they were expressed and purified for further analysis. It has been reported that the GSA-ATs are mainly purified in the pyridoxamine phosphate (pyridoxamine-P) form of the enzyme (Grimm et al., 1992). This has been reported for the GSA-AT purified from different organisms such as *Synechococcus* (Grimm et al., 1992), *A. baumannii* (Nardella et al., 2019), or pea leaves (Nair et al., 1991). Unlike the reported spectra of GSA-ATs, the UV-visible spectra of the putative HemL1 GSA-AT shows two peaks similar in size, possibly corresponding to the pyridoxamine-P form (330 nm) and pyridoxal-P form (410 nm) of the enzyme (Figure 5.5), while the spectra of the putative HemL2 GSA-AT shows a major peak (412 nm) corresponding to the pyridoxal-P form of the enzyme and a minor peak (330 nm) that could be attributable to the PLP enolimine form of the enzyme (Figure 5.5).

To detect GSA-AT activity, the substrate of the enzyme, glutamate-1-semialdehyde (GSA), was synthetised from the enantiopure material of 4-aminohex-5-enoic acid by ozonolysis. The amount of GSA was quantified by NMR and determined to be 1.1 mg of the hydrate form of the compound (RMM = 185.60). GSA-AT activity was detected for

the enzyme coded by the gene *hemL1* but not for the enzyme coded by the gene *hemL2*. Thus, we can confirm that the gene *hemL1* of *S. aureus* codes a GSA-AT while the gene *hemL2* codes a protein or enzyme whose activity remains to be elucidated.

The GSA-AT purified from *S. aureus* showed a K_m of 8.6 ± 2.9 µM, which is similar to the value reported for a GSA-AT of a purified enzyme from *Synechococcus* (12 µM) (Smith et al., 1991).

In order to determine if the enzyme could be inhibited by potential aminotransferase inhibitors, the compounds gamma-vinyl GABA, gamma-acetylenic GABA (antiepileptic drugs), and the broad range inhibitor of PLP-dependent enzymes, aminooxy-acetate (AOA), were chosen as possible inhibitors. AOA was able to inhibit the enzyme with an IC_{50} value of 41.8 ± 8.4 µM, while gamma-acetylenic GABA showed inhibitory activity with an IC_{50} of 54.5 ± 16.97 µM. The compound gamma-vinyl GABA or vigabatrin, from which the enzyme substrate was synthetised by ozonolysis, was also tested against the purified enzyme. It inhibited the enzymatic activity by 65% at a concentration of 0.1 M, highlighting the importance to remove any contaminant vigabatrin during the purification step in the GSA synthesis. From the compounds tested in this study, AOA and gamma-acetylenic GABA, showed the highest inhibitory activity against the purified GSA-AT from *S. aureus.* Since AOA has a broad spectrum of activity against different PLP-dependent enzymes and can target other enzymes of *S. aureus*, the compound gamma-acetylenic GABA was chosen for further analysis to detect if any protective effect was given by the compound against *S. aureus* infection in the *G. mellonella* model.

Gamma-acetylenic GABA was also found to inactivate a GSA-AT purified from pea leaves in a time-dependent manner at a concentration of 100 µM leaving a remaining 20% of the enzymatic activity after 60 min of incubation with the enzyme (Nair, unpublished data). The highest concentration of the inhibitor tested in the larvae of *G. mellonella* was 1.6 mM, which was thought to be able to attenuate the virulence of the wild-type strain of *S. aureus*. However, no protective effect was given by gamma-

acetylenic GABA against the *S. aureus* infection in the *G. mellonella* larvae model under the conditions tested. The lack of protective effect might be due to a low concentration of inhibitor used in the larvae, as it was reported that gamma-acetylenic GABA decreased the activity of a glutamate decarboxylase in the cortex tissue of rats when tested at 25 mg/kg and 50 mg/kg after 2.5 h and 5 h, respectively (van der Laan et al., 1985). This inhibitor was also reported to inhibit the activity of the gamma-aminobutyric acid transaminase (GABA-AT) in the cerebral cortex and cerebellum of rats when tested at 50 mg/kg after more than 5 hours of treatment (van der Laan et al., 1985). Further studies need to be carried out to elucidate why this compound is not giving protection against the *S. aureus* infection.

In conclusion, in this study we have elucidated the enzymatic activity of two out of three putative enzymes coded by genes in the genome of *S. aureus*. We showed that the putative aspartate aminotransferase (AspB) coded by *SAUSA300_1916* had aspartate aminotransferase activity and that the putative glutamate-1-semialdehyde aminotransferase (HemL1) coded by *SAUSA300_1614* had GSA-AT activity. We could not detect any GSA-AT activity in the product of the gene *SAUSA300_1845*. It might be possible that SAUSA300_1845 participates in other metabolic pathway involved in the synthesis of the elongation factor P. This assumption is based on the fact that the homologous gene to *SUSA300_1845* in *B. subtilis* is *gsaB*, which is predicted to code a glutamate-1-semialdehyde aminotransferase and/or an enzyme required for the modification of the translation factor elongation factor P (EF-P). It has been reported that the modifications required by the EF-P in *B. subtilis* involve the addition of a 5-aminopentanol moiety in its Lys32 residue and that the gene products of *ynbB*, *gsaB*, and *ymfI* would be required to carry out the modifications through a novel posttranslational pathway (Witzky et al., 2018). In this proposed new modification pathway, the GsaB might be responsible for the addition of an amine group onto pentanone in the acetylation of the Lys32 residue of the EF-P. Although Witzky and colleagues give us insights into the possible activity of the SAUSA300_1845, the

experimental determination of its activity remains to be elucidated. Even though we could only detect the enzymatic activity of two out of the three putative enzymes, we propose the three of them as possible drug targets against *S. aureus* infections as all have shown a significant defect in virulence compared to the wild-type strain in the *G. mellonella* model.

6.2 Final conclusion

The main objective of this thesis was to identify potential new drug targets for the treatment of infections caused by *S. aureus* strains. For this purpose, three putative enzymes, as their activities had not been experimentally determined until now, participating in the metabolism of *S. aureus* were selected to determine their essentiality for different characteristics of the pathogen and to detect their enzymatic activity. The enzymes SAUSA300_1916 (putative aspartate aminotransferase, AspB), SAUSA300_1614 and SAUSA300_1845 (putative glutamate-1-semialdehyde aminotransferases), were not essential for either growth (rich media or human serum) or biofilm formation of *S. aureus*. The deficiency of the three putative aminotransferases showed a significant decrease in the virulence of *S. aureus* when using a *Galleria mellonella* model. A planarian model was assessed as an alternative host-pathogen interaction model and, although it was useful to study the survival and colonisation of *S. aureus*, it was not used for further analysis as it was difficult to inject the worms with precision without having a microinjection system.

Once demonstrated that the three putative enzymes were required for the virulence of *S. aureus*, we successfully detected aspartate aminotransferase activity for SAUSA300_1916 (AspB) and glutamate-1-semialdehyde aminotransferase activity for SAUSA300_1614 (HemL1). The activity of SAUSA300_1845 needs to be detected in the future.

Both enzymes, AspB and HemL1, were characterised and their kinetic parameters determined. Moreover, the enzymes were inhibited by available inhibitors that can be

safely used in humans that might have the potential to be used in the treatment of *S. aureus* infections. However, *S. aureus* has the capacity to modify its metabolism to adapt to its nutrient environment, as reported by Alreshidi and colleagues who showed that *S. aureus* changed the concentrations of its cytoplasmic amino acids after being exposed to conditions that mimicked the wound site environment (Alreshidi et al., 2022). Thus, the metabolic flexibility of *S. aureus* represent a limitation to the inhibitors selected in this study as their use would be dependent on the metabolic requirements of either aspartate or haem biosynthesis during the infection of *S. aureus*.

6.3 Future work

In this study the aspartate aminotransferase activity of the AspB enzyme from *S. aureus* was experimentally detected and its kinetics parameters determined. The mutant strain for aspartate aminotransferase activity showed a growth defect in serum and the RPMI-1640 medium, as well as a decreased virulence and colonisation, suggesting it could serve as a target for new antimicrobials. In order to determine if this enzyme represents a good target, it would be useful to determine if AspB is the primary aspartate aminotransferase in *S. aureus* and how its deficiency might affect other metabolic routes important for the fitness and virulence of the pathogen. It would also be desirable to determine at what subclass of aspartate aminotransferases AspB belongs to since members of the Pfam family PF12897 are not found in human cells (Jansen et al., 2020). The identification of specific domains that might be unique to the bacterial enzyme, as in the case of the aspartate aminotransferase from the oomycete *Phytophthora sojae* that contains a N-terminus domain specific to the oomycetes (R. Wang et al., 2016), might also be another way to find differences between the human and the bacterial enzymes.

The inhibitors tested against the aspartate aminotransferase that have shown the most potent inhibitory effect were PF-04859989 and adapalene and can be studied further. In order to determine the *in vivo* efficacy of the compounds, it would be useful to study the

physiochemical properties of the inhibitors (solubility, lipophilicity, crystallinity, etc.), their pharmacokinetics (PK) and pharmacodynamics (PD), as well as their cytotoxicity against human cells to determine if they could be optimized to improve their metabolic stability that is required for high exposure in order to use them as inhibitors of the AspB enzyme of *S. aureus*.

We have also established glutamate-1-semialdehyde aminotransferase activity for the HemL1 enzyme coded by the *hemL1* gene (*SAUSA300_1614)* and have found a potential inhibitor, gamma-acetylenic GABA, that might be used further. However, it would be of interest to determine some characteristics of the compound like its physiochemical properties, PK, PD, and cytotoxicity in order to determine its potential as a leading compound to optimize inhibitors against the GSA-AT of *S. aureus*.

An interesting task that needs to be completed is the determination of the activity of the protein/enzyme coded by *SAUSA300_1845*. We have shown that the mutant for that gene product has a significant impairment in the *S. aureus* virulence in the *G. mellonella* model, which makes it a good target for drug development against *S. aureus* infections. Until the experimental determination of its activity is carried out, SAUSA300_1845 should be considered as a hypothetical protein rather than a putative glutamate-1-semialdehyde aminotransferase.

7. References

Abdurrahman, G., Schmiedeke, F., Bachert, C., Bröker, B. M., & Holtfreter, S. (2020). Allergy—A New Role for T Cell Superantigens of Staphylococcus aureus? *Toxins*, *12*(3), 1–21. https://doi.org/10.3390/toxins12030176

Abnave, P., Mottola, G., Gimenez, G., Boucherit, N., Trouplin, V., Torre, C., Conti, F., Ben Amara, A., Lepolard, C., Djian, B., Hamaoui, D., Mettouchi, A., Kumar, A., Pagnotta, S., Bonatti, S., Lepidi, H., Salvetti, A., Abi-Rached, L., Lemichez, E., … Ghigo, E. (2014). Screening in planarians identifies MORN2 as a key component in LC3-associated phagocytosis and resistance to bacterial infection. *Cell Host and Microbe*, *16*(3), 338–350. https://doi.org/10.1016/j.chom.2014.08.002

Agata, K., Soejima, Y., Kato, K., Kobayashi, C., Umesono, Y., & Watanabe, K. (1998). Structure of the Planarian Central Nervous System (CNS) Revealed by Neuronal Cell Markers. *Zoological Science*, *15*(3), 433–440. https://doi.org/10.2108/zsj.15.433

Allegra, E., Titball, R. W., Carter, J., & Champion, O. L. (2018). Galleria mellonella larvae allow the discrimination of toxic and non-toxic chemicals. *Chemosphere*, *198*, 469–472. https://doi.org/10.1016/j.chemosphere.2018.01.175

Alonzo, F., & Torres, V. J. (2014). The Bicomponent Pore-Forming Leucocidins of Staphylococcus aureus. *Microbiology and Molecular Biology Reviews*, *78*(2), 199–230. https://doi.org/10.1128/mmbr.00055-13

Alreshidi, M., Dunstan, H., Roberts, T., Bardakci, F., Badraoui, R., Adnan, M., Saeed, M., Alreshidi, F., Albulaihed, Y., & Snoussi, M. (2022). Changes in Amino Acid Metabolism of Staphylococcus aureus following Growth to the Stationary Phase under Adjusted Growth Conditions. *Microorganisms*, *10*(8). https://doi.org/10.3390/microorganisms10081503

Alshatwi, A. A., Ramesh, E., Periasamy, V. S., & Subash-Babu, P. (2013). The apoptotic effect of hesperetin on human cervical cancer cells is mediated through cell cycle arrest, death receptor, and mitochondrial pathways. *Fundamental and Clinical Pharmacology*, *27*(6), 581–592. https://doi.org/10.1111/j.1472-8206.2012.01061.x

Altamirano, F. L., & Barr, J. J. (2019). Phage therapy in the postantibiotic era. *Clinical Microbiology Reviews*, *32*(2), 1–25. https://doi.org/10.1128/CMR.00066-18

Andersson, D. I., & Hughes, D. (2010). Antibiotic resistance and its cost: Is it possible to reverse resistance? *Nature Reviews Microbiology*, *8*(4), 260–271. https://doi.org/10.1038/nrmicro2319

Aranganathan, S., Selvam, J. P., & Nalini, N. (2008). Effect of hesperetin, a citrus flavonoid, on bacterial enzymes and carcinogen-induced aberrant crypt foci in colon cancer rats: a dose-dependent study. *Journal of Pharmacy and Pharmacology*, *60*(10), 1385–1392. https://doi.org/10.1211/jpp/60.10.0015

Arnold, C., Merryman, M. S., Harris-Arnold, A., McKinney, S., Seidel, C., Loethen, S., Proctor, K. N., Guo, L., & Sanchez Alvarado, A. (2016). Pathogenic shifts in endogenous microbiota impede tissue regeneration via distinct activation of TAK1/MKK/p38. *ELife*, *5*, e16793. https://doi.org/10.7554/eLife.16793

Arteaga Blanco, L. A., Crispim, J. S., Fernandes, K. M., de Oliveira, L. L., Pereira, M. F., Bazzolli, D. M. S., & Martins, G. F. (2017). Differential cellular immune response of Galleria mellonella to Actinobacillus pleuropneumoniae. *Cell and Tissue Research*, *370*(1), 153–168. https://doi.org/10.1007/s00441-017-2653-5

Atabay, K., LoCascio, S., de Hoog, T., & Reddien, P. (2018). Self organization and progenitor targeting generate stable patterns in planarian regeneration. *Science*, *8179*(March).

Azam, M. A., Saha, N., & Jupudi, S. (2019). An explorative study on Staphylococcus aureus MurE inhibitor: induced fit docking, binding free energy calculation, and

molecular dynamics. *Journal of Receptors and Signal Transduction*, *39*(1), 45–54. https://doi.org/10.1080/10799893.2019.1605528

Banjerdpongchai, R., Wudtiwai, B., Khaw-on, P., Rachakhom, W., Duangnil, N., & Kongtawelert, P. (2016). Hesperidin from Citrus seed induces human hepatocellular carcinoma HepG2 cell apoptosis via both mitochondrial and death receptor pathways. *Tumor Biology*, *37*(1), 227–237. https://doi.org/10.1007/s13277-015-3774-7

Barreca, D., Gattuso, G., Bellocco, E., Calderaro, A., Trombetta, D., Smeriglio, A., Laganà, G., Daglia, M., Meneghini, S., & Nabavi, S. M. (2017). Flavanones: Citrus phytochemical with health-promoting properties. *BioFactors*, *43*(4), 495–506. https://doi.org/10.1002/biof.1363

Beeler, T., & Churchich, J. E. (1976). Reactivity of the Phosphopyridoxal Groups of Cystathionase. *The Journal of Biological Chemistry*, *251*, 5267–5271.

Beenken, K. E., Dunman, P. M., Mcaleese, F., Macapagal, D., Murphy, E., Projan, S. J., Blevins, J. S., & Smeltzer, M. S. (2004). Global Gene Expression in Staphylococcus aureus Biofilms. *Journal of Bacteriology*, *186*(14), 4665–4684. https://doi.org/10.1128/JB.186.14.4665

Benton, B., Zhang, J., Bond, S., Pope, C., Christian, T., Lee, L., Winterberg, K., Schmid, M., & Buysee, J. (2004). Large-Scale Identification of Genes Required for Full Virulence of Staphylococcus aureus Large-Scaale Identification of Genes Required for Full Virulence of Staphylococcus aureus. *Journal of Bacteriology*, *186*(24), 8478–8489. https://doi.org/10.1128/JB.186.24.8478

Berends, E. T. M., Horswill, A. R., Haste, N. M., Monestier, M., Nizet, V., & Von Köckritz-Blickwede, M. (2010). Nuclease expression by Staphylococcus aureus facilitates escape from neutrophil extracellular traps. *Journal of Innate Immunity*, *2*(6), 576–586. https://doi.org/10.1159/000319909

Berger, L. C., Wilson, J., Wood, P., & Berger, B. J. (2001). Methionine regeneration and aspartate aminotransferase in prasitic protozoa. *Journal of Bacteriology*, *183*(15), 4421–4434. https://doi.org/10.1128/JB.183.15.4421-4434.2001

Berglund, P., Humble, M. S., & Branneby, C. (2012). 7.18 C-X Bond Formation: Transaminases as Chiral Catalysts: Mechanism, Engineering, and Applications. *Comprehensive Chirality*, *7*, 390–401. https://doi.org/10.1016/B978-0-08-095167-6.00723-0

Bernanrd, B. A. (1993). Adapalene, a new chemical entity with retinoid activity. *Skin Pharmacology and Physiology*, *6*(1), 61–69.

Birolo, L., Sandmeier, E., Christen, P., & John, R. A. (1995). The Roles of Tyr70 and Tyr225 in Aspartate Aminotransferase Assessed by Analysing the Effects of Mutations on the Multiple Reactions of the Substrate Analogue Serine O-Sulphate. *European Journal of Biochemistry*, *232*(3), 859–864. https://doi.org/10.1111/j.1432-1033.1995.0859a.x

Birolo, L., Tutino, L. M., Fontanella, B., Gerday, C., Mainolfi, K., Pascarella, S., Sannia, G., Vinci, F., & Marino, G. (2000). Aspartate aminotransferase from the Antarctic bacterium Pseudoalteromonas haloplanktis TAC 125. Cloning, expression, properties, and molecular modelling. *European Journal of Biochemistry*, *267*(9), 2790–2802. https://doi.org/10.1046/j.1432-1327.2000.01299.x

Bremell, T., Lange, S., Svensson, L., Jennische, E., Gröndahl, K., Carlsten, H., & Tarkowski, A. (1990). Outbreak of spontaneous staphylococcal arthritis and osteitis in mice. *Arthritis & Rheumatism*, *33*(11), 1739–1744. https://doi.org/10.1002/art.1780331120

Brennan, L., Alves, P. M., Hewage, C., Malthouse, J. P. G., & McBean, G. J. (2006). Impact of the gliotoxin L-serine-O-sulphate on cellular metabolism in cultured rat

astrocytes. *Neurochemistry International*, *48*(8), 739–745. https://doi.org/10.1016/j.neuint.2005.12.004

Bridges, R. J., Hatalski, C. G., Shim, S. N., Cummings, B. J., Vijayan, V., Kundi, A., & Cotman, C. W. (1992). Gliotoxic actions of excitatory amino acids. *Neuropharmacology*, *31*(9), 899–907. https://doi.org/10.1016/0028-3908(92)90128-C

Brinster, S., Lamberet, G., Staels, B., Trieu-Cuot, P., Gruss, A., & Poyart, C. (2009). Type II fatty acid synthesis is not a suitable antibiotic target for Gram-positive pathogens. *Nature*, *458*(7234), 83–86. https://doi.org/10.1038/nature07772

Brown, S. E., Howard, A., Kasprzak, A. B., Gordon, K. H., & East, P. D. (2009). A peptidomics study reveals the impressive antimicrobial peptide arsenal of the wax moth Galleria mellonella. *Insect Biochemistry and Molecular Biology*, *39*(11), 792–800. https://doi.org/10.1016/j.ibmb.2009.09.004

Browne, N., Heelan, M., & Kavanagh, K. (2013). An analysis of the structural and functional similarities of insect hemocytes and mammalian phagocytes. *Virulence*, *4*(7), 597–603. https://doi.org/10.4161/viru.25906

Bugg, T. D. H., Braddick, D., Dowson, C. G., & Roper, D. I. (2011). Bacterial cell wall assembly: Still an attractive antibacterial target. *Trends in Biotechnology*, *29*(4), 167–173. https://doi.org/10.1016/j.tibtech.2010.12.006

Campbell, J., Singh, A. K., Santa Maria, J. P., Kim, Y., Brown, S., Swoboda, J. G., Mylonakis, E., Wilkinson, B. J., & Walker, S. (2011). Synthetic lethal compound combinations reveal a fundamental connection between wall teichoic acid and peptidoglycan biosyntheses in staphylococcus aureus. *ACS Chemical Biology*, *6*(1), 106–116. https://doi.org/10.1021/cb100269f

Camposano, S. E., Major, P., Halpern, E., & Thiele, E. A. (2008). Vigabatrin in the treatment of childhood epilepsy: A retrospective chart review of efficacy and safety

profile. *Epilepsia*, *49*(7), 1186–1191. https://doi.org/10.1111/j.1528-1167.2008.01589.x

Carfrae, L. A., & Brown, E. D. (2023). Nutrient stress is a target for new antibiotics. In *Trends in Microbiology* (Vol. 31, Issue 6, pp. 571–585). Elsevier Ltd. https://doi.org/10.1016/j.tim.2023.01.002

Cassini, A., Högberg, L. D., Plachouras, D., Quattrocchi, A., Hoxha, A., Simonsen, G. S., Colomb-Cotinat, M., Kretzschmar, M. E., Devleesschauwer, B., Cecchini, M., Ouakrim, D. A., Oliveira, T. C., Struelens, M. J., Suetens, C., Monnet, D. L., Strauss, R., Mertens, K., Struyf, T., Catry, B., … Hopkins, S. (2019). Attributable deaths and disability-adjusted life-years caused by infections with antibiotic-resistant bacteria in the EU and the European Economic Area in 2015: a population-level modelling analysis. *The Lancet Infectious Diseases*, *19*(1), 56–66. https://doi.org/10.1016/S1473-3099(18)30605-4

Cerenius, L., Lee, B. L., & Söderhäll, K. (2008). The proPO-system: pros and cons for its role in invertebrate immunity. *Trends in Immunology*, *29*(6), 263–271. https://doi.org/10.1016/j.it.2008.02.009

Chang, C. M., Chern, J., Chen, M. Y., Huang, K. F., Chen, C. H., Yang, Y. L., & Wu, S. H. (2015). Avenaciolides: Potential MurA-targeted inhibitors against peptidoglycan biosynthesis in methicillin-resistant staphylococcus aureus (MRSA). *Journal of the American Chemical Society*, *137*(1), 267–275. https://doi.org/10.1021/ja510375f

Chaudhuri, R. R., Allen, A. G., Owen, P. J., Shalom, G., Stone, K., Harrison, M., Burgis, T. A., Lockyer, M., Garcia-Lara, J., Foster, S. J., Pleasance, S. J., Peters, S. E., Maskell, D. J., & Charles, I. G. (2009). Comprehensive identification of essential Staphylococcus aureus genes using Transposon-Mediated Differential Hybridisation (TMDH). *BMC Genomics*, *10*, 1–18. https://doi.org/10.1186/1471-2164-10-291

Cheung, G. Y. C., Bae, J. S., & Otto, M. (2021). Pathogenicity and virulence of Staphylococcus aureus. In *Virulence* (Vol. 12, Issue 1, pp. 547–569). Bellwether Publishing, Ltd. https://doi.org/10.1080/21505594.2021.1878688

Choby, J. E., Grunenwald, C. M., Celis, A. I., Gerdes, S. Y., Dubois, J. L., & Skaar, P. (2018). Staphylococcus aureus HemX Modulates Glutamyl-tRNA Reductase Abundance To Regulate Heme Biosynthesis. *American Society for Microbiology*, *9*(1), 1–19. https://doi.org/10.1128/mBio.02287-17

Chu, J., Vila-Farres, X., Inoyama, D., Gallardo-Macias, R., Jaskowski, M., Satish, S., Freundlich, J. S., & Brady, S. F. (2018). Human Microbiome Inspired Antibiotics with Improved β-Lactam Synergy against MDR Staphylococcus aureus. *ACS Infectious Diseases*, *4*(1), 33–38. https://doi.org/10.1021/acsinfecdis.7b00056

Connolly, J., Boldock, E., Prince, L. R., Renshaw, S. A., Whyte, M. K., & Foster, S. J. (2017). Identification of Staphylococcus aureus factors required for pathogenicity and growth in human blood. *Infection and Immunity*, *85*(11). https://doi.org/10.1128/IAI.00337-17

Cooper, M. A., & Shlaes, D. (2011). Fix the antibiotics pipeline. *Nature*, *472*(7341), 32. https://doi.org/10.1038/472032a

Cornish-Bowden, A. (1986). Why is uncompetitive inhibition so rare?. A possible explanation, with implications for the design of drugs and pesticides. *FEBS Letters*, *203*(1), 3–6. https://doi.org/10.1016/0014-5793(86)81424-7

Cosgrove, S. E., Sakoulas, G., Perencevich, E. N., Schwaber, J., Karchmer, A. W., & Carmeli, Y. (2003). Comparison of mortality associated with methicillin-susceptible and methicillin-resistant Staphylococcus aureus bacteremia: An ecological analysis [6] (multiple letters). *Clinical Infectious Diseases*, *36*, 55–59. https://doi.org/10.1086/377611

Cotter, G., Doyle, S., & Kavanagh, K. (2000). Development of an insect model for the in vivo pathogenicity testing of yeasts. *FEMS Immunology and Medical Microbiology*, *27*(2), 163–169. https://doi.org/10.1016/S0928-8244(99)00185-6

Cruz, A. R., Boer, M. A. den, Strasser, J., Zwarthoff, S. A., Beurskens, F. J., de Haas, C. J. C., Aerts, P. C., Wang, G., de Jong, R. N., Bagnoli, F., van Strijp, J. A. G., van Kessel, K. P. M., Schuurman, J., Preiner, J., Heck, A. J. R., & Rooijakkers, S. H. M. (2021). Staphylococcal protein A inhibits complement activation by interfering with IgG hexamer formation. *Proceedings of the National Academy of Sciences*, *118*(7), e2016772118. https://doi.org/10.1073/pnas.2016772118

Cutuli, M. A., Petronio Petronio, G., Vergalito, F., Magnifico, I., Pietrangelo, L., Venditti, N., & Di Marco, R. (2019). Galleria mellonella as a consolidated in vivo model hosts: New developments in antibacterial strategies and novel drug testing. *Virulence*, *10*(1), 527–541. https://doi.org/10.1080/21505594.2019.1621649

Dailey, H. A., Dailey, T. A., Gerdes, S., Jahn, D., Jahn, M., O'Brian, M. R., & Warren, M. J. (2017). Prokaryotic Heme Biosynthesis: Multiple Pathways to a Common Essential Product. *Microbiology and Molecular Biology Reviews*, *81*(1), 1–62. https://doi.org/10.1128/mmbr.00048-16

Dailey, H. A., Gerdes, S., Dailey, T. A., Burch, J. S., & Phillips, J. D. (2015). Noncanonical coproporphyrin-dependent bacterial heme biosynthesis pathway that does not use protoporphyrin. *Proceedings of the National Academy of Sciences*, *112*(7), 2210–2215. https://doi.org/10.1073/pnas.1416285112

De Biase, D., Barra, D., Bossa, F., Pucci, P., & John, R. A. (1991). Chemistry of the inactivation of 4-aminobutyrate aminotransferase by the antiepileptic drug Vigabatrin. *Journal of Biological Chemistry*, *266*(30), 20056–20061. https://doi.org/10.1016/s0021-9258(18)54890-0

de Jong, N. W. M., van Kessel, K. P. M., & van Strijp, J. A. G. (2019). Immune Evasion by Staphylococcus aureus. *Microbiology Spectrum*, *7*(2), 1–27. https://doi.org/10.1128/9781683670131.ch39

De La Torre, F., Moya-García, A. A., Suárez, M. F., Rodríguez-Caso, C., Cañas, R. A., Sánchez-Jiménez, F., & Cánovas, F. M. (2009). Molecular modeling and site-directed mutagenesis reveal essential residues for catalysis in a prokaryote-type aspartate aminotransferase1[W][OA]. *Plant Physiology*, *149*(4), 1648–1660. https://doi.org/10.1104/pp.108.134510

de Oliveira, D. C., da Silva Lima, F., Sartori, T., Santos, A. C. A., Rogero, M. M., & Fock, R. A. (2016). Glutamine metabolism and its effects on immune response: molecular mechanism and gene expression. *Nutrire*, *41*(1), 1–10. https://doi.org/10.1186/s41110-016-0016-8

Dickey, S. W., Cheung, G. Y. C., & Otto, M. (2017). Different drugs for bad bugs: Antivirulence strategies in the age of antibiotic resistance. *Nature Reviews Drug Discovery*, *16*(7), 457–471. https://doi.org/10.1038/nrd.2017.23

Donlan, R. M., & Costerton, J. W. (2002). Biofilms: Survival Mechanisms of Clinically Relevant Microorganisms. *Clinical Microbiology Reviews*, *15*(2), 167–193. https://doi.org/10.1128/CMR.15.2.167

Dounay, A. B., Anderson, M., Bechle, B. M., Campbell, B. M., Claffey, M. M., Evdokimov, A., Evrard, E., Fonseca, K. R., Gan, X., Ghosh, S., Hayward, M. M., Horner, W., Kim, J. Y., McAllister, L. A., Pandit, J., Paradis, V., Parikh, V. D., Reese, M. R., Rong, S., … Verhoest, P. R. (2012). Discovery of brain-penetrant, irreversible kynurenine aminotransferase ii inhibitors for schizophrenia. *ACS Medicinal Chemistry Letters*, *3*(3), 187–192. https://doi.org/10.1021/ml200204m

Dounay, A. B., Anderson, M., Bechle, B. M., Evrard, E., Gan, X., Kim, J. Y., McAllister, L. A., Pandit, J., Rong, S., Salafia, M. A., Tuttle, J. B., Zawadzke, L. E., & Verhoest,

P. R. (2013). PF-04859989 as a template for structure-based drug design: Identification of new pyrazole series of irreversible KAT II inhibitors with improved lipophilic efficiency. *Bioorganic and Medicinal Chemistry Letters*, *23*(7), 1961–1966. https://doi.org/10.1016/j.bmcl.2013.02.039

Drilling, A., Morales, S., Boase, S., Jervis-Bardy, J., James, C., Jardeleza, C., Tan, N. C. W., Cleland, E., Speck, P., Vreugde, S., & Wormald, P. J. (2014). Safety and efficacy of topical bacteriophage and ethylenediaminetetraacetic acid treatment of Staphylococcus aureus infection in a sheep model of sinusitis. *International Forum of Allergy and Rhinology*, *4*(3), 176–186. https://doi.org/10.1002/alr.21270

Dunphy, G., & Halwani, A. (1997). Haemolymph proteins of larvae of Galleria mellonella detoxify endotoxins of the insect pathogenic bacteria Xenorhabdus nematophilus (Enterobacteriaceae). *Journal of Insect Physiology*, *43*(11), 1023–1029. https://doi.org/10.1016/S0022-1910(97)00072-3

Dunsmore, C. J., Miller, K., Blake, K. L., Patching, S. G., Henderson, P. J. F., Garnett, J. A., Stubbings, W. J., Phillips, S. E. V., Palestrant, D. J., Angeles, J. D. L., Leeds, J. A., Chopra, I., & Fishwick, C. W. G. (2008). 2-Aminotetralones: Novel inhibitors of MurA and MurZ. *Bioorganic and Medicinal Chemistry Letters*, *18*(5), 1730–1734. https://doi.org/10.1016/j.bmcl.2008.01.089

ECDC, & OECD. (2019). Antimicrobial Resistance Tackling the Burden in the European Union. In *Antimicrobial resistance: tackling the burden in the European Union 2019*.

Edwards, M. J., Clarke, T. A., Richardson, D. J., & Paquete, C. M. (2020). Role of multiheme cytochromes involved in extracellular anaerobic respiration in bacteria. *Protein Science*, *29*, 830–842. https://doi.org/10.1002/pro.3787

Elavarasan, J., Velusamy, P., Ganesan, T., Ramakrishnan, S. K., Rajasekaran, D., & Periandavan, K. (2012). Hesperidin-mediated expression of Nrf2 and upregulation of antioxidant status in senescent rat heart. *Journal of Pharmacy and*

Pharmacology, *64*(10), 1472–1482. https://doi.org/10.1111/j.2042-7158.2012.01512.x

Eliot, A. C., & Kirsch, J. F. (2004). Pyridoxal Phosphate Enzymes: Mechanistic, Structural, and Evolutionary Considerations. *Annual Review of Biochemistry*, *73*(1), 383–415. https://doi.org/10.1146/annurev.biochem.73.011303.074021

Ellens, K. W., Christian, N., Singh, C., Satagopam, V. P., May, P., & Linster, C. L. (2017). Confronting the catalytic dark matter encoded by sequenced genomes. *Nucleic Acids Research*, *45*(20), 11495–11514. https://doi.org/10.1093/nar/gkx937

Elliott, S. A., & Sánchez Alvarado, A. (2013). The history and enduring contributions of planarians to the study of animal regeneration. *Wiley Interdisciplinary Reviews: Developmental Biology*, *2*(3), 301–326. https://doi.org/10.1002/wdev.82

Erhardt, S., Schwieler, L., Nilsson, L., Linderholm, K., & Engberg, G. (2007). The kynurenic acid hypothesis of schizophrenia. *Physiology and Behavior*, *92*(1–2), 203–209. https://doi.org/10.1016/j.physbeh.2007.05.025

Falugi, F., Kim, H. K., Missiakas, D. M., & Schneewind, O. (2013). Role of protein a in the evasion of host adaptive immune responses by Staphylococcus aureus. *MBio*, *4*(5), 1–9. https://doi.org/10.1128/mBio.00575-13

Farha, M. A., Leung, A., Sewell, E. W., D'Elia, M. A., Allison, S. E., Ejim, L., Pereira, P. M., Pinho, M. G., Wright, G. D., & Brown, E. D. (2013). Inhibition of WTA synthesis blocks the cooperative action of pbps and sensitizes MRSA to β-lactams. *ACS Chemical Biology*, *8*(1), 226–233. https://doi.org/10.1021/cb300413m

Fey, P. D., Endres, J. L., Yajjala, V. K., Widhelm, T. J., Boissy, R. J., Bose, J. L., & Bayles, K. W. (2013). A genetic resource for rapid and comprehensive phenotype screening of nonessential Staphylococcus aureus genes. *MBio*, *4*(1), 1–8. https://doi.org/10.1128/mBio.00537-12

Fitzpatrick, S. M., Cooper, A. J. L., & Duffy, T. E. (1983). Use of β-Methylene-D,L-Aspartate to Assess the Role of Aspartate Aminotransferase in Cerebral Oxidative Metabolism. *Journal of Neurochemistry*, *41*(5), 1370–1383. https://doi.org/10.1111/j.1471-4159.1983.tb00835.x

Flamm, R. K., Rhomberg, P. R., Kaplan, N., Jones, R. N., & Farrell, D. J. (2015). Activity of Debio1452, a FabI inhibitor with potent activity against Staphylococcus aureus and coagulase-negative Staphylococcus spp., including multidrug-resistant strains. *Antimicrobial Agents and Chemotherapy*, *59*(5), 2583–2587. https://doi.org/10.1128/AAC.05119-14

Forsthoefel, D. J., Cejda, N. I., Khan, U. W., & Newmark, P. A. (2020). Cell-type diversity and regionalized gene expression in the planarian intestine revealed by laser-capture microdissection transcriptome profiling. *ELife*, *9*, e52613. https://doi.org/10.1101/756924

Foster, T. J. (2005). Immune evasion by staphylococci. *Nature Reviews Microbiology*, *3*(12), 948–958. https://doi.org/10.1038/nrmicro1289

Foster, T. J. (2017). Antibiotic resistance in Staphylococcus aureus. Current status and future prospects. *FEMS Microbiology Reviews*, *41*(3), 430–449. https://doi.org/10.1093/femsre/fux007

Foster, T. J., Geoghegan, J. A., Ganesh, V. K., & Höök, M. (2014). Adhesion, invasion and evasion: the many functions of the surface proteins of Staphylococcus aureus. *Nat.Rev.Microbiol.*, *12*(1740-1534 (Electronic)), 49–62. https://doi.org/10.1038/nrmicro3161

Frank, M. W., Yao, J., Batte, J. L., Gullett, J. M., Subramanian, C., Rosch, J. W., & Rock, C. O. (2020). Host fatty acid utilization by staphylococcus aureus at the infection site. *MBio*, *11*(3), 1–14. https://doi.org/10.1128/mBio.00920-20

Friberg, C., Haaber, J. K., Vestergaard, M., Fait, A., Perrot, V., Levin, B. R., & Ingmer, H. (2020). Human antimicrobial peptide, LL-37, induces non-inheritable reduced susceptibility to vancomycin in Staphylococcus aureus. *Scientific Reports*, *10*(1), 1–9. https://doi.org/10.1038/s41598-020-69962-4

Friedmann, H. C., Duban, M. E., Valasinas, A., & Frydman, B. (1992). The enantioselective participation of (S)- and (R)-diaminovaleric acids in the formation of δ-aminolevulinic acid in cyanobacteria. *Biochemical and Biophysical Research Communications*, *185*(1), 60–68. https://doi.org/10.1016/S0006-291X(05)80955-6

Gao, L., Li, A., Li, N., Liu, X., Deng, H., Zhao, B., & Pang, Q. (2017). *Innate and intrinsic immunity in planarians*. 443–452.

Girardi, N. M., Thoden, J. B., & Holden, H. M. (2020). Misannotations of the genes encoding sugar N-formyltransferases. *Protein Science*, *29*(4), 930–940. https://doi.org/10.1002/pro.3807

González, J. D., Caballero, A., Viegas, I., Metón, I., Jones, J. G., Barra, J., Fernández, F., & Baanante, I. V. (2012). Effects of alanine aminotransferase inhibition on the intermediary metabolism in Sparus aurata through dietary amino-oxyacetate supplementation. *British Journal of Nutrition*, *107*(12), 1747–1756. https://doi.org/10.1017/S000711451100496X

González-Estévez, C. (2009). Autophagy meets planarians. *Autophagy*, *5*(3), 290–297. https://doi.org/10.4161/auto.5.3.7665

Graf, A. C., Leonard, A., Schäuble, M., Rieckmann, L. M., Hoyer, J., Maaß, S., Lalk, M., Becher, D., Pané-farré, J., & Riedel, K. (2019). Virulence factors produced by Staphylococcus aureus biofilms have a moonlighting function contributing to biofilm integrity. *Molecular and Cellular Proteomics*, *18*(6), 1036–1053.

Grimm, B., Bull, A., & Breul, V. (1991). Structural genes of glutamate 1-semialdehyde aminotransferase for porphyrin synthesis in a cyanobacterium and Escherichia coli.

Molecular & General Genetics MGG, *225*(1), 1–10. https://doi.org/10.1007/BF00282635

Grimm, B., Smith, M. A., & von Wettstein, D. (1992). The role of Lys272 in the pyridoxal 5-phosphate active site of Synechococcus glutamate-1-semialdehyde aminotransferase. *European Journal of Biochemistry*, *206*(2), 579–585. https://doi.org/10.1111/j.1432-1033.1992.tb16962.x

Grishin, N. V., Phillips, M. A., & Goldsmith, E. J. (1995). Modeling of the spatial structure of eukaryotic ornithine decarboxylases. *Protein Science*, *4*(7), 1291–1304. https://doi.org/10.1002/pro.5560040705

Grosser, M. R., Paluscio, E., Thurlow, L. R., Dillon, M. M., Cooper, V. S., Kawula, T. H., & Richardson, A. R. (2018). Genetic requirements for Staphylococcus aureus nitric oxide resistance and virulence. *PLoS Pathogens*, *14*(3), 1–27. https://doi.org/10.1371/journal.ppat.1006907

Grumann, D., Nübel, U., & Bröker, B. M. (2014). Staphylococcus aureus toxins - Their functions and genetics. *Infection, Genetics and Evolution*, *21*, 583–592. https://doi.org/10.1016/j.meegid.2013.03.013

Gu, W., Song, J., Bonner, C. A., Xie, G., & Jensen, R. A. (1998). PhhC is an essential aminotransferase for aromatic amino acid catabolism in Pseudomonas aeruginosa. *Microbiology*, *144*(11), 3127–3134. https://doi.org/10.1099/00221287-144-11-3127

Guccione, E., Del Rocio Leon-Kempis, M., Pearson, B. M., Hitchin, E., Mulholland, F., Van Diemen, P. M., Stevens, M. P., & Kelly, D. J. (2008). Amino acid-dependent growth of Campylobacter jejuni: Key roles for aspartase (AspA) under microaerobic and oxygen-limited conditions and identification of AspB (Cj0762), essential for growth on glutamate. *Molecular Microbiology*, *69*(1), 77–93. https://doi.org/10.1111/j.1365-2958.2008.06263.x

Halsey, C. R., Lei, S., Wax, J. K., Lehman, M. K., Nuxoll, A. S., Steinke, L., Sadykov, M., Powers, R., & Fey, P. D. (2017). Amino acid catabolism in *Staphylococcus aureus* and the function of carbon catabolite repression. *MBio*, *8*(1), e01434-16. https://doi.org/10.1128/mBio.01434-16

Halwani, A. E., Niven, D. F., & Dunphy, G. B. (2000). Apolipophorin-III and the Interactions of Lipoteichoic Acids with the Immediate Immune Responses of Galleria mellonella. *Journal of Invertebrate Pathology*, *76*, 233–241. https://doi.org/10.1006/jipa.2000.4978

Hamada, A., Torre, C., Lepolard, C., & Ghigo, E. (2016). Inhibition of LTA4H expression promotes Staphylococcus aureus elimination by planarians. *Matters*, *2*(4), e201604000011. https://doi.org/10.19185/matters.201604000011

Hammer, N. D., Reniere, M. L., Cassat, J. E., Zhang, Y., Hirsch, A. O., Hood, M. I., & Skaar, E. P. (2013). Two heme-dependent terminal oxidases power Staphylococcus aureus organ-specific colonization of the vertebrate host. *MBio*, *4*(4), e00241-13. https://doi.org/10.1128/mBio.00241-13

Hammer, N. D., & Skaar, E. P. (2011). Molecular mechanisms of Staphylococcus aureus iron acquisition. *Annual Review of Microbiology*, *65*, 129–147. https://doi.org/10.1146/annurev-micro-090110-102851.Molecular

Hansson, M., Rutberg, L., Schroder, I., & Hederstedt, L. (1991). The Bacillus subtilis hemAXCDBL gene cluster, which encodes enzymes of the biosynthetic pathway from glutamate to uroporphyrinogen III. *Journal of Bacteriology*, *173*(8), 2590–2599. https://doi.org/10.1128/jb.173.8.2590-2599.1991

Hartmann, T., Zhang, B., Baronian, G., Schulthess, B., Homerova, D., Grubmuͤller, S., Kutzner, E., Gaupp, R., Bertram, R., Powers, R., Eisenreich, W., Kormanec, J., Herrmann, M., Molle, V., Somerville, G. A., & Bischoff, M. (2013). Catabolite control protein E (CcpE) is a LysR-type transcriptional regulator of tricarboxylic acid cycle

activity in Staphylococcus aureus. *Journal of Biological Chemistry*, *288*(50), 36116–36128. https://doi.org/10.1074/jbc.M113.516302

Hayashida, A., Bartlett, A. H., Foster, T. J., & Park, P. W. (2009). Staphylococcus aureus beta-toxin induces lung injury through syndecan-1. *American Journal of Pathology*, *174*(2), 509–518. https://doi.org/10.2353/ajpath.2009.080394

Haydon, D., Stokes, N., Ure, R., Galbraith, G., Bennet, J., Brown, D., Baker, P., Barynin, V., Rice, D., Sedelnikova, S., Heal, J., Sheridan, J., Aiwale, S., Chauhan, P., Srivastava, A., Taneja, A., Collins, I., Errington, J., & Czaplewski, L. (2008). An Inhibitor of FtsZ with Potent and Selective Anti-Staphylococcal Activity. *Science*, *321*, 1673–1676.

Hayes, M. J. (2017). Sulphated glycosaminoglycans support an assortment of planarian rhabdite structures. *Biology Open*, *6*(5), 571–581. https://doi.org/10.1242/bio.024554

Herman-Bausier, P., Labate, C., Towell, A. M., Derclaye, S., Geoghegan, J. A., & Dufrêne, Y. F. (2018). Staphylococcus aureus clumping factor A is a force-sensitive molecular switch that activates bacterial adhesion. *Proceedings of the National Academy of Sciences of the United States of America*, *115*(21), 5564–5569. https://doi.org/10.1073/pnas.1718104115

Herman-Bausier, P., Valotteau, C., Pietrocola, G., Rindi, S., Alsteens, D., Foster, T. J., Speziale, P., & Dufrêne, Y. F. (2016). Mechanical strength and inhibition of the Staphylococcus aureus collagen-binding protein Cna. *MBio*, *7*(5), 1–11. https://doi.org/10.1128/mBio.01529-16

Hershberg, R. (2017). Antibiotic-Independent Adaptive Effects of Antibiotic Resistance Mutations. *Trends in Genetics*, *33*(8), 521–528. https://doi.org/10.1016/j.tig.2017.05.003

Holdgate, G. A., Meek, T. D., & Grimley, R. L. (2018). Mechanistic enzymology in drug discovery: A fresh perspective. *Nature Reviews Drug Discovery*, *17*(2), 115–132. https://doi.org/10.1038/nrd.2017.219

Homma, T., Nuxoll, A., Gandt, A. B., Ebner, P., Engels, I., Schneider, T., Götz, F., Lewis, K., & Conlon, B. P. (2016). Dual targeting of cell wall precursors by teixobactin leads to cell lysis. *Antimicrobial Agents and Chemotherapy*, *60*(11), 6510–6517. https://doi.org/10.1128/AAC.01050-16

Howden, B. P., Davies, J. K., Johnson, P. D. R., Stinear, T. P., & Grayson, M. L. (2010). Reduced vancomycin susceptibility in Staphylococcus aureus, including vancomycin-intermediate and heterogeneous vancomycin-intermediate strains: Resistance mechanisms, laboratory detection, and clinical implications. *Clinical Microbiology Reviews*, *23*(1), 99–139. https://doi.org/10.1128/CMR.00042-09

Hrast, M., Jukič, M., Patin, D., Tod, J., Dowson, C. G., Roper, D. I., Barreteau, H., & Gobec, S. (2018). In silico identification, synthesis and biological evaluation of novel tetrazole inhibitors of MurB. *Chemical Biology and Drug Design*, *91*(6), 1101–1112. https://doi.org/10.1111/cbdd.13172

Hu, S., Zhang, X., Lu, Y., Lin, Y. C., Xie, D. F., Fang, H., Huang, J., & Mei, L. H. (2017). Cloning, expression and characterization of an aspartate aminotransferase gene from Lactobacillus brevis CGMCC 1306. *Biotechnology and Biotechnological Equipment*, *31*(3), 544–553. https://doi.org/10.1080/13102818.2017.1304181

Hubbard, A. T. M., Bulgasim, I., & Roberts, A. P. (2020). A novel hemA mutation is responsible for a small- variant phenotype in Escherichia coli. *Microbiology*, micro000962. https://doi.org/10.1099/mic.0.000962

Imanishi, I., Nicolas, A., Caetano, A. C. B., Castro, T. L. de P., Tartaglia, N. R., Mariutti, R., Guédon, E., Even, S., Berkova, N., Arni, R. K., Seyffert, N., Azevedo, V., Nishifuji, K., & Le Loir, Y. (2019). Exfoliative toxin E, a new Staphylococcus aureus

virulence factor with host-specific activity. *Scientific Reports*, *9*(1), 1–12. https://doi.org/10.1038/s41598-019-52777-3

Isoda, H., Motojima, H., Onaga, S., Samet, I., Villareal, M. O., & Han, J. (2014). Analysis of the erythroid differentiation effect of flavonoid apigenin on K562 human chronic leukemia cells. *Chemico-Biological Interactions*, *220*, 269–277. https://doi.org/10.1016/j.cbi.2014.07.006

Jansen, R. S., Mandyoli, L., Hughes, R., Wakabayashi, S., Pinkham, J. T., Selbach, B., Guinn, K. M., Rubin, E. J., Sacchettini, J. C., & Rhee, K. Y. (2020). Aspartate aminotransferase Rv3722c governs aspartate-dependent nitrogen metabolism in Mycobacterium tuberculosis. *Nature Communications*, *11*(1), 1–13. https://doi.org/10.1038/s41467-020-15876-8

Jensen, S., & Lyon, B. (2009). Genetics of Antimicrobial Resistance in Staphylococcus aureus. *Future Microbiology*, *4*(5), 565–582. https://doi.org/10.1111/j.1749-6632.1956.tb36635.x

Jochim, A., Shi, T., Belikova, D., Schwarz, S., Peschel, A., & Heilbronner, S. (2019). Methionine limitation impairs pathogen expansion and biofilm formation capacity. *Applied and Environmental Microbiology*, *85*(9), 1–16. https://doi.org/10.1128/AEM.00177-19

Jordan, P. M., Gerstmeier, J., Pace, S., Bilancia, R., Rao, Z., Börner, F., Miek, L., Gutiérrez-Gutiérrez, Ó., Arakandy, V., Rossi, A., Ialenti, A., González-Estévez, C., Löffler, B., Tuchscherr, L., Serhan, C. N., & Werz, O. (2020). Staphylococcus aureus-Derived α-Hemolysin Evokes Generation of Specialized Pro-resolving Mediators Promoting Inflammation Resolution. *Cell Reports*, *33*(2). https://doi.org/10.1016/j.celrep.2020.108247

Josse, J., Laurent, F., & Diot, A. (2017). Staphylococcal adhesion and host cell invasion: Fibronectin-binding and other mechanisms. *Frontiers in Microbiology*, *8*(DEC), 1–8. https://doi.org/10.3389/fmicb.2017.02433

Jung, M. J., Lippert, B., Metcalf, B. W., Böhlen, P., & Schechter, P. J. (1977). γ-VINYL GABA (4-amino-hex-5-enoic acid), A NEW SELECTIVE IRREVERSIBLE INHIBITOR OF GABA-T: EFFECTS ON BRAIN GABA METABOLISM IN MICE. *Journal of Neurochemistry*, *29*(5), 797–802. https://doi.org/10.1111/j.1471-4159.1977.tb10721.x

Jupudi, S., Azam, M. A., & Wadhwani, A. (2021). Design, synthesis and molecular modelling of phenoxyacetohydrazide derivatives as Staphylococcus aureus MurD inhibitors. *Chemical Papers*, *75*(3), 1221–1235. https://doi.org/10.1007/s11696-020-01380-2

Kaiser, J. C., Omer, S., Sheldon, J. R., Welch, I., & Heinrichs, E. (2015). Role of BrnQ1 and BrnQ2 in Branched-Chain Amino Acid Transport and Virulence in Staphylococcus aureus. *Infection and Immunity*, *83*(3), 1019–1029.

Kampen, A. H., Tollersrud, T., & Lund, A. (2005). Staphylococcus aureus capsular polysaccharide types 5 and 8 reduce killing by bovine neutrophils in vitro. *Infection and Immunity*, *73*(3), 1578–1583. https://doi.org/10.1128/IAI.73.3.1578-1583.2005

Kasif, S., & Roberts, R. J. (2020). We need to keep a reproducible trace of facts, predictions, and hypotheses from gene to function in the era of big data. *PLoS Biology*, *18*(11), 1–10. https://doi.org/10.1371/journal.pbio.3000999

Katayama, Y., Baba, T., Sekine, M., Fukuda, M., & Hiramatsu, K. (2013). Beta-hemolysin promotes skin colonization by Staphylococcus aureus. *Journal of Bacteriology*, *195*(6), 1194–1203. https://doi.org/10.1128/JB.01786-12

Kaul, M., Mark, L., Zhang, Y., Parhi, A. K., Lyu, Y. L., Pawlak, J., Saravolatz, S., Saravolatz, L. D., Weinstein, M. P., LaVoie, E. J., & Pilcha, D. S. (2015). TXA709,

an FtsZ-targeting benzamide prodrug with improved pharmacokinetics and enhanced in vivo efficacy against methicillin-resistant Staphylococcus aureus. *Antimicrobial Agents and Chemotherapy*, *59*(8), 4845–4855. https://doi.org/10.1128/AAC.00708-15

Kayan, T., & Torres, V. J. (2019). Staphylococcus aureus secreted toxins and extracellular enzymes. In V. Fischetti, R. Novick, J. Ferreti, D. Portnoy, M. Braunstein, & J. Rood (Eds.), *Gram-Positive Pathogens* (Third Edit, pp. 640–668). ASM Press.

Kesharwani, P., Chopra, S., & Dasgupta, A. (Eds.). (2020). *Drug Discovery Targeting Drug-Resistant Bacteria*. Academic Press. https://doi.org/10.1177/2472555220970966

Khamash, D. F., Voskertchian, A., Tamma, P. D., Akinboyo, I. C., Carroll, K. C., & Milstone, A. M. (2019). Increasing Clindamycin and Trimethoprim-Sulfamethoxazole Resistance in Pediatric Staphylococcus aureus Infections. *Journal of the Pediatric Infectious Diseases Society*, *8*(4), 351–353. https://doi.org/10.1093/jpids/piy062

Kim, H., Ikegami, K., Nakaoka, M., Yagi, M., Shibata, H., & Sawa, Y. (2003). Characterization of aspartate aminotransferase from the cyanobacterium phormidium lapideum. *Bioscience, Biotechnology and Biochemistry*, *67*(3), 490–498. https://doi.org/10.1271/bbb.67.490

Köhler, E., Seville, M., Jäger, J., Fotheringham, I., Hunter, M., Edwards, M., Jansonius, J. N., & Kirschner, K. (1994). Significant Improvement to the Catalytic Properties of Aspartate Aminotransferase: Role of Hydrophobic and Charged Residues in the Substrate Binding Pocket. *Biochemistry*, *33*(1), 90–97. https://doi.org/10.1021/bi00167a012

Komoda, T., & Matsunaga, T. (2015). Constituents of the Human Body. *Biochemistry for Medical Professionals*, 7–24. https://doi.org/10.1016/b978-0-12-801918-4.00003-7

Korangath, P., Teo, W. W., Sadik, H., Han, L., Mori, N., Huijts, C. M., Wildes, F., Bharti, S., Zhang, Z., Santa-Maria, C. A., Tsai, H., Dang, C. V., Stearns, V., Bhujwalla, Z. M., & Sukumar, S. (2015). Targeting glutamine metabolism in breast cancer with aminooxyacetate. *Clinical Cancer Research*, *21*(14), 3263–3273. https://doi.org/10.1158/1078-0432.CCR-14-1200

Krakauer, T., Pradhan, K., & Stiles, B. G. (2016). Staphylococcal superantigens spark host-mediated danger signals. *Frontiers in Immunology*, *7*(FEB). https://doi.org/10.3389/fimmu.2016.00023

Kriegeskorte, A., GrubmuЇller, S., Huber, C., Khal, B., von Eiff, C., Proctor, R., Peters, G., Eisenreich, W., & Becker, K. (2014). Staphylococcus aureus small colony variants show common metabolic features in central metabolism irrespective of the underlying auxotrophism. *Frontiers in Cellular and Infection Microbiology*, *4*(October), 1–8. https://doi.org/10.3389/fcimb.2014.00141

Kumar, G., & Khan, M. (2018). Study of the life cycle of greater wax moth (Galleria mellonella) under storage conditions in relation to different weather conditions. *Journal of Entomology and Zoology Studies*, *6*(3), 444–447.

Ladhani, S. (2003). Understanding the mechanism of action of the exfoliative toxins of Staphylococcus aureus. *FEMS Immunology and Medical Microbiology*, *39*(2), 181–189. https://doi.org/10.1016/S0928-8244(03)00225-6

Lange, M., & Mályusz, M. (1994). Fast method for the simultaneous determination of 2-oxo acids in biological fluids by high-performance liquid chromatography. *Journal of Chromatography B: Biomedical Sciences and Applications*, *662*(1), 97–102. https://doi.org/10.1016/0378-4347(94)00383-1

Lavine, M. D., & Strand, M. R. (2002). Insect Hemocytes and Their Role in Immunity. *Insect Biochemistry and Molecular Biology*, *32*(2002), 1295–1309. https://doi.org/10.1016/B978-012373976-6.50004-5

Law, J. N., Kale, S. D., & Murali, T. M. (2021). Accurate and efficient gene function prediction using a multi-bacterial network. *Bioinformatics*, *37*(6), 800–806. https://doi.org/10.1093/bioinformatics/btaa885

Layer, G., Reichelt, J., Jahn, D., & Heinz, D. W. (2010). Structure and function of enzymes in heme biosynthesis. *Protein Science*, *19*(6), 1137–1161. https://doi.org/10.1002/pro.405

Ledger, E. V. K., Mesnage, S., & Edwards, A. M. (2022). Human serum triggers antibiotic tolerance in Staphylococcus aureus. *Nature Communications*, *13*(1), 1–19. https://doi.org/10.1038/s41467-022-29717-3

Lee, H., Doud, E. H., Wu, R., Sanishvili, R., Juncosa, J. I., Liu, D., Kelleher, N. L., & Silverman, R. B. (2015). Mechanism of inactivation of γ-aminobutyric acid aminotransferase by (1 S,3 S)-3-amino-4-difluoromethylene-1-cyclopentanoic acid (CPP-115). *Journal of the American Chemical Society*, *137*(7), 2628–2640. https://doi.org/10.1021/ja512299n

Lee, K., Campbell, J., Swoboda, J. G., Cuny, G. D., & Walker, S. (2010). Development of improved inhibitors of wall teichoic acid biosynthesis with potent activity against Staphylococcus aureus. *Bioorganic and Medicinal Chemistry Letters*, *20*(5), 1767–1770. https://doi.org/10.1016/j.bmcl.2010.01.036

Li, L., Chen, H., Liu, Y., Xu, S., Wu, M., Liu, Z., Qi, C., Zhang, G., Li, J., & Huang, X. (2020). Synergistic effect of linezolid with fosfomycin against Staphylococcus aureus in vitro and in an experimental Galleria mellonella model. *Journal of Microbiology, Immunology and Infection*, *53*(5), 731–738. https://doi.org/10.1016/j.jmii.2018.12.007

Liang, J., Han, Q., Tan, Y., Ding, H., & Li, J. (2019). Current advances on structure-function relationships of pyridoxal 5'-phosphate-dependent enzymes. *Frontiers in Molecular Biosciences*, *6*(MAR). https://doi.org/10.3389/fmolb.2019.00004

Linderholm, K. R., Skogh, E., Olsson, S. K., Dahl, M. L., Holtze, M., Engberg, G., Samuelsson, M., & Erhardt, S. (2012). Increased levels of kynurenine and kynurenic acid in the CSF of patients with schizophrenia. *Schizophrenia Bulletin*, *38*(3), 426–432. https://doi.org/10.1093/schbul/sbq086

Ling, L. L., Schneider, T., Peoples, A. J., Spoering, A. L., Engels, I., Conlon, B. P., Mueller, A., Schäberle, T. F., Hughes, D. E., Epstein, S., Jones, M., Lazarides, L., Steadman, V. A., Cohen, D. R., Felix, C. R., Fetterman, K. A., Millett, W. P., Nitti, A. G., Zullo, A. M., … Lewis, K. (2015). A new antibiotic kills pathogens without detectable resistance. *Nature*, *517*(7535), 455–459. https://doi.org/10.1038/nature14098

Lippert, B., Metcalf, B. W., Jung, M. J., & Casara, P. (1977). 4-Amino-hex-5-enoic Acid, a Selective Catalytic Inhibitor of 4-Aminobutyric-Acid Aminotransferase in Mammalian Brain. *European Journal of Biochemistry*, *74*(3), 441–445. https://doi.org/10.1111/j.1432-1033.1977.tb11410.x

Liu, C. C., & Lin, M. H. (2020). Involvement of Heme in Colony Spreading of Staphylococcus aureus. *Frontiers in Microbiology*, *11*(February), 1–10. https://doi.org/10.3389/fmicb.2020.00170

Liu, G. Y., Essex, A., Buchanan, J. T., Datta, V., Hoffman, H. M., Bastian, J. F., Fierer, J., & Nizet, V. (2005). Staphylococcus aureus golden pigment impairs neutrophil killing and promotes virulence through its antioxidant activity. *The Journal of Experimental Medicine*, *202*(2), 209–215. https://doi.org/10.1084/jem.20050846

Löscher, W. (1980). A comparative study of the pharmacology of inhibitors of GABA-metabolism. *Archives of Pharmacology*, *315*(2), 119–128. https://doi.org/10.1007/BF00499254

Lowy, F. (2003). Antimicrobial resistance: the example of Staphylococcus aureus. *Journal of Clinical Investigation*, *111*, 1265–1273. https://doi.org/10.1172/JCI200318535.In

Lu, C., Chan, K., Li, W., Atkinson, G. C., Thakor, N. S., Tenson, T., Schulten, K., Wilson, K. S., Hauryliuk, V., & Frank, J. (2013). Mechanism of tetracycline resistance by ribosomal protection protein Tet (O). *Nature Communications*, *4*(1), 1–8. https://doi.org/10.1038/ncomms2470

Lv, X., Fan, J., Ge, H., Gao, Y., Zhang, X., Teng, M., & Niu, L. (2006). Cloning, expression, purification, crystallization and preliminary X-ray diffraction analysis of the glutamate-1-semialdehyde aminotransferase from Bacillus subtilis. *Acta Crystallographica Section F: Structural Biology and Crystallization Communications*, *62*(5), 483–485. https://doi.org/10.1107/S1744309106013121

Macgowan, A. P., & Wise, R. (2001). Establishing MIC breakpoints and the interpretation of in vitro susceptibility tests. *Journal of Antimicrobial Chemotherapy*, *48*, 17–28.

Maciel, E., Jiang, C., Barghouth, P., Nobile, C., & Oviedo, N. (2019). The planarian Schmidtea mediterranea is a new model to study host-pathogen interactions during fungal infections. *Developmental and Comparative Immunology*, *93*, 18–27. https://doi.org/10.1016/j.dci.2018.12.005

Maksymiuk, C., Ioerger, T., Balakrishnan, A., Bryk, R., Sacchettini, J., & Nathan, C. (2015). Comparison of transposon and deletion mutants in Mycobacterium tuberculosis: The case of rv1248c, encoding 2-hydroxy-3-oxoadipate synthase. *Tuberculosis*, *95*(6), 689–694. https://doi.org/10.1016/j.tube.2015.08.009.Comparison

Malin, J. J., & De Leeuw, E. (2019). Therapeutic compounds targeting Lipid II for antibacterial purposes. *Infection and Drug Resistance*, *12*, 2613–2625. https://doi.org/10.2147/IDR.S215070

Manandhar, S., Singh, A., Varma, A., Pandey, S., & Grant, G. (2018). Biofilm Producing Clinical Staphylococcus aureus Isolates Augmented Prevalence of Antibiotic Resistant Cases in Tertiary Care Hospitals of Nepal. *Frontiers in Microbiology*, *9*, 2749. https://doi.org/10.3389/fmicb.2018.02749

Mann, P. A., Müller, A., Xiao, L., Pereira, P. M., Yang, C., Ho Lee, S., Wang, H., Trzeciak, J., Schneeweis, J., Dos Santos, M. M., Murgolo, N., She, X., Gill, C., Balibar, C. J., Labroli, M., Su, J., Flattery, A., Sherborne, B., Maier, R., … Roemer, T. (2013). Murgocil is a highly bioactive staphylococcal-specific inhibitor of the peptidoglycan glycosyltransferase enzyme MurG. *ACS Chemical Biology*, *8*(11), 2442–2451. https://doi.org/10.1021/cb400487f

Martin, J. K., Sheehan, J. P., Bratton, B. P., Moore, G. M., Mateus, A., Li, S. H. J., Kim, H., Rabinowitz, J. D., Typas, A., Savitski, M. M., Wilson, M. Z., & Gitai, Z. (2020). A Dual-Mechanism Antibiotic Kills Gram-Negative Bacteria and Avoids Drug Resistance. *Cell*, *181*(7), 1518-1532.e14. https://doi.org/10.1016/j.cell.2020.05.005

Mason, W. J., & Skaar, E. P. (2009). Assessing the contribution of heme-iron acquisition to Staphylococcus aureus pneumonia using computed tomography. *PLoS ONE*, *4*(8). https://doi.org/10.1371/journal.pone.0006668

McBean, G. J. (2007). Sulfur-Containing Amino Acids. In *Handbook of Neurochemistry and Molecular Neurobiology* (Third Edit, pp. 133–154). Springer.

Mccallum, N., Berger-Bächi, B., & Senn, M. M. (2010). Regulation of antibiotic resistance in Staphylococcus aureus. *International Journal of Medical Microbiology*, *300*, 118–129. https://doi.org/10.1016/j.ijmm.2009.08.015

Meeske, A. J., Sham, L. T., Kimsey, H., Koo, B. M., Gross, C. A., Bernhardt, T. G., & Rudner, D. Z. (2015). MurJ and a novel lipid II flippase are required for cell wall biogenesis in Bacillus subtilis. *Proceedings of the National Academy of Sciences of the United States of America*, *112*(20), 6437–6442. https://doi.org/10.1073/pnas.1504967112

Mehta, P., & Christen, P. (2000). The molecular evolution of Pyridoxal-5'-phosphate-dependent enzymes. *Advances in Enzymology and Related Areas of Molecular Biology*, *74*.

Ménard, G., Rouillon, A., Ghukasyan, G., Emily, M., Felden, B., & Donnio, P. Y. (2021). Galleria mellonella Larvae as an Infection Model to Investigate sRNA-Mediated Pathogenesis in Staphylococcus aureus. *Frontiers in Cellular and Infection Microbiology*, *11*. https://doi.org/10.3389/fcimb.2021.631710

Menetrey, A., Janin, A., Pullman, J., Overcash, J. S., Haouala, A., Leylavergne, F., Turbe, L., Wittke, F., Nicolas-, & Nicolas-Métral, V. (2019). Bone and Joint Tissue Penetration of the Staphylococcus-Selective Antibiotic Afabicin in Patients Undergoing Elective Hip Replacement Surgery. *Antimicrobial Agents and Chemotherapy*, *63*(3), e01669-18.

Micoli, F., Bagnoli, F., Rappuoli, R., & Serruto, D. (2021). The role of vaccines in combatting antimicrobial resistance. *Nature Reviews Microbiology*, 1–16. https://doi.org/https://doi.org/10.1038/s41579-020-00506-3

Miller, W. R., Bayer, A. S., & Arias, C. A. (2016). Mechanism of action and resistance to daptomycin in Staphylococcus aureus and enterococci. *Cold Spring Harbor Perspectives in Medicine*, *6*(11). https://doi.org/10.1101/cshperspect.a026997

Mollace, V., Sacco, I., Janda, E., Malara, C., Ventrice, D., Colica, C., Visalli, V., Muscoli, S., Ragusa, S., Muscoli, C., Rotiroti, D., & Romeo, F. (2011). Hypolipemic and

hypoglycaemic activity of bergamot polyphenols From animal models to human studies. *Fitoterapia*, *82*, 309–316. https://doi.org/10.1016/j

Möller, N., Ziesemer, S., Hildebrandt, P., Assenheimer, N., Völker, U., & Hildebrandt, J. P. (2020). S. aureus alpha-toxin monomer binding and heptamer formation in host cell membranes-Do they determine sensitivity of airway epithelial cells toward the toxin? *PLoS ONE*, *15*(5), 1–21. https://doi.org/10.1371/journal.pone.0233854

Moormeier, D. E., & Bayles, K. W. (2017). Staphylococcus aureus Biofilm: A Complex Developmental Organism Graphical Abstract. *Mol Microbiol*, *104*(3), 365–376. https://doi.org/10.1111/mmi.13634.Staphylococcus

Moormeier, D. E., Bose, J., Horswill, A. R., & Bayles, K. W. (2014). Temporal and stochastic control of Staphylococcus aureus biofilm developement. *MBio*, *5*(5), e01341-14. https://doi.org/10.3389/fmicb.2017.01290

Morales, G., Picazo, J. J., Baos, E., Candel, F. J., Arribi, A., Pela, B., Andrade, R., Torre, D., & Sa, M. (2010). Resistance to Linezolid Is Mediated by the cfr Gene in the First Report of an Outbreak of Linezolid- Resistant Staphylococcus aureus. *Clinical Infectious Diseases*, *50*(6), 821–825. https://doi.org/10.1086/650574

Moreno-Sánchez, R., Marín-Hernández, Á., Del Mazo-Monsalvo, I., Saavedra, E., & Rodríguez-Enríquez, S. (2017). Assessment of the low inhibitory specificity of oxamate, aminooxyacetate and dichloroacetate on cancer energy metabolism. *Biochimica et Biophysica Acta - General Subjects*, *1861*(1), 3221–3236. https://doi.org/10.1016/j.bbagen.2016.08.006

Morita, M. (1991). Phagocytic response of planarian reticular cells to heat-killed bacteria. *Hydrobiologia*, *227*(1), 193–199. https://doi.org/10.1007/BF00027602

Murima, P., Mckinney, J. D., & Pethe, K. (2014). Targeting Bacterial Central Metabolism for Drug Development. *Chemistry and Biology*, *21*, 1423–1432.

Murray, C. J., Ikuta, K. S., Sharara, F., Swetschinski, L., Robles Aguilar, G., Gray, A., Han, C., Bisignano, C., Rao, P., Wool, E., Johnson, S. C., Browne, A. J., Chipeta, M. G., Fell, F., Hackett, S., Haines-Woodhouse, G., Kashef Hamadani, B. H., Kumaran, E. A. P., McManigal, B., … Naghavi, M. (2022). Global burden of bacterial antimicrobial resistance in 2019: a systematic analysis. *The Lancet*, *399*(10325), 629–655. https://doi.org/10.1016/S0140-6736(21)02724-0

Nadvi, N. A., Salam, N. K., Park, J., Akladios, F. N., Kapoor, V., Collyer, C. A., Gorrell, M. D., & Church, W. B. (2017). High resolution crystal structures of human kynurenine aminotransferase-I bound to PLP cofactor, and in complex with aminooxyacetate. *Protein Science*, *26*(4), 727–736. https://doi.org/10.1002/pro.3119

Nair, S. P., Harwood, J. L., & John, R. A. (1991). Direct identification and quantification of the cofactor in glutamate semialdehyde aminotransferase from pea leaves. *FEBS Letters*, *283*(1), 4–6. https://doi.org/10.1016/0014-5793(91)80540-J

Nardella, C., Boi, D., di Salvo, M. L., Barile, A., Stetefeld, J., Tramonti, A., & Contestabile, R. (2019). Isolation of a complex formed between acinetobacter baumannii HemA and HemL, key enzymes of tetrapyrroles biosynthesis. *Frontiers in Molecular Biosciences*, *6*(FEB), 1–11. https://doi.org/10.3389/fmolb.2019.00006

Nathwani, D., Morgan, M., Masterton, R. G., Dryden, M., Cookson, B. D., French, G., & Lewis, D. (2008). Guidelines for UK practice for the diagnosis and management of methicillin-resistant Staphylococcus aureus (MRSA) infections presenting in the community. *Journal of Antimicrobial Chemotherapy*, *61*(5), 976–994. https://doi.org/10.1093/jac/dkn096

Newmark, P. A., & Sánchez Alvarado, A. (2002). NOT YOUR FATHER'S PLANARIAN A CLASSIC MODEL ENTERS THE ERA OF FUNCTIONAL GENOMICS. *Nature Reviews Genetics*, *3*(3), 210–219. https://doi.org/10.1038/nrg759

Nurjadi, D., Schäfer, J., Friedrich-Jänicke, B., Mueller, A., Neumayr, A., Calvo-Cano, A., Goorhuis, A., Molhoek, N., Lagler, H., Kantele, A., Van Genderen, P. J. J., Gascon, J., Grobusch, M. P., Caumes, E., Hatz, C., Fleck, R., Mockenhaupt, F. P., & Zanger, P. (2015). Predominance of dfrG as determinant of trimethoprim resistance in imported Staphylococcus aureus. *Clinical Microbiology and Infection*, *21*(12), 1095.e5-1095.e9. https://doi.org/10.1016/j.cmi.2015.08.021

Nuxoll, A. S., Halouska, S. M., Sadykov, M. R., Hanke, M. L., Bayles, K. W., Kielian, T., Powers, R., & Fey, P. D. (2012). CcpA Regulates Arginine Biosynthesis in Staphylococcus aureus through Repression of Proline Catabolism. *PLoS Pathogens*, *8*(11), p.e1003033.

Nygaard, T. K., Pallister, K. B., DuMont, A. L., DeWald, M., Watkins, R. L., Pallister, E. Q., Malone, C., Griffith, S., Horswill, A. R., Torres, V. J., & Voyich, J. M. (2012). Alpha-toxin induces programmed cell death of human T cells, B cells, and monocytes during USA300 infection. *PLoS ONE*, *7*(5). https://doi.org/10.1371/journal.pone.0036532

O'Brien, M. M., Walsh, E. J., Massey, R. C., Peacock, S. J., & Foster, T. J. (2002). Staphylococcus aureus clumping factor B (ClfB) promotes adherence to human type I cytokeratin 10: Implications for nasal colonization. *Cellular Microbiology*, *4*(11), 759–770. https://doi.org/10.1046/j.1462-5822.2002.00231.x

Ogston, A. (1881). Report upon microorganisms in surgical diseases. *The British Medical Journal*, *1*, 369–375.

Oliveira, D., Borges, A., & Simões, M. (2018). Staphylococcus aureus toxins and their molecular activity in infectious diseases. *Toxins*, *10*(6). https://doi.org/10.3390/toxins10060252

Olsson, S. K., Samuelsson, M., Saetre, P., Lindström, L., Jönsson, E. G., Nordin, C., Engberg, G., Erhardt, S., & Landén, M. (2010). Elevated levels of kynurenic acid in

the cerebrospinal fluid of patients with bipolar disorder. *Journal of Psychiatry and Neuroscience*, *35*(3), 195–199. https://doi.org/10.1503/jpn.090180

O'Neill, E., Houston, P., Humphreys, H., Robinson, D. A., Loughman, A., Foster, T. J., & O'Gara, J. P. (2008). A novel Staphylococcus aureus biofilm phenotype mediated by the fibronectin-binding proteins, FnBPA and FnBPB. *Journal of Bacteriology*, *190*(11), 3835–3850. https://doi.org/10.1128/JB.00167-08

O'Neill, J. (2016). *TACKLING DRUG-RESISTANT INFECTIONS GLOBALLY: FINAL REPORT AND RECOMMENDATIONS*.

Oogai, Y., Matsuo, M., Hashimoto, M., Kato, F., Sugai, M., & Komatsuzawa, H. (2011). Expression of Virulence Factors by Staphylococcus aureus Grown in Serum. *Applied and Environmental Microbiology*, *77*(22), 8097–8105. https://doi.org/10.1128/aem.05316-11

Oshima, T., Okamoto, A., & Kuramitsu, S. (1996). An aspartate aminotransferase from an extremely thermophilic bacterium , Thermus thermopilus HB8. *Journal of Biochemistry*, *144*(1), 135–144.

Otto, M. (2008). Staphylococcal Biofilms. *Current Topics in Microbiology and Immunology*, *322*, 207–228.

Otto, M. (2014). Staphylococcus aureus toxins. *Current Opinion in Microbiology*, *17*(1), 32–37. https://doi.org/10.1016/j.mib.2013.11.004

Paharik, A. E., & Horswill, A. R. (2016). The Staphylococcal Biofilm: Adhesins, Regulation, and Host Response. *Microbiology Spectrum*, *4*(2), 529–566. https://doi.org/10.1128/9781555819286.ch19

Painter, K. L., Hall, A., Ha, K. P., & Edwards, A. M. (2017). The Electron Transport Chain Sensitizes Staphylococcus aureus and Enterococcus faecalis to the Oxidative Burst. *Infection and Immunity*, *85*(12), 1–13.

Panche, A. N., Diwan, A. D., & Chandra, S. R. (2016). Flavonoids: An overview. *Journal of Nutritional Science*, *5*. https://doi.org/10.1017/jns.2016.41

Pang, Q., Gao, L., Bai, Y., Deng, H., Han, Y., Hu, W., Zhang, Y., Yuan, S., Sun, W., Lu, Y., Zhang, X., Liu, B., & Zhao, B. (2017). Identification and characterization of a novel multifunctional placenta specific protein 8 in Dugesia japonica. *Gene*, *613*, 1–9. https://doi.org/10.1016/j.gene.2017.02.024

Pasquina, L. W., Santa Maria, J. P., & Walker, S. (2013). Teichoic acid biosynthesis as an antibiotic target. *Current Opinion in Microbiology*, *16*(5), 531–537. https://doi.org/10.1016/j.mib.2013.06.014

Pavlović, D., Mutak, S., Andreotti, D., Biondi, S., Cardullo, F., Paio, A., Piga, E., Donati, D., & Lociuro, S. (2014). Synthesis and structure-activity relationships of α-Amino-γ-lactone Ketolides: A novel class of macrolide antibiotics. *ACS Medicinal Chemistry Letters*, *5*(10), 1133–1137. https://doi.org/10.1021/ml500279k

Peiris, T. H., Hoyer, K. K., & Oviedo, N. J. (2014). Innate immune system and tissue regeneration in planarians: An area ripe for exploration. *Seminars in Immunology*, *26*(4), 295–302. https://doi.org/10.1016/j.smim.2014.06.005

Percudani, R., & Peracchi, A. (2003). A genomic overview of pyridoxal-phosphate-dependent enzymes. *EMBO Reports*, *4*(9), 850–854. https://doi.org/10.1038/sj.embor.embor914

Percudani, R., & Peracchi, A. (2009). The B6 database: A tool for the description and classification of vitamin B6-dependent enzymatic activities and of the corresponding protein families. *BMC Bioinformatics*, *10*, 273. https://doi.org/10.1186/1471-2105-10-273

Petrovic Fabijan, A., Lin, R. C. Y., Ho, J., Maddocks, S., Ben Zakour, N. L., Iredell, J. R., Khalid, A., Venturini, C., Chard, R., Morales, S., Sandaradura, I., & Gilbey, T.

(2020). Safety of bacteriophage therapy in severe Staphylococcus aureus infection. *Nature Microbiology*, *5*(3), 465–472. https://doi.org/10.1038/s41564-019-0634-z

Pietta, P. G. (2000). Flavonoids as antioxidants. *Journal of Natural Products*, *63*(7), 1035–1042. https://doi.org/10.1021/np9904509

Pinto, A., Tamborini, L., Pennacchietti, E., Coluccia, A., Silvestri, R., Cullia, G., De Micheli, C., Conti, P., & De Biase, D. (2016). Bicyclic γ-amino acids as inhibitors of γ-aminobutyrate aminotransferase. *Journal of Enzyme Inhibition and Medicinal Chemistry*, *31*(2), 295–301. https://doi.org/10.3109/14756366.2015.1021251

Pishchany, G., McCoy, A. L., Torres, V. J., Krause, J. C., Crowe, J. E., Fabry, M. E., & Skaar, E. P. (2010). Specificity for human hemoglobin enhances Staphylococcus aureus infection. *Cell Host and Microbe*, *16*(8), 544–550. https://doi.org/10.1016/j.chom.2010.11.002.Specificity

Pishchany, G., Sheldon, J. R., Dickson, C. F., Alam, M. T., Read, T. D., Gell, D. A., Heinrichs, D. E., & Skaar, E. P. (2014). IsdB-dependent hemoglobin binding is required for acquisition of heme by Staphylococcus aureus. *Journal of Infectious Diseases*, *209*(11), 1764–1772. https://doi.org/10.1093/infdis/jit817

Piskin, S., & Uzunali, E. (2007). A review of the use of adapalene for the treatment of acne vulgaris. In *Therapeutics and Clinical Risk Management* (Vol. 3, Issue 4).

Postma, B., Poppelier, M. J., van Galen, J. C., Prossnitz, E. R., van Strijp, J. A. G., de Haas, C. J. C., & van Kessel, K. P. M. (2004). Chemotaxis Inhibitory Protein of Staphylococcus aureus Binds Specifically to the C5a and Formylated Peptide Receptor. *The Journal of Immunology*, *172*(11), 6994–7001. https://doi.org/10.4049/jimmunol.172.11.6994

Potter, A. D., Butrico, C. E., Ford, C. A., Curry, J. M., Trenary, I. A., Tummarakota, S. S., Hendrix, A. S., Young, J. D., & Cassat, J. E. (2020). Host nutrient milieu drives an essential role for aspartate biosynthesis during invasive Staphylococcus aureus

infection. *Proceedings of the National Academy of Sciences of the United States of America*, *117*(22), 12394–12401. https://doi.org/10.1073/pnas.1922211117

Powers, M. E., Kim, H. K., Wang, Y., & Wardenburg, J. B. (2012). ADAM10 mediates vascular injury induced by staphylococcus aureus α-hemolysin. *Journal of Infectious Diseases*, *206*(3), 352–356. https://doi.org/10.1093/infdis/jis192

Presctott, L. M., Harley, J. P., & Klein, D. A. (2002). *Microbiology* (Fifth Edit). McGraw-Hill.

Public Health England. (2021). *Annual epidemiological commentary: Gram-negative bacteraemia, MRSA bacteraemia, MSSA bacteraemia and C. difficile infections, up to and including financial year April 2020 to March 2021*. 1–96.

Pugh, C. E., Nair, S. P., Harwood, J. L., & John, R. A. (1991). *Conditions for the assay of glutamate semialdehyde aminotransferase that overcome the problem of substrate instability*. *46*, 43–46.

Pujol, M., Miró, J. M., Shaw, E., Aguado, J. M., Puig-Asensio, M., Pigrau, C., Calbo, E., Montejo, M., Rodriguez-Álvarez, R., Garcia-Pais, M. J., Pintado, V., Escudero-Sánchez, R., Lopez-Contreras, J., Morata, L., Montero, M., Andrés, M., Pasquau, J., Arenas, M. D. M., Padilla, B., … Carratalà, J. (2021). Daptomycin Plus Fosfomycin Versus Daptomycin Alone for Methicillin-resistant Staphylococcus aureus Bacteremia and Endocarditis: A Randomized Clinical Trial. *Clinical Infectious Diseases*, *72*(9), 1517–1525. https://doi.org/10.1093/cid/ciaa1081

Purves, J., Cockayne, A., Moody, P. C. E., & Morrissey, J. A. (2010). Comparison of the regulation, metabolic functions, and roles in virulence of the glyceraldehyde-3-phosphate dehydrogenase homologues gapA and gapB in Staphylococcus aureus. *Infection and Immunity*, *78*(12), 5223–5232. https://doi.org/10.1128/IAI.00762-10

Qin, J. Z., Xin, H., & Nickoloff, B. J. (2010). Targeting glutamine metabolism sensitizes melanoma cells to TRAIL-induced death. *Biochemical and Biophysical Research Communications*, *398*(1), 146–152. https://doi.org/10.1016/j.bbrc.2010.06.057

Rammelkamp, C. H., & Maxon, T. (1942). Resistance of Staphylococcus aureus to the Action of Penicillin. *Proceedings of the Society for Experimental Biology and Medicine*, *51*(3), 386–389. https://doi.org/10.3181/00379727-51-13986

Rani, N., Kumar, C., Arunachalam, A., & PTV, L. (2018). Rutin as a potential inhibitor to target peptidoglycan pathway of Staphylococcus aureus cell wall synthesis. *Clinical Microbiology and Infectious Diseases*, *3*(3), 1–9. https://doi.org/10.15761/cmid.1000142

Rausch, S., Hänchen, A., Denisiuk, A., Löhken, M., Schneider, T., & Süssmuth, R. D. (2011). Feglymycin is an Inhibitor of the Enzymes MurA and MurC of the Peptidoglycan Biosynthesis Pathway. *ChemBioChem*, *12*(8), 1171–1173. https://doi.org/10.1002/cbic.201100120

Reddien, P. W., Bermange, A. L., Murfitt, K. J., Jennings, J. R., & Sánchez Alvarado, A. (2005). Identification of genes needed for regeneration, stem cell function, and tissue homeostasis by systematic gene perturbation in planaria. *Developmental Cell*, *8*(5), 635–649. https://doi.org/10.1016/j.devcel.2005.02.014

Reddien, P. W., & Sánchez Alvarado, A. (2004). Fundamentals of Planarian Regeneration. *Annual Review of Cell and Developmental Biology*, *20*, 725–757. https://doi.org/10.1146/annurev.cellbio.20.010403.095114

Redgrave, L. S., Sutton, S. B., Webber, M. A., & Piddock, L. J. V. (2014). Fluoroquinolone resistance: Mechanisms, impact on bacteria, and role in evolutionary success. *Trends in Microbiology*, *22*(8), 438–445. https://doi.org/10.1016/j.tim.2014.04.007

Reitzer, L. (2004). Biosynthesis of Glutamate, Aspartate, Asparagine, L -Alanine, and D -Alanine . *EcoSal Plus*, *1*(1). https://doi.org/10.1128/ecosalplus.3.6.1.3

Réjasse, A., Gilois, N., Barbosa, I., Huillet, E., Bevilacqua, C., Tran, S., Ramarao, N., Stenfors Arnesen, L. P., & Sanchis, V. (2012). Temperature-dependent production of various PlcR-controlled virulence factors in Bacillus weihenstephanensis strain KBAB4. *Applied and Environmental Microbiology*, *78*(8), 2553–2561. https://doi.org/10.1128/AEM.07446-11

Rembeza, E., & Engqvist, M. K. M. (2021). Experimental and computational investigation of enzyme functional annotations uncovers misannotation in the EC 1.1.3.15 enzyme class. *PLoS Computational Biology*, *17*(9), 1–22. https://doi.org/10.1371/journal.pcbi.1009446

Renwick, J., Reeves, E. P., Wientjes, F. B., & Kavanagh, K. (2007). Translocation of proteins homologous to human neutrophil p47phox and p67phox to the cell membrane in activated hemocytes of Galleria mellonella. *Developmental and Comparative Immunology*, *31*(4), 347–359. https://doi.org/10.1016/j.dci.2006.06.007

Renwick, M. J., Brogan, D. M., & Mossialos, E. (2016). A systematic review and critical assessment of incentive strategies for discovery and development of novel antibiotics. *Journal of Antibiotics*, *69*(2), 73–88. https://doi.org/10.1038/ja.2015.98

Resch, A., Rosenstein, R., Nerz, C., Go, F., & Götz, F. (2005). Differential Gene Expression Profiling of Staphylococcus aureus Cultivated under Biofilm and Planktonic Conditions. *Applied and Environmental Microbiology*, *71*(5), 2663–2676. https://doi.org/10.1128/AEM.71.5.2663

Richardson, A. R. (2019). Virulence and Metabolism. *Microbiology Spectrum*, *7*(2), 7–2.

Richardson, A. R., Somerville, G. A., & Sonenshein, A. L. (2015). Regulating the Intersection of Metabolism and Pathogenesis in Gram-positive Bacteria. *Metabolism and Bacterial Pathogenesis*, 129–165. https://doi.org/10.1128/microbiolspec.mbp-0004-2014

Rödström, K. E. J., Elbing, K., & Lindkvist-Petersson, K. (2014). Structure of the Superantigen Staphylococcal Enterotoxin B in Complex with TCR and Peptide–MHC Demonstrates Absence of TCR–Peptide Contacts. *The Journal of Immunology*, *193*(4), 1998–2004. https://doi.org/10.4049/jimmunol.1401268

Roggenkamp, A., Sing, A., Hornef, M., Brunner, U., Autenrieth, I. B., & Heesemann, J. (1998). Chronic prosthetic hip infection caused by a small-colony variant of Escherichia coli. *Journal of Clinical Microbiology*, *36*(9), 2530–2534. https://doi.org/10.1128/jcm.36.9.2530-2534.1998

Rotelli, A. E., Guardia, T., Juárez, A. O., De La Rocha, N. E., & Pelzer, L. E. (2003). Comparative study of flavonoids in experimental models of inflammation. *Pharmacological Research*, *48*(6), 601–606. https://doi.org/10.1016/S1043-6618(03)00225-1

Rusu, A., Tanase, C., Pascu, G.-A., & Todoran, N. (2020). Recent Advances Regarding the Therapeutic Potential of Adapalene. *Pharmaceuticals*, *13*(9), 217. https://doi.org/10.3390/ph13090217

Sadykov, M. R., Thomas, V. C., Marshall, D. D., Wenstrom, C. J., Moormeier, D. E., Widhelm, T. J., Nuxoll, A. S., Powers, R., & Bayles, W. (2013). Inactivation of the Pta-AckA Pathway Causes Cell Death in Staphylococcus aureus. *Journal of Bacteriology*, *195*(13), 3035–3044. https://doi.org/10.1128/JB.00042-13

Sadykov, M. R., Zhang, B., Halouska, S., Nelson, J. L., Kreimer, L. W., Zhu, Y., Powers, R., & Somerville, G. A. (2010). Using NMR Metabolomics to Investigate Tricarboxylic Acid Cycle-dependent Signal Transduction in Staphylococcus. *The Journal of Biological Chemistry*, *285*(47), 36616–36624. https://doi.org/10.1074/jbc.M110.152843

Saghatelian, A., & Cravatt, B. F. (2005). Assignment of protein function in the postgenomic era. *Nature Chemical Biology*, *1*(3), 129. https://doi.org/10.1038/nchembio0805-130

Sakr, A., Brégeon, F., Mège, J. L., Rolain, J. M., & Blin, O. (2018). Staphylococcus aureus nasal colonization: An update on mechanisms, epidemiology, risk factors, and subsequent infections. *Frontiers in Microbiology*, *9*(OCT), 1–15. https://doi.org/10.3389/fmicb.2018.02419

Sawicki, E., Hauser, T. R., Stanley, T. W., & Elbert, W. (1961). The 3-Methyl-2-benzothiazolone Hydrazone Test: Sensitive New Methods for the Detection, Rapid Estimation, and Determination of Aliphatic Aldehydes. *Analytical Chemistry*, *33*(1), 93–96. https://doi.org/10.1021/ac60169a028

Sebaugh, J. L. (2011). Guidelines for accurate EC50/IC50 estimation. *Pharmaceutical Statistics*, *10*(2), 128–134. https://doi.org/10.1002/pst.426

Seetharamappa, J., Oke, M., Liu, H., McMahon, S. A., Johnson, K. A., Carter, L., Dorward, M., Zawadzki, M., Overton, I. M., Van Niekirk, C. A. J., Graham, S., Botting, C. H., Taylor, G. L., White, M. F., Barton, G. J., Coote, P. J., & Naismith, J. H. (2007). Expression, purification, crystallization, data collection and preliminary biochemical characterization of methicillin-resistant Staphylococcus aureus Sar2028, an aspartate/tyrosine/phenylalanine pyridoxal-5′-phosphate- dependent aminotransferase. *Acta Crystallographica Section F: Structural Biology and Crystallization Communications*, *63*(5), 452–456. https://doi.org/10.1107/S1744309107019562

Seidl, K., Goerke, C., Wolz, C., Mack, D., Berger-Bächi, B., & Bischoff, M. (2008). Staphylococcus aureus CcpA affects biofilm formation. *Infection and Immunity*, *76*(5), 2044–2050. https://doi.org/10.1128/IAI.00035-08

Seidl, K., Müller, S., François, P., Kriebitzsch, C., Schrenzel, J., Engelmann, S., Bischoff, M., & Berger-bächi, B. (2009). Effect of a glucose impulse on the CcpA regulon in Staphylococcus aureus. *BMC Microbiology*, *9*(1), 95. https://doi.org/10.1186/1471-2180-9-95

Seif, Y., Monk, J. M., Mih, N., Tsunemoto, H., Poudel, S., Zuniga, C., Broddrick, J., Zengler, K., & Palsson, B. O. (2019). A computational knowledge-base elucidates the response of Staphylococcus aureus to different media types. *PLoS Computational Biology*, *15*(1), 1–27. https://doi.org/10.1371/journal.pcbi.1006644

Seilie, S. E., & Wardenburg, J. B. (2017). Staphylococcus aureus pore-forming toxins: the interface of pathogen and host complexity. *Seminars in Cell and Developmental Biology*, *72*, 101–116. https://doi.org/10.1016/j.semcdb.2017.04.003.Staphylococcus

Shatalin, K., Nuthanakanti, A., Kaushik, A., Shishov, D., Peselis, A., Shamovsky, I., Pani, B., Lechpammer, M., Vasilyev, N., Shatalina, E., Rebatchouk, D., Mironov, A., Fedichev, P., Serganov, A., & Nudler, E. (2021). Inhibitors of bacterial H2S biogenesis targeting antibiotic resistance and tolerance. *Science*, *1175*(June), 1169–1175.

Sheehan, G., Dixon, A., & Kavanagh, K. (2019). Utilization of galleria mellonella larvae to characterize the development of staphylococcus aureus infection. *Microbiology*, *165*(8), 863–875. https://doi.org/10.1099/mic.0.000813

Sherrard, L. J., Tunney, M. M., & Elborn, J. S. (2014). Antimicrobial resistance in the respiratory microbiota of people with cystic fibrosis. *The Lancet*, *384*(9944), 703–713. https://doi.org/10.1016/S0140-6736(14)61137-5

Shi, T., Shi, Y., Gao, H., Ma, Y., Wang, Q., Shen, S., Shao, X., Gong, W., Chen, X., Qin, J., Wu, J., Jiang, Q., & Xue, B. (2022). Exercised accelerated the production of muscle-derived kynurenic acid in skeletal muscle and alleviated the

postmenopausal osteoporosis through the Gpr35/NFκB p65 pathway. *Journal of Orthopaedic Translation*, *35*, 1–12. https://doi.org/10.1016/j.jot.2022.03.003

Shroot, B., Michel, S., & Antipolis, S. (1997). Pharmacology and chemistry of adapalene. *Journal of the American Academy of Dermatology*, *36*(6 II SUPPL.), 96–103. https://doi.org/10.1016/s0190-9622(97)70050-1

Siddiqui, S. (2019). Resistance in Pathogenic Microorganisms. In *New and Future Developments in Microbial Biotechnology and Bioingineering: Microbial Secondary Metabolites Biochemistry and Applications* (pp. 183–191).

Sikes, J. M., & Newmark, P. A. (2013). Restoration of anterior regeneration in a planarian with limited regenerative ability. *Nature*, *500*(7460), 77–80. https://doi.org/10.1038/nature12403

Silva, L. N., Da Hora, G. C. A., Soares, T. A., Bojer, M. S., Ingmer, H., Macedo, A. J., & Trentin, D. S. (2017). Myricetin protects Galleria mellonella against Staphylococcus aureus infection and inhibits multiple virulence factors. *Scientific Reports*, *7*(1), 1–16. https://doi.org/10.1038/s41598-017-02712-1

Sinha, N., Eirich, J., Finkemeier, I., & Grimm, B. (2022). Glutamate 1-semialdehyde aminotransferase is connected to GluTR by GluTR-binding protein and contributes to the rate-limiting step of 5-aminolevulinic acid synthesis. *The Plant Cell*, *34*(11), 4623–4640. https://doi.org/10.1093/plcell/koac237

Skaar, E. P., Humayun, M., Bae, T., DeBord, K., & Schneewind, O. (2004). Iron-source preference of Staphylococcus aureus infections. *Science*, *305*, 1626–1628.

Smith, M., Kannangara, G., Grimm, B., & von Wettstein, D. (1991). Characterization of glutamate-1-semialdehyde aminotransferase of Synechococcus Steady-state kinetics analysis. *European Journal of Biochemistry*, *202*, 749–757.

Somerville, G. A., & Proctor, R. A. (2009). At the Crossroads of Bacterial Metabolism and Virulence Factor Synthesis in Staphylococci. *Microbiology and Molecular Biology Reviews*, *73*(2), 233–248. https://doi.org/10.1128/mmbr.00005-09

Son, H. F., & Kim, K. J. (2016). Structural insights into a novel class of aspartate aminotransferase from Corynebacterium glutamicum. *PLoS ONE*, *11*(6), 1–15. https://doi.org/10.1371/journal.pone.0158402

Song, Y., Pu, H., Jiang, T., Zhang, L., & Ouyang, M. (2016). Crystal structure of glutamate-1-semialdehyde-2,1-aminomutase from Arabidopsis thaliana. *Acta Crystallographica Section:F Structural Biology Communications*, *72*, 448–456. https://doi.org/10.1107/S2053230X16007263

Spahich, N. A., Vitko, N. P., Thurlow, L. R., Temple, B., & Richardson, A. R. (2016). Staphylococcus aureus lactate- and malate-quinone oxidoreductases contribute to nitric oxide resistance and virulence. *Molecular Microbiology*, *100*(5), 759–773.

Sprouffske, K., & Wagner, A. (2016). Growthcurver: An R package for obtaining interpretable metrics from microbial growth curves. *BMC Bioinformatics*, *17*(1), 17–20. https://doi.org/10.1186/s12859-016-1016-7

Storici, P., De Biase, D., Bossa, F., Bruno, S., Mozzarelli, A., Peneff, C., Silverman, R. B., & Schirmer, T. (2004). Structures of γ-Aminobutyric Acid (GABA) Aminotransferase, a Pyridoxal 5′-Phosphate, and [2Fe-2S] Cluster-containing Enzyme, Complexed with γ-Ethynyl-GABA and with the Antiepilepsy Drug Vigabatrin. *Journal of Biological Chemistry*, *279*(1), 363–373. https://doi.org/10.1074/jbc.M305884200

Sung, M. H., Tanizawa, K., Tanaka, H., Kuramitsu, S., Kagamiyama, H., & Soda, K. (1990). Purification and characterization of thermostable aspartate aminotransferase from a thermophilic Bacillus species. *Journal of Bacteriology*, *172*(3), 1345–1351. https://doi.org/10.1128/jb.172.3.1345-1351.1990

Swarupa, V., Chaudhury, A., & Krishna Sarma, P. V. G. (2017). Effect of 4-methoxy 1-methyl 2-oxopyridine 3-carbamide on Staphylococcus aureus by inhibiting UDP-MurNAc-pentapeptide, peptidyl deformylase and uridine monophosphate kinase. *Journal of Applied Microbiology*, *122*(3), 663–675. https://doi.org/10.1111/jam.13378

Swoboda, J., Meredith, T., Campbell, J., Brown, S., Suzuki, T., Bollenbach, T., Malhowski, A., Kishony, R., Gilmore, M., & Walker, S. (2009). Discovery of a Small Molecule that Blocks Wall Teichoic Acid Biosynthesis in Staphylococcus aureus. *ACS Chemical Biology*, *4*(10), 875–883.

Tan, C. M., Therien, A. G., Lu, J., Lee, S. H., Caron, A., Gill, C. J., Lebeau-Jacob, C., Benton-Perdomo, L., Monteiro, J. M., Pereira, P. M., Elsen, N. L., Wu, J., Deschamps, K., Petcu, M., Wong, S., Daigneault, E., Kramer, S., Liang, L., Maxwell, E., … Roemer, T. (2012). Restoring methicillin-resistant Staphylococcus aureus susceptibility to β-lactam antibiotics. *Science Translational Medicine*, *4*(126). https://doi.org/10.1126/scitranslmed.3003592

Tan, X., Ramond, E., Jamet, A., Barnier, J.-P., Decaux-Tramoni, B., Dupuis, M., Euphrasie, D., Tros, F., Nemazanyy, I., Ziveri, J., Nassif, X., Charbit, A., & Coureuil, M. (2019). Transketolase of Staphylococcus aureus in the Control of Master Regulators of Stress Response During Infection. *The Journal of Infectious Diseases*, *220*, 1967–1976. https://doi.org/10.1093/infdis/jiz404

Tanaka, M., Wang, T., Onodera, Y., Uchida, Y., & Sato, K. (2000). Mechanism of quinolone resistance in Staphylococcus aureus. *Journal of Infection and Chemotherapy*, *6*, 131–139.

Thornburg, J. M., Nelson, K. K., Clem, B. F., Lane, A. N., Arumugam, S., Simmons, A., Eaton, J. W., Telang, S., & Chesney, J. (2008). Targeting aspartate aminotransferase in breast cancer. *Breast Cancer Research*, *10*(5), 1–12. https://doi.org/10.1186/bcr2154

Thorpe, K. E., Joski, P., & Johnston, K. J. (2018). Antibiotic-resistant infection treatment costs have doubled since 2002, now exceeding $2 billion annually. *Health Affairs*, *37*(4), 662–669. https://doi.org/10.1377/hlthaff.2017.1153

Toney, M. D. (2005). Reaction specificity in pyridoxal phosphate enzymes. *Archives of Biochemistry and Biophysics*, *433*(1), 279–287. https://doi.org/10.1016/j.abb.2004.09.037

Tong, S. Y. C., Lye, D. C., Yahav, D., Sud, A., Robinson, J. O., Nelson, J., Archuleta, S., Roberts, M. A., Cass, A., Paterson, D. L., Foo, H., Paul, M., Guy, S. D., Tramontana, A. R., Walls, G. B., McBride, S., Bak, N., Ghosh, N., Rogers, B. A., … Davis, J. S. (2020). Effect of Vancomycin or Daptomycin with vs Without an Antistaphylococcal β-Lactam on Mortality, Bacteremia, Relapse, or Treatment Failure in Patients with MRSA Bacteremia: A Randomized Clinical Trial. *JAMA - Journal of the American Medical Association*, *323*(6), 527–537. https://doi.org/10.1001/jama.2020.0103

Torres, V. J., Pishchany, G., Humayun, M., Schneewind, O., & Skaar, E. P. (2006). Staphylococcus aureus IsdB is a hemoglobin receptor required for heme iron utilization. *Journal of Bacteriology*, *188*(24), 8421–8429. https://doi.org/10.1128/JB.01335-06

Torres, V. J., Stauff, D. L., Pishchany, G., Bezbradica, J. S., Laura, E., Iturregui, J., Anderson, K. L., Dunman, P. M., Joyce, S., & Skaar, P. (2007). A Staphylococcus aureus regulatory system that responds to host heme and modulates virulence. *Cell Host and Microbe*, *1*(2), 109–119.

Tsai, C. J.-Y., Loh, J. M. S., & Proft, T. (2016). *Galleria mellonella* infection models for the study of bacterial diseases and for antimicrobial drug testing. *Virulence*, *7*(3), 214–229. https://doi.org/10.1080/21505594.2015.1135289

Tsoumtsa, L. L., Torre, C., Trouplin, V., Coiffard, B., Gimenez, G., Mege, J. L., & Ghigo, E. (2017). Antimicrobial capacity of the freshwater planarians against S. aureus is

under the control of Timeless. *Virulence*, *8*(7), 1160–1169. https://doi.org/10.1080/21505594.2016.1276689

Tuttle, J. B., Anderson, M., Bechle, B. M., Campbell, B. M., Chang, C., Dounay, A. B., Evrard, E., Fonseca, K. R., Gan, X., Ghosh, S., Horner, W., James, L. C., Kim, J. Y., McAllister, L. A., Pandit, J., Parikh, V. D., Rago, B. J., Salafia, M. A., Strick, C. A., … Verhoest, P. R. (2013). Structure-based design of irreversible human KAT II inhibitors: Discovery of new potency-enhancing interactions. *ACS Medicinal Chemistry Letters*, *4*(1), 37–40. https://doi.org/10.1021/ml300237v

Valentino, M. D., Foulston, L., Sadaka, A., Kos, V. N., Villet, R. A., Maria, J. S., Lazinski, D. W., Camilli, A., Walker, S., Hooper, D. C., & Gilmore, M. S. (2014). Genes contributing to Staphylococcus aureus fitness in abscess- and infection-related ecologies. *MBio*, *5*(5), 1–10. https://doi.org/10.1128/mBio.01729-14

van Belkum, A., Verkaik, N. J., de Vogel, C. P., Boelens, H. A., Verveer, J., Nouwen, J. L., Verbrugh, H. A., & Wertheim, H. F. L. (2009). Reclassification of *Staphylococcus aureus* Nasal Carriage Types. *The Journal of Infectious Diseases*, *199*(12), 1820–1826. https://doi.org/10.1086/599119

van der Laan, J. W., Weick, G., & van Bleek, G. (1985). Effects of inhibitors of GABA-transaminase on hole-board exploration and on temperature. Relation with effects on quasi-morphine abstinence behaviour induced by sodium dipropylacetate. *Biochemical Pharmacology*, *34*(21), 3789–3794. https://doi.org/10.1016/0006-2952(85)90426-5

Vazquez, V., Liang, X., Horndahl, J. K., Ganesh, V. K., Smeds, E., Foster, T. J., & Hook, M. (2011). Fibrinogen is a ligand for the Staphylococcus aureus Microbial Surface Components Recognizing Adhesive Matrix Molecules (MSCRAMM) Bone sialoprotein-binding protein (Bbp). *Journal of Biological Chemistry*, *286*(34), 29797–29805. https://doi.org/10.1074/jbc.M110.214981

Vestergaard, M., Frees, D., & Ingmer, H. (2019). Antibiotic Resistance and the MRSA Problem. *Microbiology Spectrum*, *7*(2), GPP3-0057–2018. https://doi.org/10.1128/9781683670131.ch47

Vitko, N. P., Spahich, N. A., & Richardson, A. R. (2015). Glycolytic Dependency of High-Level Nitric Oxide Resistance and Virulence in Staphylococcus aureus. *MBio*, *6*(2), p.e00045-15.

Vuong, C., Yeh, A. J., Cheung, G. Y. C., & Otto, M. (2016). Investigational drugs to treat methicillin-resistant Staphylococcus aureus. *Expert Opinion on Investigational Drugs*, *25*(1), 73–93. https://doi.org/10.1517/13543784.2016.1109077

Walsh, C., & Wencewicz, T. (2016). *Antibiotics: Challenges Mechanisms Opportunities* (First Edit). ASM Press.

Wang, Q., Zhang, Q., Luan, S., Yang, K., Zheng, M., Li, K., Chen, L., & Li, H. (2019). Adapalene inhibits ovarian cancer ES-2 cells growth by targeting glutamic-oxaloacetic transaminase 1. *Bioorganic Chemistry*, *93*(April), 103315. https://doi.org/10.1016/j.bioorg.2019.103315

Wang, R., Braughton, K. R., Kretschmer, D., Bach, T. H. L., Queck, S. Y., Li, M., Kennedy, A. D., Dorward, D. W., Klebanoff, S. J., Peschel, A., DeLeo, F. R., & Otto, M. (2007). Identification of novel cytolytic peptides as key virulence determinants for community-associated MRSA. *Nature Medicine*, *13*(12), 1510–1514. https://doi.org/10.1038/nm1656

Wang, R., Zhang, M., Liu, H., Xu, J., Yu, J., He, F., Zhang, X., Dong, S., & Dou, D. (2016). PsAAT3, an oomycete-specific aspartate aminotransferase, is required for full pathogenicity of the oomycete pathogen Phytophthora sojae. *Fungal Biology*, *120*(4), 620–630. https://doi.org/10.1016/j.funbio.2016.01.005

Wang, X., Li, W., Wang, W., Wang, S., Xu, T., Chen, J., & Zhang, W. (2021). Involvement of Small Colony Variant-Related Heme Biosynthesis Genes in Staphylococcus

aureus Persister Formation in vitro. *Frontiers in Microbiology*, *12*(December), 756809. https://doi.org/10.3389/fmicb.2021.756809

Waterhouse, E. J., Mims, K. N., & Gowda, S. N. (2009). Treatment of refractory complex partial seizures: Role of vigabatrin. *Neuropsychiatric Disease and Treatment*, *5*(1), 505–515. https://doi.org/10.2147/ndt.s5236

Weiss, J. S. (1997). Current Options for the Topical Treatment of Acne Vulgaris. *Pediatric Dermatology*, *14*(6), 480–488.

Wermser, C., & Lopez, D. (2018). Identification of Staphylococcus aureus genes involved in the formation of structured macrocolonies. *Microbiology*, *164*(5), 801–815. https://doi.org/10.1099/mic.0.000660

Wertheim, H., Melles, D. C., Vos, M. C., van Leeuwen, W., van Belkum, A., Verbrugh, H. a, & Nouwen, J. L. (2005). The role of nasal carriage in Staphylococcus aureus infections. *The Lancet Infectious Diseases*, *5*(12), 751–762. https://doi.org/10.1016/S1473-3099(05)70295-4

Whitten, M. M. A., Tew, I. F., Lee, B. L., & Ratcliffe, N. A. (2004). A Novel Role for an Insect Apolipoprotein (Apolipophorin III) in β-1,3-Glucan Pattern Recognition and Cellular Encapsulation Reactions. In *The Journal of Immunology* (Vol. 172, Issue 4, pp. 2177–2185). https://doi.org/10.4049/jimmunol.172.4.2177

WHO. (2020). Antibacterial Agents in Clinical and Preclinical Development: An Overview and Analysis. *World Health Organization, Geneva, Switzerland*.

Wiesner, A., Losen, S., Kopáček, P., Weise, C., & Götz, P. (1997). Isolated Apolipophorin III from Galleria mellonella stimulates the immune reactions of this insect. *Journal of Insect Physiology*, *43*(4), 383–391. https://doi.org/10.1016/S0022-1910(96)00113-8

Wilcox, L. J., Borradaile, N. M., De Dreu, L. E., & Huff, M. W. (2001). Secretion of hepatocyte apoB is inhibited by the flavonoids, naringenin and hesperetin, via reduced activity and expression of ACAT2 and MTP. *Journal of Lipid Research*, *42*(5), 725–734.

Wilkie, S. E., & Warren, M. J. (1998). Recombinant expression, purification, and characterization of three isoenzymes of aspartate aminotransferase from Arabidopsis thaliana. *Protein Expression and Purification*, *12*(3), 381–389. https://doi.org/10.1006/prep.1997.0845

Wishart, D. S., Guo, A. C., Oler, E., Wang, F., Anjum, A., Peters, H., Dizon, R., Sayeeda, Z., Tian, S., Lee, B. L., Berjanskii, M., Mah, R., Yamamoto, M., Jovel, J., Torres-Calzada, C., Hiebert-Giesbrecht, M., Lui, V. W., Varshavi, D., Varshavi, D., … Gautam, V. (2022). HMDB 5.0: The Human Metabolome Database for 2022. *Nucleic Acids Research*, *50*(D1), D622–D631. https://doi.org/10.1093/nar/gkab1062

Witzky, A., Hummels, K. R., Rajkovic, A., Jones, L. A., Kearns, D. B., & Ibba, M. (2018). EF-P Posttranslational modification has variable impact on polyproline translation in Bacillus subtilis. *MBio*, *9*(2), 306–318.

Wu, G., Liu, Y., Ding, Y., & Yi, Y. (2016). Ultrastructural and functional characterization of circulating hemocytes from Galleria mellonella larva: Cell types and their role in the innate immunity. *Tissue and Cell*, *48*(4), 297–304. https://doi.org/10.1016/j.tice.2016.06.007

Wu, H. J., Yang, Y., Wang, S., Qiao, J. Q., Xia, Y. F., Wang, Y., Wang, W. D., Gao, S. F., Liu, J., Xue, P. Q., & Gao, X. W. (2011). Cloning, expression and characterization of a new aspartate aminotransferase from Bacillus subtilis B3. *FEBS Journal*, *278*(8), 1345–1357. https://doi.org/10.1111/j.1742-4658.2011.08054.x

Xie, W., Dolder, S., Siegrist, M., Wetterwald, A., & Hofstetter, W. (2016). Glutamate Receptor Agonists and Glutamate Transporter Antagonists Regulate Differentiation of Osteoblast Lineage Cells. *Calcified Tissue International*, *99*(2), 142–154. https://doi.org/10.1007/s00223-016-0129-3

Xing, R., & Whitman, W. B. (1992). Characterization of amino acid aminotransferases of Methanococcus aeolicus. *Journal of Bacteriology*, *174*(2), 541–548. https://doi.org/10.1128/jb.174.2.541-548.1992

Yagi, T., Kagamiyama, H., Nozaki, M., & Soda, K. (1985). Glutamate aspartate transaminase from microorganisms. *Methods in Enzymology*, *113*(1985), 83–89.

Yang, D., Ho, Y. X., Cowell, L. M., Jilani, I., Foster, S. J., & Prince, L. R. (2019). A genome-wide screen identifies factors involved in S. Aureus - Induced human neutrophil cell death and pathogenesis. *Frontiers in Immunology*, *10*(JAN). https://doi.org/10.3389/fimmu.2019.00045

Yee, R., Feng, J., Wang, J., Chen, J., & Zhang, Y. (2019). Identification of Genes Regulating Cell Death in Staphylococcus aureus. *Frontiers in Microbiology*, *10*. https://doi.org/10.3389/fmicb.2019.02199

Yelamanchi, S. D., & Surolia, A. (2021). Targeting amino acid metabolism of Mycobacterium tuberculosis for developing inhibitors to curtail its survival. *IUBMB Life*, *73*(4), 643–658. https://doi.org/10.1002/iub.2455

Yoshida, T., Yamasaki, S., Kaneko, O., Taoka, N., Tomimoto, Y., Namatame, I., Yahata, T., Kuromitsu, S., Cantley, L. C., & Lyssiotis, C. A. (2020). A covalent small molecule inhibitor of glutamate-oxaloacetate transaminase 1 impairs pancreatic cancer growth. *Biochemical and Biophysical Research Communications*, *522*(3), 633–638. https://doi.org/10.1016/j.bbrc.2019.11.130

Yoshida, Y., Fujigaki, H., Kato, K., Yamazaki, K., Fujigaki, S., Kunisawa, K., Yamamoto, Y., Mouri, A., Oda, A., Nabeshima, T., & Saito, K. (2019). Selective and competitive

inhibition of kynurenine aminotransferase 2 by glycyrrhizic acid and its analogues. *Scientific Reports*, *9*(1), 1–11. https://doi.org/10.1038/s41598-019-46666-y

Yu, A. C., Schousboec, A., & Hertz, L. (1982). Metabolic Fate of 14C-Labeled Glutamate in Astrocytes in Primary Cultures. *Journal of Neurochemistry*, *39*(4), 954–960. https://doi.org/10.1111/j.1471-4159.1982.tb11482.x

Yu, F., Lu, C., Liu, Y., Sun, H., Shang, Y., Ding, Y., Li, D., Qin, Z., Parsons, C., Huang, X., Li, Y., Hu, L., & Wang, L. (2014). Emergence of quinupristin / dalfopristin resistance among livestock-associated Staphylococcus aureus ST9 clinical isolates. *International Journal of Antimicrobial Agents*, *44*, 416–419.

Yu, L., & Sivitz, W. I. (2020). Oxaloacetate Mediates Mitochondrial Metabolism and Function. *Current Metabolomics and Systems Biology*, *7*(1), 11–23. https://doi.org/10.2174/2213235x07666191008103247

Zareei, S., Boojar, M. M. A., & Amanlou, M. (2017). Inhibition of liver alanine aminotransferase and aspartate aminotransferase by hesperidin and its aglycone hesperetin: An in vitro and in silico study. *Life Sciences*, *178*, 49–55. https://doi.org/10.1016/j.lfs.2017.04.001

Zdybicka-Barabas, A., Palusińska-Szysz, M., Gruszecki, W. I., Mak, P., & Cytryńska, M. (2014). Galleria mellonella apolipophorin III - An apolipoprotein with anti-Legionella pneumophila activity. *Biochimica et Biophysica Acta - Biomembranes*, *1838*(10), 2689–2697. https://doi.org/10.1016/j.bbamem.2014.07.003

Zeng, D., Debabov, D., Hartsell, T. L., Cano, R. J., Adams, S., Schuyler, J. A., McMillan, R., & Pace, J. L. (2016). Approved glycopeptide antibacterial drugs: Mechanism of action and resistance. *Cold Spring Harbor Perspectives in Medicine*, *6*(12), 1–16. https://doi.org/10.1101/cshperspect.a026989

Zhang, J., Kang, Z., Chen, J., & Du, G. (2015). Optimization of the heme biosynthesis pathway for the production of 5-aminolevulinic acid in Escherichia coli. *Scientific Reports*, *5*, 1–7. https://doi.org/10.1038/srep08584

Zhang, L. (2011). *Heme biology: the secret life of heme in regulating diverse biological processes*. World Scientific Publishing Company.

Zhu, Y., Nandakumar, R., Sadykov, M. R., Madayiputhiya, N., Luong, T. T., Gaupp, R., Lee, C. Y., & Somerville, G. A. (2011). RpiR Homologues May Link Staphylococcus aureus RNAIII Synthesis and Pentose Phosphate Pathway Regulation. *Journal of Bacteriology*, *193*(22), 6187–6196. https://doi.org/10.1128/JB.05930-11

8. Appendix

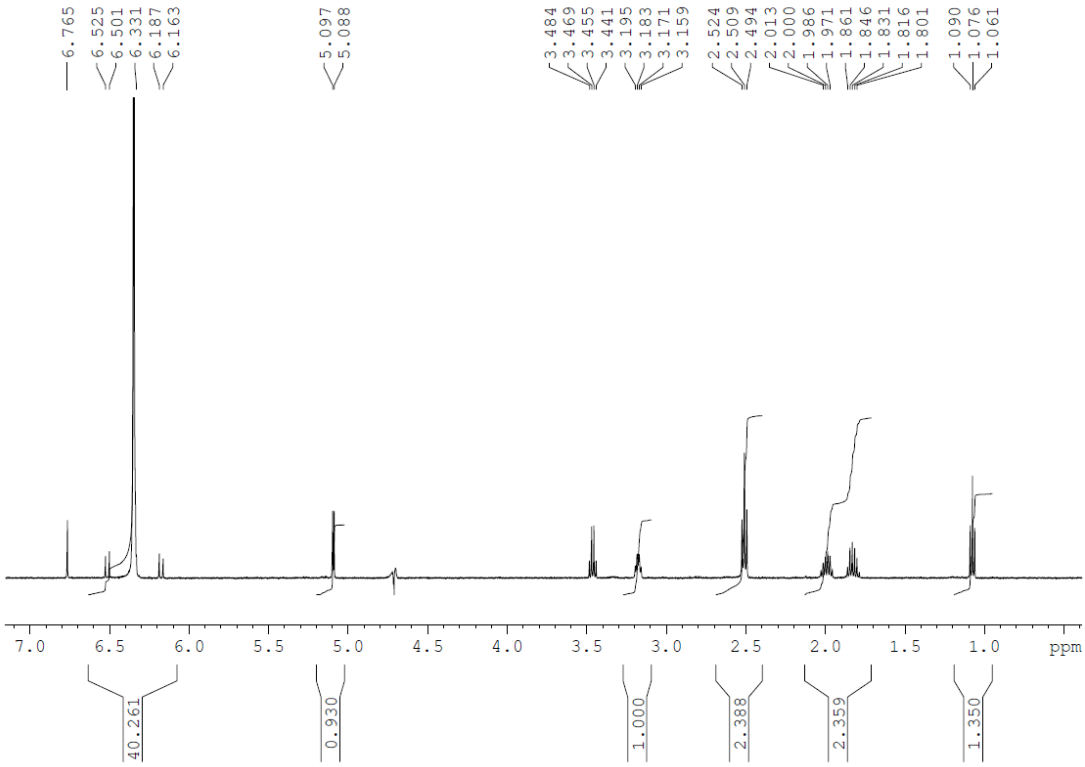

Appendix 1 - Proton NMR spectrum of the glutamate-1-semialdehyde in D_2O.